SPATIOTEMPORAL STIMULUS EFFECTS ON RESPONSE PROPERTIES OF NEURONS IN THE PRIMARY SOMATOSENSORY CORTEX OF OWL MONKEYS

By

Jamie Lynn Reed

Dissertation

Submitted to the Faculty of the

Graduate School of Vanderbilt University

in partial fulfillment of the requirements

for the degree of

DOCTOR OF PHILOSOPHY

in

Neuroscience

December, 2009

Nashville, Tennessee

Approved:

Dr. Jon H. Kaas

Dr. A.B. Bonds, III

Dr. Troy A. Hackett

Dr. Anna W. Roe

ACKNOWLEDGEMENTS

I am grateful for the stipend support from the National Institutes of Health Training Grant to the Vanderbilt University Neuroscience Graduate program, T32-MH64913, and the University Graduate Fellowship for my first few years. For my last three years I was fortunate to be supported by the Ruth L. Kirschstein National Research Service Award, NIH/NINDS grant F31-NS053231. This research was supported by funds to Dr. Jon H. Kaas from the James S. McDonnell Foundation and NIH/NINDS grant NS16446. Sources of support for collaborators are listed within individual chapters.

Foremost, I am forever grateful to my advisor, Dr. Jon Kaas, for his support and direction, for his exemplary example, and for his confidence in me to explore research directions and collaborations. I look forward to continuing work with Jon. My committee members provided exceptional guidance. I appreciate advice from my committee chair, Dr. Anna Roe, especially regarding the NRSA. Dr. A.B. Bonds collaborated with us when I revised my proposal to utilize techniques in his laboratory, and he provided his array placement wizardry in each experiment. Dr. Troy Hackett generously supplied his time and knowledge, particularly with technical aspects of our early, challenging projects.

Dr. Huixin Qi has been called my research "big sister" and has been a part of almost every project I have done. I am lucky to have had her guidance, and I look forward to continuing collaborations. Dr. Pierre Pouget was instrumental in teaching me analysis methods using Matlab, and he was extremely generous with his time and code. I also hope we continue collaborations, as his enthusiasm for neuroscience is infectious. Dr. Ford Ebner and Dr. Vivien Casagrande were part of my qualifying committee and

both contributed to the ideas and techniques in this work long after my qualifying exam. I am so appreciative of their generosity. I thank Dr. Jeff Schall, also a member of my qualifying committee, for his support of my collaboration with Pierre, as well as for suggesting I start a Neurophysiology Discussion Group. And I thank all members for making the group worthwhile, particularly Corrie Camalier and Jeremiah Cohen for helping to start and keep the group operating for so long.

I thank current and former members of the Kaas and Hackett labs for the ideal lab environment (we were spoiled). Dr. Yoshi Kajikawa and Dr. Bill D'Angelo advised me in early projects not included in this dissertation. Dr. Mike Remple was a primary force outside of Jon guiding me to join the Kaas lab, and he has been a great mentor. To co-authors of manuscripts not already named, including Dr. Mark Burish, Dr. Zhiyi Zhou, and Dr. Melanie Bernard: I thank you for help, along with Dr. Omar Gharbawie and Corrie Camalier for taking shifts during the 1-3 day experiments. Advice from Dr. Robert Friedman (working with Dr. Roe) was essential for setting up stimulation equipment.

Thanks to Corrie and Dr. Lisa de la Mothe for reading portions of this dissertation. Special thanks to Lisa for guidance through this process. Lisa and Suzanne Blumell were awesome office-mates, and Erik Emeric was generous with Matlab knowledge while we worked on our dissertations in our shared office my final year.

The Vanderbilt Brain Institute and administration within the Psychology Department deserve recognition, especially Trisha James and former staff members Dr. Mary Early-Zald and Carol Wiley for all of their assistance. Everyone named and unnamed who has crossed my path, my heartfelt thanks to you for providing invaluable experiences to comprise this extended period of my life, my graduate career.

TABLE OF CONTENTS

LIST OF TABLES

LIST OF FIGURES

Figure Page

LIST OF ABBREVIATIONS

Adj D.	Adjacent digits or palm pads
Adj Ph.	Adjacent phalanges within a digit
ANOVA	Analysis of variance
CN_IN	One, stimulus probe inside the Response Field, but not in the center, one probe in the center of the Response Field
CN_OUT	One stimulus probe in the center of the Response Field, one probe outside the Response Field of a neuron
CS	Central sulcus
d	Distal
D(1-5)	Digit
ECG	Electrocardiogram
EEG	Electroencephalogram
fMRI	Functional magnetic resonance imaging
GABA	Gamma-aminobutyric acid
GMFR	Geometric mean firing rate
ICA	Independent Component Analysis
IN_BOTH	Two stimulus probes inside the Response Field of a neuron
IN_IN	Two stimulus probes inside the Response Field of a neuron, simplified
IN_OUT	One stimulus probe inside the Response Field, one probe outside the Response Field of a neuron
JPETH	Joint perievent time histogram
JPSTH	Joint peristimulus time histogram
LS	Lateral sulcus
m	Middle
MAR	Missing at random
MCAR	Missing completely at random
MEG	Magnetoencephalography
MNAR	Missing not at random
mRF	Minimal receptive field
MU	Multi-unit
NonA D.	Nonadjacent digits or palm pads
NonA Ph.	Nonadjacent phalanges or phalange and palm pad
OUT_OUT	Two stimulus probes outside the Response Field of one neuron
p	Proximal
P(1-4)	Digital palm pad
PC	Principal Component
PCA	Principal Component Analysis
PETH	Perievent time histogram
PH	Hypothenar palm pad
Pi(1-3)	Insular palm pad
PR	Rostrolateral parietal area
PSTH	Peristimulus time histogram

PTh	Thenar palm pad
PV	Parietal ventral area
RA	Rapidly-adapting
RF	Receptive field
S1	Primary somatosensory cortex
S2	Secondary somatosensory cortex
SA	Slowly-adapting
SD	Standard Deviation
SI	Supporting Information
STS	Superior temporal sulcus
SU	Single unit
VP	Ventroposterior nucleus of the thalamus
VPI	Ventorposterior inferior nucleus
VPL	Ventroposterior lateral nucleus
VPM	Ventroposterior medial nucleus
VPS	Ventroposterior superior nucleus
VS	Ventral somatosensory area

CHAPTER I

INTRODUCTION

Background and Significance

The primate somatosensory cortex has been well-studied; however, functional implications of the known anatomical connections are incompletely understood. Such information is necessary to relate to human neurological phenomena including phantom limb syndrome and recovery after nerve injury. Determining functional organization of intact cortex is a step toward modeling mechanisms of plasticity underlying these phenomena, since a requirement for understanding injury to the somatosensory system is the understanding of the basic intact network. As tactile object recognition depends on integration of information from different parts of the hand, it is logical to presume that neurons somewhere in the somatosensory system integrate information from locations across the hand or hands, and even beyond. This thesis proposes that much of this integration occurs at the level of primary somatosensory cortex and to a more limited extent, subcortically. An evaluation of the extent of this integration in primary somatosensory cortex, area 3b, is a critical step in determining how and where the somatosensory system mediates object perception and other abilities.

Owl monkeys were selected as an experimental model for several reasons. Primate studies offer the closest approximation to studies that cannot be performed in humans and are thus essential to apply results related to cortical function. For technical

reasons, a primate that has area 3b on the cortical surface and is hardy for surgery and experiments is preferred. Finally, the somatosensory cortex of owl monkeys has been well-studied (e.g., Merzenich et al., 1983; Garraghty et al., 1989; Wang et al., 1995; Nicolelis et al., 1998; Xerri et al., 1999) and is thus a good model to use to expand our knowledge of somatosensory cortical processing.

Anatomical Organization of the Primate Somatosensory System

Even a brief review of the primate somatosensory system reveals the complexity of its organization. Sensations of pain, temperature, and proprioception are not isolated from tactile sensation, but this review focuses on the sense of touch; specifically on the organization of the afferent path of tactile information from the glaborous hand to the cortex, with emphasis on our area of interest, area 3b (Figure 1-1). Feedback influences on the primary somatosensory cortex are noted as well. Tactile sensation in primates is mediated by rapidly adapting Meissner corpuscles and slowly adapting Merkel cells, as well as very rapidly adapting Pacinian corpuscles. Slowly adapting Ruffini corpuscles are sensitive to skin stretch and have been identified in humans but not in monkeys. Pacinian corpuscles respond best to high frequency vibrations; therefore, the low frequency skin indentations presented in these studies are likely to activate mainly Meissner corpuscles and Merkel cells (Mountcastle, 2005, p. 113-128). The spinothalamic tract is a secondary pathway for tactile information and there is some convergence of the areas activated by pain and temperature with those responding to touch (Mountcastle, 2005, p. 397). For example, nociceptive C-fibers are believed to be tonically active and blocking their activity has been shown to affect tactile receptive fields (for review, Calford, 2002). The

dorsal column pathway is the major pathway for tactile information from the hand to reach the brain, and thus descriptions are concentrated on this pathway.

Tactile inputs from the hand project to the brainstem cuneate nucleus and then to the ventroposterior lateral nucleus of the thalamus. Anterior parietal cortex can be subdivided into areas 3a, 3b, 1, and 2; and area 3b is the homologue of primary somatosensory cortex (S1) in other mammals (Kaas, 1983). This designation is made because activating tactile inputs from the ventroposterior lateral nucleus project to area 3b, while modulating inputs project to areas 1 and 2 (Kaas, 1983, 2000). Area 3b neurons then project to areas 1 and 2, as well as to 3a (which receives activating proprioceptive input). The neurons in the anterior parietal cortex project to the secondary somatosensory area, S2, and the parietal ventral area, PV. (Kaas, 2000) From these neurons in the lateral Sylvian cortex, tactile information travels to the insular and retroinsular cortical areas (Sewards and Sewards, 2002; Mountcastle, 2005, p. 383-397). Reciprocal connections and callosal connections provide feedback within the system. There are sparse callosal connections between the hand representations in areas 3a and 3b, moderately sparse connections in area 1, with denser connections in area 2 (Killackey et al., 1983). Higher-order somatosensory areas have callosal connections of the hand representation (e.g., Manzoni et al., 1984). Some callosal connections are homotopic, others are not (e.g., Pandya and Vignolo, 1969; Jones et al., 1979). While the somatosensory system is connected to additional areas not discussed, this brief review of somatosensory pathways provides the basic information relevant to the studies in primary somatosensory cortex of anesthetized monkeys described in this thesis.

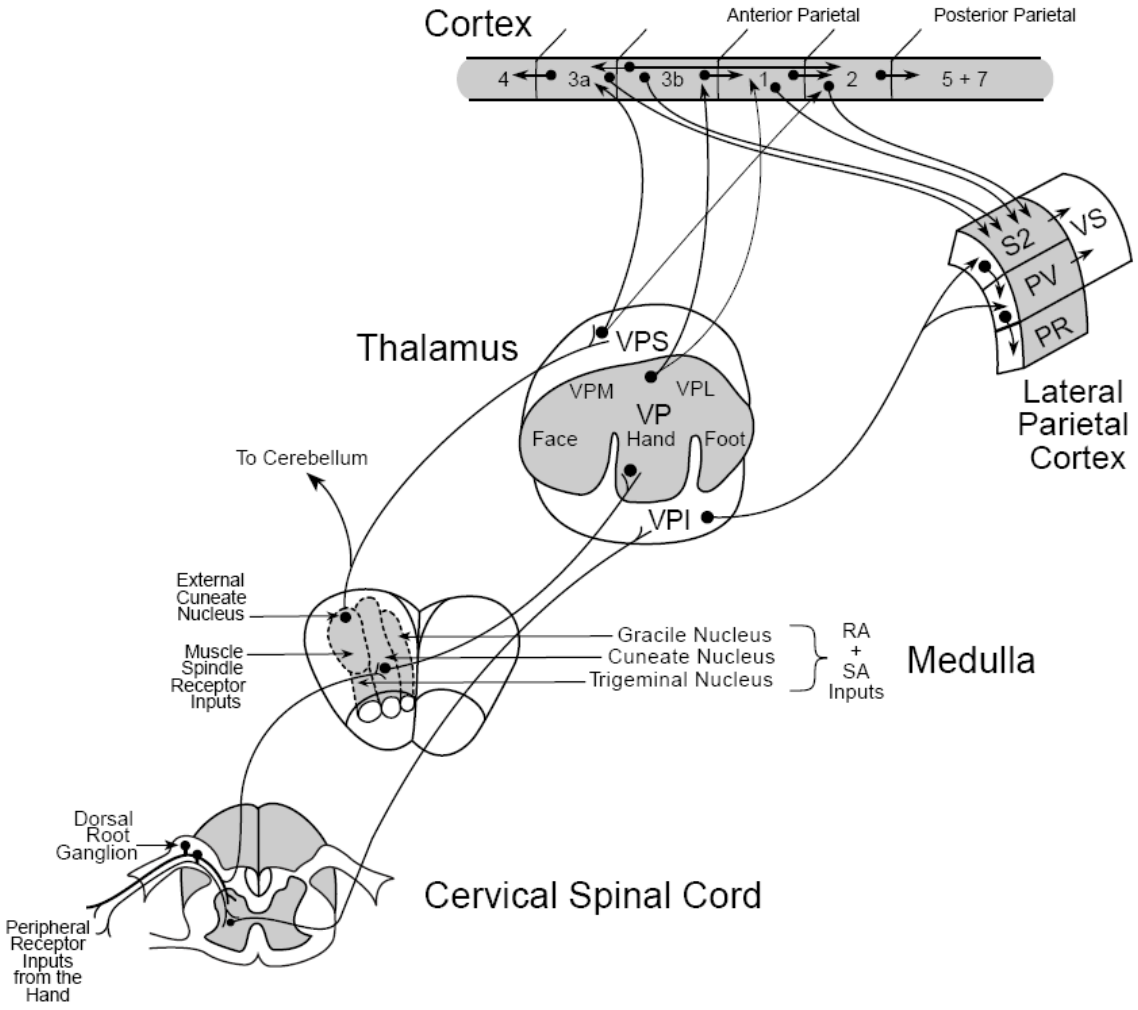

Figure 1-1. Highlights of the ascending somatosensory pathway for inputs from the hand in primates. Activating inputs originating from rapidly adapting (RA) and slowly adapting (SA) peripheral mechanoreceptors in the hand are depicted traveling from the cervical spinal cord, to the brainstem cuneate nucleus, to the ventroposterior lateral nucleus (VPL) of the thalamus, and to area 3b of anterior parietal cortex. Modulating inputs from the thalamus also project to other parts of anterior parietal cortex. Muscle spindle inputs primarily project from ventroposterior superior nucleus (VPS) of the thalamus to 3a, as well as to area 2. Spinothalamic projections to the ventroposterior inferior nucleus (VPI) modulate S2 and PV, as well as anterior parietal cortex (projection not shown). Anterior parietal cortical areas are interconnected, and project to secondary somatosensory area, S2, and parietal ventral area, PV. The ventral somatosensory area (VS) and rostrolateral parietal area (PR) have connections with S2 and PV. Anterior parietal cortex also projects to primary motor cortex (area 4) via 3a and to posterior parietal cortex (areas 5 and 7). Figure adapted from Jain et al., 1998 and Kaas et al., 2002.

Receptive Field Properties

One of the metrics used in sensory research is the receptive field, which is the area of the receptor sheet where stimulation influences cell firing (e.g., Freeman et al., 2001). Visual research uses the term classical receptive field (Allman et al., 1985), and stimuli outside the field can affect neuron responses to stimuli within the classical receptive field. In the somatosensory system, mechanical forces that spread in the skin complicate identification of the receptors that make up the receptive field; therefore, the minimal receptive field (mRF) is referred to as the regions of the body that evoke a reliable excitatory neural response to near-threshold stimulation (e.g., Merzenich et al., 1983; Xerri et al., 1999; Wu and Kaas, 2003). Like the classical receptive field, the mRF, or near-threshold excitatory field can be surrounded by regions that, when stimulated, modulate responses from within the mRF (e.g., DiCarlo et al., 1998).

Receptive fields increase in complexity as signals propagate from the periphery to the central cortical processing areas. Both rapidly adapting and slowly adapting afferents have very small receptive fields, but they have some differences in sensitivity to indentation depth and stimulus frequency (Mountcastle, 2005, p. 319). At this first level of somatosensory processing, afferents demonstrate response complexity. Due to the biomechanical properties of the skin (rather than neural properties), presenting a second stimulus at the edge of the receptive field of an afferent can suppress the response to a stimulus presented in the center of the field (Phillips and Johnson, 1981). Many complex stimulus features can be represented by artificially reconstructing population responses from the afferents (Goodwin and Wheat, 1999, 2002), and naturally, population responses are reconstructed by higher-order neurons.

The properties of receptive fields are more complex in primary somatosensory cortex than in the peripheral afferents. Neurons in the hand representation of area 3b of monkeys have receptive fields with dynamic excitatory and inhibitory components (e.g., DiCarlo et al., 1998; Sripati et al., 2006). Such components likely underlie many of the response properties of the neurons including motion detection (e.g., Whitsel et al., 1972; Gardner et al.,1992) and motion direction perception (e.g., Hyvärinen and Poranen, 1978; Warren et al., 1986). No bilateral receptive fields have been described in the hand representation of area 3b neurons in monkeys; however, bilateral receptive fields exist in areas 1 and 2 (Iwamura, 2000, review). There are no known ipsilateral projections to mediate the bilateral receptive fields in the cortex; thus, callosal pathways are acknowledged to be responsible for their existence (Mountcastle, 2005, p. 393).

The complexity of receptive fields increases in cortical areas beyond primary somatosensory cortex, as receptive fields become larger and bilateral fields become more common (Robinson and Burton, 1980a,b; Mountcastle 2005, p. 391). Selectivity for stimulus properties such as orientation is found in greater proportions of neurons (e.g., Hsiao et al., 2002) and the high-level process of attention more strongly affects neurons in S2 than in S1 (Hsiao et al., 1993). Receptive fields are large in insular neurons and bilateral fields are also common (Robinson and Burton, 1980a,b).

Response Modulation in Primary Somatosensory Cortex

This dissertation focuses on the properties of neurons in primary somatosensory cortex, which have been described to be of intermediate complexity between primary afferents and higher-order cortical areas. Despite the relative simplicity of their receptive

fields, the spatiotemporal integration properties of neurons in area 3b were investigated in response to paired stimuli presented on one or both hands. In visual cortex, stimuli presented outside the classical receptive field modulate neuron responses, mostly via surround inhibition (e.g., Allman et al., 1985; Bretzner et al., 2000; Walker et al., 2000; Freeman et al., 2001; Brown et al., 2003). Reports on "surround modulation" due to neural mechanisms in somatosensory cortex are less prevalent. In this context, surround modulation is considered the change in neuronal response that occurs when the mRF and a site outside the mRF are stimulated compared to the response when the mRF is stimulated alone. The functional significance of surround modulation in somatosensory cortex is not known, but may be related to directing attention to salient stimuli (Burton and Sinclair, 2000; Hupe et al., 2001) or allowing stimuli to be perceived as related parts within a context (e.g., Allman et al., 1985; Albright and Stoner, 2002). This aspect of somatosensory processing has not been well studied.

Modulation of responses to stimulation inside the mRF due to stimulation outside the mRF could arise from many sources including: feedforward thalamocortical connections (e.g., Friedman and Jones, 1980; Garraghty et al., 1989); intrinsic cortical connections (Manger et al., 1997; Fang et al., 2002); and extrinsic cortical connections, including intrahemispheric feedback and callosal connections (e.g., Ergenzinger et al., 1998; Calford, 2002). Thalamocortical projections, believed to be the main contributors to the excitatory mRF, synapse onto layer 4 cells, as well as onto layer 3 and layer 5 pyramidal cells with dendrites in layer 4 (e.g., White, 1989, p. 53, 80-81). In addition to these excitatory effects, GABAergic mechanisms shape neural responses and receptive fields (Hicks and Dykes, 1983; Alloway and Burton, 1986; Alloway et al., 1989;

Chowdhury and Rasmusson, 2003). Contributions to the surround are likely to come from horizontal connections and feedback connections (e.g., Thomson and Deuchars, 1994; Salin and Bullier, 1995; Lamme and Roelfsema, 2000). Distal structures such as the hands have few to no callosal connections in area 3b (Killackey et al., 1983); however, human studies indicate that ipsilateral cortex receives activation from hand stimulation (e.g., Schnitzler et al., 1995; Kurth et al., 1998; Hansson and Brismar, 1999; Tanosaki et al., 2002), likely due to feedback from areas outside 3b. Callosal projections come from pyramidal cells and are assumed to be excitatory. Few studies implicate non-pyramidal cells in callosal projections (Conti and Manzoni, 1994). Thus, callosal projections can be regarded as extrinsic connections that either act directly as excitatory or recruit GABAergic neurons and act as inhibitory inputs (Calford, 2002).

Electrophysiological Measures of Neuronal Activity

Receptive field properties are determined by using extracellular electrodes to record the activity of single neurons and multi-neuron clusters. Electrophysiological recordings provide excellent spatial and temporal resolution of neural activity; and current technology allow us to record from 100 electrodes simultaneously, covering a large spatial extent of the hand presentation in primary somatosensory cortex. Our experiments describe effects on single neurons (single-units) or small groups of neurons (multi-unit clusters) in the 3b hand representation of stimulating two sites on the body with mechanical probes providing simultaneous or asynchronous stimulation.

Based on the spiking activity collected from each monkey, analyses focused on three basic measures: firing rate, response latency, and spike timing correlations between

neuron pairs. Firing rate and latency describe the response properties of individual neurons, and these basic measures were used to examine how neuron responses were modulated by stimulation that varied in spatiotemporal features. Spike timing correlations measure the relationship of the timings of spikes in two different neurons. Such correlations are thought to increase the probability that postsynaptic neurons will be driven to fire, and correlations can indicate the relationship between neurons. The effects of varying the spatiotemporal stimulus features on spike timing correlations were quantified. These physiological measures provide functional relationships which can imply anatomical relationships; however, they do not provide specific anatomical relationships between neurons within the hand representation of primary somatosensory cortex.

Broad Significance

The global aims of this dissertation were two-fold. First, we investigated the ways in which neurons in somatosensory cortex respond to a stimulus inside the receptive field, in the context of a distant stimulus which could be presented to the contralateral hand or the ipsilateral hand. These studies quantified intrahemispheric and interhemispheric spatiotemporal processing in intact monkeys. Second, the role of interhemispheric processing on the responses to contralateral hand stimulation was further investigated by blocking signaling from an ipsilateral digit. The normal functions of neurons in the somatosensory system are relevant not only for understanding the sense of touch, but also to understanding recoveries from damage to the somatosensory system (i.e., understanding the extent to which processing is altered by lesions and to what extent

normal function returns to the area with or without therapy). These studies will lead to improved models of functional circuitry of the somatosensory cortex in primates, which will aid in understanding changes that produce neurological phenomena following denervation-induced cortical reorganization in humans. Future experiments will test this further, but the work in this dissertation is part of the foundation necessary to interpret such future studies.

Objective

A central problem in systems neuroscience is determining how sensory information is represented in the brain. The objective of this dissertation is to investigate this question specifically for the hand representation in primary somatosensory cortex in primates. Humans and nonhuman primates use the hands extensively to manipulate objects and make perceptual discriminations that can guide behavior. The idea directing the dissertation research is that object discrimination requires integration of information from across the hand, and when used together, between the hands; and this integration is likely to involve primary somatosensory cortex (area 3b).

To investigate the spatiotemporal properties of how area 3b neurons integrate information from across the hand or hands, groups of neurons were recorded simultaneously using a multielectrode array implanted in the 3b hand representation of owl monkeys (*Aotus trivirgatus*) while presenting tactile stimuli to one or both hands. This technique allowed many stimulus conditions to be recorded for each neuron unit and provided multiple pair-wise comparisons to examine the spike timing correlations in a

relatively large region of cortex (4 mm x 4 mm). The design was to place one stimulus probe within the minimal receptive field (mRF) of reference neurons to drive neural activity, and place a second probe outside the mRF to modulate the activity. The goal of this research was to examine how area 3b neurons integrate information from outside the neuron's minimal receptive field.

Specific Aims

This research investigated the effects on primate area 3b neurons of applying two tactile stimuli that varied in spatial and temporal proximity. We expected that responses of area 3b neurons are modulated when two stimuli are nearer in spatial and temporal proximity, but that modulations occur even when stimuli are separated by substantial distances. This premise was based on evidence that 1) stimuli close in proximity (on adjacent digits) applied closely in time modulate the neuron response to the stimulus in the receptive field and 2) stimulation or deafferentation of the ipsilateral hand can affect responses to stimulation on the contralateral hand in area 3b neurons. Our broad hypothesis was that neuronal processing of a stimulus presented to a single site on the contralateral hand is affected by the state of the rest of the hand, and even the state of the ipsilateral hand. The first test of this hypothesis involved stimulating two skin locations in intact monkeys to determine normal response modulations in area 3b neurons. The second test of this hypothesis focused on the possible effects that the state of the ipsilateral hand would have on processing a contralateral stimulus after blocking

spontaneous activity from an ipsilateral digit. To address this hypothesis, the following specific aims were proposed.

Aim 1. Characterize Response Modulation to Paired Stimulation Inside the Minimal Receptive Field (mRF) and Outside the mRF

We predicted that when the 'outside' probe is near the probe inside the mRF spatially and temporally, neuronal responses in area 3b are modulated more than when stimuli are widely separated, but that modulations occur even when the two probes are separated by substantial distances (i.e., nonadjacent digit sites within the hand and paired sites on the two hands). We expected to find classical suppressive interactions that resembled surround inhibition, as well as response facilitations, depending on stimulus parameters, when stimuli were delivered to two locations. This aim is divided into two sub-aims.

*Aim1a. Characterize Response Modulation When the **Spatial Proximity** Between Stimuli is Varied*

We hypothesized that stimulation outside the mRF modulates neuron responses to stimulation in the mRF, and the greatest modulation occurs when "surround" sites were close to the mRF. Two sites were stimulated simultaneously and modulations that occurred when paired sites differed in spatial proximity were characterized. If primate hands are similar to rat whisker fields, we would expect to find facilitation when adjacent sites are simultaneously stimulated (Ghazanfar and Nicolelis, 1997; Shimegi et al., 1999, 2000). Several studies report mostly suppression (e.g., Simons, 1985; Simons and Carvell, 1989; Moore and Nelson, 1998; Moore et al., 1999; Mirabella et al., 2001;

Derdikman et al., 2003; Melzer et al., 2006); but facilitation may predominate in layer 2/3 and occur widely in layer 5, similar to the findings of Shimegi et al. (1999, 2000) and Ghazanfar and Nicolelis (1997). The approach was to stimulate adjacent and nonadjacent digits, as stimulus interactions between nonadjacent digits should represent effects from 'beyond the classical receptive field' (e.g., Chowdhury and Rasmusson, 2003; Greek et al., 2003). Sites on both hands were also stimulated, as interactions will depend on direct or indirect callosal connections.

*Aim1b. Characterize Response Modulation When the **Temporal Proximity** Between Stimuli is Varied*

We hypothesized that stimuli presented close in time interact more strongly than stimuli separated in time. When stimuli are offset by more than a few milliseconds, the effects in the somatosensory system are reported to be mostly suppressive (e.g., Jänig et al., 1977, 1979; Laskin and Spencer, 1979; Gardner and Costanzo, 1980b; Brumberg et al., 1996; Moore et al., 1999; Chowdhury and Rasmusson, 2003; Greek et al., 2003). These effects occur for condition-test paradigms, in which stimulating a surround site prior to stimulating inside the receptive field results in suppression compared to stimulating inside the receptive field alone. While the effects are largely unexplored for the hand area in primate 3b, we also expected to find suppressive interactions when stimuli are offset in time. Typical spatiotemporal receptive fields for 3b neurons in the monkey hand region include a small excitatory region (that could include inhibitory surround), followed by a prolonged inhibition (e.g., Sripati et al., 2006). Sources of the prolonged inhibition and its spatial spread are not fully known. Depending on the spread

of this long inhibition, we expected that stimulating a surround site would suppress responses to stimuli applied inside the mRF later in time.

Paired sites (as in Aim 1a) were tested with stimuli separated by a range of stimulus onset asynchronies to obtain spatiotemporal profiles of stimulus interactions. We expected that the distance between stimulus sites would likely affect maximum interaction time; thus, a spatiotemporal interaction effect would exist. Condition-test intervals resulting in maximum suppression in S1 cortex are 10-30 ms for adjacent whisker stimulation in rats (Moore et al., 1999, review) and 20-40 ms for adjacent digit stimulation in raccoons (Greek et al., 2003). Within receptive fields on the monkey arm, Gardner and Costanzo (1980) found maximum suppression intervals of 10-20 ms. Thus, we expected to find maximum suppression in owl monkey 3b for adjacent digit stimulation at similar condition-test intervals (10-40 ms). Stimulation on two distant locations, such as the two hands, would require longer intervals for maximum effects.

Aim 2. Block Input from One Hand and Characterize the Change in Responses to Stimulation on the Opposite Hand

We hypothesized that neurons in area 3b are influenced by the spontaneous activity of neurons with receptive fields outside the recorded neuron's mRF, including from the opposite hemisphere. Local anesthetic injections were used to reduce some of the spontaneous activity from outside the mRF to deduce the effects of normal levels of spontaneous activity. Digit denervation in bats and monkeys reveals expanded receptive fields on the opposite hand, suggesting that tonic interhemispheric inhibition has been removed (Calford and Tweedale, 1991a,b). Neuron activity was measured before and after a local anesthetic block of input from the ipsilateral hand to determine if neurons

become more or less responsive to stimulation on the contralateral hand and determine the spatial extent of the effects. Human evoked potential recordings indicate that cortical activity increases, along with tactile spatial acuity (Werhahn et al., 2002). We predicted that some of the recorded neurons would show response facilitations and neurons that did not respond to stimulation prior to the ipsilateral block would respond to the stimulation after the block. We expected to demonstrate and quantify interactions between the hand representations in area 3b of the two hemispheres, including the topographic specificity of the effects.

Aim 3. Describe the Synchrony of Firing Between Neurons When One Stimulus Is Presented Repeatedly and When Two Stimuli Are Presented Either Simultaneously or at Different Stimulus Onset Delays

Synchronous or asynchronous firing may be an indication of how groups of neurons respond to tactile stimulation that cannot be directly assessed by single electrode recordings. Modulation of responses may be in the form of synchrony or asynchrony of firing that does not change neuronal response properties of firing rate and latency (e.g., Vaadia et al., 1995; DeCharms and Merzenich, 1996). In the visual system, perceptual grouping, attention, and stimulus discrimination have been shown to generate synchrony of firing when integration of multiple features from a single object is necessary (for review, Singer and Gray, 1995). Interpretations of synchrony have been largely limited to the high-level integration processes of perception and attention in both the visual (for review, Bichot and Desimone, 2006) and somatosensory systems (for review, Niebur et al., 2002). However, there is evidence that modulations in the levels of correlated firing can be related to stimulus features, even in anesthetized animals, in the primary visual

cortex (e.g., Samonds et al., 2003, 2004, 2006; Zhou et al., 2008) and primary somatosensory cortex (e.g., Roy and Alloway 1999; Zhang and Alloway 2004, 2006). We hypothesized that spike timing correlations, a form of synchrony, occur widely between neurons in area 3b to facilitate the processing of information from across the hand. We also predicted that the spatiotemporal characteristics of paired stimuli alter the degree of correlated firing between neurons in area 3b.

This work will lay a foundation for understanding stimulus interactions in the monkey 3b hand representation by determining spatiotemporal interactions of systematically-delivered tactile stimuli (Aims 1 and 3) and exploring interhemispheric interactions that may normally produce subthreshold effects for spike activity, but can be revealed after temporary digit denervation (Aim 2). These widespread effects are likely to be important for normal somatic sensation as well as for substrates of synaptic plasticity in recovery from injury. The results of this thesis will guide future investigations into the amount and types of integration that occur during somatosensory processing.

Overview of the Dissertation

Although the aims of this work are divided into three parts, the studies can be thought of as characterizing two main issues: 1) intrahemispheric and 2) inter-hemispheric processing. Aim 1 includes both issues, as the spatial and temporal stimulus effects was studied by providing tactile stimulation to the contralateral hand, as well as by providing paired stimulation on the ipsilateral and contralateral hands. Aim 2 focused on interhemispheric processing by determining the effects of using local anesthetic

injections to block signals from the peripheral nerves in an ipsilateral digit on the responses to single-site stimulation on the contralateral hand. Aim 3 focused on intra-hemispheric processing by analyzing correlated spike timings in pairs of neurons within the contralateral hemisphere during stimulation on the contralateral hand. The organization of the dissertation chapters does not directly correspond to the order of the specific aims, but corresponds to the two main ideas of intrahemispheric and inter-hemispheric processing.

Chapter 2 provides our initial evidence for widespread spatial processing within primary somatosensory cortex based on pair-wise correlations in spike timing (Aim 3). Chapter 3 describes response properties of individual neurons and multi-neuron clusters when tactile stimuli are presented with varying spatial and temporal relationships (Aim 1a and b). Spatial and temporal properties of spike timing correlations are discussed in Chapter 4, to complete Aim 3. Interhemispheric effects are described in Chapter 5 and 6. The spatiotemporal effects on responses that occur when the ipsilateral and contralateral hand are stimulated simultaneously or asynchronously are discussed in Chapter 5, which completes the conditions from Aim 1. Chapter 6 is devoted to the results from Aim 2, in which interhemispheric processing is deduced based on blocking the nerves of one ipsilateral digit and analyzing the response properties to single-site stimulation on the contralateral hand before and after the local anesthetic. Chapter 7 summarizes the results from the previous five chapters and includes a discussion of the implications of this work.

References

Albright TD, Stoner GR. 2002. Contextual influences on visual processing. *Annu Rev Neurosci* 25: 339-379.

Allman J, Miezin F, McGuinness E. 1985. Stimulus specific responses from beyond the classical receptive field: Neurophysiological mechanisms for local-global comparisons in visual neurons. *Annu Rev Neurosci* 8: 407-430.

Alloway KD, Burton H. 1986. Bicuculline-induced alterations in neuronal response to controlled tactile stimuli in the second somatosensory cortex of the cat: a microiontophoretic study. *Somato Mot Res* 3: 197-211.

Alloway KD, Rosenthal P, Burton H. 1989. Quantitative measurements of receptive field changes during antagonism of GABAergic transmission in primary somatosensory cortex of cats. *Exp Brain Res* 78: 514-532.

Bichot NP, Desimone R. 2006. Finding a face in the crowd: parallel and serial neural mechanisms of visual selection. Chapter 9 In *Progress in Brain Research*, ed. S. Martinez-Conde, SL Macknik, LM Martinez, J-M Alonso, and PU Tse, 155: 147-156. Amsterdam: Elsevier Science B.V.

Blake DT, Strata F, Kempter R, Merzenich MM. 2005. Experience-dependent plasticity in S1 caused by noncoincident inputs. *J Neurophysiol* 94: 2239-2250.

Bretzner F, Aïtoubah J, Shumikhina S, Tan Y-F, Molotchnikoff S. 2000. Stimuli outside the classical receptive field modulate the synchronization of action potentials between cells in visual cortex of cats. *Neuroreport* 11: 1313-1317.

Brown HA, Allison JD, Samonds JM, Bonds AB. 2003. Nonlocal origin of response suppression from stimulation outside the classic receptive field in area 17 of the cat. *Vis Neurosci* 20: 85-96.

Brumberg JC, Pinto DJ, Simons DJ. 1996. Spatial gradients and inhibitory summation in the rat whisker barrel system. *J Neurophysiol* 76: 130-140.

Buonomano DV, Merzenich MM. 1998. Cortical plasticity: from synapses to maps. *Annu Rev Neurosci* 21: 149-186.

Burton H, Sinclair RJ. 2000. Tactile-spatial and cross-modal attention effects in the primary somatosensory cortical areas 3b and 1-2 of rhesus monkeys. Somato Mot Res 17: 213-228.

Calford MB. 2002. Dynamic representational plasticity in sensory cortex. *Neuroscience* 111: 709-738.

Calford MB, Tweedale R. 1991a. Acute changes in cutaneous receptive fields in primary somatosensory cortex after digit denervation in adult flying fox. *J Neurophysiol* 65: 178-187.

Calford MB, Tweedale R. 1991b. Immediate expansion of receptive fields of neurons in area 3b of macaque monkeys after digit denervation. *Somato Mot Res* 8: 249-260.

Chowdhury SA, Rasmusson DD. 2003. Corticocortical inhibition of peripheral inputs within primary somatosensory cortex: the role of GABAA and GABAB receptors. *J Neurophysiol* 90: 851-856.

Conti F, Manzoni T. 1994. The neurotransmitters and postsynaptic action of callosally projecting neurons. *Behav Brain Res* 64: 37-53.

DeCharms RC, Merzenich MM. 1996. Primary cortical representation of sounds by the coordination of action-potential timing. *Nature* 381: 610-613.

Derdikman D, Hildesheim R, Ahissar E, Arieli A, Grinvald A. 2003. Imaging spatiotemporal dynamics of surround inhibition in the barrels somatosensory cortex. *J Neurosci* 23: 3100–3105.

DiCarlo JJ, Johnson KO, Hsiao SS. 1998. Structure of receptive fields in area 3b of primary somatosensory cortex in the alert monkey. *J Neurosci* 18: 2626-2645.

Ergenzinger ER, Glasier MM, Hahm JO, Pons TP. 1998. Cortically induced thalamic plasticity in the primate somatosensory system. *Nat Neurosci* 1: 226-229.

Fang P-C, Jain N, Kaas JH. 2002. Few intrinsic connections cross the hand-face border of area 3b of new world monkeys. *J Comp Neurol* 454: 310-319.

Freeman RD, Ohzawa I, Walker G. 2001. Beyond the classical receptive field in the visual cortex. Chapter 11 In *Progress in Brain Research*, ed. C Casanova and M Ptito, 134: 157-170. Amsterdam: Elsevier Science B.V.

Friedman DP, Jones EG. 1980. Focal projection of electophysiologically defined groupings of thalamic cells on the monkey somatic sensory cortex. *Brain Res* 191: 249-252.

Gandevia SC, Phagan CML. 1999. Perceptual distortions of the human body image produced by local anaesthesia, pain and cutaneous stimulation. *J Physiol* 514: 609-616.

Gardner EP, Palmer CI, Hämäläinen HA, Warren S. 1992. Simulation of motion on the skin. V. Effect of stimulus temporal frequency on the representation of moving bar patterns in primary somatosensory cortex of monkeys. *J Neurophysiol* 67: 37-63.

Gardner EP, Costanzo RM. 1980. Temporal integration of multiple-point stimuli in primary somatosensory cortical receptive fields of alert monkeys. *J Neurophysiol* 43: 444-468.

Garraghty PE, Pons TP, Sur M, Kaas JH. 1989. The arbors of axons terminating in middle cortical layers of somatosensory area 3b in owl monkeys. *Somato Mot Res* 6: 401-411.

Ghazanfar AA, Nicolelis MAL. 1997. Nonlinear processing of tactile information in the thalamocortical loop. *J Neurophysiol* 78: 506-510.

Goodwin AW, Wheat HE. 1999. Effects of nonuniform fiber sensitivity, innervation geometry, and noise on informationi relayed by a population of slowly adapting type I primary afferents from the fingerpad. *J Neurosci* 19: 8057-8070.

Goodwin AW, Wheat HE. 2002. How is tactile information affected by parameters of the population such as non-uniform fiber sensitivity, innervation geometry, and response variability? *Behav Brain Res* 135: 5-10.

Greek KA, Chowdhury SA, Rasmusson DD. 2003. Interactions between inputs from adjacent digits in somatosensory thalamus and cortex of the raccoon. *Exp Brain Res* 151: 364-371.

Hansson T, Brismar T. 1999. Tactile stimulation of the hand causes bilateral cortical activation: a functional magnetic resonance study in humans. *Neurosci Lett* 271: 29-32.

Hicks TP, Dykes RW. 1983. Receptive field size for certain neurons in primary somatosensory cortex is determined by GABA-mediated intracortical inhibition. *Brain Res* 274: 160-164.

Hoechstetter K, Rupp A, Stančák A, Meinck H-M, Stippich C, Berg P, Scherg M. 2001. Interaction of tactile input in the human primary and secondary somatosensory cortex—A magnetoencephalographic study. *Neuroimage* 14: 759-767.

Hsiao SS, Lane J, Fitzgerald P. 2002. Representation of orientation in the somatosensory system. *Behav Brain Res* 135: 93-103.

Hsiao SS, O'Shaughnessy DM, Johnson KO. 1993. Effects of selective attention on spatial form processing in monkey primary and secondary somatosensory cortex. *J Neurophysiol* 70: 444-447.

Hupe JM, James AC, Girard P, Lomber SG, Payne BR, Bullier J. 2001. Feedback connections act on the early part of the responses in monkey visual cortex. *J Neurophysiol* 85: 134-145.

Hyvärinen J, Poranen A. 1978. Movement-sensitive and direction and orientation-selective cutaneous receptive fields in the hand area of the post-central gyrus in monkeys. *J Physiol London* 283: 523-537.

Iwamura Y. 2000. Bilateral receptive field neurons and callosal connections in the somatosensory cortex. *Phil Trans R Soc Lond B* 355: 267-273.

Jain N, Florence SL, Kaas JH. 1998. Reorganization of somatosensory cortex after nerve and spinal cord injury. *News Physiol Sci* 13: 143-149.

Jänig W, Schoultz T, Spencer WA. 1977. Temporal and spatial parameters of excitation and afferent inhibition in cuneothalamic relay neurons. *J Neurophysiol* 40: 822-835.

Jänig W, Spencer WA, Younkin SG. 1979. Spatial and temporal features of afferent inhibition of thalamocortical relay cells. *J Neurophysiol* 42: 1450-1460.

Jones EG, Coulter JD, Wise SP. 1979. Commissural columns in the sensory-motor cortex of monkeys. *J Comp Neurol* 188: 113-136.

Kaas JH. 1983. What, if anything, is SI? Organization of first somatosensory area of cortex. *Physiol Rev* 63: 206-231.

Kaas JH. 2000. The reorganization of somatosensory and motor cortex after peripheral nerve or spinal cord injury in primates. *Prog Brain Res* 128: 173-179.

Kaas JH, Jain N, Qi H-X. 2002. The organization of the somatosensory system in primates. Chapter 1 In *The Somatosensory System: Deciphering the brain's own body image*, ed. RJ Nelson, 1-26. Boca Raton, FL: CRC Press LLC.

Killackey HP, Gould HJ, III, Cusick CG, Pons TP, Kaas JH. 1983. The relation of corpus callosum connections to architectonic fields and body surface maps in sensorimotor cortex of new and old world monkeys. *J Comp Neurol* 219: 328-419.

Kitada R, Kochiyama T, Hashimoto T, Naito E, Matsumura M. 2003. Moving tactile stimuli of fingers are integrated in the intraparietal and inferior parietal cortices. *Neuroreport* 14: 719-724.

Kurth R, Villringer K, Mackert B-M, Schwiemann J, Braun J, Curio G, Villringer A, Wolf K-J. 1998. fMRI assessment of somatotopy in human Brodmann area 3b by electrical finger stimulation. *Neuroreport* 9: 207-212.

Lamme VAF, Roelfsema PR. 2000. The distinct modes of vision offered by feedforward and recurrent processing. *Trends Neurosci* 23: 571-579.

Laskin SE, Spencer WA. 1979. Cutaneous masking. II. Geometry of excitatory and inhibitory receptive fields of single units in somatosensory cortex of the cat. *J Neurophysiol* 42: 1061-1082.

Manger PR, Woods TM, Muñoz A, Jones EG. 1997. Hand/face border as a limiting boundary in the body representation in monkey somatosensory cortex. *J Neurosci* 17: 6338-6351.

Manzoni T, Barbaresi P, Conti F. 1984. Callosal mechanism for the interhemispheric transfer of hand somatosensory information in the monkey. *Behav Brain Res* 11:155-170.

Melzer P, Champney GC, Maguire MJ, Ebner FF. 2006. Rate code and temporal code for frequency of whisker stimulation in rat primary and secondary somatic sensory cortex. *Exp Brain Res* 172: 370-386.

Merzenich MM, Kaas JH, Wall J, Nelson RJ, Sur M, Felleman D. 1983. Topographic reorganization of somatosensory cortical areas 3b and 1 in adult monkeys following restricted deafferentation. *Neuroscience* 8: 33-55.

Mirabella G, Battiston S, Diamond ME. 2001. Integration of multiple-whisker inputs in rat somatosensory cortex. *Cereb Cortex* 11: 164-170.

Moore CI, Nelson SB. 1998. Spatio-temporal subthreshold receptive fields in the vibrissa representation of rat primary somatosensory cortex. *J Neurophysiol* 80: 2882-2892.

Moore CI, Nelson SB, Sur M. 1999. Dynamics of neuronal processing in rat somatosensory cortex. *Trends Neurosci* 22: 513-520.

Mountcastle VB. 2005. *The Sensory Hand: Neural mechanisms of somatic sensation*. Cambridge, MA: Harvard University Press.

Niebur E, Hsiao SS, and Johnson KO. 2002. Synchrony: a neuronal mechanism for attentional selection? *Curr Opin Neurobiol* 12: 190-194.

Pandya D, Vignolo LA. 1969. Interhemispheric projections of the parietal lobe in the rhesus monkey. *Brain Res* 15: 49-65.

Phillips JR, Johnson KO. 1981. Tactile spatial resolution. III. A continuum mechanics model of skin predicting mechanoreceptor responses to bars, edges and gratings. *J Neurophysiol* 46: 1204-1225.

Robinson CJ, Burton H. 1980a. Organization of somatosensory receptive fields in cortical areas 7b, retroinsula, postauditory and granular insula of M. fascicularis. *J Comp Neurol* 192: 69-92.

Robinson CJ, Burton H. 1980b. Somatic submodality distribution within the second somatosensory (SII), 7b, retroinsular, postauditory, and granular insular cortical areas of M. fascicularis. *J Comp Neurol* 192: 93-108.

Roelfsema PR, Lamme VA, Spekreijse H. 2004. Synchrony and covariation of firing rates in the primary visual cortex during contour grouping. *Nat Neurosci* 7: 982-991.

Roy SA and Alloway KD. 1999. Synchronization of local neural networks in the somatosensory cortex: a comparison of stationary and moving stimuli. *J Neurophysiol* 81: 999–1013.

Salin P-A, Bullier J. 1995. Corticocortical connections in the visual system: structure and function. *Physiol Rev* 75: 107-154.

Samonds JM, Allison JD, Brown HA, Bonds AB. 2003. Cooperation between area 17 neuron pairs enhances fine discrimination of orientation. *J Neurosci* 23: 2416-2425.

Samonds JM, Allison JD, Brown HA, Bonds AB. 2004. Cooperative synchronized assemblies enhance orientation discrimination. *Proc Natl Acad Sci USA* 101: 6722-6727.

Samonds JM, Zhou Z, Bernard MR, and Bonds AB. 2006. Synchronous activity in cat visual cortex encodes collinear and cocircular contours. *J Neurophysiol* 95: 2602-2616.

Schnitzler A, Salmelin R, Salenius S, Jousmäki V, Hari R. 1995. Tactile information from the human hand reaches the ipsilateral primary somatosensory cortex. *Neurosci Lett* 200: 25-28.

Sewards TV, Sewards M. 2002. Separate, parallel sensory and hedonic pathways in the mammalian somatosensory system.*Brain Res Bull* 58: 243-260.

Shimegi S, Akasaki T, Ichikawa T, Sato H. 2000. Physiological and anatomical organization of multiwhisker response interactions in the barrel cortex of rats. *J Neurosci* 20: 6241-6248.

Shimegi S, Ichikawa T, Akasaki T, Sato H. 1999. Temporal characteristics of response integration evoked by multiple whisker stimulations in the barrel cortex of rats. *J Neurosci* 19: 10164-10175.

Simons DJ. 1985. Temporal and spatial integration in the rat SI vibrissa cortex. *J Neurophysiol* 54: 615-633.

Simons DJ, Carvell GE. 1989. Thalamocortical response transformation in the rat vibrissa/barrel system. *J Neurophysiol* 61: 311-330.

Singer W and Gray CM. 1995. Visual feature integration and the temporal correlation hypothesis. *Annu Rev Neurosci* 18: 555-586.

Sripati AP, Yoshioka T, Denchev P, Hsiao SS, Johnson KO. 2006. Spatiotemporal receptive fields of peripheral afferents and cortical area 3b and 1 neurons in the primate somatosensory system. *J Neurosci* 26: 2101-2114.

Tanosaki M, Suzuki A, Takino R, Kimura T, Iguchi Y, Kurobe Y, Haruta Y, Hoshi Y, Hashimoto I. 2002. Neural mechanisms for generation of tactile interference effects on somatosensory evoked magnetic fields in humans. *Clin Neurophysiol* 113: 672-680.

Thomson AM, Deuchars J. 1994. Temporal and spatial properties of local circuits in neocortex. *Trends Neurosci* 17: 119-126.

Vaadia E, Haalman I, Abeles M, Bergman H, Prut Y, Slovin H, Aertsen A. 1995. Dynamics of neuronal interactions in monkey cortex in relation to behavioural events. *Nature* 373: 515-518.

Walker GA, Ohzawa I, Freeman RD. 2000. Suppression outside the classical cortical receptive field. *Vis Neurosci* 17: 1-11.

Wang X, Merzenich MM, Sameshima K, Jenkins WM. 1995. Remodelling of hand representation in adult cortex determined by timing of tactile stimulation. *Nature* 378: 71-75.

Warren S, Hämäläinen HA, Gardner EP. 1986. Objective classification of motion- and direction-sensitive neurons in primary somatosensory cortex of awake monkeys. *J Neurophysiol* 56: 598-622.

Werhahn KJ, Mortensen J, Van Boven RW, Zeuner KE, Cohen LG. 2002. Enhanced tactile spatial acuity and cortical processing during acute hand deafferentation. *Nat Neurosci* 5: 936-938.

White EL. 1989. *Cortical circuits: synaptic organization of the cerebral cortex structure, function, and theory*. Boston: Birkhäuser Boston, Inc.

Whitsel BL, Roppolo JR, Werner G. 1972. Cortical information processing of stimulus motion on primate skin. *J Neurophysiol* 35: 691-717.

Wu CW-H, Kaas JH. 2003. Somatosensory cortex of prosimian galagos: physiological recording, cytoarchitecture, and cortiocortical connections of anterior parietal cortex and cortex of the lateral sulcus. *J Comp Neurol* 457: 263-292.

Xerri C, Merzenich MM, Jenkins W, Santucci S. 1999. Representational plasticity in cortical area 3b paralleling tactual-motor skill acquisition in adult monkeys. *Cereb Cortex* 9: 264-276.

Zhang M, Alloway KD. 2004. Stimulus-induced intercolumnar synchronization of neuronal activity in rat barrel cortex: a laminar analysis. *J Neurophysiol* 92: 1464–1478.

Zhang M, Alloway KD. 2006. Intercolumnar synchronization of neuronal activity in rat barrel cortex during patterned airjet stimulation: A laminar analysis. *Exp Brain Res* 169: 311-325.

Zhou Z, Bernard MR, Bonds AB. 2008. Deconstruction of spatial integrity in visual stimulus detected by modulation of synchronized activity in cat visual cortex. *J Neurosci* 28: 3759-3768.

CHAPTER II

WIDESPREAD SPATIAL INTEGRATION IN PRIMARY SOMATOSENSORY CORTEX

This chapter reproduces the published work: Reed JL, Pouget P, Qi HX, Zhou Z, Bernard MR, Burish MJ, Haitas J, Bonds AB, Kaas JH. 2008. Widespread spatial integration in primary somatosensory cortex. Proc Natl Acad Sci USA. 105(29):10233-10237. The figure numbers have been changed to reflect the chapter number and the references have been reformatted. The article content is otherwise unaltered.

Abstract

Tactile discrimination depends on integration of information from the discrete receptive fields (RFs) of peripheral sensory afferents. Because this information is processed over a hierarchy of subcortical nuclei and cortical areas, the integration likely occurs at multiple levels. The current study presents results indicating that neurons across most of the extent of the hand representation in monkey primary somatosensory cortex (area 3b) interact, even when these neurons have separate RFs. We obtained simultaneous recordings by using a 100-electrode array implanted in the hand representation of primary somatosensory cortex of two anesthetized owl monkeys. During a series of 0.5-s skin indentations with single or dual probes, the distance between the electrodes from which neurons with synchronized spike times were recorded exceeded 2 mm. The results provide evidence that stimuli on different parts of the hand influence the degree of synchronous firing among a large population of neurons. Because spike synchrony potentiates the activation of commonly targeted neurons, synchronous neural activity in primary somatosensory cortex can contribute to discrimination of complex tactile stimuli.

Introduction

Humans and other primates use their hands to make tactile discriminations that guide choices and actions. The vast majority of those choices are based on stimuli that are presented to sites across the hand or hands. The transformation of these scattered information sources from receptors in distinct patches of skin into one percept presumes integration within the central nervous system. This integration could occur at several levels, but here we consider the primary somatosensory cortex (S1, i.e., area 3b). While area 3b contains a detailed somatotopic representation of the hand and neurons with small receptive fields (RFs), considerable integration across hand locations could already occur at this level via horizontal connections within area 3b.

One way of examining neuronal interactions is through spike timing synchrony. When the spikes of two neurons occur together more often than expected by chance, we can infer that those neurons are part of the same local network. The two neurons could receive a common input that drives the synchronous firing or the neurons could be synaptically connected. Our focus was on quantifying integration in the form of spike synchrony collected from neuronal activity in layers 2/3 of S1 in anesthetized owl monkeys (*Aotus trivirgatus)*. Analysis of firing rate data will be presented elsewhere.

Using a 100-electrode array (Cyberkinetics) covering 4 mm x 4 mm of cortical area (Figure 2-1A,B), our approach to examine sensory input integration in the area 3b hand representation focused on correlations in spike timing in pairs of neurons responding to the same or different stimulus probes (1 mm diameter contact surface). We

examined interactions across, rather than within, digit and palm pads to determine the extent of spatial integration in the area 3b hand representation.

Correlations between neurons have been proposed as a biophysical mechanism by which neurons at lower levels in processing hierarchies more effectively increase the responsiveness of neurons at higher levels (e.g., Azouz and Gray, 2000; Salinas and Sejnowski, 2001). In the primate somatosensory system, spike timing correlations have been studied primarily in secondary somatosensory cortex (S2) in awake macaque monkeys performing attention tasks (e.g., Niebur et al., 2002; Roy et al., 2007), as firing rate changes without spike synchrony changes have been associated with attention in S1 (Hsiao et al., 1993). Here we examined spike synchrony occurring in S1 of anesthetized owl monkeys. Rather than studying synchrony as neural correlate of attention, we studied the role of spike synchrony as a low-level correlate of stimulus processing and integration. We examined spike timing synchrony using the joint peristimulus time histogram analysis (JPSTH) based on methods from Aertsen and colleagues (1989). The analysis focuses on the subset of spike timing correlations that likely arise from functional connections rather than correlations due to stimulus-related changes in firing rate. In particular, our purpose is to infer the influences of common input and lateral connections in area 3b. The data presented include dual-site stimulation on nonadjacent hand locations, as stimulus interactions between nonadjacent digits would be strict indicators of effects from "beyond the classical receptive field" (Allman et al., 1985).

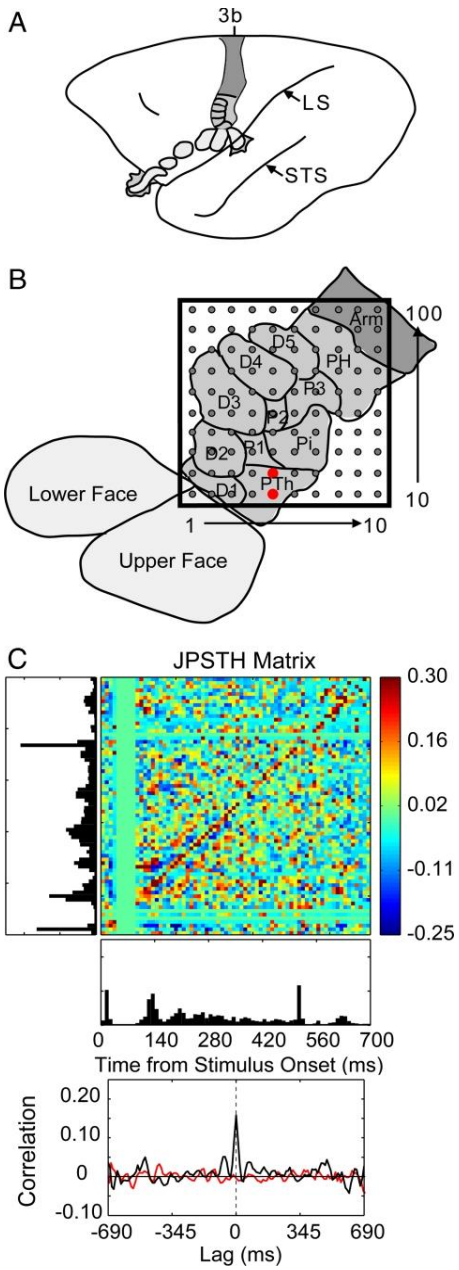

Figure 2-1. An example of correlated spike activity recorded from two adjacent electrodes in monkey 1. A. A lateral schematic view of an owl monkey brain with area 3b shaded. Subdivisions representing the face and hand are outlined, including those that cannot be seen from a surface view. LS = lateral sulcus, STS = superior temporal sulcus. B. The location of the array for case 1 within the area 3b hand representation. The approximate representations of the digits (D1-5) and the digital (P1-3), thenar (PTh), hypothenar (PH) and insular (Pi) pads of the hand are identified and outlined. The red dots mark the electrodes where the two neurons were recorded for the analysis shown in C. Both neurons had receptive fields on PTh. C. An example of the spike timing synchrony between units recorded from adjacent electrodes. Two probes simultaneously indented the skin on PTh and P1. Spike synchrony between the two neurons is shown in the normalized joint peristimulus time histogram, the JPSTH matrix. The two PSTHs of the responses to 100 repetitions of 0.5 s skin indentations are shown to the left and below the matrix, with the cross-correlation histogram derived from the JPSTH analysis directly below. The colored pixels in the JPSTH matrix represent the magnitude of the normalized correlation at different lag times over a poststimulus time of 700 ms. Strong spike synchrony occurred around 0 ms lag time throughout the period. The cross-correlation histogram (black) revealed a peak correlation of 0.16 that exceeded the mean correlation from the shuffled trials (red).

Neurons with overlapping RFs might be expected to show spike timing correlations based on common input and synaptic connections. Neurons with nonoverlapping RFs might be less likely to share information and fire synchronous spikes. Simultaneous recordings in S1 and S2 in cats revealed that neurons with synchronized spike times tended to have overlapping RFs, while the pairs that did not show synchrony tended to have nonoverlapping RFs (Roy et al., 2001). However, recent studies in visual cortex have led to the proposal that synchrony is related to stimulus properties (e.g., Samonds et al., 2003, 2006). Therefore, we tested whether we could drive synchronous firing between neurons with nonoverlapping RFs responding to stimulation on nonadjacent locations, as a signal of information integration from beyond the classical RF.

Results

Recordings were obtained using a 100-electrode array implanted in layers 2/3 of S1 of two anesthetized owl monkeys when one or two sites on the hand were stimulated. We selected 182 units from the two monkeys based on response criteria to the stimulation conditions (see Methods). From monkey 1, 28 units were classified as single units and 66 were multi-units. From monkey 2, 42 units were single units and 46 were multi-units. Across all stimulation conditions, this resulted in 1244 single unit pairs and 2476 multi-unit pairs for spike timing analysis. Paired nonadjacent locations selected for stimulation included digit 1 (D1) with digit 3 (D3), digit 2 (D2) with digit 4 (D4), and the thenar palm pad (PTh) with palm pad 2 (P2). We obtained responses from 50 single units and 63

multi-units, while analyzing 316 single unit pairs and 473 multi-unit pairs for synchrony. Only one unit was selected per electrode for analysis so that no spike timing correlations were performed between units from the same electrode. This restriction ensured that spike correlations were unlikely calculated between contaminated spikes (Gerstein, 2000). Our measure of synchrony was the peak magnitude of correlation between pairs of neurons based on JPSTH analysis with spike trains aligned on the start of a 0.5 s skin indentation. Pairs with significant correlations showed synchronous spiking during the sustained skin indentation, not only at the stimulus onset and removal (Figure 2-1C).

Multi-Electrode Recordings Indicate Widespread Stimulus Effects

Responses of area 3b neurons to 0.5 s skin indentations within the minimal RF (based on traditional mapping techniques) included a sharp onset response followed by some response depression, a variable level of maintained activity, and often an off response, depression, and a return to prestimulus levels of spontaneous activity. Neurons included in the analysis showed sustained activity in response to the 0.5 s stimulations on at least one of the hand locations in the recording conditions (see Methods). Although rapidly-adapting neuron types with low levels of spontaneous activity and transient responses to stimulation were recorded, these were not included in the analysis since the JPSTH calculation requires many spikes to obtain an estimate of spike timing synchrony (Aertsen et al., 1989; Gerstein et al., 1989; Gerstein, 2000). The recorded responses were similar to those reported previously from area 3b neurons in monkeys (e.g., Mountcastle et al., 1969; Sur et al., 1984).

We found correlated spike times occurred between pairs of neuron-units recorded from adjacent electrodes (0.4 mm center-to-center distance) as well as from distant electrodes (over 2 mm apart). An example of the extent of correlations when a single site on the palm (PTh) was stimulated repeatedly is shown in Figure 2-2. A representation of the peak firing rate for the subset of units analyzed for synchrony is shown in conjunction with the peak correlations between unit pairs.

Quantification of Spatial Integration across Area 3b Indicates Extensive Interactions

The proportions of unit pairs with synchronous spike timings decreased when two sites were stimulated compared to single-site stimulation. During single-site stimulation, 49.6% of the pairs recorded showed synchrony in their spike timings. During dual-site stimulation, 28.2% of the pairs were synchronized. For both single- and dual-site stimulation conditions, the proportions of correlated pairs decreased as the cortical distance separating the two units increased (Table 2-1). When one site was stimulated, 58.7% of the neuron pairs recorded less than 1.0 mm apart had significant spike timing correlations. This proportion dropped to 16.7% for pairs that were separated by 4.0 to 5.0 mm. When two nonadjacent sites were stimulated, 35.6% of the neuron pairs recorded less than 1.0 mm apart were synchronized. This proportion dropped to 7.5% for pairs separated by 3.0 to 4.0 mm. We speculate that information provided by synchronous activity became more specific when two sites were stimulated.

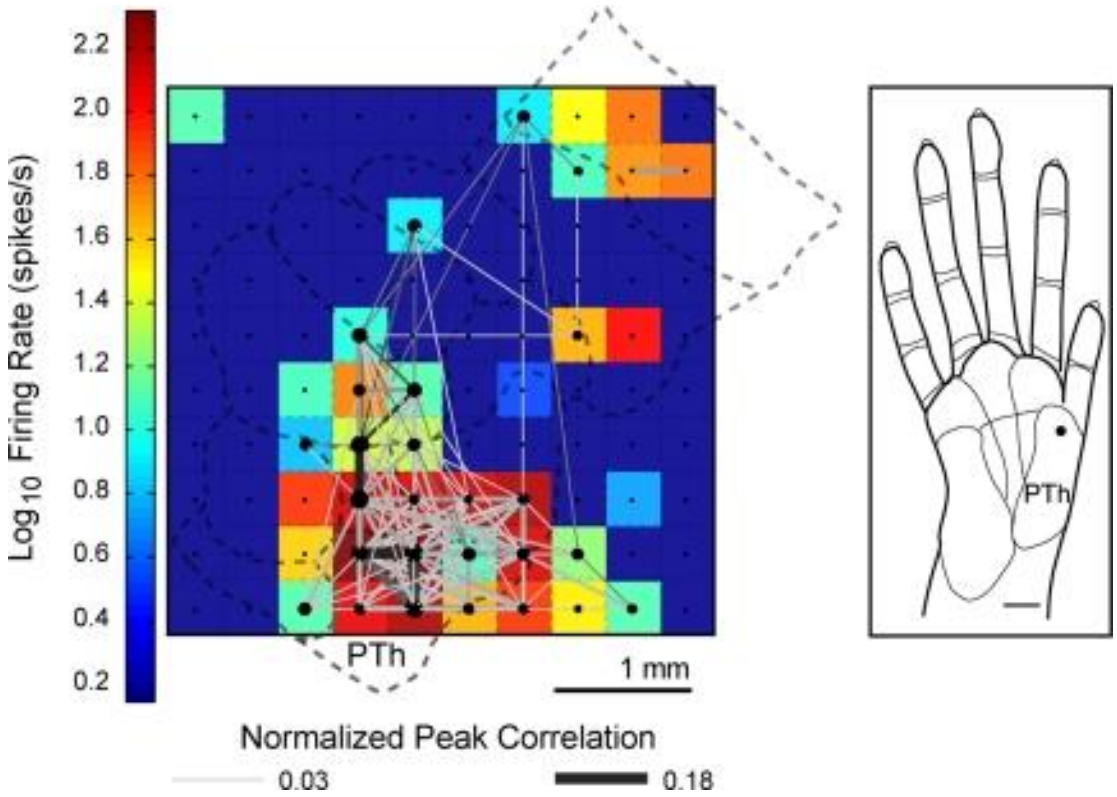

Figure 2-2. An example of widespread spike timing correlations and firing activity. Significant peak correlations across the sampled neuron-units in the 100-electrode array are displayed in a grid with a color map representing the peak firing rates of the units overlaid on the schematic of the area 3b hand representation to indicate the approximate spatial locations of the electrodes. Shown is one example from case 1 when a single site on the thenar palm (PTh) was stimulated repeatedly (100 trials). Dots indicate electrode sites and significant correlations between units are represented by the lines connecting the dots. The size of the dots and the thickness of the connecting lines are visual representations of the peak magnitude of the correlation. Each colored box represents the peak firing rate of a unit at one electrode site. Peak firing rates are shown for those units included in the synchrony analysis. Dark blue squares indicate electrodes not analyzed for spike synchrony because units did not show sustained responses to stimulation.

Table 2-1. Proportions of correlated pairs across cortical distance in S1.

	Cortical distance, mm						
Site stimulation	0–1.0	1.0–2.0	2.0–3.0	3.0–4.0	4.0–5.0	5.0–6.0	Total
Single							
Recorded pairs, *n*	264	378	321	100	12	0	1,075
Synchronized pairs, *n*	155	205	134	37	2	0	533
Proportion, %	58.7	54.2	41.7	37.0	16.7	—	49.6
Dual							
Recorded pairs, *n*	146	223	192	67	6	0	634
Synchronized pairs, *n*	52	75	47	5	0	0	179
Proportion, %	35.6	33.6	24.5	7.5	0	—	28.2

—, not applicable.

As a next step, we examined the relationship of the distance between correlated pairs and the magnitude of the peak correlation. The data were summarized for both monkeys in a scatter plot (Figure 2-3) to determine if strong correlations tended to occur between neurons on adjacent electrodes. We found a weak, but significant trend for stronger correlations occurring between neurons recorded from nearby electrodes when a single site was stimulated ($r = -0.2247$, $p < 0.0001$, $n = 533$), as well as when two nonadjacent sites were simultaneously stimulated ($r = -0.2048$, $p = 0.006$, $n = 179$). We found that significant correlations occurred between neurons recorded from distant electrodes, over 2 mm apart.

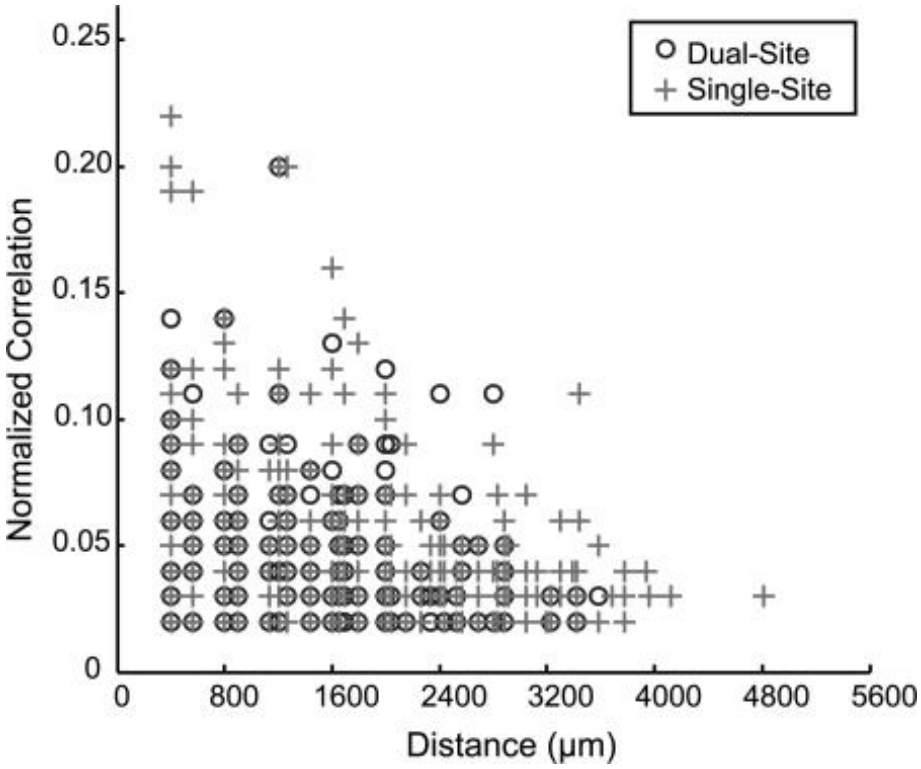

Figure 2-3. Relationship of spike timing peak correlation magnitude to the distance between electrodes. The normalized, significant peak correlation magnitudes are plotted as a function of distance between the correlated unit pairs, summarized for monkeys 1 and 2 when nonadjacent sites were simultaneously stimulated (Dual-Site) and when single sites were stimulated as controls (Single-Site).

Discussion

One might expect that spatial integration by 3b neurons is very limited, as RFs have been consistently described as restricted in size, usually confined to part of a phalanx of a single digit or palm pad (Iwamura et al., 1983; Pons et al., 1987; DiCarlo et al., 1998), and appear uniformly excitatory when probed with punctate stimuli (Mountcastle et al., 1959; Sur, 1980; Sur et al., 1985; Sripati et al., 2006). Studies indicate that inhibitory surrounds of area 3b neurons in hand cortex do not substantially enlarge the RF area (DiCarlo et al., 1998; Sur, 1980; Sripati et al., 2006). Here we show that traditional depictions of RFs do not reflect the extent of integration that occurs in area 3b.

The ability to record from 100 electrodes simultaneously allows us to examine responses and spike synchrony across a large extent within a single cortical area or between areas. Our experiment, using tactile stimulation of nonadjacent hand sites of anesthetized owl monkeys, demonstrates the widespread spatial integration of sensory inputs present in the area 3b hand representation. When even a single site was stimulated with repeated skin indentations, neurons on numerous electrodes responded to the 1 mm diameter stimulus. These results are in agreement with findings in which chronic multi-site recordings in owl monkey somatosensory cortex areas 3b, 2, and S2 showed widespread activity in response to single-site tactile stimulation and evidence for ensemble coding of stimulus location using firing rates (Nicolelis et al., 1998). Spike timing correlations occurred between neurons separated by millimeters of cortex, beyond the predicted extent of the representation of the palm pad location at that site (Figure 2-2), suggesting a functional connectivity that has been largely overlooked.

Correlated firing among neurons can occur through four basic ways: 1) a common input arriving nearly simultaneously to the neurons; 2) lateral connections within cortex; 3) responses in unconnected neurons to a common stimulus; and 4) statistical coincidence due to firing rate. Our corrections in the correlation calculations remove or reduce the impact of 3) and 4), although "uncorrected correlations" likely have roles in stimulus processing (Gerstein et al., 1989). Thus, we are left to determine if the correlations we find are due to common input or lateral connections. We recorded from neuron pairs with the same or overlapping RFs, which are likely to receive a common, activating input as well as have strong lateral connections (e.g., Gilbert, 1993; Burton and Fabri, 1995). These neurons were in close proximity (adjacent electrodes, 0.4 mm apart). Significant spike correlations also occurred for neurons with nonoverlapping RF across larger regions of cortex (over 2 mm apart). Synchronies between neuron pairs with dissimilar RFs induced by stimulating two nonadjacent digits simultaneously are unlikely due to common thalamocortical input, as the densest thalamocortical projections are topographically matched, although a few projections spread across distinct representations in area 3b of owl monkeys (Garraghty et al., 1989; Garraghty and Sur, 1990). Lateral projections extend across segregated digit representations in monkey area 3b (e.g., De Felipe et al., 1986; Manger et al., 1997; Fang et al., 2002). Thus, we propose that common thalamic inputs together with dense lateral connections result in strong correlations between neurons across a localized area of cortex in which neurons have overlapping RFs, while longer and less dense intrinsic lateral connections (De Felipe et al., 1986; Garraghty et al., 1989; Garraghty and Sur, 1990; Manger et al., 1997; Fang et al., 2002) contribute to weaker correlations that are spread across a larger area. An

additional source of correlated activity between distant neurons could be common feedback connections from higher-order somatosensory areas with large RFs.

Evidence for Widespread Correlated Neural Assemblies in Area 3b

Recent studies have shown measurable changes in spike time synchrony between pairs of neurons with changes in attention in primate somatosensory cortex (e.g., Hsiao et al., 1993; Steinmetz et al., 2000; Niebur et al., 2002; Roy et al., 2007). To a large extent, such synchronies have been interpreted as a high-level integration process based on feedback connections from higher levels, despite the evidence for robust presence of synchrony in anesthetized preparations (Alloway et al., 1993, 2002; Roy and Alloway, 1999; Samonds et al., 2003, 2006; Bruno and Sakmann, 2006; Eggermont, 2006). The manifestation of synchrony in unconscious animals implies specific anatomical connectivity between neurons and populations of neurons and furthermore emphasizes that higher levels of integration must consider such low-level integration.

Our results, using paired stimuli on multiple locations across the hand, expand previous correlation studies in somatosensory cortex which found that neurons with overlapping RFs have strong correlations when probed with single stimuli inside the RF and moving stimulation (e.g., Alloway et al., 1993, 2002; Roy and Alloway, 1999). Similar to findings in cat S2 (Alloway et al., 2002), we found that the magnitude of correlated activity decreased with increasing electrode distance (Figure 2-3). However, the spatial distance between correlated neurons was surprising, as significant correlations occurred between neurons separated by over 2 mm (Table 2-1, Figure 2-3). As suggested by Roy and Alloway (1999), we have found that spike timing synchrony in S1 may be

related to stimulus properties in anesthetized animals, indicating that low-level integration processes play an important role in neural coding, in addition to the role played by higher-level processes (such as attention).

In conclusion, we have shown evidence for extensive sensory input integration in S1 cortex of anesthetized owl monkeys. Traditional minimal receptive field mapping is only the "tip of the iceberg" in terms of reflecting the actual stimulus interactions that take place in the area 3b hand representation. Interactions extend across nonadjacent digit sites, despite the lack of RF mapping studies in primates showing such large fields in area 3b. The differences in our findings compared to traditional RF mapping can be explained in part by our stimulus. We use a suprathreshold stimulus to drive responses, whereas RF mapping is typically done with near-threshold stimulation. Our suprathreshold stimulus may activate a larger pool of inputs, allowing us to measure interactions that are likely to occur during natural tactile stimulation. Using our methods, we found sensory input integration across regions much larger than the small RFs and discrete digit representations predict. We propose that neurons even at the first level of somatosensory cortex participate in global aspects of stimulus processing, upon which higher-level processing is based.

Materials and Methods

Preparation

Two adult owl monkeys (1 kg) were prepared for electrophysiological recordings in primary somatosensory cortex under the guidelines established by the National

Institutes of Health and the Animal Care and Use Committee at Vanderbilt University. Animals were anesthetized with propofol and N_2O and paralyzed with vecuronium bromide. See supporting information (SI) for detailed methods. A small craniotomy was made over the primary somatosensory cortex, and the dura was removed. The electrode array was inserted into the cortex pneumatically to a depth of 600 μm, so that electrode tips are expected to be within layers 2/3. The opening was covered with agar mixed with Ringer's solution to provide stability. Similar methods have been described elsewhere (Samonds et al., 2003; Xu et al., 2003).

Stimulation Procedures

Computer-controlled stimuli were generated in a custom-designed Visual Basic program and executed with two independent force- and position-feedback controlled motor systems (300B, Aurora Scientific Inc., Aurora, ON, CA). Round Teflon probes 1 mm in diameter delivered tactile stimuli to the glaborous hand. Stimuli consisted of pulses that indented the skin 0.5 mm for 0.5 s, followed by 2.0 s off of the skin, repeated for 255-300 s. These parameters allowed us to detect responses to stimulus on and off times and classify phasic or sustained responses (Sur et al., 1984). Paired sites were selected for stimulation and the pulses were delivered simultaneously. Single-site control stimuli were delivered to each of the sites in the pair prior to simultaneous stimulation. For practical purposes, reference units were identified and probes were positioned so that one probe was inside and one probe was outside the minimal receptive field (mRF) of the reference neuron. Procedures for mRF mapping have been published elsewhere

(Merzenich et al., 1978; Nelson et al., 1980; Jain et al., 2001). See SI for details regarding mRF mapping and stimulation procedures.

Data Acquisition

Recordings were made using the 10 x 10 Utah array and the Bionics Data Acquisition System (Cyberkinetics Neurotechnology Systems Inc., Salt Lake City, UT). The signals on each channel were amplified by 5000 and band-pass filtered between 250 Hz and 7.5 kHz. The threshold for each electrode was automatically set for 3.25 times the mean activity and the waveforms were sampled at 30 kHz for 1.5 ms windows (Samonds et al., 2003).

Histology

Following data collection, animals were perfused and the brains were prepared for histological analysis as described previously (Jain et al., 2001). The cortex was flattened and cut frozen at 40 µm. Sections were processed for myelin to aid in determining the electrode sites relative to the area 3b hand representation. SI Figure 2-4 shows the tissue quality that may be obtained using the 100-electrode array.

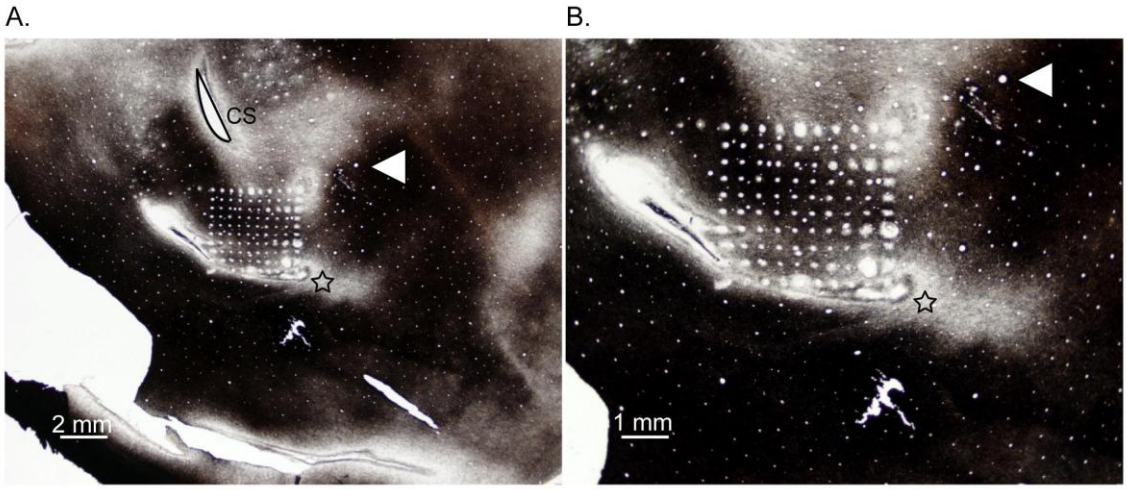

SI Figure 2-4. Illustration of tissue quality with use of the 100-electrode array. The damage produced by *inserting* the array appears to be minimal in most cases, but tears in the tissue caused by the array *removal* and tissue processing are common and did occur for both of the presented cases. Photomicrographs were adjusted for brightness and contrast in Adobe Photoshop CS and were not altered in any other way. Graphics and text were added in Adobe Illustrator 10. Medial is upward and rostral is to the right in A and B. White arrowheads mark matching blood vessels and the stars indicate approximately matched sites near the lateral sulcus. A. The individual electrode sites are visible in this section at 0.5 x magnification (section 13) from one owl monkey in which the 100-electrode array was acutely implanted and removed after recording for over 2 days. CS indicates the location of the central sulcus. B. The same section in A is shown at 1 x magnification to show the detail of the electrode tracks. We find that the majority of the tissue damage comes from removing the electrode array from the brain prior to perfusion and from processing the tissue.

Data Analysis

Spike Sorting and Data Selection

Spike signals were sorted offline with an automatic spike classification program for Matlab (The Mathworks, Inc., Natick, MA) based on the t-distribution Expectation Maximization algorithm (Shoham et al., 2003). All recordings for a given stimulation series were sorted together to standardize sorting across recordings. We reviewed each recording with a second spike sorter program, Plexon Offline Sorter (Plexon Inc., Dallas, TX). See SI Methods and SI Figure 2-5 for sorting details. We used the Plexon software

to verify the quality of unit isolation such that single units had refractory periods ≥ 1.2 ms; p values ≤ 0.05 for multivariate ANOVA related to cluster separation; and distinct waveform amplitudes and shapes when compared with other activity on the same electrode (Nicolelis et al., 2003). Single- and multi-units were grouped separately. In each monkey, several of the electrodes recorded single unit activity (45 electrodes and 65 electrodes in cases 1 and 2, respectively); however, not all single units responded significantly under each stimulus condition. Only units that responded to a given stimulus condition with peak firing rates above the upper 99% confidence limit of the expected mean firing rate were included in the analyses for that condition. Confidence limits were calculated with NeuroExplorer software (Nex Technologies, Littleton, MA) based on the assumption that the spike counts have a Poisson distribution.

Additionally, neurons included in the analysis showed sustained activity in at least one of the stimulus conditions such that spiking activity was maintained during the 0.5 s skin indentation. In practice, both of the following criteria had to be reached for a unit to be included in the correlation analysis. The activity between 100 and 500 ms after stimulus onset must reach the upper 95% confidence limit of the mean firing rate for 3 or more consecutive 1 ms bins, and the activity within this 400 ms period must exceed the expected mean firing rate for at least 50 1 ms bins. Units showing only rapidly-adapting response properties typically had relatively low spike counts, which makes the interpretation of JPSTH analysis difficult or even biased, so these units were excluded from analysis. Finally, we selected one unit per electrode for JPSTH analysis, choosing single units over multi-units when possible.

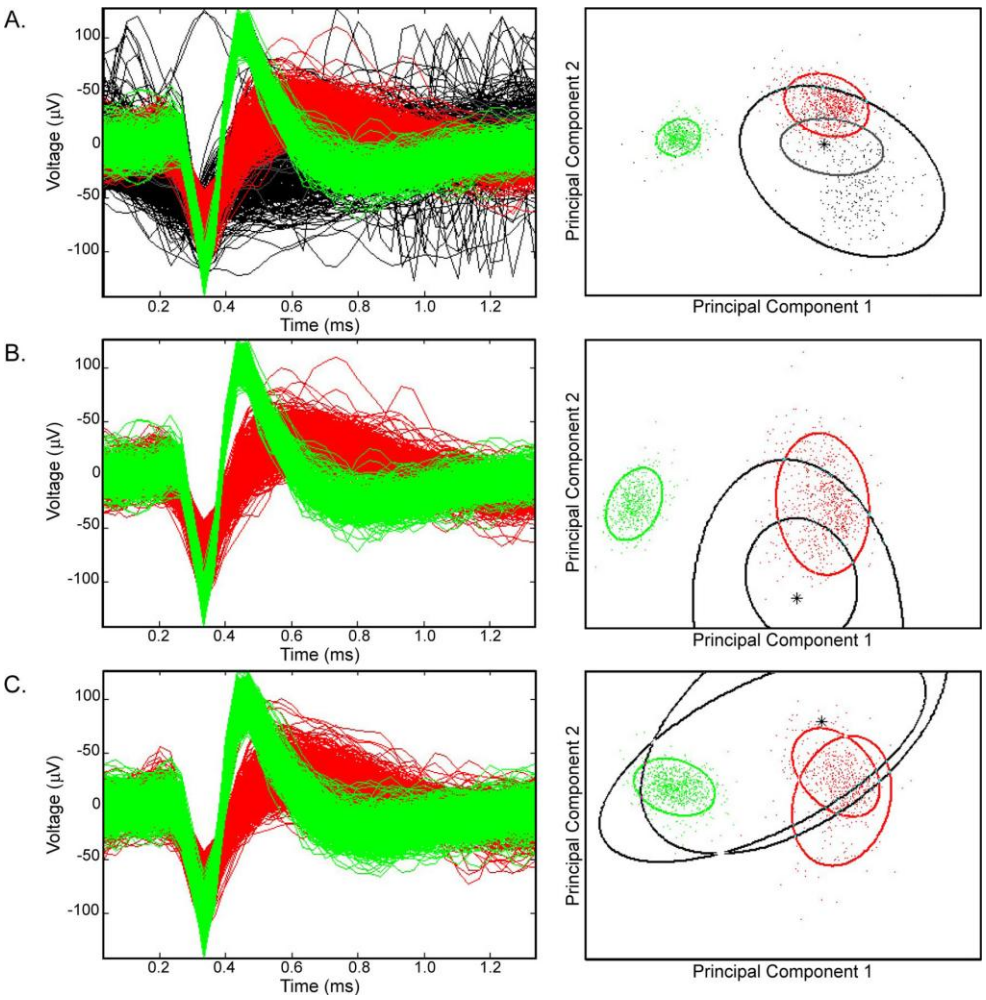

SI Figure 2-5. Examples of spike sorting quality. A. The left plot shows waveforms recorded from electrode 95 in monkey 2 from the Cyberkinetics Matlab-based automatic spike sorting program during stimulation on distal D2. The 539 waveforms classified as a single unit (green) were distinguishable from other waveforms. The black waveforms are classified as noise by the Matlab-based automatic spike sorter program. We considered the red unit a multi-unit due to the lack of separation from the background noise spikes. The right plot of the first and second principal components (PC1 and PC2) shows separate clustering of the single unit (green) from the background spikes (black). Since it was possible to record from multiple units per electrode, we examined the recorded files individually using Plexon Offline Sorter to ensure that the appropriate units were compared across recordings. In most cases, spikes that belong to one unit but are counted as "noise" in the automatic spike sorter can be added to the appropriate unit using the Plexon program. (See large amplitude "noise" waveforms and spikes within the green cluster.) B. The same plot style and units in A are shown after the "erase noise" feature is used in the Matlab-based automatic spike sorting program to focus on the spikes from the green unit and the cluster separation. When two units were recorded simultaneously from one electrode, we only selected one unit per electrode for synchrony analysis, choosing single units over multi-units. In this case, we chose the single unit shown in green (designated as 95b). C. One way to view the stability of the recordings and unit designations is to show the appearance of waveforms and clusters across a series of stimulations. (This function cannot be performed using the Plexon spike sorting program unless all of the stimulations are recorded in the same file.) Shown here are the recordings for the single-site stimulation on D2 and D4, simultaneous stimulation on D2 and D4, and temporally offset stimulation on D2 and D4 (data not presented here), encompassing 620 trials recorded over 79 minutes. The plot style is the same as B with "noise" spikes hidden to focus on the isolation of single unit 95b (green) over the time course of the stimulus series.

Spike Time Synchrony

Spike synchrony between pairs of neurons was measured from the cross-correlation histogram derived from the JPSTH with all the spike trains aligned on the onset of skin indentation following previous conventions (Aertsen et al., 1989; Gerstein, 2000; Ventura et al., 2005). See SI for detailed methods. We compared the peak correlation value from the cross-correlation histogram derived from the normalized JPSTH of neurons across stimulus conditions. SI Figure 2-6 shows examples of JPSTHs during stimulation and no stimulation; however, the very low spike counts in anesthetized animals in absence of tactile stimulation typically did not reach an appropriate number of spikes for use of the JPSTH calculation (Aertsen et al., 1989; Gerstein et al., 1989; Gerstein, 2000) and were not analyzed.

We tallied the proportions of synchronized neuron pairs to the total recorded pairs for groups of cortical distances separating the neurons in the pair. To represent the relationship of the electrode distance between the correlated neurons with the magnitude of the spike timing correlations, we measured the distance between electrodes and the correlation strength for the given stimulus condition. We examined these paired values of distance and spike timing correlation magnitude in a scatter plot and performed linear regression on the population summary to obtain the correlation coefficient using Matlab.

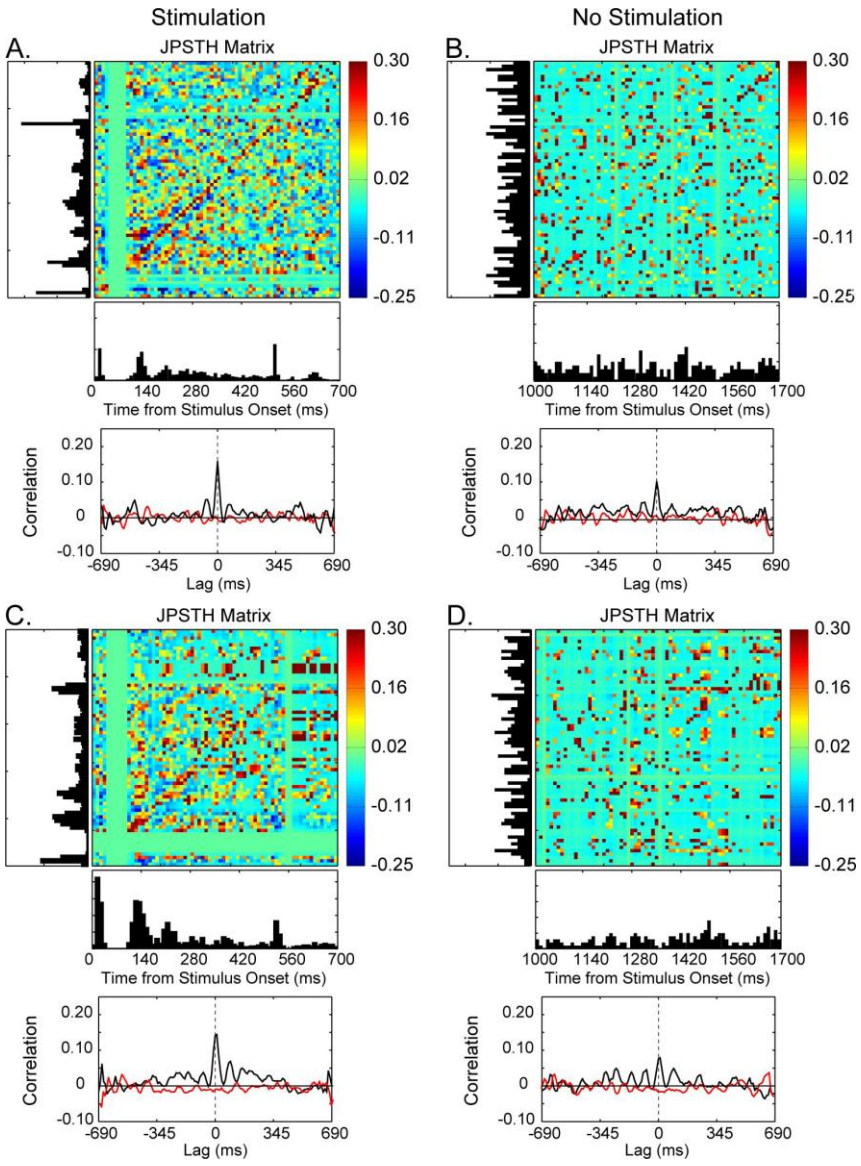

SI Figure 2-6. Examples of spike time synchrony during trials with stimulation or without tactile stimulation. The left column includes results during stimulation with the 500 ms indentation from 0 to 700 ms. The right column includes results during the stimulus off periods from the same trials from 1000 to 1700 ms. The same conventions as Fig. 1 are used for the JPSTH plot. A. The JPSTH matrix and associated cross-correlation histogram are shown for multi-units 5a and 15a from case 1 during 100 trials of dual-site stimulation on palm sites PTh and P1. The normalized peak correlation is 0.16, centered on 0 ms. Unit 5a has 1439 spikes, and unit 15a has 2359 spikes. B. The JPSTH and cross-correlation histogram are shown for the same units as A during the portion of the trials when the tactile probes were off of the skin. (Each trial contained a 2 s interstimulus interval when the probes were not touching the skin.) The normalized peak correlation is 0.11, centered on 0 ms. Unit 5a has 246 spikes, and unit 15a has 419 spikes. C. The JPSTH and cross-correlation histogram are shown for single units 85a and 95b from case 2 during 100 trials of dual-site stimulation on digit sites distal D2 and D4. The normalized peak correlation is 0.14, centered on 0 ms. Unit 85a has 784 spikes, and unit 95b has 790 spikes. D. The JPSTH and cross-correlation histogram are shown for the same units as C during the portion of the trials when the tactile probes were off of the skin. The normalized peak correlation is 0.08, centered on 0 ms. Unit 85a has 200 spikes, and unit 95b has 386 spikes. Since the spike numbers were typically very low when no tactile stimulation was provided, we did not analyze the correlations from these data in the present study. The presence of these correlations in absence of a driving stimulus confirms that the peak correlations measured and interpreted did not result from spike coincidence due to only brief and extreme changes in firing rate at the initiation and removal of the stimulation.

Acknowledgements

This work was supported by the James S. McDonnell Foundation (JHK) and NIH grants NS16446 (JHK), F31-NS053231 (JLR), EY014680-03 (ABB), T32-GM07347 (MJB), P30-EY08126, and P30-HD015052. We thank Dr. Jeff Schall for comments and insight regarding development of analysis methods and Dr. O. Gharbawie and C. Camalier for help collecting data from case 2.

References

Aertsen AMHJ, Gerstein GL, Habib M, Palm G. 1989. Dynamics of neuronal firing correlation: modulation of "effective connectivity". *J Neurophysiol* 61: 900-917.

Allman J, Miezin F, McGuinness E. 1985. Stimulus specific responses from beyond the classical receptive field: Neurophysiological mechanisms for local-global comparisons in visual neurons. *Annu Rev Neurosci* 8: 407-430.

Alloway KD, Johnson MJ, Wallace MB. 1993. Thalamocortical interactions in the somatosensory system: interpretations of latency and cross-correlation analyses. *J Neurophysiol* 70: 892–908.

Alloway KD, Zhang M, Dick SH, Roy SA. 2002. Pervasive synchronization of local neural networks in the secondary somatosensory cortex of cats during focal cutaneous stimulation. *Exp Brain Res* 147: 227–242.

Azouz R, Gray CM. 2000. Dynamic spike threshold reveals a mechanism for synaptic coincidence detection in cortical neurons *in vivo*. *Proc Natl Acad Sci USA* 97: 8110-8115.

Bruno RM, Sakmann B. 2006. Cortex is driven by weak but synchronously active thalamocortical synapses. *Science* 312: 1622-1627.

Burton H, Fabri M. 1995. Ipsilateral intracortical connections of physiologically defined cutaneous representations in area 3b and 1 of macaque monkeys: projections in the vicinity of the central sulcus. *J Comp Neurol* 355: 508-538.

De Felipe J, Conley M, Jones EG. 1986. Long-range focal collateralization of axons arising from corticocortical cells in monkey sensory-motor cortex. *J Neurosci* 6: 3749-3766.

DiCarlo JJ, Johnson KO, Hsiao SS. 1998. Structure of receptive fields in area 3b of primary somatosensory cortex in the alert monkey. *J Neurosci* 18: 2626-2645.

Eggermont JJ. 2006. Properties of correlated neural activity clusters in cat auditory cortex resemble those of neural assemblies. *J Neurophysiol* 96: 746-764.

Fang PC, Jain N, Kaas JH. 2002. Few intrinsic connections cross the hand-face border of area 3b of new world monkeys. *J Comp Neurol* 454: 310-319.

Garraghty PE, Pons TP, Sur M, Kaas JH. 1989. The arbors of axons terminating in middle cortical layers of somatosensory area 3b in owl monkeys. *Somatosens Mot Res* 6: 401-411.

Garraghty PE, Sur M. 1990. Morphology of single intracellularly stained axons terminating in area 3b of macaque monkeys. *J Comp Neurol* 294: 583-593.

Gerstein GL. 2000. Cross-correlation measures of unresolved multi-neuron recordings. *J Neurosci Methods* 100: 41–51.

Gerstein GL, Bedenbaugh P, Aertsen AMHJ. 1989. Neuronal assemblies. *IEEE Trans Biomed Eng* 36: 4-14.

Gilbert CD. 1993. Circuitry, architecture, and functional dynamics of visual cortex. *Cereb Cortex* 3: 373-386.

Hsiao SS, O'Shaughnessy DM, Johnson KO. 1993. Effects of selective attention on spatial form processing in monkey primary and secondary somatosensory cortex. *J Neurophysiol* 70: 444-447.

Iwamura Y, Tanaka M, Sakamoto M, Hikosaka O. 1983. Functional subdivisions representing different finger regions in area 3b or the first somatosensory cortex of the conscious monkey. *Exp Brain Res* 51: 315-326.

Jain N, Qi H-X, Kaas JH. 2001. Long-term chronic multichannel recordings from sensorimotor cortex and thalamus of primates. Chapter 5 In *Progress in Brain Research*, ed. MAL Nicolelis, 130: 1-10. Amsterdam: Elsevier Science B.V.

Manger PR, Woods TM, Muñoz A, Jones EG. 1997. Hand/face border as a limiting boundary in the body representation in monkey somatosensory cortex. *J Neurosci* 17: 6338-6351.

Merzenich MM, Kaas JH, Sur M, Lin CS. 1978. Double representations of the body surface within cytoarchitectonic areas 3b and 1 in "SI" in the owl monkey (*Aotus trivirgatus*). *J Comp Neurol* 181: 41-74.

Mountcastle VB, Powell TPS. 1959. Neural mechanisms subserving cutaneous sensibility, with special reference to the role of afferent inhibition in sensory perception and discrimination. *Bull Johns Hopkins Hosp* 105: 201-232.

Mountcastle VB, Talbot WH, Sakata H, Hyvarinen J. 1969. Cortical neuronal mechanisms in flutter-vibration studied in unanesthetized monkeys. Neuronal periodicity and frequency discrimination. *J Neurophysiol* 32: 452-484.

Nelson RJ, Sur M, Felleman DJ, Kaas JH. 1980. Representations of the body surface in postcentral parietal cortex of *Macaca fascicularis*. *J Comp Neurol* 192: 611-643.

Nicolelis MAL, Ghazanfar AA, Stambaugh CR, Oliveira LMO, Laubach M, Chapin JK, Nelson RJ, Kaas JH. 1998. Simultaneous encoding of tactile information by three primate cortical areas. *Nat Neurosci* 1: 621-630.

Nicolelis MAL, Dimitrov D, Carmena JM, Crist R, Lehew G, Kralik JD, Wise SP. 2003. Chronic, multisite, multielectrode recordings in macaque monkeys. *Proc Natl Acad Sci USA* 100: 11041-11046.

Niebur E, Hsiao SS, Johnson KO. 2002. Synchrony: a neuronal mechanism for attentional selection? *Curr Opin Neurobio* 12: 190-194.

Pons TP, Wall JT, Garraghty PE, Cusick CG, Kaas JH. 1987. Consistent features of the representation of the hand in area 3b of macaque monkeys. *Somatosens Res* 4: 309-331.

Roy A, Steinmetz PN, Hsiao SS, Johnson KO, Niebur E. 2007. Synchrony: a neural correlate of somatosensory attention. *J Neurophysiol* 98: 1645-1661.

Roy S, Alloway KD. 1999. Synchronization of local neural networks in the somatosensory cortex: a comparison of stationary and moving stimuli. *J Neurophysiol* 81: 999-1013.

Roy SA, Dear SP, Alloway KD. 2001. Long-range cortical synchronization without concomitant oscillations in the somatosensory system of anesthetized cats. *J Neurosci* 21: 1795-1808.

Salinas E, Sejnowski TJ. 2001. Correlated neuronal activity and the flow of neural information. *Nat Rev Neurosci* 2: 539-550.

Samonds JM, Allison JD, Brown HA, Bonds AB. 2003. Cooperation between Area 17 neuron pairs enhances fine discrimination of orientation. *J Neurosci* 23: 2416-2425.

Samonds JM, Zhou Z, Bernard MR, Bonds AB. 2006. Synchronous activity in cat visual cortex encodes collinear and cocircular contours. *J Neurophysiol* 95: 2602-2616.

Shoham S, Fellows MR, Normann RA. 2003. Robust, automatic spike sorting using mixtures of multivariate t-distributions. *J Neurosci Methods* 127:111-122.

Sripati AP, Yoshioka T, Denchev P, Hsiao SS, Johnson KO. 2006. Spatiotemporal receptive fields of peripheral afferents and cortical area 3b and 1 neurons in the primate somatosensory system. *J Neurosci* 26: 2101-2114.

Steinmetz PN, Roy A, Fitzgerald PJ, Hsiao SS, Johnson KO, Niebur E. 2000. Attention modulates synchronized neuronal firing in primate somatosensory cortex. *Nature* 404: 187–190.

Sur M. 1980. Receptive fields of neurons in areas 3b and 1 of somatosensory cortex in monkeys.*Brain Res* 198: 465-471.

Sur M, Wall, JT, Kaas JH. 1984. Modular distribution of neurons with slowly adapting and rapidly adapting responses in area 3b of somatosensory cortex in monkeys. *J Neurophysiol* 51: 724-744.

Ventura V, Cai C, Kass RE. 2005. Statistical assessment of time-varying dependency between two neurons. *J Neurophysiol* 94: 2940-2947.

Xu X, Collins CE, Kaskan PM, Khaytin I, Kaas JH, Casagrande VA. 2003. Optical imaging of visually evoked responses in prosimian primates reveals conserved features of the middle temporal visual area. *Proc Natl Acad Sci USA* 101: 2566-2571.

Supporting Information

SI Materials and Methods

Preparation

Each monkey was given an initial ketamine injection (10-30 mg/kg, intramuscular) for sedation during surgical preparations. Anesthesia was induced with 2-4% halothane gas and maintained with intravenous propofol (10 mg/kg/hr) during surgery. The monkey was secured in a stereotaxic device. Rectal temperature was monitored and maintained between 37-39°C with a servo-controlled heating pad. Paralysis was induced with 1-3 ml vecuronium bromide and maintained by intravenous vecuronium bromide (0.1-0.3 mg/kg/hr) mixed with 5% dextrose and Lactated Ringer's solution. Once paralyzed, animals were artificially ventilated with a mixture of N_2O: O_2: CO_2 (75: 23.5: 1.5) at a rate sufficient to maintain peak end tidal CO_2 at ~ 4%. Paralysis was necessary to keep the hand stable during long stimulus blocks. Depth of anesthesia was monitored by electrocardiogram and electroencephalogram. Supplemental anesthesia was provided by 0.3 mg/kg/hr propofol.

Stimulation Procedures

The detailed mapping procedures can be found elsewhere (Merzenich et al., 1978; Nelson et al., 1980). Briefly, we located responsive regions on the hand for units on each electrode first by stimulating lightly with a hand-held probe and listening to the responses on an audio monitor. For well-isolated units, we mapped minimal receptive fields (mRFs)

at a finer level by stimulating with graded Semmes-Weinstein filaments (starting with the 10 g filament), finding the threshold, and then drawing mRFs on hand diagrams (Jain et al., 2001). We marked the estimated excitatory center of the mRF for probe placement. This procedure was followed at the beginning, end, and periodically throughout the recording experiment. Using hand-plotted mRFs was a practical way to determine probe placement (inside and outside the mRF of reference neurons).

Before stimulation, the fingernails were glued (cyanoacrylic) to Teflon screws that were fixed in plasticine to keep the hand position stable during recording. Adhesive was removed from the fingernails using acetone.

Histology

The myelin-stained sections of flattened cortex were used to help reconstruct the location of the electrodes within S1 by examining the patterns of myelin staining. Area 3b is myelin-rich and darkly stained, and characteristic "ovals" representing the face and oral cavity can be identified (Jain et al., 1998, 2001). Electrode depth can be estimated by tracking the appearance and disappearance of electrode tracks across sections. Two primary factors were considered. First, the cortex was cut parallel to the pia, which is not always precisely parallel to the electrode locations. Second, tissue shrinking and stretching may occur during processing. We estimated this by comparing the observed distance between electrodes across the array to the expected distance (4 mm). By taking these issues into account, we can obtain an approximation of the electrode depth and location.

Data Analysis

Spike sorting and data selection. Initial spike sorting was performed using the automatic spike classification software available from Cyberkinetics. This method using an adaptation of the Expectation Maximization algorithm with t-distributions has been shown to perform more reliably than statistical methods that rely on the Gaussian model of waveform variability (Shoham et al., 2003). The automatic nature of the classification and the capacity of the software to be used with data collected from the Bionics recording system made this method of spike sorting the preferred first step. Due to memory limitations and the large amounts of data recorded during an experiment, not all of the possible conditions (recorded over the course of two days) were able to be sorted simultaneously within the automatic classification software. (As mentioned in the text, all of the recordings for a given stimulation protocol were sorted together.) For the purpose of the project (beyond the scope of this paper), we want to not only compare the responses of the same unit within a given stimulation protocol, but also to compare the responses of the same unit across different stimulation types when the same unit was held. Since the automatic spike sorter program does not designate the units by the same name across multiple recorded files not sorted together, we used the Plexon Offline Sorter program (Plexon Inc., Dallas, TX) to review and sort each recorded file individually. This was necessary to ensure that the same units were compared across stimulus conditions. For example, when more than one unit was recorded on an electrode, the unit called "95b" in recording 1 must be called "95b" in recording 5 if those recordings will be compared. Plexon Offline Sorter allowed us to swap unit names if

necessary and perform semi-automatic sorting (such as Valley-Seeking) if needed to obtain better unit isolation.

In addition, Plexon Offline Sorter allowed us to check the stability of the recordings by viewing the unit clustering in Principal Component space in three dimensions with the z-axis as timestamps (x-axis as PC1, y-axis as PC2). None of the units included in the analysis were found to drift over time or change unit identities over the course of the stimulation protocol. The manual adjustment capabilities in the Plexon software allowed us to ensure that we used the same populations of units in our control conditions (single-site stimulation) and experimental conditions (nonadjacent dual-site stimulation). We also examined the stability of the recordings by sorting multiple recorded files simultaneously using the Cyberkinetics Matlab-based automatic spike sorting program and viewing the unit isolation in multiple files simultaneously (equivalent to approximately 2 hours of recording at one time). Units included in the analysis were observed to be stable using both methods of examination (with Plexon and Cyberkinetics spike sorter programs).

Spike time synchrony. There are multiple time scales for which temporal correlation can be examined. To assess very precise spike synchrony, small time bins (1-5 ms) have been used; however, such small bins require relatively high spike counts. Coarse temporal correlation is considered at time scales > 20 ms (e.g., Vaadia et al., 1995; Oram et al., 2001). Bin sizes between 1-15 ms are commonly reported (e.g., Vaadia et al., 1995; Benda et al., 2006; Narayanan and Laubach, 2006). In our case, spike correlation was examined in 700 ms windows divided into 70 bins—we use 10 ms bins since only the brief on and off response transients will peak with firing rates above 100

Hz. This appears for these data to be a reasonable compromise to be able to extract the fine temporal correlation especially for the period of relatively low firing during the sustained portion of the stimulus (Figure 2-1, SI Figure 2-6). The peri-stimulus time histograms (PSTH) of spike counts aligned on stimulation onset with 10 ms bins were obtained for each of a pair of neurons:

$$\langle n_{(i)(u)} \rangle = \frac{1}{K} \sum_{k=1}^{K} n_i^{(k)}(u)$$

Where $n_{(i)}^{(k)}(u)$ is the number of spikes per bin in the k^{th} of K total trials. Using the same notation, the contribution to the joint peri-event time histogram (JPETH) of spikes in the k^{th} trial is just the product of the counts in each time bin in the matrix for each neuron in the pair:

$$n_{ij}^{k}(u, v) = n_i^{k}(u) \cdot n_j^{k}(v)$$

The average raw JPSTH is obtained by:

$$\text{JPSTH}_{\text{raw}} = \langle n_{ij}(u, v) \rangle = \frac{1}{K} \sum_{k=1}^{K} n_{ij}^{(k)}(u, v)$$

The raw JPSTH measures the average incidence of common spike occurrences, but of course, this incidence naturally will be affected by modulation of the discharge rate of either neuron in the pair. The fraction of coincident spikes resulting from such modulation (also known as the shift-predictor) is estimated by calculating the cross-product matrix of the individual peri-event time histograms:

$$\langle \bar{n}_{ij}(u, v) \rangle = \langle n_i(u) \rangle \langle n_j(v) \rangle$$

In abbreviated notation, the normalized JPSTH was determined by subtracting this shift-predictor from the raw JPSTH and scaling each bin by the square root of the product of the standard deviations from the individual neurons:

$$\mathrm{JPSTH}_{\mathrm{normalized}} = \frac{\langle n_{ij} \rangle - \langle \bar{n}_{ij}(u, v) \rangle}{\sqrt{\langle n_i(u) \rangle (1 - \langle n_i(u) \rangle) \cdot \langle n_j(v) \rangle (1 - \langle n_j(v) \rangle)}}$$

Thus, the normalized JPSTH measures the probability of coincident spikes in the pair of neurons corrected for overall modulation of discharge rates; the values are treated as correlation coefficients, ranging from -1 to +1 (Aertsen et al., 1989).

The JPSTH matrix represents time from earlier in the lower left to later in the upper right; the bins along this main diagonal measure the coincidences with 0 time lag (Figure 2-1C). The JPSTH can be summarized in two additional plots. First, the time-averaged cross-correlogram is computed by summing the JPSTH bins parallel to the main diagonal; the cross-correlogram measures the average positive or negative correlation across the entire interval of analysis (Figure 2-1C). Second, the coincidence histogram (not shown) represents the coincident or near-coincident firing of the cells time-locked to the event on which the PETH are aligned. Although the dynamics of the correlation are not analyzed here, examination of the JPSTH revealed that the correlated spike times occur during the sustained portion of the stimulus-driven activity, rather than at the

transient responses to stimulus onset and removal. The spike timing coincidence will be examined elsewhere.

To test the reliability of the normalized JPSTH, we repeated the JPSTH calculation on two sets of spike trains in which no correlation should be present but where in the first case the spike train variability is preserved or in the second case the spike train variability is derived from a non-homogeneous Poisson process. The first was the *shuffled* JPETH generated by shuffling the order of the trials for one of each pair of neurons. It is important to emphasize that the trial-by-trial variability present in the normalized JPETH is preserved within the *shuffled* JPETH even if no correlation should be observed. Only pairs showing a normalized JPSTH correlation value significantly larger than the *shuffled* JPSTH were considered for further analysis. In practice, a bootstrapping (5000 iterations) procedure was used to test each correlation value against the distribution of the entire population of shuffled correlation values. Only the pairs for which the correlation value exceeded two times the standard deviation over the mean of the bootstrapped distribution were considered as significant.

Firing rate spike density function. Peak firing rate of individual neuron-units was determined from spike density functions. A spike density function was produced by convolving the spike train from each trial with a function resembling a postsynaptic potential specified by τ_g, the time constant for the growth phase, and τ_d, the time constant for the decay phase as:

$R(t) = (1 - \exp(-t/\tau_d)*\exp(-t/\tau_d)$. Based on physiological data from excitatory synapses, τ_g was set to 1 ms (e.g., Mason et al., 1991; Moore and Nelson, 1998). We set τ_d to 5 ms (Mason et al., 1991; Moore and Nelson, 1998; Steinmetz et al., 2000; Veredas et al.,

2005) rather than 20 ms because the transient nature of the on and off responses in primary somatosensory neurons was excessively smoothed using the commonly used decay constant of 20 ms. Other stimulus conditions in the same monkeys included dual-site stimulation delivered at temporal offsets of 10 and 30 ms (results will be presented elsewhere); therefore, we selected a smaller value for τ_d that best fit the data.

We visualized the peak firing rates across the sampled neurons in the 100-electrode array by creating a color map in Matlab. In some cases, to view the extent of high and low firing rates, we converted the firing rate values to logarithmic values. These graphics are for visualization purposes only.

SI References

Benda J, Longtin A, Maler L. 2006. A synchronization-desychronization code for natural communication signals. *Neuron* 52: 347-358.

Jain N, Catania KC, Kaas JH. 1998. A histologically visible representation of the fingers and palm in primate area 3b and its immutability following long-term deafferentations. *Cereb Cortex* 8: 227-236.

Jain N, Qi HX, Catania KC, Kaas JH. 2001. Anatomical correlates of the face and oral cavity representations in the somatosensory area 3b of monkeys. *J Comp Neurol* 429: 455-468.

Mason A, Nicoll A, Stratford K. 1991. Synaptic transmission between individual pyramidal neurons of the rat visual cortex in vitro. *J Neurosci* 11: 72-84.

Moore CI, Nelson SB. 1998. Spatio-temporal subthreshold receptive fields in the vibrissa representation of rat primary somatosensory cortex. *J Neurophysiol* 80: 2882-2892.

Narayanan NS, Laubach M. 2006. Top-down control of motor cortex ensembles by dorsomedial prefrontal cortex. *Neuron* 52: 921-931.

Oram MW, Hatsopoulos NG, Richmond BJ, Donoghue JP. 2001. Excess synchrony in motor cortical neurons provides redundant direction information with that from coarse temporal measures. *J Neurophysiol* 86: 1700-1716.

Vaadia E, Haalman I, Abeles M, Bergman H, Prut Y, Slovin H, Aertsen A. 1995. Dynamics of neuronal interactions in monkey cortex in relation to behavioural events. *Nature* 373: 515-518.

Veredas FJ, Vico FJ, Alonso JM. 2005. Factors determining the precision of the correlated firing generated by a monosynaptic connection in the cat visual pathway. *J Physiol 5*67.3: 1057-1078.

CHAPTER III

RESPONSE PROPERTIES OF NEURONS IN PRIMARY SOMATOSENSORY CORTEX OF OWL MONKEYS REFLECT WIDESPREAD SPATIOTEMPORAL INTEGRATION

This chapter reproduces the manuscript submitted to the Journal of Neurophysiology on August 4, 2009 with contributions from Drs. Hui-Xin Qi, Zhiyi Zhou, Melanie R. Bernard, Mark J. Burish, A.B. Bonds, and Jon H. Kaas.

Abstract

Receptive fields of neurons in somatosensory area 3b of monkeys are typically described as restricted to part of a single digit or palm pad. However, such neurons are likely involved in integrating stimulus information from across the hand. To evaluate this possibility, we recorded from area 3b neurons in anesthetized owl monkeys with 100-electrode arrays, stimulating two hand locations with electro-mechanical probes simultaneously or asynchronously. Response magnitudes and latencies of single- and multi-units varied with stimulus conditions, and multi-unit responses were similar to single unit responses. The mean peak firing rate for single neurons stimulated within the preferred location was estimated to be ~26 spikes/s. Simultaneous stimulation with a second probe outside the preferred location slightly decreased peak firing rates to ~22 spikes/s. When the non-preferred stimulus preceded the preferred stimulus by 10–500 ms, peak firing rates were suppressed, with greatest suppression when the non-preferred stimulus preceded by 30 ms (~7 spikes/s). The mean latency for single neurons stimulated within the preferred location was ~23 ms, and latency was little affected by

paired stimulation. However, when the non-preferred stimulus preceded the preferred stimulus by 10 ms, latencies shortened to ~16 ms. Response suppression occurred even when stimuli were separated by long distances spatially (nonadjacent digits) and temporally (500 ms onset asynchrony). Facilitation, though rare, occurred most often when the stimulus onsets were within 0-30 ms of each other. These findings quantify spatiotemporal interactions and support the hypothesis that area 3b is involved in widespread stimulus integration.

Introduction

As tactile object recognition depends on the integration of information from different parts of the hand, it is logical to presume that neurons somewhere in the somatosensory system integrate information from locations across the hand. Primary somatosensory cortex (S1) is the first cortical level at which this integration could take place. In primates, anterior parietal cortex can be subdivided into somatosensory areas 3a, 3b, 1, and 2; with area 3b, the homologue of S1 in other mammals (Kaas, 1983), as the first site for processing tactile information. We selected owl monkeys because the cortical area of interest, area 3b, is not buried in a central sulcus in this primate, and the somatosensory cortex has been well studied (e.g., Merzenich et al., 1978; Cusick et al., 1989; Garraghty et al., 1989; Nicolelis et al., 2003). An evaluation of the extent of this integration in area 3b is a critical step in determining how and where the somatosensory system mediates object perception and other abilities.

Do Widespread Spatial Interactions Exist in Area 3b?

Area 3b receptive fields in monkeys have been consistently described as restricted in size, usually confined to part of a single digit phalanx or palm pad (e.g., Sur, 1980; Iwamura et al., 1983; Sur et al., 1985; Pons et al., 1987; DiCarlo et al., 1998). Previous studies in several species have examined spatial and temporal response properties in primary sensory cortical areas, including area 3b, and there is good evidence for stimuli that are spatially distant to modulate neuron behavior, reviewed as follows. Stimuli "beyond the classical receptive field" are known to modulate responses of neurons in primary visual cortex to stimuli within the receptive field (e.g., Allman et al., 1985; Wang et al., 1995; Walker et al., 2000; Brown et al., 2003). Like the classical receptive field defined in vision research, the tactile minimal receptive field (mRF; e.g., Merzenich et al., 1983; Xerri et al., 1999), or the excitatory field to near-threshold stimuli, of the monkey hand can be surrounded by regions that, when stimulated, modulate responses within the mRF (e.g., DiCarlo et al., 1998; Mountcastle, 2005; Sripati et al., 2006). In S1 of rats, neuron responses are modulated by stimulating whiskers beyond the traditional receptive field of a primary whisker and immediately adjacent whiskers (e.g., Armstrong-James and Fox, 1987; Ghazanfar and Nicolelis, 1997, 1999; Moore and Nelson, 1998; Zhu and Connors, 1999), and even by stimulating the forepaw (Berwick et al., 2004). Studies in the forelimb representation of the somatosensory system in several species have examined effects of stimuli within the receptive field and at sites near, but outside of the excitatory receptive field of neurons in cortex (e.g., Mountcastle and Powell, 1959; Laskin and Spencer, 1979; Gardner and Costanzo, 1980a,b; Burton et al., 1998; DiCarlo et al., 1998, 2000, 2002; Greek et al., 2003; Sripati et al., 2006), thalamus (e.g., Jänig et

al., 1979; Canedo and Aguilar, 2000; Greek et al., 2003), and brainstem (e.g., Jänig et al., 1977; Canedo and Aguilar, 2000). Although the proximity of the second stimulus to the receptive field varies, the overall finding is that inhibition caused by the second stimulus is maximal at the receptive field center and decreases with distance from center. Similarly, human psychophysics (e.g., Schweizer et al., 2000; Braun et al., 2005) and evoked potential and magnetic field responses (e.g., Hoechstetter et al., 2001; Tanosaki et al., 2002a,b; Pilz et al., 2004) indicate that a second stimulus will interfere with the response to the first stimulus in a topographic manner, such that near stimuli have a greater effect than distant stimuli. We extended these studies by testing paired stimuli within and across digits on the monkey hand, to relate to findings in humans in which invasive studies are rarely performed.

How Might Temporal Factors Influence Spatial Interactions?

Previous work on area 3b has shown that after a single stimulus is presented within the mRF, there is an initial excitation peak surrounded by inhibition; over time that excitatory peak is replaced by inhibition (Sripati et al., 2006). These dynamics can shape the responses of neurons when stimulation is provided beyond the minimal receptive field. Temporal stimulus relationships may signal object relatedness and play a role in forming cortical topography and receptive fields (Xing and Gerstein, 1996; Wiemer et al., 2000). For example, Merzenich and colleagues (1988, 1995) found that increasing co-activation of the digits resulted in multi-digit receptive fields and concluded that receptive fields do not simply reflect anatomical connections, but are derived from a subset of inputs based on temporal correlations of activity. Similarly,

human fMRI showed that after simultaneous stimulation of digits 2, 3, and 4 for three hours, the S1 cortical representations for the co-activated fingers moved closer together (Pilz et al., 2004). Additionally, later testing for detection of tactile stimuli resulted in increased mislocalizations. When digits were stimulated asynchronously, the cortical representations moved apart and mislocalizations were reduced (Pilz et al., 2004).

To examine the effects of temporal stimulus relationships on neuronal response properties, we designed a modification of condition-test paradigms in which the conditioning stimulus is presented outside the minimal receptive field and the test stimulus is within or outside of the suprathreshold receptive field for a given neuron. We selected onset delays between the conditioning stimulus and the test stimulus based on studies in raccoons (e.g., Chowdhury and Rasmusson, 2003; Greek et al., 2003) and macaque monkeys (Gardner and Costanzo, 1980b; Burton et al., 1998) that involved similar condition-test paradigms. Condition-test paradigms have also been studied extensively in the rat whisker barrel system with wide-ranging intervals between the conditioning and test stimuli (e.g., Simons, 1985; Shimegi et al., 1999; Boloori and Stanley, 2006).

How Will the Current Study Extend Previous Studies?

In this study of single- and multi-unit response properties, we sought to determine the properties of the dynamic interactions that could result in such dramatic changes. To do so, we studied the immediate effects of simultaneous and asynchronous stimulation of adjacent and nonadjacent hand locations on neuron responses in area 3b in owl monkeys. We compared stimulation at paired locations within a single digit with stimulation at

locations on two separate digits to determine how the stimulus interactions depend on spatial topography. We sought to investigate whether interactions *within* a digit differ from interactions *across* digits, as the local connections within area 3b are denser distal-to-proximally within a single digit representation than across digit representations (Fang et al., 2002). Additionally, we presented the paired stimuli simultaneously and at selected temporal onset asynchronies to determine if temporal interactions influence the responses of area 3b neurons.

In our design, a conditioning stimulus is referred to as the "non-preferred stimulus" because this stimulus always evokes fewer spikes from the reference neuron than the "test" or "preferred stimulus". We presented tactile stimuli that indented the skin for 500 ms, followed by 2.0 s off of the skin, in blocks of 100-120 trials so that each stimulus had the potential to cause sustained activation. Then, we selected paired skin sites and delivered pulses simultaneously (0 ms delay) and at selected stimulus onset asynchronies of 10, 30, 50, 100, and 500 ms to study the effects of varying the temporal proximity of stimuli. Thus, the paired 500 ms stimuli variably overlapped in time. (For the 500 ms stimulus onset asynchrony condition, as the conditioning stimulus is lifting off of the skin, the test stimulus is contacting the skin. Depending on the spatial proximity of the stimuli, this conditioning stimulus may not affect the response to the test stimulus since the stimuli occur far apart in time.) Here, we consider that when the presence of a non-preferred stimulus affects the responses of one neuron to a preferred stimulus, a stimulus "interaction" occurs. The term "widespread interaction" can then be applied when the effects on the reference neuron occur when stimuli are presented widely separated in space or time. Thus, differences in response properties due to paired

stimulation with varying spatial and temporal parameters allow us to quantify spatiotemporal stimulus interactions.

Materials and Methods

The present study examines the effects on firing rate and latency of neurons in area 3b of owl monkeys (*Aotus trivirgatus*) when two 500 ms skin indentations were presented simultaneously or at stimulus onset asynchronies to adjacent or nonadjacent hand locations. One stimulus was within the "Response Field" and the other was within or outside of the Response Field of the reference neuron (see *Response Field* section).

Preparation for Recording

Two adult male owl monkeys (cases 1 and 2; each 1 kg) and one adult female owl monkey (case 3; 1.2 kg) were prepared for electrophysiological recordings in primary somatosensory cortex following procedures detailed previously (Reed et al., 2008). Monkeys 1 and 2 were part of a previous study related to spike timing correlations (Reed et al., 2008). All procedures followed the guidelines established by the National Institutes of Health and the Animal Care and Use Committee at Vanderbilt University. Each monkey was given a ketamine injection (10-30 mg/kg, intramuscular) for sedation during surgical preparations. Anesthesia was induced with 2-4% halothane gas and maintained with propofol (10 mg/kg/hr, intravenous) during surgery. Rectal temperature was monitored and maintained between 37-39°C with a servo-controlled heating pad. The monkey was secured in a stereotaxic device for surgery and throughout the experiment.

After anesthetizing the animal, paralysis was induced with 1-3 ml vecuronium bromide and maintained by intravenous vecuronium bromide (0.1-0.3 mg/kg/hr) mixed with 5% dextrose and Lactated Ringer's solution. Once paralyzed, animals were artificially ventilated with a mixture of N_2O: O_2: CO_2 (75: 23.5: 1.5) at a rate sufficient to maintain peak end tidal CO_2 at ~ 4%. Paralysis was induced to keep the hand stable during long stimulus blocks. Electrocardiograms (ECG) and electroencephalograms (EEG) were monitored to gauge depth of anesthesia. The skull and dura overlying primary somatosensory cortex were removed. The pneumatic inserter for the electrode array was set to a depth of 600 µm, so that electrode tips were expected to be within cortical layer 3. After the insertion of the electrode array, the opening was covered with 1% agar mixed with Ringer's solution to provide electrode stability and prevent desiccation. Following surgical procedures, supplemental anesthesia during recordings was provided by 0.3 mg/kg/hr propofol. Similar methods have been described elsewhere (Samonds et al., 2003; Xu et al., 2003). In one monkey (case 3), 1.2 mg/kg sufentanil was added to the Lactated Ringer's solution for slow infusion during the surgical procedures in order to stabilize anesthetic depth. Following delivery of this amount of sufentanil, the monkey was maintained under propofol anesthesia and vecuronium bromide paralysis without supplemental sufentanil during extracellular recordings. All monkeys were maintained approximately within sleep stage 2 during the recording experiments, as estimated by inspection of the EEG and ECG.

Stimulation Procedures

We focused on comparing neuron responses to paired stimulation on adjacent digits versus nonadjacent digits; however, we also collected responses to paired stimulation on adjacent and nonadjacent phalanges within a single digit. Stimuli were provided by two independent force- and position-feedback controlled motor systems (300B, Aurora Scientific Inc., Aurora, ON, CA). The lever arms of the motors were tipped with round Teflon probes 1 mm in diameter; thus, the stimulus probes represented a small contact surface. Stimuli consisted of square wave pulses that indented the skin 0.5 mm for 0.5 s, followed by 2.0 s off of the skin, repeated for 255-300 s (100 to 120 trials). We used the minimal ramp time allowed by the stimulation equipment, which had a length step response time of 1.3 ms. The long duration of the indentation allowed us to record phasic and sustained responses (Sur et al., 1984). Paired skin sites were selected for stimulation and the indentations were delivered simultaneously (0 ms delay) and at selected stimulus onset asynchronies of 10, 30, 50, 100, and 500 ms, with the conditioning stimulus preceding the test stimulus, to study the effects of varying the temporal proximity of stimuli. Single-site control stimuli were delivered to each of the sites prior to paired stimulation. These stimulus parameters were selected to analyze spatiotemporal effects on response properties of neurons in primary somatosensory cortex. For practical purposes, reference units were identified and probes were positioned so that one probe was inside and one probe was outside the minimal receptive field (mRF) of the reference neuron. The mRF was defined as the region of skin where a near-threshold light touch with a probe reliably evoked spikes from the recorded neurons. Procedures for mRF mapping have been published elsewhere (e.g., Merzenich et al.,

1978; Nelson et al., 1980), and our general procedures have been published (Reed et al., 2008). Receptive field mapping also helped locate electrodes as within and outside of area 3b in a manner that complemented our subsequent histological identification of area 3b. The fingernails were glued (cyanoacrylic) to Teflon screws fixed in plasticine to keep the hand in place during stimulus blocks. Adhesive was removed from the fingernails using acetone.

Data Acquisition

Recordings were made using the 10 x 10 "Utah" array and the Bionics Data Acquisition System (Blackrock Microsystems, Salt Lake City, UT). The signals on each channel were amplified by 5000 and band-pass filtered between 250 Hz and 7.5 kHz. The threshold for each electrode was automatically set for 3.25 times the mean activity and the waveforms were sampled at 30 kHz for 1.5 ms windows (Samonds et al., 2003).

Histology

Following data collection, animals were perfused with saline followed by fixative, and the brains were prepared for histological analysis as described previously (Jain et al., 2001). The cortex was flattened, frozen, and cut parallel to the surface at 40 µm. Sections were processed for myelin to aid in determining the electrode sites relative to the area 3b hand representation. (See Reed et al., 2008 for an example of the tissue quality that may be obtained using the 100-electrode array and a description of how electrode depths and locations are estimated.) We estimated electrode depth by tracking the appearance and disappearance of electrode tracks across serial sections.

Data Analysis

Spike Sorting

The details of the spike sorting procedures have been described previously (Reed et al., 2008). Recorded signals were sorted offline with an automatic spike classification program based on the t-distribution Expectation Maximization algorithm (Shoham et al., 2003) which is part of the data acquisition system. The recordings for a given stimulus block were sorted together to standardize sorting across recordings. We used a second spike sorter program, Plexon Offline Sorter (Plexon Inc., Dallas, TX) to verify the quality of unit isolation such that single units had refractory periods ≥ 1.2 ms; p values ≤ 0.05 for multivariate ANOVA related to cluster separation; and distinct waveform amplitudes and shapes when compared with other activity on the same electrode (Nicolelis et al., 2003). Single- and multi-units were categorized separately but grouped together for factor analysis. If multiple single units were collected from one electrode, all were included in the analysis, and at most only one multi-unit per electrode was included in the analysis. Typically, our multi-unit recordings were of multiple neuron clusters that could not be isolated into individual units, but the waveforms had typical neuron-like negative and positive deflections.

Peak Firing Rate

As described in Reed et al. (2008), spike trains were smoothed with a spike density function to determine peak firing rate using Matlab (The Mathworks, Inc., Natick, MA). A spike density function was produced by convolving the spike train from each

trial with a function resembling a postsynaptic potential specified by τ_g, the time constant for the growth phase, and τ_d, the time constant for the decay phase as:

$R(t) = (1 - \exp(-t/\tau_d)*\exp(-t/\tau_d)$.

Based on physiological data from excitatory synapses, τ_g was set to 1 ms (e.g., Mason et al., 1991; Moore and Nelson, 1998). We set τ_d to 5 ms (Mason et al., 1991; Moore and Nelson, 1998; Veredas et al., 2005) because the transient nature of the on and off responses in primary somatosensory neurons was excessively smoothed at larger values, particularly for cases in which stimuli were presented at stimulus onset asynchronies of 10 and 30 ms. For stimuli presented with onset asynchronies, we focused on responses that occurred within a response time window of 50 ms following the onset of the second stimulus; thus, the first stimulus acted as "conditioning stimulus" as used in many other studies (e.g., Gardner and Costanzo, 1980b; Chowdhury and Rasumusson, 2003; Greek et al., 2003).

For excitatory responses, the peak firing rate was determined as the maximum of the spike density function within the response time window, and the average baseline firing rate (calculated over a 500 ms window prior to stimulation onset) was subtracted from this value. This peak firing rate value was required to be greater than a threshold value, which was the average baseline firing rate plus two standard deviations of this baseline with a minimum value of 5 spikes/s. To determine if this value was significant, the nonparametric Mann-Whitney U test and the parametric Student's t-test with two tails were performed and results compared. The U test and t test resulted in the same categorizations of significance ($\alpha = 0.05$). If no excitatory response was detected in the response window, responses were examined for possible suppressive effects. Our criteria

for suppressive responses were average firing rates from the spike density function less than the average baseline firing rate below 1.65 times the standard deviation of the baseline, and this low firing had to be sustained for 10 ms or more. We used the average peak firing rate over 100 trials as our measure of interest because neuron responses in area 3b (for rapidly-adapting and slowly-adapting responses) tend to show an initial transient onset response, followed by a variable amount of firing suppression (e.g., Sur, 1980). Therefore, peak firing rate acts as a general measure of responsiveness that would not depend on the presence of sustained responsiveness to the stimuli and would indicate if the onset responses were influenced by the presence of the conditioning stimulus.

Response Latency

Response latencies were calculated using Matlab and determined from spike density function histograms as the initial time when the rate meets the half-height over the threshold value of the peak firing rate within the response time window (see above). The peak latency was calculated using the greater of the half-height or the threshold value. Since the data were not continuous, polynomial fitting of the spike density function was used to determine the time of the half-height. The value that was found at the least distance from the time of the peak and preceding the peak such that the rate values followed an increasing trend (upward slope towards the peak) was called the response latency. This method of determining latency is similar to measures that determine the width or duration of peaks in histograms (e.g., Tutunculer et al., 2006; Davidson et al., 2007). Latencies were only calculated when response criteria were met

for excitatory or suppressive responses (see *Peak Firing Rate*). Results were checked individually to ensure proper assignments.

Firing Rate Modulation Index

A modulation index was developed for Matlab based on methods used to describe multisensory integration (Stanford et al., 2005; Alvarado et al., 2007). The observed average response in the 50 ms window of interest during a given 2-site stimulation condition was compared with the distribution of expected average responses based on simple summation of the unit's response to the two stimuli presented individually. The expected distribution is based on the sum of two control values computed for every combination of trials, for 100 trials (100 x 100). From the distribution, 100 trials were randomly selected (without replacement) and averaged to give the predicted average response to 2-site stimulation. This was repeated 10,000 times to build a reference distribution of predicted responses, and the observed response was compared to this distribution, following the methods of Alvarado et al. (2007). The Kolmogorov-Smirnov test of normality was used for the observed responses (100 trials each) and the predicted responses (100 trials selected from 10,000 bootstrapped samples). When normality assumptions were met, paired t tests for matched samples were used; otherwise, nonparametric Wilcoxon signed rank tests were used ($\alpha = 0.05$). The modulation categories were "superadditive", "subadditive", "additive", "suppressive", or "no difference" from the response to the preferred single stimulus, similar to the methods of Stanford et al. (2005). "Superadditive" responses were greater than the predicted distribution by 2 times the standard deviation of the distribution, and "subadditive"

responses were less than the predicted distribution by 2 times the standard deviation of the distribution. Responses were classified as "suppressive" when the magnitude of the response to 2-site stimulation was less than that of the response to the preferred single stimulus. These categories were determined for individual neuron units across conditions and tallied.

Response Field

While the placement of our stimulus probes was guided by the previously determined mRF, we also defined large excitatory "Response Fields" with our above-threshold skin indentations with our stimulus probes. Since we recorded from multiple neurons simultaneously using a 100-electrode array, the stimulus locations did not always coincide with the receptive fields of each neuron. We defined an excitatory "Response Field" based on the neuron unit firing rates in response to suprathreshold tactile stimulation. We devised the classification of the Response Field to relate the neurons' receptive field to the stimulus locations in expectation that this categorization would help explain why condition-test paradigms in S1 variably caused suppression, facilitation, or no change in neuron subsets.

First, the peak firing rate of each unit was corrected by subtracting the average baseline firing rate of that unit. Then, the corrected peak firing rates of all of the neurons recorded from the array were averaged, resulting in a population average firing rate. When a single site on the hand was stimulated, that site was classified as *inside* that unit's excitatory Response Field if the corrected peak firing rate was greater than or equal to 3 times the standard deviation of the population firing rate. For a given neuron, responses

for all of the locations that were stimulated for a given experiment were compared and the maximum firing rate was found, with the location becoming designated as in the *center* of that unit's Response Field. When the unit firing rate did not meet the criteria to be categorized as *inside*, the location was considered *outside* of the Response Field. This Response Field is a firing-rate-based estimate similar to the concept of the receptive field (as measured by suprathreshold stimulation) and was used to examine and classify spatial integration. Although two sites were routinely stimulated together, the Response Field classification was based on the responses to stimulation at the single sites.

Data Selection and Classification

The data were classified based on several factors that were used in a statistical model to estimate the contributions of those factors to the observed latencies and firing rates. These factors were the temporal proximity of the stimuli, the spatial proximity of the stimuli, and the neuron's Response Field relationship to the stimuli.

Temporal Asynchrony Condition

For each stimulus block, two stimulation sites were selected and stimulated individually for comparison with paired stimulus presentations. The firing rates of individual neurons for stimulation at a "preferred" site were examined compared to paired stimulation at "preferred" and "non-preferred" sites. The "non-preferred" site was designated to be the skin location to which the neuron responded with the lower peak firing rate. The "preferred control" was assigned as the skin location to which the neuron responded with the higher peak firing rate. Results from stimulation at the preferred

control site alone represented the first level of the temporal condition factor for analysis. Paired stimuli were presented simultaneously (0 ms delay) and at selected stimulus onset asynchronies of 10, 30, 50, 100, and 500 ms, with the non-preferred stimulus preceding the preferred control stimulus, for a total of seven levels. See Figure 3-1A. The data were selected such that the preferred stimulus for a given neuron was presented second and the non-preferred stimulus was presented first.

Spatial Proximity Condition

The paired hand locations stimulated included adjacent hand sites distal digit 2 (dD2) with distal digit 3 (dD3) (monkey 1, 2, 3), dD3 with distal digit 4 (dD4) (monkey 2, 3), dD4 with distal digit 5 (dD5) (monkey 3), and distal thenar palm pad (dPTh) with center palm pad 1 (P1) (monkey 1). Nonadjacent hand locations included dD2 with dD4 (monkey 2), dD3 with dD5 (monkey 3), dD2 with dD5 (monkey 3), middle digit 1 (mD1) with dD3 (monkey 2), and dPTh with center palm pad 2 (P2) (monkey 1). From monkey case 2, stimuli within digit 2 including paired stimulation on adjacent phalanges dD2 and middle D2 (mD2), mD2 and proximal D2 (pD2), and nonadjacent phalanges dD2 with pD2. From monkey case 3, we recorded responses during paired stimulation on adjacent phalanges dD4 and mD4, and nonadjacent phalanges dD4 and pD4, as well as dD4 with center palm pad 3 (P3). Recordings with stimulation on adjacent phalanges were grouped for analysis as were those with stimulation on nonadjacent phalanges or palm pads. These stimulus conditions allowed us to have four levels of the spatial proximity condition, which we abbreviated as follows: adjacent digits= Adj D.; nonadjacent digits= NonA D.;

within a digit, adjacent phalanges = Adj Ph.; within a digit, nonadjacent phalanges = NonA Ph. See Figure 3-1B.

Response Field Condition

The relationship of the paired stimuli to the Response Field of the reference unit was included as a factor that could influence the firing rate and latency of the unit. We collected the following relationships under our stimulus conditions: 1) one probe in the center of the unit's Response Field, and the other probe also inside but not in the center "hotspot" of the Response Field, abbreviated as CN_IN; 2) both probes inside the unit's Response Field (but not in the center), abbreviated as IN_BOTH; 3) one probe in the center and one probe outside the Response Field, abbreviated as CN_OUT; 4) one probe inside the Response Field and one probe outside the Response Field, abbreviated as IN_OUT; and 5) both probes outside the Response Field, abbreviated as OUT_OUT. We never had an instance in which both stimulus probes were located in the center of a unit's Response Field. Thus, the Response Field factor had five levels. See Figure 3-1C.

Signal Isolation Category

We classified the data as single unit (SU) and multi-unit (MU) signal isolation based on our spike sorting criteria and included this two-level factor in the analysis to determine the influence on the response latency and peak firing rate. See Figure 3-1D.

Summary Statistics

Data from Matlab calculations for firing rate and latency measures were compiled and summarized in Excel to select units and conditions in which the non-preferred location was stimulated first in the series. Data for which the preferred location was stimulated first and the non-preferred location stimulated second were not included in this analysis of firing rate and latency. To be included in the summary analysis for firing rate and latency, units had to respond to at least one single-site stimulation condition and at least one dual-site stimulation condition. If a unit's response was suppressed in all stimulus conditions after the control stimulation so that no significant peak firing rates or latencies could be detected, then that unit was not included in the analysis. Only excitatory responses were included in this analysis. The data subset was imported into SPSS 17.0 (SPSS, Inc., Chicago, IL) for further statistical analysis. The alpha level for all significance tests was 0.05. We examined the raw data values for firing rate and latency, but for comparison across stimulus conditions, we also duplicated the data and normalized the values to those for the control stimulation for each unit in order to evaluate how the response properties changed when two sites were stimulated compared to the single preferred control site.

Across all conditions we performed the Kolmogorov-Smirnov 1-sample distribution test (SPSS 17.0) on the values we obtained for response latency and firing rate, and we determined that the distributions differed from the normal and Poisson distributions; therefore, we analyzed firing rate and latency using an extension of the Generalized Linear Model, which is becoming more widely used in psychological sciences (Tuerlinckx et al., 2006, review), known as the Generalized Estimating

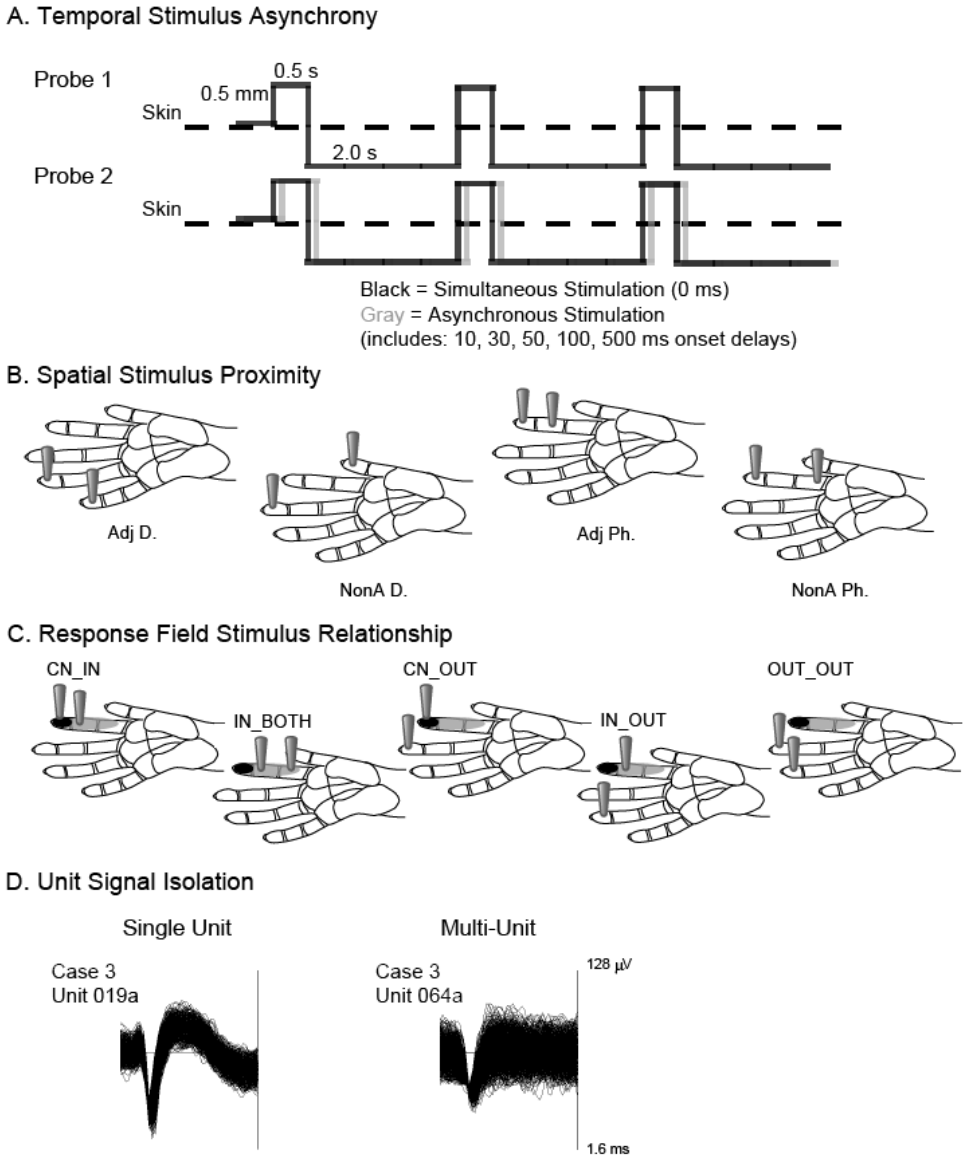

Figure 3-1. Schematic representations of data categories. A. The pattern of stimulation is depicted by solid lines indicating the duration the stimulus probe indents the skin (0.5 s), the depth of indentation (0.5 mm), and the duration the stimulus probe is off of the skin per stimulus cycle (2.0 s). Paired stimulation, indicated by the schematics of Probe 1 and Probe 2, may be simultaneous or asynchronous. To depict asynchronous stimulation generally, the gray solid line representing Probe 2 is shifted relative to the black solid line. The two probes are presented to different skin sites on the hand; however, the schematic depicts the overlap in contact time of the stimuli presented via Probe 1 and Probe 2. B. The spatial stimulus relationships were divided into 4 categories. Locations of the two stimulus probes on schematics of the owl monkey hand illustrate the proximity category. Scale bars on hand diagrams are 1 mm. Adj D. = adjacent digits (or palm pads); NonA D. = nonadjacent digits (or palm pads); Adj Ph. = adjacent phalanges; NonA Ph. = nonadjacent phalanges. C. The Response Field category is determined by the unit's Response Field relative to the stimulation location. Black shading on schematics of the owl monkey hand indicates the center of the Response Field for a hypothetical unit. Gray shading on the hand indicates locations inside the Response Field, but outside the center "hotspot" for the hypothetical reference unit. The locations of the two gray probes indicate the location of the stimulation relative to the Response Field for each Response Field category. D. Data were also classified by the quality of the signal isolation into single units or multi-units. Examples of each unit type are shown from monkey case 3. The trace window for each unit type shown spanned 128 µV and 1.6 ms.

Equations approach (e.g., Liang and Zeger, 1986; Zeger and Liang, 1986). We specifically employed Generalized Estimating Equations because this method estimates the contributions of multiple factors resulting in the observed responses and is able to take into account the presence of correlated data in the sample, unlike other methods which require that observations are independent. This analysis has fewer assumptions regarding the data distribution than parametric analysis of variance (e.g., Liang and Zeger, 1986), and while it accounts for the correlated data, it does not specify the within-subject effects (Tuerlinckx et al., 2006, review). Both the firing rate and latency data were better fit by a gamma distribution function than the normal distribution, and the Generalized Estimating Equations analysis using SPSS allowed us to select the gamma distribution with a log link function (e.g., Hardin and Hilbe, 2003) as the model distribution.

We used this approach on our peak firing rate and response latency data sets to estimate the sources of variance related to the temporal stimulus condition, the spatial proximity of the stimuli, and the Response Field relationship of the neuron unit subjects. In our case, neuron properties were measured across the temporal conditions and therefore could be correlated within subjects (neuron units). A model was made for the dependent variable (response latencies or peak firing rates) and the effects of the between-subjects predictors are estimated by solving the generalized estimating equation based on the parameters provided. Thus, in these models, latency or peak firing rate acted as the dependent variable, the within-subject variable was the stimulation condition, while the predictor factors included: the temporal stimulation condition, the spatial proximity of stimuli (Adj D., NonA D., Adj Ph., NonA Ph.), the relationship of the

stimulus to the Response Field of the neuron unit, and the classification of the unit as a single- or multi-unit. Then we analyzed single unit data separately from multi-unit data in additional statistical analyses.

The model parameters for both latency and firing rate results were based on a gamma probability distribution with the log link function, a first-order autoregressive correlation matrix, and a robust model estimator. We tested other probability distributions including Poisson and Gaussian (normal); however, the gamma distribution with the log link fit the data best (according to data fitting and model goodness-of-fit tests). We tested possible working correlation matrix structures to determine which estimate of the dependency within the data resulted in the best fitting models. We used an autoregressive correlation matrix for the model because this incorporates the time dependence of the repeated measures, but we also tested other correlation matrix structures for the best fit (e.g., Hardin and Hilbe, 2003). We selected a robust model estimator rather than a model-based estimator because the robust model estimator is consistent even when the working correlation matrix structure is mis-specified (Hardin and Hilbe, 2003, p 30). We applied the Bonferroni correction for multiple comparisons. The Wald Chi-Square statistic was used to test the significance of the model effects resulting from the Generalized Estimating Equations analysis. The results of the Generalized Estimating Equations analysis provide estimated values to fit the observed data, and calculations to indicate the likely significance of the differences; therefore, the values reported in the Results are the predictions from the analysis. These predicted values did not differ greatly from the observed values and followed the same trends. See Supplemental Material for plots of the observed data values.

Results

We recorded from 100-electrode arrays implanted in layer 3 of anterior parietal cortex, primarily area 3b, of three anesthetized owl monkeys during stimulation on selected hand locations and analyzed the contributions of spatiotemporal stimulus properties to the observed response latencies and peak firing rates. Figure 3-2 depicts the placement of the electrode arrays in each of the three monkey cases as determined from patterns of myelin staining in sections of flattened cortex and from receptive field mapping during the recording procedures. Several electrodes recorded single unit activity in each monkey (45 electrodes in case 1 and 65 electrodes in both cases 2 and 3); however, not all single units responded significantly under each stimulus condition. Note, the numbers of single units reported for firing rate and latency are higher than the numbers of electrodes recording single units as more than one single unit could be recorded from the same electrode. The same units were not always maintained during the 1-3 days of recording. The numbers of units in each summary analysis are those studied for each stimulus condition. The numbers of units meeting the criteria for analysis were as follows: 19 single units (SUs) and 64 multi-units (MUs) from monkey 1; 44 SUs and 71 MUs from monkey 2; and 99 SUs and 71 MUs from monkey 3. Data from SUs and MUs were collapsed for summary analysis to determine statistical differences between SU and MU responses for peak firing rate and latency, and then these categories were analyzed separately. Typical response histograms of a single neuron are shown in Figure 3-3.

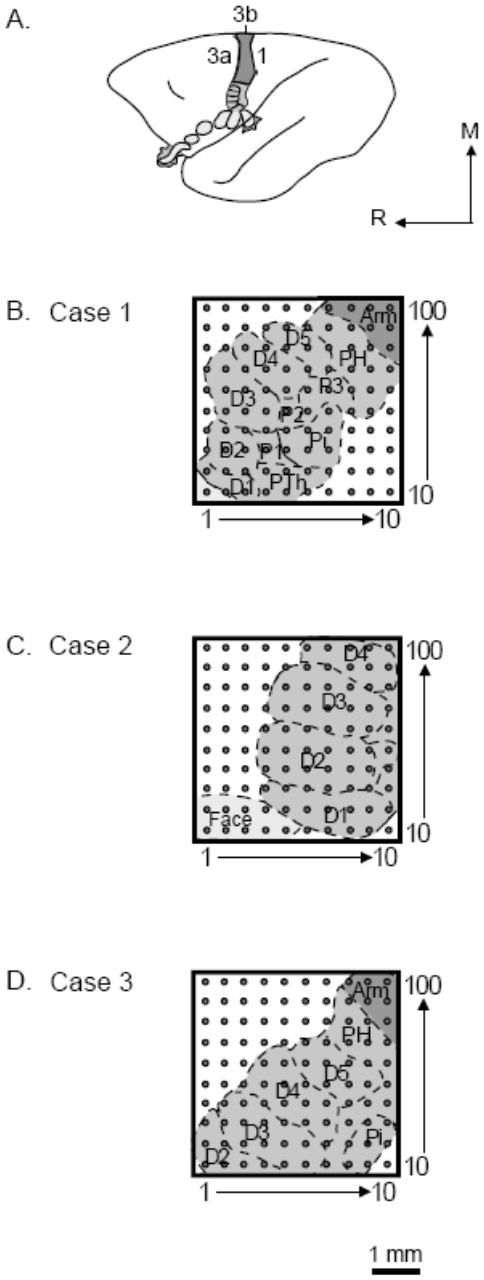

Figure 3-2. Schematic reconstructions show 100-electrode array placement in area 3b of three owl monkey cases. A. A schematic of the owl monkey brain is shown with the area 3b body representations highlighted as area 3a and area 1 neurons tended not to respond well to light tactile stimulation under the anesthetic conditions of these experiments. B-D. Electrode locations in each owl monkey case were approximated based on examination of myelin-stained sections of flattened cortex, in which area 3b stains more darkly than surrounding areas, with a myelin-poor septum indicating the border of the hand and face representation. Occasionally, myelin-poor septa can seen between digit representations in flattened cortex preparations, but in our cases we used the results of receptive field mapping during recording experiments to estimate the digit and palm pad representations. The placements of the 4 mm x 4 mm array in each case tended to cover a large part of the hand representation. The 1mm scale bar corresponds to the size of the array schematics for all three owl monkey cases.

Spatiotemporal Stimulus Effects on Peak Firing Rate and Response Latency

Peak firing rates varied with spatiotemporal features of the stimulus conditions. We collected 1385 SU firing rate responses and 2213 MU firing rate responses that met the inclusion criteria under the spatiotemporal stimulus conditions. These values are slightly higher than the number of latencies collected because firing rate responses could have a zero value when the firing rate did not differ from the spontaneous rate; however, latencies could not be given zero values. We collected 1098 SU response latencies and 1771 MU response latencies that met our inclusion criteria under the spatiotemporal stimulus conditions. The mean of the observed peak firing rates for the dataset was 28.70 spikes/s (SD 36.04), and the median of the peak firing rates was 14.95 spikes/s. The mean of the observed response latency for the dataset over all conditions was 20.67 ms (SD 6.31), and the median was 19.80 ms.

In Supplemental Figure S3-1 the group medians of the peak firing rates and latencies are plotted in three dimensions to show the distributions along the four main categories: temporal asynchrony, spatial proximity, Response Field relationship, and signal isolation (SU vs. MU). Peak firing rates tended to cluster based on these categories, with a tendency to be lowest when stimulation probes were both outside the Response Field (OUT_OUT), highest when both were located inside the Response Field (CN_IN and IN_BOTH), and intermediate when one stimulus probe was inside and one probe was outside the Response Field (CN_OUT and IN_OUT). Latencies tended to be longer when both stimuli were located outside the Response Field (OUT_OUT), but latencies were dispersed across the categories rather than falling into clusters.

We used Generalized Estimating Equations analysis on the full data set to determine the contributions of these categories on the variability of peak firing rate responses and response latencies. Our analysis indicated that several factors influenced the neuron response properties of peak firing rate and latency.

Signal Isolation Category

As one might expect, the multi-unit peak firing rates were significantly higher than those of single units (MU = 27.46 spikes/s ± 2.21; SU = 19.17 spikes/s ± 1.81; P = 0.002). Excitatory response latencies in a MU cluster were slightly but significantly shorter than those of SUs (MUs = 19.48 ms ± 0.26; SUs = 21.24 ms ± 0.36; P < 0.0005). The differences between single unit and multi-unit peak firing rates and latencies are plotted in Supplemental Figure S3-5, along with the effects of the spatiotemporal stimulus conditions on the population of single- and multi-units combined. Although our analysis indicated that single units and multi-units did not follow different trends, we separated single units from multi-units for the subsequent analysis to determine the effects on the variance of single unit responses and multi-unit responses separately (see Supplemental Tables S3-1-S3-4).

Temporal Asynchrony Category

For the temporal stimulation condition, peak firing rates were suppressed by co-stimulation with a non-preferred stimulus compared to stimulation by the preferred control stimulus alone (see SU results in Figure 3-4A; combined results in Supplemental

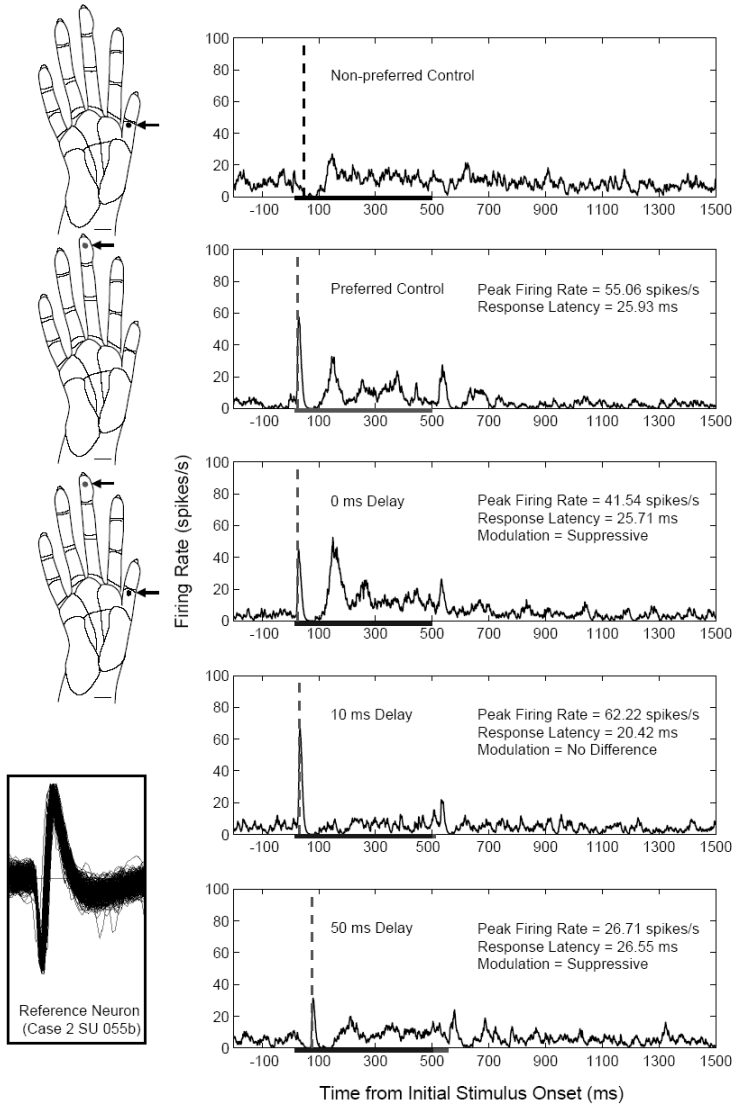

Figure 3-3. Example histograms from a single unit depict peak firing rate and latency changes across selected spatiotemporal stimulus conditions. Arrows point to dots on the diagrams of the owl monkey hand which indicate the stimulus locations on digit 1 and digit 3 for a series of recordings in monkey case 2. Inset. The trace of the single unit in each histogram is shown at the lower left corner in a trace window that spanned 128 μV and 1.6 ms. Histograms are shown for the neuron's responses when the two locations stimulated individually, then for both locations simultaneously, and finally for two stimulus blocks in which the non-preferred, or conditioning, stimulus was presented at 10 ms and 50 ms before the onset of the preferred stimulus. Stimulation was presented in blocks of 100 trials. Histograms are smoothed by a spike density function as described in the *Methods*. Vertical dashed lines indicate when the latency was determined using the criteria described in the Methods. The duration for each stimulus was 500 ms, as indicated by the line on the x-axis; therefore, paired stimulation overlapped in time for all stimulus onset delays tested except for 500 ms (not shown). The measures we examined included the peak firing rate within 50 ms of the preferred stimulus onset and the associated latency of that response. The peak firing rates and response latencies following stimulation of the preferred location are given for each excitatory response. The firing rate modulation category is listed for examples of paired stimulation. While the 10ms delay resulted in an average peak firing rate value that was about 13% larger than the response during control stimulation alone, the analysis for firing rate modulation found that this difference was not statistically significant in this example.

Figure S3-2A). Significant decreases in peak response magnitudes compared to single-site control stimulation (SU = 26.11 spikes/s ± 1.15) occurred for all of the paired stimulation conditions at stimulus onset asynchronies as follows: 0 ms: SU = 22.04 spikes/s ± 1.08, P = 0.007; 10 ms: SU = 11.78 spikes/s ± 0.88, P < 0.0005; 30 ms: SU = 6.76 spikes/s ± 0.68, P < 0.0005; 50 ms: SU = 10.85 spikes/s ± 1.03, P < 0.0005; 100 ms: SU = 20.34 spikes/s ± 1.79, P = 0.033; and 500 ms, 15.10 ± 1.17, P < 0.0005. On average, peak firing rate responses of single units were suppressed by the presence of the non-preferred stimulus at all delays tested, with maximal suppression when the non-preferred stimulus preceded the preferred stimulus by 30 ms. Thus, peak firing rates indicate that stimulus information is integrated across time up to 500 ms, with strong effects when the non-preferred stimulus is presented between 10-50 ms before the preferred stimulus. Multi-units followed the same trend, and these data are presented in Supplemental Material.

In contrast to the results for peak firing rates, we found shortened response latencies occurred when stimuli were paired and presented simultaneously (SU = 21.55 ms ± 0.37; P = 0.003) or when the preferred (test) stimulus was presented at a 10 ms delay (SU = 15.64 ms ± 0.61; P < 0.0005) compared to single-site stimulation (SU = 22.89 ms ± 0.38), as shown in Figure 3-4B. Latencies in response to stimulations at onset delays of 30 ms (SU = 20.41 ms ± 0.91; P = 0.235), 50 ms (SU = 23.09 ms ± 0.58; P = 1.000), 100 ms (SU = 23.79 ms ± 0.47; P = 1.000), and 500 ms (SU = 23.83 ms ± 0.63; P = 1.000) were not significantly different from the latency during single-site stimulation (SU = 22.89 ms ± 0.38). Multi-units followed the same trend (see Supplemental

Material). Thus, latencies were reduced by paired stimulus presentations within 10 ms and did not show clear relationships to stimulus integration across time.

Relationship between response latency and firing rate. The shortened mean latency we observed when the non-preferred stimulus preceded the preferred stimulus by 10 ms compared to the latency in response to the preferred control stimulus alone (Figure 3-4B) appeared to conflict with the decreased peak firing rate in response to the 10 ms onset delay compared to the response to the preferred control stimulus alone (Figure 3-4A). To investigate this result further, we performed a Wilcoxon signed ranks test between matched samples such that the peak firing rate for each neuron was compared between the control stimulation condition and the condition in which the onset of the preferred stimulus was delayed by 10 ms relative to the onset of the non-preferred stimulus. We performed the same test for the response latency for each neuron in our data set. From the test of firing rate values, 294 values were negative differences and 127 values were positive differences (0 ties); therefore, the majority of firing rates decreased in the 10 ms delay group relative to the control group ($Z = -7.788$, $P < 0.0005$). From the test of latency values, 235 values were negative differences and 69 values were positive differences (0 ties); therefore most of the latencies were shortened in the 10 ms delay group compared to the control group ($Z = -10.503$, $P < 0.0005$). Thus, the summary results in Figures 3-4A and 3-4B reflect the response properties of the majority of the neurons in the dataset; however, some neurons responded differently. We determined the nonparametric Spearman correlation coefficient (ρ) to relate response latency with peak firing rates *paired for each* neuron across *all* of the spatiotemporal stimulus conditions. A

weak negative correlation existed between latency and peak firing rate ($\rho = -0.141$, $P < 0.0005$), such that latencies shortened as peak firing rates increased overall, as expected.

Spatial Proximity Category

Peak firing rates were generally suppressed by paired stimulation compared to single-site stimulation (Single-site: SU = 26.11 spikes/s ± 1.15; Adj D.: SU = 12.92 spikes/s ± 1.92, $P < 0.0005$; NonA D.: SU = 20.37 spikes/s ± 2.33, $P = 0.074$; Adj Ph.: SU = 7.94 spikes/s ± 1.08, $P < 0.0005$; NonA Ph.: SU = 15.53 spikes/s ± 1.90, $P < 0.0005$), with the greatest suppression when stimuli were presented to adjacent phalanges (Figure 3-4C). While latencies were slightly delayed when stimuli were presented to adjacent phalanges (Adj Ph.: SU = 24.23 ms ± 0.64) compared to single-site stimulation (Single-site: SU = 22.89 ms ± 0.38), this difference was not statistically significant ($P = 0.660$). However, latencies were slightly shortened when adjacent digits were stimulated (Adj D.: SU = 18.59 ms ± 0.69) compared to single-site stimulation (Single-site: SU = 22.89 ms ± 0.38; $P < 0.0005$). These spatially-dependent effects on latency indicate stronger facilitative effects (shorter latencies) between adjacent digits and stronger suppressive effects (longer latencies) between adjacent phalanges within a digit. The trends for both peak firing rates and latencies were mirrored by multi-units (see Supplemental Material). Thus, widespread integration of stimulus information from different parts of the hand was demonstrated by differences in peak firing rates in response to single-site stimulation compared to dual-site stimulations even when paired locations were nonadjacent digits. Response latencies were somewhat affected by the

spatial proximity of paired stimuli, and therefore also demonstrated some relationship to stimulus integration across the hand.

Response Field Relationship Category

The relationship of the location of the stimulation sites to the Response Field affected peak firing rates (Figure 3-4E), but did not affect latencies (Figure 3-4F). As may be expected, the peak firing rates were significantly lower when both stimuli were outside of the Response Field (OUT_OUT: SU = 3.72 spikes/s ± 0.49) compared to other conditions when one or both stimuli were inside the Response Field, as follows: IN_OUT: SU = 9.64 spikes/s ± 1.19; $P < 0.0005$; CN_OUT: SU = 14.60 spikes/s ± 2.48; $P < 0.0005$; IN_BOTH: SU = 39.56 spikes/s ± 6.50; $P < 0.0005$; and CN_IN: SU = 24.08 spikes/s ± 2.63; $P < 0.0005$. The highest firing rates were found when both stimuli were within the Response Field of the reference unit, and the responses in these two categories were not significantly different (IN_BOTH and CN_IN, $P = 0.272$). Similarly, there was no significant difference in firing rates when the Response Field was classified as IN_OUT compared to CN_OUT ($P = 0.713$). Overall, peak firing rates were lowest when both stimuli were outside the Response Field and highest when both stimuli were within the Response Field, and presenting one stimulus outside the Response Field reduced peak firing rates approximately 50%. When both stimuli were outside of the Response Field, the latencies were slightly longer (OUT_OUT: SU = 23.02 ms ± 1.06) than when both stimuli were inside the Response Field (IN_BOTH: SU = 20.05 ms ± 0.76), but this small difference was not statistically significant ($P = 0.228$). Thus, the Response Field relationship influenced peak firing rates but not latencies (and these results were also

found in multi-units as reported in Supplemental Material). We expected that the categorization of the Response Field relationship with the stimulation parameters would be related to the ways neurons integrate widespread stimulus information in time and space.

Since we recorded from multiple neuron units simultaneously using the 100-electrode array, we expected that not all of the neurons recorded under each condition would behave the same way, given the differences in Response Field relationships to the stimulus locations. For visualization of the activity patterns across the spatial extent of the electrode array under different stimulus conditions, Figure 3-5 shows color map plots of the peak firing rate values for single- and multi-units recorded from the 100-electrode array during a subset of the stimulus parameters for each block. Individual units had different changes in peak firing rates with each change in stimulation parameters. To address these individual changes and determine the population effects across spatiotemporal stimulation parameters, we calculated a modulation index for each unit across the levels of our temporal stimulation variable. For further treatment of spatiotemporal interactions, see Supplemental Material and Tables S3-5-S3-6.

Firing Rate Modulation Index

To further describe the effects of spatiotemporal stimulation on peak firing rate, we used a modulation index to categorize how the responses to the paired stimuli compared to the linear sum of the responses to both of the single sites alone. In this analysis, mean firing rate responses to each single-site stimulus alone were summed for comparison to mean firing rate responses to co-stimulation, as described in the Methods.

For these data, there was no significant difference between single- and multi-units (P = 0.948), so the results are plotted together. In total across the conditions, 51.1% (N = 1671 out of 3272) of the responses were classified as "suppressive"; 39.2% (N = 1283) of the responses were classified as "no difference"; 5.7% (N = 187) were classified as "superadditive"; and 4.0% (N = 131) were classified as "subadditive". We found no instances of "additive" modulation in which the response to paired stimulation was not statistically different from the linear sum of the two single-site responses. The counts for each modulation index category are shown in Figure 3-6, divided into the stimulation categories on the x-axis and grouped by the proximity of the stimuli in each panel. We collected fewer conditions for stimulation within a digit (N = 543, Adj Ph.; N = 389, NonA Ph.) compared to stimulation across two digits (N = 936, Adj D.; N = 1402, NonA D.); however, the majority of the responses under all conditions were "no difference" from the best control response and "suppressive" compared to the best control response. An interesting effect due to the temporal stimulation parameters appears prominent when reviewing the panels for stimulation on adjacent (Adj D.) and nonadjacent (NonA D.) digit pairs in Figure 3-6. As the stimulus onset asynchrony increases from 0 to 500 ms, the number of responses classified as "no difference" decreases, and the number of responses classified as "suppressive" increases.

We present the same data in a second way in Figure 3-7 in order to illustrate the findings based on percent of responses within each stimulation category. Suppression dominated the response modulation types averaged across categories (~59% for Adj D., ~50% for NonA D., ~50% for Adj Ph., and ~35% for NonA Ph.). But this effect was not found uniformly across the stimulus conditions, as also indicated by the counts in Figure

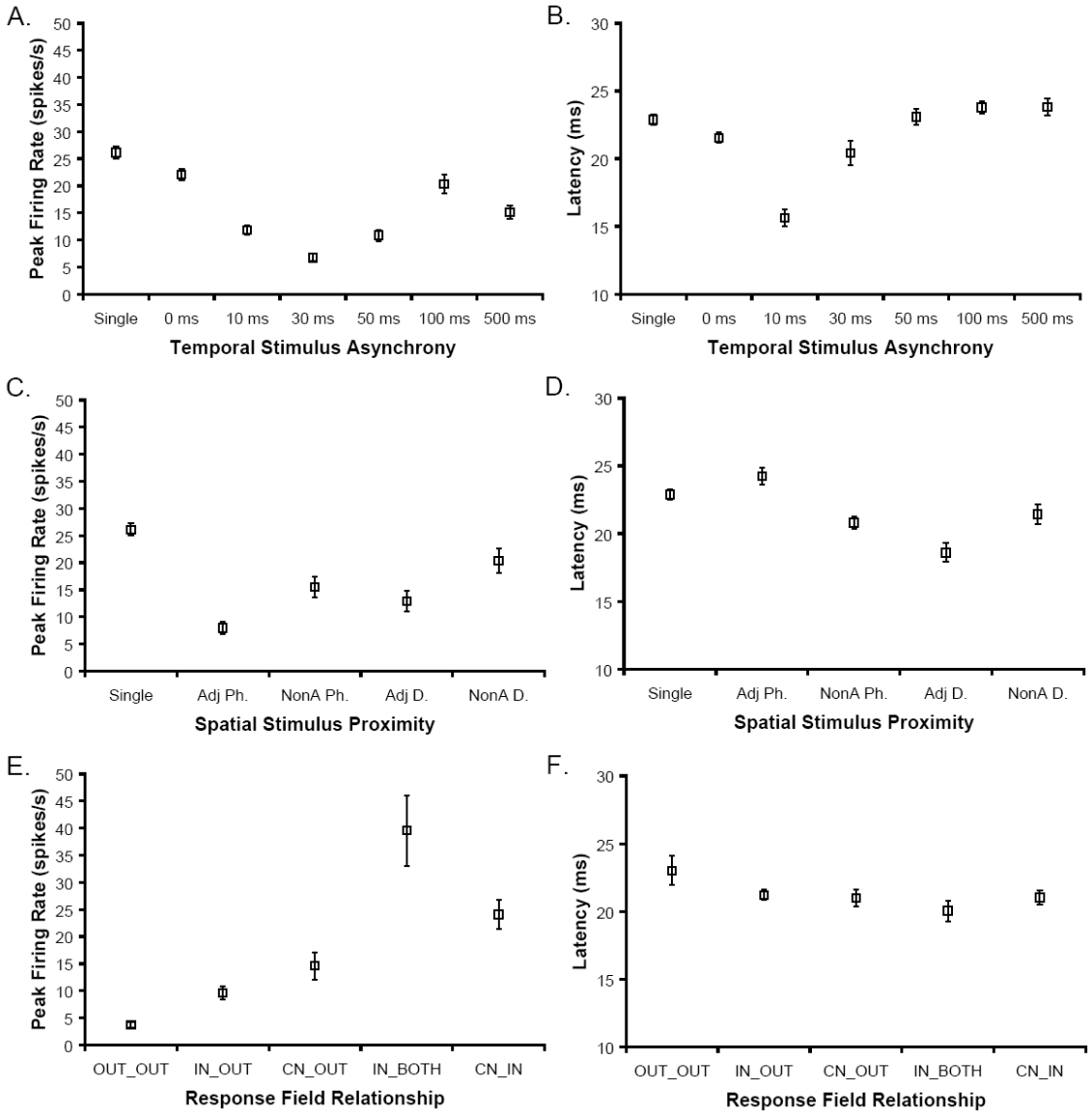

Figure 3-4. Main effects for peak firing rate and response latency from single units across spatiotemporal stimulus conditions. Estimated mean values from Generalized Estimating Equations analysis of 309 single units are shown with error bars representing ± 1 standard error of the mean. A. Means of peak firing rates (spikes/s) are plotted for each temporal stimulation category, comparing the preferred control stimulation (Single) to paired stimulation at 0, 10, 30, 50, 100, and 500 ms stimulus onset asynchronies. Dual-site stimulation suppressed peak firing rates relative to single-site stimulation. The 30 ms onset delay resulted in the greatest suppression. B. Means of response latencies (ms) plotted for each temporal stimulation condition show that 0 and 10 ms onset delays resulted in faster latencies than single-site stimulation. C. Means of peak firing rates plotted for each spatial condition in which the stimuli were presented on adjacent digits (Adj D.), nonadjacent digits (NonA D.), adjacent phalanges (Adj Ph.), or nonadjacent phalanges (NonA Ph.). Dual-site stimulation suppressed firing rates compared to single-site stimulation for all conditions except when NonA digits were stimulated. Peak firing rates were higher for stimulation on NonA D. than Adj Ph. D. Latencies were slightly faster for stimulation on Adj D. and NonA Ph. compared to single-site stimulation. E. Means of peak firing rates are plotted for each Response Field relationship. Firing rates were lower when the stimuli were outside of the Response Field (OUT_OUT) compared to all other conditions. CN_IN was not different from IN_BOTH or CN_OUT, and IN_OUT was not different from CN_OUT. F. Latencies were slightly, but not significantly longer when both stimuli were presented outside of the neuron's Response Field (OUT_OUT) compared to all other Response Field relationships.

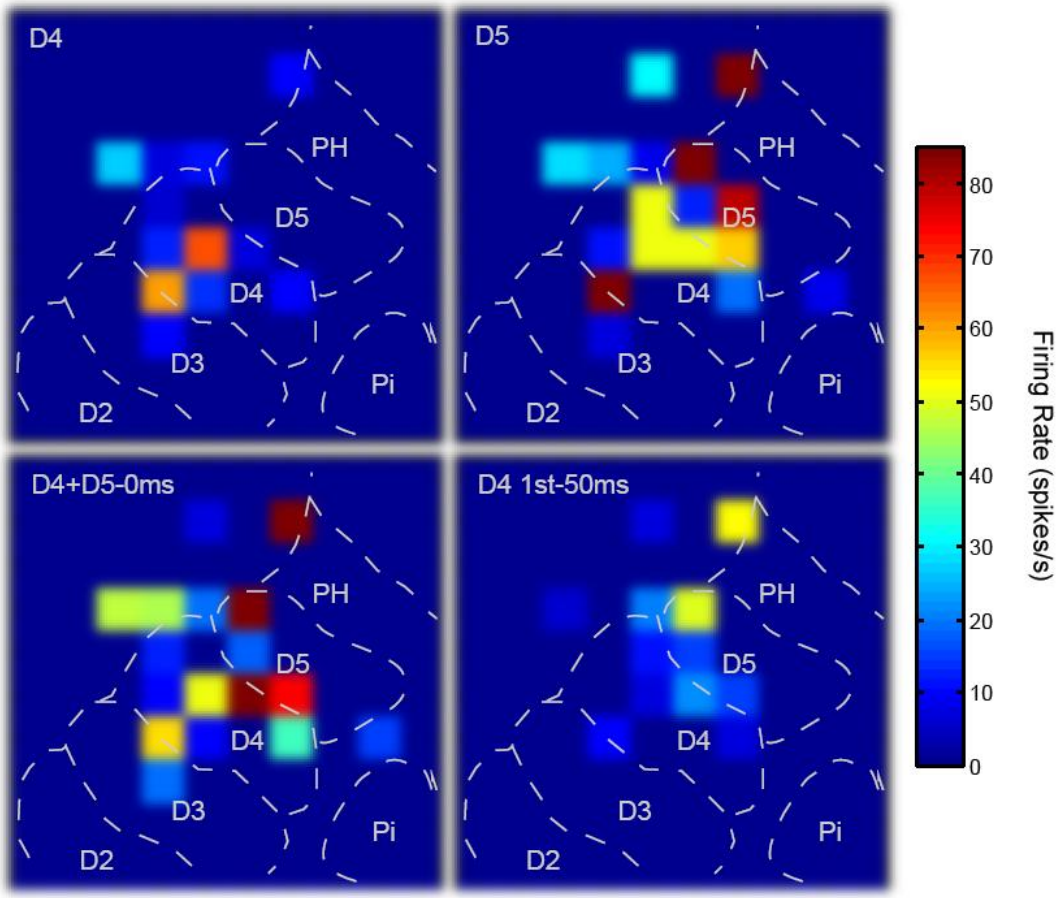

Figure 3-5. Peak firing rate values represented across the 100-electrode array under selected stimulus conditions. Color maps of the peak firing rate responses across the array were generated in Matlab with hot colors representing higher peak firing rates. Each square represents an electrode in the array and the peak firing rate value during the 50 ms response window. Electrodes from which no significant responses were obtained during the stimulations shown are indicated in dark blue (no squares). The dashed lines indicate approximate locations of the representations within area 3b in monkey 3. Upper Left panel shows the responses when a single site on distal digit 4 (D4) was stimulated for 100 trials. Upper Right panel shows the responses when a single site on the adjacent digit 5 (D5) was stimulated. Both single-site stimulation conditions show that the hotspots of activity occurred in the expected representations, but the activity could cross into adjacent representations and be non-uniform. In the Lower Left panel, both single site locations were stimulated simultaneously, resulting in a pattern of activity that one would not expect from simple summation across electrodes. The Lower Right panel shows the responses when D4 was stimulated 50 ms before D5 was stimulated, with the responses after D5 stimulation captured. The responding electrodes appear to show suppressed or unchanged responses.

3-6. For example, we found that when paired stimuli were presented simultaneously, most of the responses showed "no difference" compared to the best control site across each of the four stimulus proximity factors (~51% for Adj D., ~59% for NonA D., ~61% for Adj Ph., and ~69% for NonA Ph.). Facilitation was rare. Summing the proportions of total facilitation (from "subadditive" and "superadditive" categories), we found that stimuli presented on nonadjacent sites resulted in the highest proportion of facilitation (~11%); followed by stimulation within a digit on adjacent phalanges (~10%), adjacent site stimulation on separate digits (~8%), and stimulation within a digit on nonadjacent phalanges (~6%). However, when facilitation occurred ("subadditive" and "superadditive" categories), the stimuli were more likely to be presented at short stimulus onset asynchronies (0, 10, 30 ms) across each of the proximity factors (~81% for Adj D., ~81% for NonA D., ~79% for Adj Ph., and ~96% for NonA Ph.). Thus, using this response modulation index, we found that responses were suppressed in large proportions across the temporal stimulation and spatial proximity categories. In addition, spatiotemporal characteristics of stimulus presentations influenced the proportions of neurons showing "no difference", "suppression", and "subadditive" and "superadditive" facilitation of firing rate when two sites were stimulated compared to the sum of the rates when each site was stimulated separately.

The proportion of SU and MU neurons falling into the response modulation categories of "suppression", "no difference", "subadditive" facilitation, and "superadditive" facilitation were similar across the relations of the stimulation locations to the neurons Response Fields (Figure 3-8). The response modulation types were distributed across the Response Field categories such that no one category contained the

majority of any one response modulation type. Neurons that responded with facilitation, for example, did not fall into one specific category. The response categories of "suppression", "no difference", "subadditive" facilitation, and "superadditive" facilitation were similarly distributed across the Response Field categories.

Discussion

We examined peak firing rate and excitatory response latency during stimulation conditions that varied in spatiotemporal characteristics in order to quantify how neurons in primary somatosensory cortex integrate information from paired stimuli presented inside and outside their receptive fields at various stimulus onset asynchronies. The ranges of stimulus onset asynchronies along with the stimulus pairings on locations within single digits and across digits have not been reported previously, nor has the categorization of the Response Field been applied to extracting the contributions of stimulus properties to the response properties. The hypothesis that both spatial and temporal stimulus properties shape responses to paired stimuli was supported and the intricacies of the effects were explored. As predicted, we found that peak firing rate and latency were affected by the spatial and temporal stimulus parameters, but some of the effects were unexpected, including how far in space and time paired stimuli interact to influence neuron responses. Our results are consistent with those from previous studies, but we provide new information regarding spatiotemporal stimulus integration. Here we treat each aspect of the analysis individually, and then discuss the possible mechanisms that mediate the effects and the functional implications of the results.

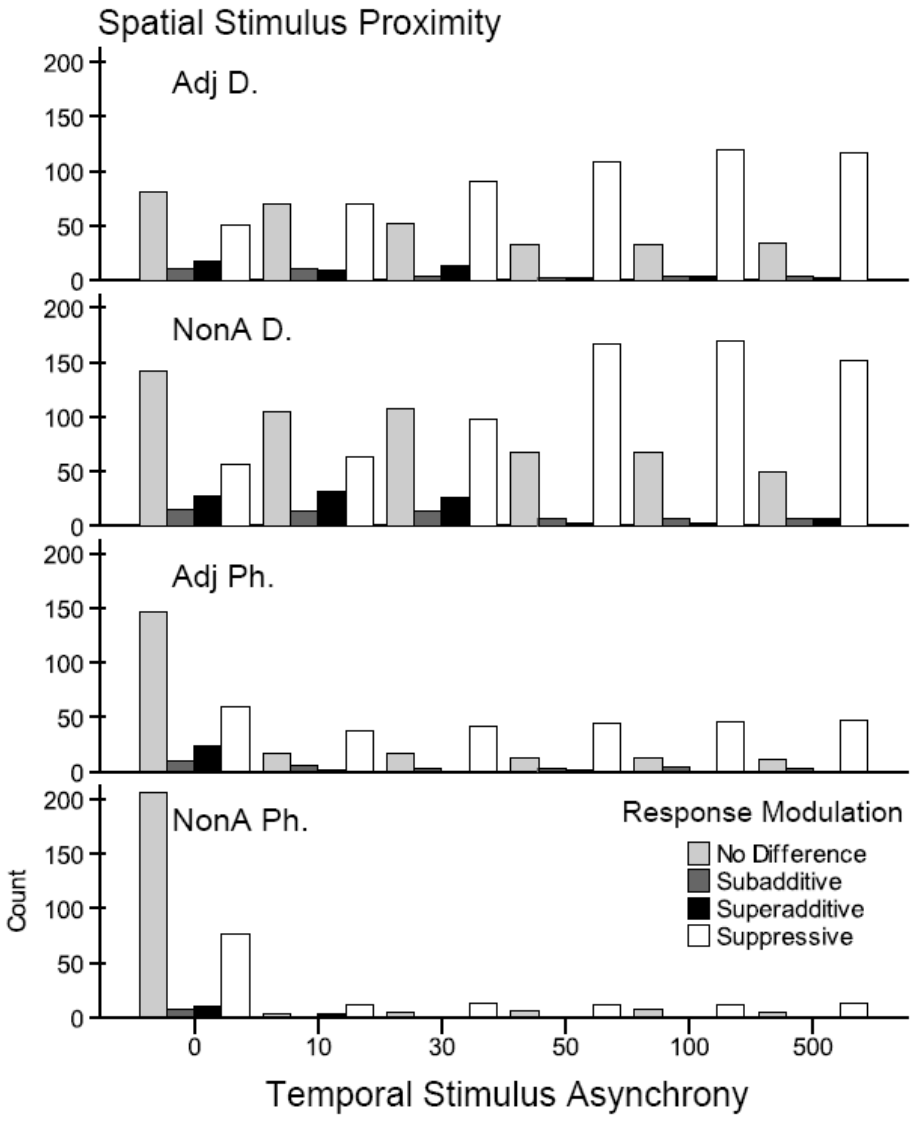

Figure 3-6. Total counts of firing rate modulation classes categorized by spatial and temporal stimulation parameters. Individual bar shades indicate the classes of firing rate modulation in response to paired stimulation which occurred in these data: "No Difference" compared to the response to the preferred control, "Subadditive" compared to the summation of the responses of both controls, "Superadditive" compared to the summation of the responses of the controls, and "Suppressive" compared to the response to the preferred control. The types of paired stimulation conditions are grouped on the x-axis referring to the stimulus onset asynchronies from 0 to 500 ms, in which the preferred stimulus was always presented after the non-preferred stimulus. The panels show the total counts of these categories for each of the four tested stimulus proximity categories. Fewer recordings were made with paired stimuli within a single digit (Adj Ph., NonA Ph.). Suppression and no difference compared to the preferred control stimulation dominate the modulation classification types. Note the pattern such that many responses are classified as "no difference" during stimulation at short stimulus onset delays (0-30 ms) and there are fewer at longer delays (50-500 ms). Responses classified as "suppressive" show the reverse effect, particularly in the panels for adjacent and nonadjacent digit stimulation conditions. Facilitation (subadditive, superadditive) occurred less often, but was predominantly found when the delays were short (0-30 ms).

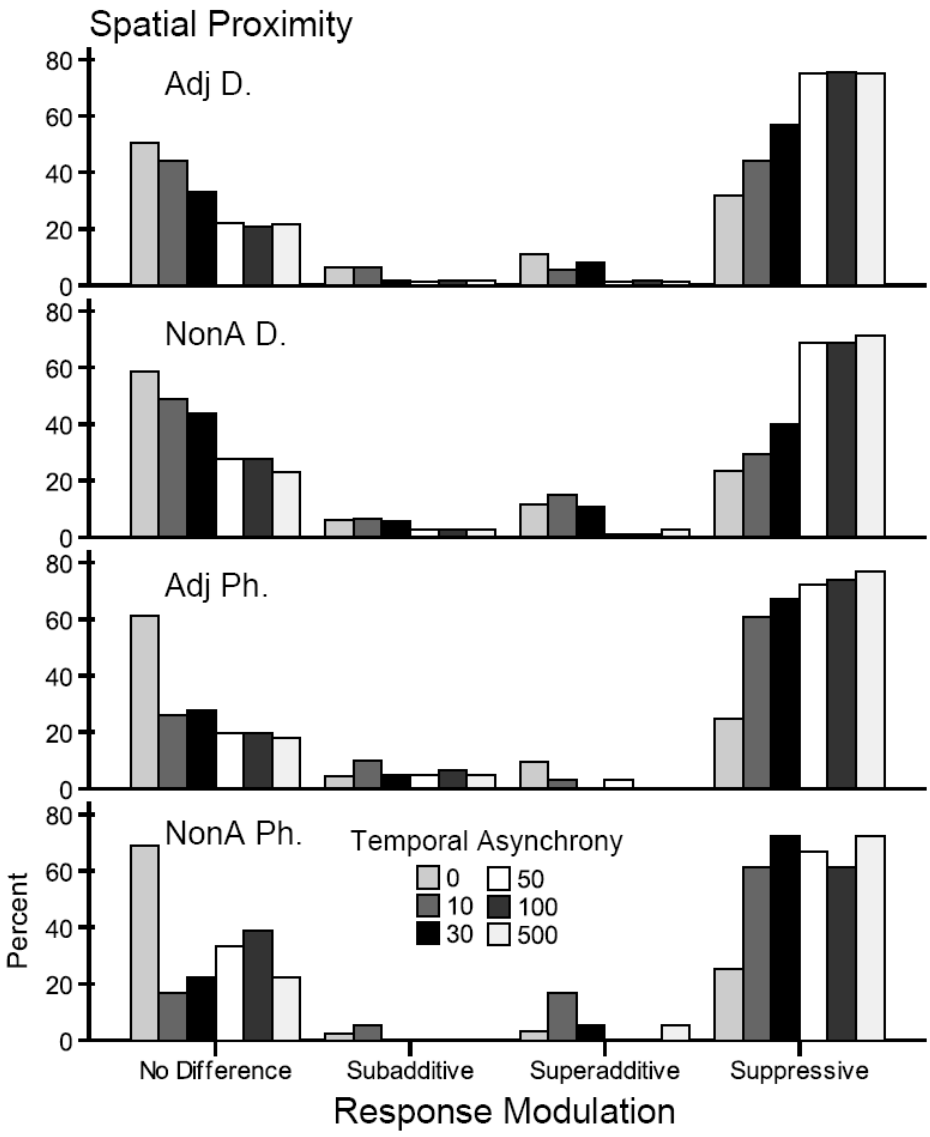

Figure 3-7. Percentages of response types for firing rate modulation categorized by spatial and temporal stimulation parameters. Four classes of firing rate modulation in response to paired stimulation occurred in these data: "no difference" compared to the response to the preferred control, "subadditive" compared to the summation of the responses of both controls, "superadditive" compared to the summation of the responses of the controls, and "suppressive" compared to the response to the preferred control; and these are displayed on the x-axis. Individual bar shades indicate the paired stimulation type referring to the stimulus onset asynchronies in which the preferred stimulus was always presented after the non-preferred stimulus. The panels show the total counts of these categories for each of the four tested stimulus proximity categories. Note that fewer recordings were made for the categories stimulating within a single digit (Adj Ph., NonA Ph.). Percent on the y-axis refers to the percentage of occurrences of each response type category, calculated within each panel for the four proximity categories. This view of the same data from Figure 3-6 shows that when stimuli were presented at short delays (0-30 ms), response types tended to be "no difference" and "facilitative" (subadditive, superadditive). At these short delays, paired stimuli presented within a single digit (Adj Ph., NonA Ph.) were suppressive modulators of firing rate in greater proportions than when paired stimuli were presented on adjacent or nonadjacent digits.

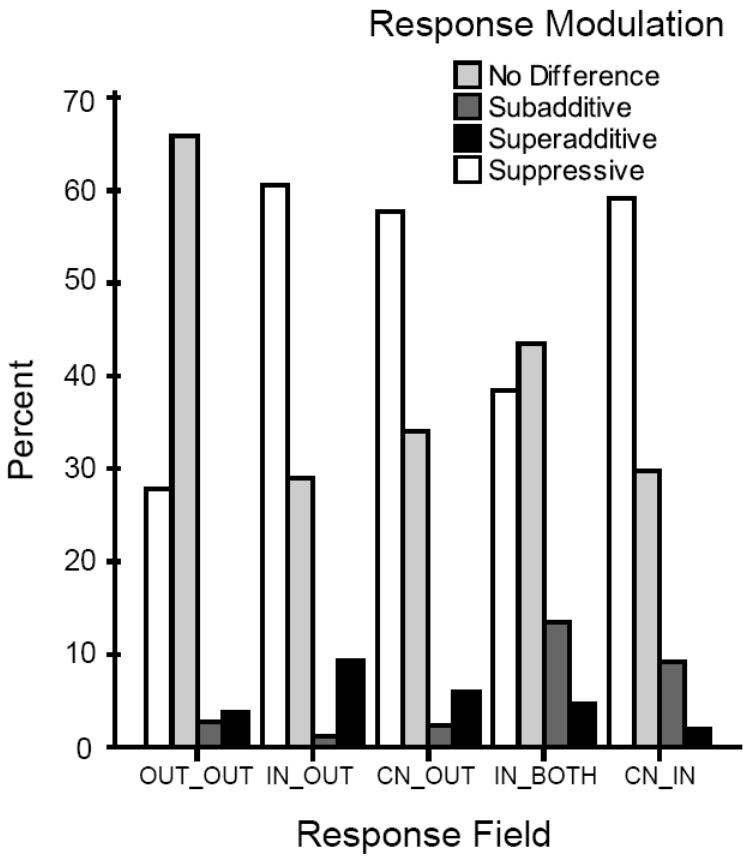

Figure 3-8. Percentages of response types for firing rate modulation categorized by Response Field relationships. The Response Field categories are shown on the x-axis. On the y-axis, the percentages of occurrences of the four response classes of "no difference", "subadditive", "superadditive", and "suppressive" were determined within each Response Field relationship category. The response classes were distributed across the Response Field categories rather than grouped within the categories.

Response Field Mapping and Cortical Topography

The first step in our analysis of the data from each monkey was to reconstruct the location of the electrodes in the array relative to the hand representation. This was done based on histological reconstruction from myelin stained sections of flattened cortex, minimal receptive field mapping data, and the classification of the Response Field based on the mechanical stimulation. Locations of multi-digit receptive fields based on minimal receptive field mapping helped us to draw approximate borders between representations. Our classification of the excitatory Response Field was based on neuron firing rate to suprathreshold stimuli. While minimal receptive fields studied with near-threshold stimuli have been described as small and localized within a single digit, the suprathreshold Response Fields we characterized can be large, often encompassing different digits. The idea that primary somatosensory cortex, area 3b, responds only to small and discrete body locations is now supplemented by a growing awareness of how stimulation "beyond the classical receptive field" influences neuron responses (e.g., Clark et al., 1988; Nicolelis et al., 1998; Chen et al., 2003; Friedman et al., 2008; Reed et al., 2008). The inclusion of separate digits within the Response Field indicates that the large receptive fields are not simply artifacts caused by the spread of deformations in the skin. Since near-threshold stimuli are commonly used to map minimal receptive fields in the somatosensory system, small receptive fields usually contained within a single digit have been primarily reported within area 3b. We used mechanical stimulation that indented the skin 0.5 mm, and this stimulus would be suprathreshold for some neurons; therefore, two-digit receptive fields may not be surprising, even for single neurons. Ours is not the first report of receptive fields encompassing multiple digits. For example, Tremblay et al.

(1996) reported 59 out of 96 single neurons recorded from area 3b in macaque monkeys had single digit receptive fields, which was a higher proportion of single digit receptive fields than found in areas 1 and 2. There may be some differences when our study compared with others which use traditional receptive field mapping with near-threshold stimulation due to our naming conventions regarding the "center", "inside", and "outside" of the Response Field characterized by suprathreshold stimulation. Our study may have revealed fewer "surround" effects than would be reported using near-threshold measures of the receptive field and suprathreshold stimulation outside the minimal receptive field. Finer mapping of receptive fields or stimulating a specific set of several locations across the hand may reveal even more spatiotemporal interactions and increase the specificity of the effects.

While we do not presume that these approximate topographic maps are permanent, we did not specifically test how the topography may or may not be affected by the passive mechanical stimulation employed in this experiment. We had reason to believe that in our anesthetized preparation with passive stimulation, the topography of area 3b would not change significantly due to the spatiotemporal stimulation (e.g., Darian-Smith, 2009), and that stimuli need to be behaviorally relevant (Clark et al., 1988; Xerri et al., 1999; Pilz et al., 2004) or applied for extended periods of time (Kalisch et al., 2007) in order to cause the cortical maps to reorganize. While we applied stimuli for extended periods of time, the locations to which the stimuli were applied varied throughout the experiment. The basic techniques we applied could be used to extend the study to investigate changes in cortical topography due to spatiotemporal stimulation.

Spatiotemporal Contributions to Peak Firing Rate and Response Latency Changes

Our analyses support the hypothesis that spatiotemporal interactions modulate response magnitudes during paired stimulation (Supplemental Tables S3-1, S3-2 - S3-5). Notably, these results indicate that presentation of a conditioning stimulus affects the response to a test stimulus that may be presented far apart in space (nonadjacent digits) and time (50-500 ms), and we examined the effects of paired stimulus presentation when stimuli were presented closely in space (within the same digit) and time (simultaneously to 30 ms stimulus onset delays). Our results are consistent with our premise that widespread spatiotemporal stimulus interactions occur in area 3b, and these results quantify the relationships of specific spatiotemporal stimulus characteristics to neuron response properties. We added a new level of analysis in which we related the neuron's Response Field to the location of the paired stimulation. As expected, the peak firing rates differed among these categories such that when both probes were outside the Response Field (OUT_OUT), the peak firing rate was low; and when both probes were inside the Response Field (CN_IN, IN_BOTH), the peak firing rate was much higher (Figure 3-4E). Using this categorization, we were able to detect the interaction of this factor with the other prediction factors of temporal and spatial stimulus proximity (Supplemental Tables S3-1- S3-2, and Supplemental Figure S3-6). These trends include the suppression of peak firing rates in general by a preceding conditioning stimulus, particularly when test stimuli within the neuron's Response Field were presented after a 30 or 50 ms delay. Co-stimulating adjacent phalanges resulted in strong suppression of the peak firing rate across all Response Field relationships when the conditioning stimulus was presented 30 or 50 ms ahead of the test stimulus. Overall, stimulating

nonadjacent digits resulted in less suppression, particularly when one stimulus was inside and the other was outside the Response Field. Suppression of the response peak was found when the stimulation locations were close spatially (within a digit) or both within the neuron's suprathreshold receptive field. The suppression was lessened (or more facilitation was present) when stimulation locations were distant (nonadjacent digits) and the conditioning stimulus was located outside the neuron's Response Field.

The influences of the relationship of the stimulation sites to the Response Field on response latencies were mostly predictable. Paired stimuli outside the Response Field resulted in the longest latencies and paired stimuli inside the Response Field resulted in the shortest latencies (Figure 3-4F). The response was primed for paired stimulation within a single digit across all of the Response Field categories, and also for paired stimulation on adjacent digits when the conditioning stimulus was within the neuron's Response Field. This indicates a facilitative effect specific for when the stimulated locations are close spatially or both within the neuron's suprathreshold receptive field. In these situations in which latencies are shortened, excitatory drive must outweigh the "in-field inhibition" (e.g., Mountcastle and Powell, 1959; Jänig et al., 1979; Gardner and Costanzo, 1980a,b; DiCarlo et al., 1998; Sripati et al., 2006; Helmstaedter et al., 2009) and lateral inhibition effects (e.g., Hicks and Dykes, 1983; Chowdhury and Rasmusson, 2003; Helmstaedter et al., 2009) that depress firing and instead allow the increase in spike rate to occur a few milliseconds quicker than when the conditioning stimulus is not present.

We found the maximal suppression of firing rates when stimulus onsets were presented 30-50 ms apart (Figure 3-4A, Supplemental Figure S3-2A), and this coincides

well with results from other studies. Condition-test intervals resulting in maximum suppression in S1 cortex were 10-30 ms for adjacent whisker stimulation in rats (Moore et al., 1999, review) and 20-40 ms for adjacent digit stimulation in raccoons (Greek et al., 2003). Within the large receptive fields on the arm in awake macaque monkeys, Gardner and Costanzo (1980b) found maximum suppression intervals of 10-20 ms using air jet stimulation (mostly to hairs). Our suppressive effects for tactile stimulation on paired locations within a digit and across separate digits, rather than on adjacent whiskers or within larger receptive fields, are most similar to the values found for adjacent digit stimulation in raccoons (Greek et al., 2003).

We expected that latencies would be generally lengthened by co-stimulating digits with varying spatiotemporal stimulus parameters as firing rates were typically reduced. Instead, response latencies decreased compared to single-site stimulation on the preferred location when the two stimuli were presented simultaneously or when a conditioning, non-preferred stimulus preceded the test stimulus by 30 ms or less. The shortest latencies occurred when the conditioning stimulus preceded the test stimulus by 10 ms. This result occurred across the spatial categories of stimulus proximity and the relationship of the Response Field to the stimuli (Figures 3-4B, Supplemental Figure S3-2B). Latencies were longer when the test stimulus was preceded by a conditioning stimulus by more than 30 ms, but most latencies were not significantly longer compared to the latency when the preferred site was stimulated alone (Figures 3-4B, Supplemental Figure S3-2B). Boloori and Stanley (2006), who used stimulation of pairs of whiskers in rats to examine the spatiotemporal response properties in S1 neurons (in layers 2/3 and 4), found that the conditioning stimulus increased the latencies of the test responses, and they did not

describe neurons with shortened latencies. In addition, Boloori and Stanley (2006) found that response latency was longer than baseline for short interstimulus delays but recovered to baseline as the delay lengthened. Our finding that the shortest latencies occur when stimuli are presented within 10 ms of each other demonstrates a facilitative effect in which the response to conditioning stimulus, which is often subthreshold, facilitates the response to the preferred stimulus. The facilitative effect peaked when the conditioning stimulus preceded the test stimulus by 10 ms and decreased in strength when the delay increased to 30 ms. Stimuli presented farther apart in time had insignificant effects on response latencies.

Latencies were shortened when paired locations were stimulated on separate digits compared to paired locations within a single digit (Figure 3-4D). Co-stimulating adjacent digits resulted in the shortest latencies, and co-stimulating adjacent phalanges within a single digit resulted in the longest latencies. The result from stimulating adjacent digits is similar to the finding in the superior colliculus of cats that multisensory stimulation shortens response latencies of neurons compared to the preferred unisensory stimulus (Rowland et al., 2007). Instead of providing two stimuli from different sensory modalities, our pairing tactile stimuli at short delays likely resulted in the summation of subthreshold inputs to allow the spiking threshold to be reached sooner.

Single Unit and Multi-Unit Data Comparisons

We reported results for single unit peak firing rates and latencies throughout this article and referred to similar trends in multi-unit data in the Supplemental Material. We found that the population means from multi-units resulted in higher peak firing rates than

those from single units (MU = 27.46 spikes/s ± 2.21; SU = 19.17 spikes/s ± 1.81; P = 0.002), and latencies from the multi-unit population were slightly shorter than those from single units (MUs = 19.48 ms ± 0.26; SUs = 21.24 ms ± 0.36; $P < 0.0005$). This appeared to be a shift in the multi-unit means compared to single units by recording signals that were averaged over multiple single neurons. This mean shift did not appear to influence the responses of multi-units to spatiotemporal stimulation differently than the responses of single neurons. Multi-unit results appeared to closely reflect the single unit results; therefore, we do not expect that single unit activity reflects an unusual subset of neurons sampled by the 100-electrode array. Using single electrodes that can be adjusted in depth may result in sampling bias as experimenters isolate the spikes from the largest neurons; however, our method used immovable electrodes. Thus, isolated single units were likely to be those that happened to be closest to the recording electrodes, all of which were within cortical layer 3. When we examined how the firing rate was modulated when paired sites were stimulated compared to the expected response (based on the sum of the responses to stimulation on each site alone), data from single units and multi-units were not significantly different ($P = 0.948$); and we analyzed those data together.

Relationship of Peak Response Magnitudes and Latencies

The relationship between response latency and peak firing rate (paired neuron-by-neuron) followed expectations overall, such that across all spatiotemporal stimulation conditions tested, latencies tended to shorten as firing rates increased ($\rho = -0.141$, $P < 0.0005$). Our findings differ somewhat from those of Boloori and Stanley (2006), who found a correlation of -0.76 ($P < 0.00001$) between latency and firing rate, such that

longer response latencies were strongly associated with firing rate suppression in rat S1 neurons (for the second whisker deflection in a stimulus pair). Because our summary analysis of the effects of the spatiotemporal stimulus conditions on response latency (Figure 3-4B) and peak firing rate (Figure 3-4A) did not consistently reveal the expected inverse relationship between latency and firing rate, we used Wilcoxon signed ranks tests for paired samples to specifically examine the condition in which the trend was clearly violated. When the non-preferred stimulus preceded the preferred stimulus by 10 ms, some neurons responded with shorter latencies but lower firing rates compared to the response to the preferred stimulus alone. However, in a subset of units, we found relative increases in firing rates when paired stimuli were presented within short delays (Figures 3-6, 3-7), so some underlying facilitative drive must exist to result in shortened latencies and firing rate increases compared to single-site stimulation on the preferred skin location. (See Figure 3-3 for one example neuron which shows an increased firing rate and shortened latency when the preferred stimulus is delayed 10 ms compared to the response to the preferred stimulus alone.) The underlying cause for the response diversity within our dataset is uncertain.

Spatiotemporal Contributions to Deviations from Simple Summation of Peak Firing Rates in Response to Paired Stimulation

Based on the analyses of firing rate modulation, small subsets of neurons were facilitated, primarily when stimuli were presented at the shortest delays of 0, 10, and 30 ms (Figure 3-7). Although the average value of the peak firing rate was maximally suppressed for 30 ms delays across all spatial parameters, this delay also resulted in response facilitation in a subset of neurons; and particularly for conditions in which

stimulation occurred on separate digits. Additionally, we found that with increasing stimulus onset asynchronies, peak response suppression increased (Figure 3-6). Even at 100 and 500 ms delays, the instances of suppression were still high, particularly for stimulation on adjacent and nonadjacent digits. Studies with condition-test paradigms typically do not use intervals as long as 500 ms, as they tend to use stimuli that are shorter in duration than ours. At their longest interval tested of 260 ms, Boloori and Stanley (2006) found that test responses had not fully recovered to control levels. Our stimuli may have been capable of interacting over such large time intervals because the stimulus duration was long (500 ms) and the 0.5 mm indentation was suprathreshold stimulation for a subset of neurons; therefore, our stimuli may recruit more neurons and activate them for longer periods than brief stimulus pulses at low intensities.

While suppression tends to dominate the results of condition-test paradigms (e.g., Jänig et al., 1977, 1979; Laskin and Spencer, 1979; Gardner and Costanzo, 1980b; Simons, 1985; Simons and Carvell, 1989; Brumberg et al., 1996; Burton et al., 1998; Moore et al., 1999; Mirabella et al., 2001; Chowdhury and Rasmusson, 2003; Derdikman et al., 2003; Greek et al., 2003; Melzer et al., 2006), we and others (e.g., Shimegi et al., 1999, 2000; Greek et al., 2003) report mixed effects on responses after the conditioning stimulus. We hypothesized that the relationship of the Response Field to the stimulus sites might account for the different response types, and reveal why most neuron responses are suppressed in condition-test paradigms, while subsets of others are facilitated or unchanged. We found, however, that each of the Response Field categories included units showing no change, suppression, or facilitation of response peaks (Figure 3-8).

While their studies focused on other issues, results from optical imaging experiments in squirrel monkeys (Chen et al., 2003; Friedman et al., 2008) and a supporting sample of single electrode recordings (Friedman et al., 2008) apply to the issues of widespread spatial interactions in area 3b. Optical imaging results showed that simultaneous stimulation on two adjacent digits reduced the signal amplitude at the individual cortical sites for digits. As the signal reduction was not significant when nonadjacent digits were stimulated (Chen et al., 2003; Friedman et al., 2008), suppressive effects were likely stronger when the cortical locations were closer in proximity. While "no effect," "facilitatory," and "suppressive" categories were calculated differently than our modulation index categories, more than one third of the neuron responses in their sample (N = 27 area 3b neurons) were suppressed by simultaneous stimulation on adjacent or nonadjacent digits, 30% of the neuron responses were facilitated, and one-third of the responses were unchanged by paired stimulation (Friedman et al., 2008). The differences in the proportions of responses categorized as no effect, facilitative, or suppressive in the two studies may relate to the sample sizes and differences in categorization calculations. Together with our findings, these studies suggest a spatial gradient of inhibition-facilitation interactions exists such that simultaneous stimulation on adjacent digits results in stronger suppression than that on nonadjacent digits. Our results suggest further that suppression is strongest between locations on adjacent phalanges within a single digit.

Possible Origins of Spatiotemporal Interactions in the 3b Hand Representation

While our study has not defined all aspects of spatiotemporal interactions in area 3b, we can consider the possible anatomical substrates underlying the effects. Clearly there are facilitative and suppressive components contributing to the responses across the digit representation. These proposed underlying components are shown in Figure 3-9, which is a summary of our findings focused on how peak firing rate and response latency are modulated by stimulation on paired locations and the proportions of units that show facilitative versus suppressive interactions overall. Suppressive effects on firing rate were found over all of the spatial and temporal stimulus conditions; but the largest proportion of suppressive effects occurred between adjacent phalanges within a single digit, followed by nonadjacent phalanges within a single digit. The shortened latencies and increased firing rates indicate that facilitative mechanisms occurred when adjacent digits were stimulated; and our temporal stimulus conditions revealed that facilitation occurred more often when two stimuli were presented within 0 to 30 ms of each other. Interactions between stimuli presented to nonadjacent digits resulted in the highest proportions of neurons with facilitated firing rates in response to co-stimulation (11%); however, since the response latencies and peak firing rates showed facilitative effects when adjacent digits were stimulated (Figures 3-4B, 3-7B), we estimated that facilitation between stimuli presented to nonadjacent digits is similar in strength to that when adjacent digits are stimulated.

Intracortical connections are the most likely sources of the spatiotemporal interactions we observed. Primate area 3b has dense horizontal connections overall (De Felipe et al., 1986; Burton and Fabri, 1995; Manger et al., 1997), with particularly dense

connections within individual digit regions and between digit and adjoining palm regions rather than across adjacent digits (Fang et al., 2002). However, horizontal connections also extend across digit representations (Burton and Fabri, 1995; Manger et al., 1997), and the distribution of projections is likely to decrease in density as distance from the soma increases (Tanosaki et al., 2002a,b). We found that co-stimulating adjacent phalanges on the same digits had a suppressive effect. Yet, sites within a single digit are close in physical proximity and have dense intracortical connections in area 3b (Fang et al., 2002).Thus, our results suggest that intrinsic, horizontal connections primarily have suppressive effects that result in both delayed latencies and decreased firing rates, within the cortical representation of a digit while the less dense horizontal connections between the representations of digits have mainly a facilitative effect. Of course, other connections may mediate the response differences.

As horizontal collaterals of pyramidal cells in layers 3 and 5 extend over 3–6mm in monkey 3b (De Felipe et al., 1986); they form a substrate for widespread spatial interactions. Surround receptive fields of neurons in S1 barrel cortex of rats are primarily derived by intracortical mechanisms (e.g., Li and Waters, 1996; Fox et al., 2003). Intracellular recording studies confirm that subthreshold receptive fields are more extensive than suprathreshold receptive fields (e.g., Smits et al., 1991; Moore and Nelson, 1998; Brecht and Sakmann, 2002; Fox, 2002), and neurons in S1 of rats receive subthreshold inputs from 3 or more digits (Li and Waters, 1996; Arnold et al., 2001). Similarly, in primary visual cortex, horizontal connections appear to mediate integration of information from larger regions of visual space than the classical receptive fields predict (e.g., Gilbert, 1992, review).

The responses of neurons in the present study to spatially distributed stimuli are not necessarily only the result of interactions through cortical connections within area 3b. Area 3b neurons have other ways of being responsive to spatially separate stimuli in addition to using intra-areal connections. 1) The ascending system is divergent in its connections, and receptive fields are maintained in part by lateral inhibition, with relays in the brainstem (cuneate nucleus) and thalamus (ventroposterior nucleus) (e.g., Hicks and Dykes, 1983; Jones et al., 1982, 1997; Garraghty and Sur, 1990; Rausell et al., 1995, 1998; Xu and Wall, 1999). Thalamocortical axon arbors have been traced in owl monkeys (Garraghty et al., 1989) and macaque monkeys (Garraghty and Sur, 1990) to reveal that these arbors can span across cortical columns and can have secondary branches terminating away from the main branch. Adjacent thalamic neurons can project to targets up to 1.5 mm apart in area 3b of macaque monkeys (Rausell and Jones, 1995), reflecting dispersion greater than 3b receptive field mapping reveals. These thalamo-cortical projections could account for some of the interactions within digits and possibly across adjacent digits. Most notably, theoretical modeling of neuron responses in primary visual cortex suggests that many response properties are mediated by thalamocortical connections, including some of the suppression caused by stimuli considered outside the classical receptive field (Carandini et al., 2002); these findings could be relevant to S1 as well. 2) Cortical feedback to thalamic and subthalamic levels appears to sharpen or diminish the receptive field size in visual (e.g., Murphy et al., 1987, 1999; Sillito and Jones, 2002), auditory (e.g., Yan and Suga, 1996; Zhang et al., 1997, 2000), and somatosensory systems (e.g., Shin and Chapin, 1990; Ghosh et al., 1994; Ghazanfar et al., 1997, 1999, 2001; Ergenzinger et al., 1998; Temereanca and Simons, 2004). Thus,

spatial interactions of some extent occur subcortically. Feedback that adjusts subcortical receptive fields will in turn influence cortical responses. 3) Area 3b receives feedback connections from other somatosensory representations, especially those in areas 3a, 1, 2, S2, and PV (e.g., Cusick et al., 1989; Kaas, 1990; Darian-Smith et al., 1993; Krubitzer and Burton et al., 1995a,b; Qi et al., 2002; Wu and Kaas, 2003) that influence response properties. 4) Finally, callosal connections reach 3b directly (albeit, few; see Killackey et al., 1983 for owl monkeys) and via feedback from other fields with denser callosal connections (Calford, 2002, review). Our stimuli were presented only within the contralateral hand; therefore, these callosal connections are expected to contribute little to the response properties observed.

Functional Relevance of Spatiotemporal Interactions in the Hand Representation

The spatiotemporal effects on neuron responses to somatosensory stimuli we report here affect stimulus processing, and therefore, perception. Although our procedure of stimulating one or two hand locations does not mimic many natural stimulation situations, this simplified stimulation allowed us to quantitatively evaluate how sensory information from the hand is integrated in area 3b. Spatiotemporal response characteristics have been suggested to account for motion detection (e.g., Whitsel et al., 1972; Hyvärinen and Poranen, 1978; Warren et al., 1986; Gardner et al., 1992), motion direction perception (e.g., Hyvärinen and Poranen, 1978; Warren et al., 1986), feature detection regardless of stimulus velocity (DiCarlo et al., 2002), and orientation detection (e.g., Hyvärinen and Poranen, 1978; Warren et al., 1986; DiCarlo et al., 2002). While our stimuli are unlikely to elicit perceptions of continuous motion across the paired sites on

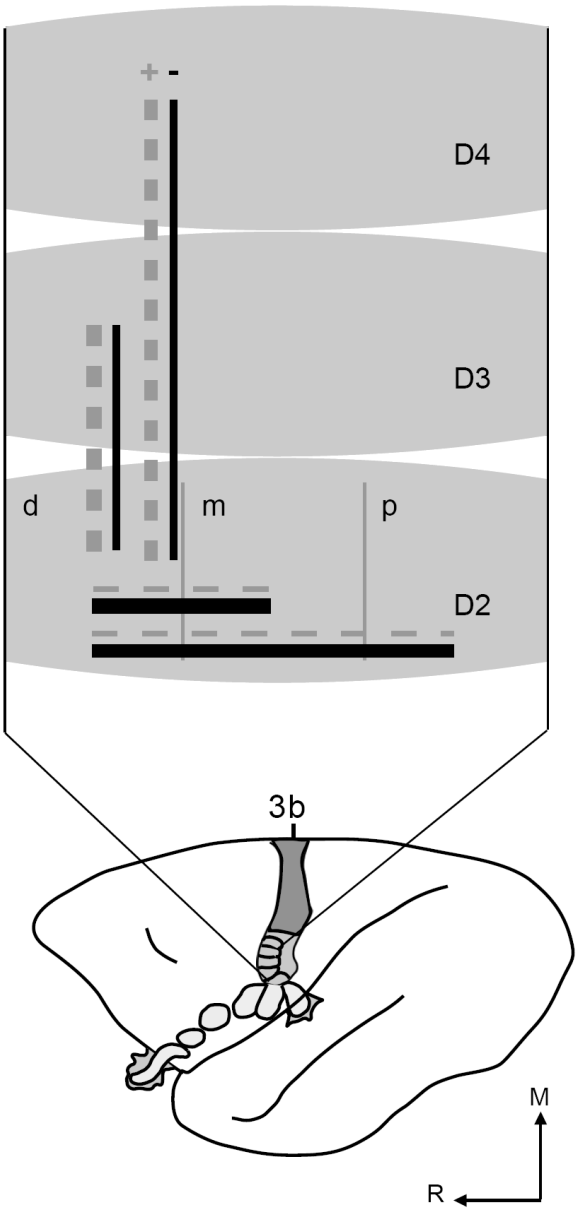

Figure 3-9. A summary diagram of the spatiotemporal interactions resulting from functional connections between parts of the hand representation in area 3b. Representations of three digits (D2, D3, D4) in area 3b are shown above the schematic of the owl monkey brain indicating the location of area 3b. These represent stimulation applied to adjacent and nonadjacent locations rather than to the specific digits. One digit is divided into distal (d), middle (m), and proximal (p) sections to represent the stimulation on phalanges within each digit. Line thickness between sites is an approximate representation of the proportion of suppression or facilitation recorded from the selected locations. Black lines refer to suppressive interactions (-) that occurred when stimuli were presented on the paired locations indicated, and these lines are solid to indicate that suppressive interactions were found at all stimulus onset asynchronies tested, from 0-500 ms. Gray lines refer to facilitative interactions (+) that occurred when stimuli were presented on the paired sites indicated. All of the gray lines are dashed to indicate that facilitative interactions tended to dominate during short stimulus onset delays from 0-30 ms. The most facilitation via effects on firing rate and latency was found when adjacent digits were stimulated; thus, the lines are the thickest.

the digits, these simple stimuli allowed us to investigate basic neuron response properties that underlie more complex stimulus discriminations.

Our electrophysiological results relate to a recent human psychophysical study by Horner (2006) which compared tactile pattern discrimination along adjacent locations on the index finger and found that 1) performance was best when patterns were presented to the same location rather than separate digit locations; 2) discrimination was best on the distal phalange compared to the middle phalange; and 3) short stimulus onset asynchronies (120 ms) impaired performance compared to long onset asynchronies (540 and 990 ms). Horner described the results as consistent with the idea that since the distal digits are more densely innervated than the proximal parts of the hand (e.g., Johansson and Vallbo, 1979); the distal digits have a performance advantage. We found shortened latencies and higher peak firing rates when adjacent and nonadjacent digits were stimulated, and our stimulation locations were primarily distal digits (see Methods). Thus, the facilitative effect on firing rates and latencies we observed in area 3b neurons when stimulating separate digits may be related to the innervation density and the performance advantage of distal digits.

While Horner did not discuss the contributions to impaired discrimination when stimuli were applied with short stimulus onset asynchronies, our data along with others (e.g., Jänig et al., 1977, 1979; Laskin and Spencer, 1979; Gardner and Costanzo, 1980b; Burton et al., 1998; Chowdhury and Rasmusson, 2003; Greek et al., 2003), suggest that the impaired discrimination may be related to the firing rate suppression that occurs when two stimuli are applied to locations on the hand (or forelimb) synchronously or asynchronously. Long-term passive tactile stimulation on all fingers of the human hand

has been shown to improve tactile acuity when the stimulation was synchronous, while asynchronous stimulation did not improve tactile acuity and showed trends for reducing acuity (Kalisch et al., 2007). Taken with human psychophysical studies, our results predict that tactile perception and discrimination would be impaired when paired stimuli are presented within one digit compared to across separate digits and that asynchronous presentation of stimuli would impair the perception of a second, target stimulus.

Acknowledgements

This work was supported by the James S. McDonnell Foundation (J.H. Kaas) and NIH grants NS16446 (J.H. Kaas), F31-NS053231 (J.L. Reed), EY014680-03 (A.B. Bonds), T32-GM07347 (M.J. Burish). Matlab scripts were written primarily by Dr. Pierre Pouget and John Haitas in collaboration with J.L. Reed and Jurnell Cockhren. Dr. Omar Gharbawie and Corrie Camalier helped collect data from 2 of the 3 monkey cases.

References

Allman J, Miezin F, McGuinness E. 1985. Stimulus specific responses from beyond the classical receptive field: Neurophysiological mechanisms for local-global comparisons in visual neurons. *Annu Rev Neurosci* 8: 407-430.

Alvarado JC, Vaughan JW, Stanford TR, Stein BE. 2007. Multisensory versus unisensory integration: contrasting modes in the superior colliculus. *J Neurophysiol* 97: 3193-205.

Armstrong-James M, Fox K. 1987. Spatiotemporal convergence and divergence in the rat S1 "barrel" cortex. *J Comp Neurol* 236: 265-281.

Arnold PB, Li CX, Waters RS. 2001. Thalamocortical arbors extend beyond single

cortical barrels: an in vivo intracellular tracing study in rat. *Exp Brain Res* 136: 152-168.

Berwick J, Redgrave P, Jones M, Hewson-Stoate N, Martindale J, Johnston D, Mayhew JEW. 2004. Integration of neural responses originating from different regions of the cortical somatosensory map. *Brain Res* 1030: 284-293.

Boloori AR, Stanley GB. 2006. The dynamics of spatiotemporal response integration in the somatosensory cortex of the vibrissa system. *J Neurosci* 26: 3767-3782.

Braun C, Hess H, Burkhardt M, Wühle A, Preissl H. 2005. The right hand knows what the left hand is feeling. *Exp Brain Res* 162: 366-373.

Brecht M, Sakmann B. 2002. Dynamic representation of whisker deflection by synaptic potentials in spiny stellate and pyramidal cells in the barrels and septa of layer 4 rat somatosensory cortex. *J Physiol* 543: 49-70.

Brown HA, Allison JD, Samonds JM, Bonds AB. 2003. Nonlocal origin of response suppression from stimulation outside the classic receptive field in area 17 of the cat. *Vis Neurosci* 20: 85-96.

Brumberg JC, Pinto DJ, Simons DJ. 1996. Spatial gradients and inhibitory summation in the rat whisker barrel system. *J Neurophysiol* 76: 130-140.

Burton H, Fabri M. 1995a. Ipsilateral intracortical connections of physiologically defined cutaneous representations in area 3b and 1 of macaque monkeys: projections in the vicinity of the central sulcus. *J Comp Neurol* 355: 508-538.

Burton H, Fabri M, Alloway K. 1995b. Cortical areas within the lateral sulcus connected to cutaneous representations in areas 3b and 1: a revised interpretation of the second somatosensory area in macaque monkeys. *J Comp Neurol* 355: 539-562.

Burton H, Sinclair RJ, Whang K. 1998. Vibrotactile stimulus order effects in somatosensory cortical areas of rhesus monkeys. *Somato Mot Res* 15: 316-324.

Calford MB. 2002. Dynamic representational plasticity in sensory cortex. *Neuroscience* 111: 709-738.

Canedo A, Aguilar J. 2000. Spatial and cortical influences exerted on cuneothalamic and thalamocortical neurons of the cat. *Eur J Neurosci* 12: 2515-2533.

Chen LM, Friedman RM, Roe AW. 2003. Optical imaging of a tactile illusion in area 3b of the primary somatosensory cortex. *Science* 302: 881-885.

Chowdhury SA, Rasmusson DD. 2003. Corticocortical inhibition of peripheral inputs within primary somatosensory cortex: the role of $GABA_A$ and $GABA_B$ receptors.

J Neurophysiol 90: 851-856.

Clark SA, Allard T, Jenkins WM, Merzenich MM. 1988. Receptive fields in the body-surface map in adult cortex defined by temporally correlated inputs. *Nature* 332: 444-445.

Cusick CG, Wall JT, Felleman DJ, Kaas JH. 1989. Somatotopic organization of the lateral sulcus of owl monkeys: area 3b, S-II, and a ventral somatosensory area. *J Comp Neurol* 282: 169-190.

Darian-Smith C. Somatosensory plasticity. 2009. In *Encyclopedia of Neuroscience*, ed. LR Squire. Amsterdam: Elsevier, 99-110.

Darian-Smith C, Darian-Smith I, Burman K, Ratcliffe N. 1993. Ipsilateral cortical projections to areas 3a, 3b, and 4 in the macaque monkey. *J Comp Neurol* 335: 200-213.

Davidson AG, O'Dell R, Chan V, Schieber MH. 2007. Comparing effects in spike-triggered averages of rectified EMG across different behaviors. *J Neurosci Methods* 163: 283-294.

De Felipe J, Conley M, Jones EG. 1986. Long-range focal collateralization of axons arising from corticocortical cells in monkey sensory-motor cortex. *J Neurosci* 6: 3749-3766.

Derdikman D, Hildesheim R, Ahissar E, Arieli A, Grinvald A. 2003. Imaging spatio-temporal dynamics of surround inhibition in the barrels somatosensory cortex. *J Neurosci* 23: 3100–3105.

DiCarlo JJ, Johnson KO, Hsiao SS. 1998. Structure of receptive fields in area 3b of primary somatosensory cortex in the alert monkey. *J Neurosci* 18: 2626-2645.

DiCarlo JJ, Johnson KO. 2000. Spatial and temporal structure of receptive fields in primate somatosensory area 3b: effects of stimulus scanning direction and orientation. *J Neurosci* 20: 495-510.

DiCarlo JJ, Johnson KO. 2002. Receptive field structure in cortical area 3b of the alert monkey. *Behav Brain Res* 135: 167-178.

Ergenzinger ER, Glasier MM, Hahm JO, Pons TP. 1998. Cortically induced thalamic plasticity in the primate somatosensory system. *Nat Neurosci* 1: 226-229.

Fang P-C, Jain N, Kaas JH. 2002. Few intrinsic connections cross the hand-face border of area 3b of new world monkeys. *J Comp Neurol* 454: 310-319.

Fox K. 2002. Anatomical pathways and molecular mechanisms for plasticity in the barrel

cortex. *Neuroscience* 111: 799-814.

Fox K, Wright N, Wallace H, Glazewski S. 2003. The origin of cortical surround receptive fields studied in the barrel cortex. *J Neurosci* 23: 8380-8391.

Friedman RM, Chen LM, Roe AW. 2008. Responses of areas 3b and 1 in anesthetized squirrel monkeys to single- and dual-site stimulation of the digits. *J Neurophysiol* 100: 3185-3196.

Gardner EP, Palmer CI, Hämäläinen HA, Warren S. 1992. Simulation of motion on the skin. V. Effect of stimulus temporal frequency on the representation of moving bar patterns in primary somatosensory cortex of monkeys. *J Neurophysiol* 67: 37-63.

Gardner EP, Costanzo RM. 1980a. Spatial integration of multiple-point stimuli in primary somatosensory cortical receptive fields of alert monkeys. *J Neurophysiol* 43: 420-443.

Gardner EP, Costanzo RM. 1980b. Temporal integration of multiple-point stimuli in primary somatosensory cortical receptive fields of alert monkeys. *J Neurophysiol* 43: 444-468.

Garraghty PE, Pons TP, Sur M, Kaas JH. 1989. The arbors of axons terminating in middle cortical layers of somatosensory area 3b in owl monkeys. *Somatosens Motor Research* 6: 401-411.

Garraghty PE, Sur M. 1990. Morphology of single intracellularly stained axons terminating in area 3b of macaque monkeys. *J Comp Neurol* 294: 583-593.

Ghazanfar AA, Krupa DJ, Nicolelis MAL. 2001. Role of cortical feedback in the receptive field structure and nonlinear response properties of somatosensory thalamic neurons. *Exp Brain Res* 141: 88-100.

Ghazanfar AA, Nicolelis MAL. 1997. Nonlinear processing of tactile information in the thalamocortical loop. *J Neurophysiol* 78: 506-510.

Ghazanfar AA, Nicolelis MAL. 1999. Spatiotemporal properties of layer V neurons of the rat primary somatosensory cortex. *Cereb Cortex* 9: 348-361.

Ghosh S, Murray GM, Turman AB, Rowe MJ. 1994. Corticothalamic influences on transimission of tactile information in the ventroposterolateral thalamus of the cat: effect of reversible inactivation of somatosensory cortical areas I and II. *Exp Brain Res* 100: 276-286.

Gilbert CD. 1992. Horizontal integration and cortical dynamics. *Neuron* 9: 1-13.

Greek KA, Chowdhury SA, Rasmusson DD. 2003. Interactions between inputs from adjacent digits in somatosensory thalamus and cortex of the raccoon. *Exp Brain Res* 151: 364-371.

Hardin JW, Hilbe JM. 2003. *Generalized estimating equations*. Boca Raton, FL: Chapman and Hall/CRC.

Helmstaedter M, Sakmann B, Feldmeyer D. 2009. Neuronal correlates of local, lateral, and translaminar inhibition with reference to cortical columns. *Cereb Cortex* 19: 926-937.

Hicks TP, Dykes RW. 1983. Receptive field size for certain neurons in primary somatosensory cortex is determined by GABA-mediated intracortical inhibition. *Brain Res* 274: 160-164.

Hoechstetter K, Rupp A, Stančák A, Meinck H-M, Stippich C, Berg P, Scherg M. 2001. Interaction of tactile input in the human primary and secondary somatosensory cortex—A magnetoencephalographic study. *NeuroImage* 14: 759-767.

Horner DT. 2006. Tactile pattern discrimination at adjacent locations along the proximal-distal axis of the index finger. *Perception* 35: 125-136.

Hsieh C-L, Shima F, Tobimatsu S, Sun S-J, Kato M. 1995. The interaction of the somatosensory evoked potentials to simultaneous finger stimuli in the human central nervous system. A study using direct recordings. *Electroencephalogr Clin Neurophysiol* 96: 135-142.

Hyvärinen J, Poranen A. 1978. Movement-sensitive and direction and orientation-selective cutaneous receptive fields in the hand area of the post-central gyrus in monkeys. *J Physiol London* 283: 523-537.

Iwamura Y, Tanaka M, Sakamoto M, Hikosaka O. 1983. Functional subdivisions representing different finger regions in area 3b or the first somatosensory cortex of the conscious monkey. *Exp Brain Res* 51: 315-326.

Jain N, Qi H-X, Kaas JH. 2001. Long-term chronic multichannel recordings from sensorimotor cortex and thalamus of primates. Chapter 5 In *Progress in Brain Research*, ed. MAL Nicolelis, 130: 1-10. Amsterdam: Elsevier Science B.V.

Jänig W, Schoultz T, Spencer WA. 1977. Temporal and spatial parameters of excitation and afferent inhibition in cuneothalamic relay neurons. *J Neurophysiol* 40: 822-835.

Jänig W, Spencer WA, Younkin SG. 1979. Spatial and temporal features of afferent inhibition of thalamocortical relay cells. *J Neurophysiol* 42: 1450-1460.

Johansson RS, Vallbo AB. 1979. Tactile sensibility in the human hand: relative and absolute densities of the four types of mechanoreceptive units in glaborous skin. *J Physiol* 286: 283-300.

Jones EG, Friedman DP, Hendry SHC. 1982. Thalamic basis of place- and modality-specific columns in monkey somatosensory cortex: a correlative anatomical and physiological study. *J Neurophysiol* 48: 545-568.

Jones EG, Manger PR, Woods TM. 1997. Maintenance of a somatotopic cortical map in the face of diminishing thalamocortical inputs. *Proc Natl Acad Sci USA* 94: 11003-11007.

Kaas JH. 1983. What, if anything, is SI? Organization of first somatosensory area of cortex. *Physiol Rev* 63: 206-231.

Kalisch T, Tegenthoff M, Dinse HR. 2007. Differential effects of synchronous and asynchronous multifinger coactivation on human tactile performance. *BMC Neurosci* 8: 58.

Killackey HP, Gould HJ III, Cusick CG, Pons TP, Kaas JH. 1983. The relation of corpus callosum connections to architectonic fields and body surface maps in sensori-motor cortex of new and old world monkeys. *J Comp Neurol* 219: 384-419.

Krubitzer LA, Kaas JH. 1990. The organization and connections of somatosensory cortex in marmosets. *J Neurosci* 10: 952-974.

Laskin SE, Spencer WA. 1979. Cutaneous masking. II. Geometry of excitatory and inhibitory receptive fields of single units in somatosensory cortex of the cat. *J Neurophysiol* 42: 1061-1082.

Li CX, Waters RS. 1996. In vivo intracellular recording and labeling of neurons in the forepaw barrel subfield (FBS) of rat somatosensory cortex: possible physiological and morphological substrates for reorganization. *Neuroreport* 7: 2261-2272.

Liang K-Y, Zeger SL. 1986. Longitudinal data analysis using generalized linear models. *Biometrika* 73: 13-22.

Manger PR, Woods TM, Muñoz A, Jones EG. 1997. Hand/face border as a limiting boundary in the body representation in monkey somatosensory cortex. *J Neurosci* 17: 6338-6351.

Mason A, Nicoll A, Stratford K. 1991. Synaptic transmission between individual pyramidal neurons of the rat visual cortex in vitro. *J Neurosci* 11: 72-84.

Melzer P, Champney GC, Maguire MJ, Ebner FF. 2006. Rate code and temporal code for frequency of whisker stimulation in rat primary and secondary somatic sensory cortex. *Exp Brain Res* 172: 370-386.

Merzenich MM, Kaas JH, Sur M, Lin CS. 1978. Double representations of the body surface within cytoarchitectonic areas 3b and 1 in "SI" in the owl monkey (*Aotus trivirgatus*). *J Comp Neurol* 181: 41-74.

Mirabella G, Battiston S, Diamond ME. 2001. Integration of multiple-whisker inputs in rat somatosensory cortex. *Cereb Cortex* 11: 164-170.

Moore CI, Nelson SB. 1998. Spatio-temporal subthreshold receptive fields in the vibrissa representation of rat primary somatosensory cortex. *J Neurophysiol* 80: 2882-2892.

Moore CI, Nelson SB, Sur M. 1999. Dynamics of neuronal processing in rat somatosensory cortex. *Trends Neurosci* 22: 513-520.

Mountcastle VB. 2005. *The Sensory Hand: Neural mechanisms of somatic sensation*. Cambridge, MA: Harvard University Press.

Mountcastle VB, Powell TPS. 1959. Neural mechanisms subserving cutaneous sensibility, with special reference to the role of afferent inhibition in sensory perception and discrimination. *Bull Johns Hopkins Hosp* 105: 201-232.

Murphy PC, Sillito AM. 1987. Corticofugal feedback influences the generation of length tuning in the visual pathway. *Nature* 329: 727-729.

Murphy PC, Duckett SG, Sillito AM. 1999. Feedback connections to the lateral geniculate nucleus and cortical response properties. *Science* 286: 1552-1554.

Nelson RJ, Sur M, Felleman DJ, Kaas JH. 1980. Representations of the body surface in postcentral parietal cortex of *Macaca fascicularis*. *J Comp Neurol* 192: 611-643.

Nicolelis MAL, Ghazanfar AA, Stambaugh CR, Oliveira LMO, Laubach M, Chapin JK, Nelson RJ, Kaas JH. 1998. Simultaneous encoding of tactile information by three primate cortical areas. *Nat Neurosci* 1: 621-630.

Nicolelis MAL, Dimitrov D, Carmena JM, Crist R, Lehew G, Kralik JD, Wise SP. 2003. Chronic, multisite, multielectrode recordings in macaque monkeys. *Proc Natl Acad Sci USA* 100: 11041-11046.

Pilz K, Veit R, Braun C, Godde B. 2004. Effects of co-activation on cortical organization and discrimination performance. *Neuroreport* 15: 2669-2672.

Pons TP, Wall JT, Garraghty PE, Cusick CG, Kaas JH. 1987. Consistent features of the representation of the hand in area 3b of macaque monkeys. *Somatosens Res* 4: 309-331.

Qi H-X, Lyon DC, Kaas JH. 2002. Cortical and thalamic connections of the parietal ventral somatosensory area in marmoset monkeys (*Callithrix jacchus*). *J Comp Neurol* 443: 168-182.

Rausell E, Jones EG. 1995. Extent of intracortical arborization of thalamocortical axons as a determinant of representational plasticity in monkey somatic sensory cortex. *J Neurosci* 15: 4270-4288.

Rausell E, Bickford L, Manger PR, Woods TM, Jones EG. 1998. Extensive divergence and convergence in the thalamocortical projection to monkey somatosensory cortex. *J Neurosci* 18: 4216-4232.

Reed JL, Pouget P, Qi H-X, Zhou Z, Bernard MR, Burish MJ, Haitas J, Bonds AB, Kaas JH. 2008. Widespread spatial integration in primary somatosensory cortex. *Proc Natl Acad Sci USA* 105: 10233-10237.

Rowland BA, Quessy S, Stanford TR, Stein BE. 2007. Multisensory integration shortens physiological response latencies. *J Neurosci* 27: 5879-5884.

Samonds JM, Allison JD, Brown HA, Bonds AB. 2003. Cooperation between area 17 neuron pairs enhances fine discrimination of orientation. *J Neurosci* 23: 2416-2425.

Schweizer R, Maier M, Braun C, Birbaumer N. 2000. Distribution of mislocalizations of tactile stimuli on the fingers of the human hand. *Somatosens Motor Res* 17: 309-316.

Shimegi S, Akasaki T, Ichikawa T, Sato H. 2000. Physiological and anatomical organization of multiwhisker response interactions in the barrel cortex of rats. *J Neurosci* 20: 6241-6248.

Shimegi S, Ichikawa T, Akasaki T, Sato H. 1999. Temporal characteristics of response integration evoked by multiple whisker stimulations in the barrel cortex of rats. *J Neurosci* 19: 10164-10175.

Shin H-C, Chapin JK. 1990. Mapping the effects of SI cortex stimulation on somatosensory relay neurons in the rat thalamus: direct responses and afferent modulation. *Somatosens Motor Res* 7: 421-434.

Shoham S, Fellows MR, Normann RA. 2003. Robust, automatic spike sorting using mixtures of multivariate t-distributions. *J Neurosci Methods* 127: 111-122.

Sillito AM, Jones HE. 2002. Corticothalamic interactions in the transfer of visual information. *Philos Trans R Soc Lond B Biol Sci* 357: 1739-1752.

Simons DJ. 1985. Temporal and spatial integration in the rat SI vibrissa cortex. *J Neurophysiol* 54: 615-633.

Simons DJ, Carvell GE. 1989. Thalamocortical response transformation in the rat vibrissa/barrel system. *J Neurophysiol* 61: 311-330.

Smits E, Gordon DC, Witte S, Rasmusson DD, Zarzecki P. 1991. Synaptic potentials evoked by convergent somatosensory and corticocortical inputs in raccoon somatosensory cortex: substrates for plasticity. *J Neurophysiol* 66: 688-695.

Sripati AP, Yoshioka T, Denchev P, Hsiao SS, Johnson KO. 2006. Spatiotemporal receptive fields of peripheral afferents and cortical area 3b and 1 neurons in the primate somatosensory system. *J Neurosci* 26: 2101-2114.

Stanford TR, Quessy S, Stein BE. 2005. Evaluating the operations underlying multisensory integration in the cat superior colliculus. *J Neurosci* 25: 6499-6508.

Sur M. 1980. Receptive fields of neurons in areas 3b and 1 of somatosensory cortex in monkeys. *Brain Res* 198: 465-471

Sur M, Garraghty PE, Bruce CJ. 1985. Somatosensory cortex in macaque monkeys: laminar differences in receptive field size in areas 3b and 1. *Brain Res* 342: 391–395,

Sur M, Wall, JT, Kaas JH. 1984. Modular distribution of neurons with slowly adapting and rapidly adapting responses in area 3b of somatosensory cortex in monkeys. *J Neurophysiol* 51: 724-744.

Tanosaki M, Suzuki A, Kimura T, Takino R, Haruta Y, Hoshi Y, Hashimoto I. 2002a. Contribution of primary somatosensory area 3b to somatic cognition: a neuromagnetic study. *Neuroreport* 13: 1519-1522.

Tanosaki M, Suzuki A, Takino R, Kimura T, Iguchi Y, Kurobe Y, Haruta Y, Hoshi Y, Hashimoto I. 2002b. Neural mechanisms for generation of tactile interference effects on somatosensory evoked magnetic fields in humans. *Clin Neurophysiol* 113: 672-680.

Temereanca S, Simons DJ. 2004. Functional topography of corticothalamic feedback enhances thalamic spatial response tuning in the somatosensory whisker/barrel system. *Neuron* 41: 639-651.

Tremblay F, Ageranioti-Bélanger SA, Chapman CE. 1996. Cortical mechanisms

underlying tactile discrimination in the monkey. I. Role of primary somatosensory cortex in passive texture discrimination. *J Neurophysiol* 76: 3382-3403.

Tuerlinckx F, Rijmen F, Verbeke G, De Boeck P. 2006. Statistical inference in generalized linear mixed models: A review. *Br J Math Stat Psychol* 59: 225-255.

Tutunculer B, Foffani G, Himes BT, Moxon KA. 2006. Structure of the excitatory receptive fields of infragranular forelimb neurons in the rate primary somatosensory cortex responding to touch. *Cereb Cortex* 16: 791-810.

Veredas FJ, Vico FJ, Alonso JM. 2005. Factors determining the precision of the correlated firing generated by a monosynaptic connection in the cat visual pathway. *J Physiol* 567.3: 1057-1078.

Walker GA, Ohzawa I, Freeman RD. 2000. Suppression outside the classical cortical receptive field. *Vis Neurosci* 17: 1-11.

Wang X, Merzenich MM, Sameshima K, Jenkins WM. 1995. Remodelling of hand representation in adult cortex determined by timing of tactile stimulation. *Nature* 378: 71-75.

Warren S, Hämäläinen HA, Gardner EP. 1986. Objective classification of motion- and direction-sensitive neurons in primary somatosensory cortex of awake monkeys. *J Neurophysiol* 56: 598-622.

Whitsel BL, Roppolo JR, Werner G. 1972. Cortical information processing of stimulus motion on primate skin. *J Neurophysiol* 35: 691-717.

Wiemer J, Spengler F, Joublin F, Stagge P, Wacquant S. 2000. Learning cortical topography from spatiotemporal stimuli. *Biol Cybern* 82: 173-187.

Wu CW-H, Kaas JH. 2003. Somatosensory cortex of prosimian galagos: physiological recording, cytoarchitecture, and cortiocortical connections of anterior parietal cortex and cortex of the lateral sulcus. *J Comp Neurol* 457: 263-292.

Xerri C, Merzenich MM, Jenkins W, Santucci S. 1999. Representational plasticity in cortical area 3b paralleling tactual-motor skill acquisition in adult monkeys. *Cereb Cortex* 9: 264-276.

Xing J, Gerstein GL. 1996. Networks with lateral connectivity. III. Plasticity and reorganization of somatosensory cortex. *J Neurophysiol* 75: 217-232.

Xu J, Wall JT. 1999. Functional organization of tactile inputs from the hand in the cuneate nucleus and its relationship to organization in the somatosensory cortex. *J Comp Neurology* 411: 369-389.

Xu X, Collins CE, Kaskan PM, Khaytin I, Kaas JH, Casagrande VA. 2003. Optical imaging of visually evoked responses in prosimian primates reveals conserved features of the middle temporal visual area. *Proc Natl Acad Sci USA* 101: 2566-2571.

Yan J, Suga N. 1996. Corticofugal modulation of time-domain processing of biosonar information in bats. *Science* 273: 1100-1103.

Zeger SL, Liang K-Y. 1986. Longitudinal data analysis for discrete and continuous outcomes. *Biometrics* 42: 121-130.

Zhang Y, Suga N. 2000. Modulation of responses and frequency tuning of thalamic and collicular neurons by cortical activation in mustached bats. *J Neurophysiol* 84: 325-333.

Zhang Y, Suga N, Yan J. 1997. Corticofugal modulation of frequency processing in bat auditory system. *Nature* 387: 900-903.

Zhu JJ, Connors BW. 1999. Intrinsic firing patterns and whisker-evoked synaptic responses of neurons in the rat barrel cortex. *J Neurophysiol* 81: 1171-1183.

Supplemental Material

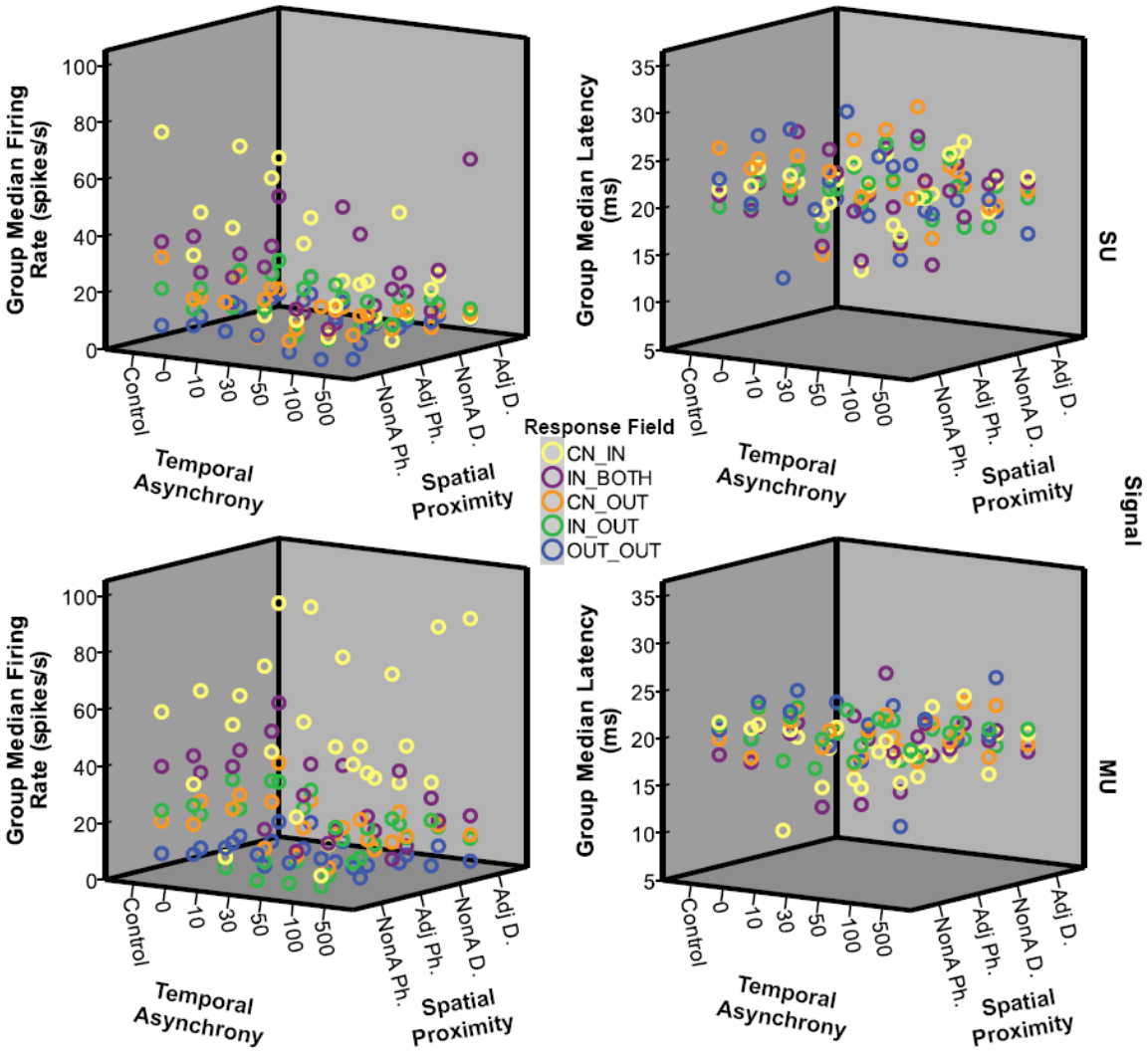

Figure S3-1. Peak firing rates and response latencies plotted to show distributions across spatiotemporal stimulation categories. These plots indicate the distributions of peak firing rates along the four categories we analyzed: temporal asynchrony, spatial proximity, Response Field relationship, and signal isolation. The temporal stimulation conditions are plotted in the x-axis and the spatial proximity conditions are plotted in the z-axis. "Control" refers to single-site stimulation on the preferred location in a stimulus pair. Other stimulation categories refer to the time between the onset of the non-preferred stimulus (first) and the preferred control stimulus (second). The Response Field relationship is designated by the color of each data point. Single unit (SU) recordings are plotted in the upper panels across the figure, and multi-unit recordings (MU) are plotted in the lower panels. Left. Within each category, the group median peak firing rates (spikes/s) are plotted in three dimensions to summarize the data distributions within the spatiotemporal stimulation categories (medians calculated from 1385 SU observations; 2213 MU observations). Right. Within each category, the group median response latencies (ms) are plotted in three dimensions to summarize the data distributions within the spatiotemporal stimulation categories.(medians calculated from 1098 SU observations; 1771 MU observations).

Table S3-1. Tests of model effects for variance in peak firing rate of single units classified by spatial and temporal stimulus characteristics and interactions

Variance Source	Wald Chi-Square	df	P value
(Intercept)	2072.941	1	< 0.0005
Temporal Asynchrony	236.079	5	< 0.0005
Spatial Proximity	29.313	3	< 0.0005
Response Field (RF)	186.435	4	< 0.0005
Temporal x Spatial	170.040	15	< 0.0005
Temporal x RF	240.727	20	< 0.0005
Spatial x RF	378.704	12	< 0.0005
Temporal x Spatial x RF	8938.891	60	< 0.0005

Tests of model effects from Generalized Linear Modeling with Generalized Estimating Equations on the dependent variable peak firing rate. N = 309 single neurons with correlated measures from the repeated stimulus measures taken from three monkeys.

Table S3-2. Tests of model effects for variance in peak firing rate of multi-units classified by spatial and temporal stimulus characteristics and interactions

Variance Source	Wald Chi-Square	df	P value
(Intercept)	1493.265	1	< 0.0005
Temporal Asynchrony	376.422	5	< 0.0005
Spatial Proximity	34.262	3	< 0.0005
Response Field (RF)	105.149	4	< 0.0005
Temporal x Spatial	488.131	15	< 0.0005
Temporal x RF	239.996	20	< 0.0005
Spatial x RF	88.345	12	< 0.0005
Temporal x Spatial x RF	11848.445	50	< 0.0005

Tests of model effects using Generalized Linear Modeling with Generalized Estimating Equations on the dependent variable peak firing rate. N = 392 multi-units with correlated measures from the repeated stimulus measures taken from three monkeys.

Table S3-3. Tests of model effects for variance in latency of single units classified by spatial and temporal stimulus characteristics and interactions

Variance Source	Wald Chi-Square	df	P value
(Intercept)	52754.790	1	< 0.0005
Temporal Asynchrony	233.939	5	< 0.0005
Spatial Proximity	44.598	3	< 0.0005
Response Field (RF)	3.965	4	0.411
Temporal x Spatial	78.747	15	< 0.0005
Temporal x RF	53.032	20	< 0.0005
Spatial x RF	60.742	12	< 0.0005
Temporal x Spatial x RF	1456.038	54	< 0.0005

Tests of model effects from Generalized Linear Modeling with Generalized Estimating Equations on the dependent variable latency. N = 309 single neurons with correlated measures from the repeated stimulus measures taken from three monkeys.

Table S3-4. Tests of model effects for variance in latency of multi-units classified by spatial and temporal stimulus characteristics and interactions

Variance Source	Wald Chi-Square	df	P value
(Intercept)	110651.394	1	< 0.0005
Temporal Asynchrony	253.505	5	< 0.0005
Spatial Proximity	45.452	3	< 0.0005
Response Field (RF)	46.881	4	< 0.0005
Temporal x Spatial	56.186	15	< 0.0005
Temporal x RF	87.030	20	< 0.0005
Spatial x RF	59.097	12	< 0.0005
Temporal x Spatial x RF	316.791	43	< 0.0005

Tests of model effects from Generalized Linear Modeling with Generalized Estimating Equations on the dependent variable latency. N = 392 multi-units with correlated measures from the repeated stimulus measures taken from three monkeys.

Supplemental Results

Spatiotemporal Stimulus Effects on Peak Firing Rate and Response Latency

Temporal asynchrony category. Significant decreases in peak response magnitudes compared to control stimulation (MU = 34.17 spikes/s ± 1.62) were predicted to occur statistically for all of the paired stimulation conditions at stimulus onset asynchronies as follows: 10 ms: SU = 14.40 spikes/s ± 1.59, $P < 0.0005$; 30 ms: MU = 4.64 spikes/s ± 0.46, $P < 0.0005$; 50 ms: MU = 5.25 spikes/s ± 0.62, $P < 0.0005$; 100 ms: MU = 16.24 spikes/s ± 1.63, $P < 0.0005$; and 500 ms, 17.80 ± 1.66, $P < 0.0005$. Unlike the results for SUs, MUs did not show a significant difference between single-site control stimulation and simultaneous stimulation (0 ms: MU = 33.84 spikes/s ± 1.59, $P = 1.000$). On average, peak firing rate responses of single units were suppressed by the presence of the non-preferred stimulus at all delays tested, with maximal suppression when the non-preferred stimulus preceded the preferred stimulus by 30 ms. Thus, peak firing rates of both single units and multi-units indicate that stimulus information is integrated across time up to 500 ms, with strong effects when the non-preferred stimulus is presented between 10-50 ms before the preferred stimulus (see Figure S3-2A for effects when SUs and MUs were combined).

Similar to results for single units, we found shortened response latencies for multi-units occurred when the preferred (test) stimulus was presented at a 10 ms delay (MU = 13.99 ms ± 0.53; $P < 0.0005$) compared to single-site stimulation (MU = 20.37 ms ± 0.32). We found that presenting the test stimulus at a 50 ms delay (MU = 22.76 ms ± 0.43; $P < 0.0005$) lengthened response latency slightly for multi-units when no significant effects were found for single units compared to control stimulation. Latencies of multi-

units in response to stimulations at the remaining onset delays were not significantly different from the latency during single-site stimulation (0 ms: MU = 19.44 ms ± 0.22, P = 0.051; 30 ms: MU = 19.61 ms ± 0.34, P = 1.000; 100 ms: MU = 21.42 ms ± 0.40, P = 0.292; 500 ms: MU = 20.44 ms ± 0.27; P = 1.000). See Figure S3-2B for effects when SUs and MUs were combined.

Spatial proximity category. Peak firing rates were generally suppressed by paired stimulation compared to single-site stimulation (Single-site: MU = 34.17 spikes/s ± 1.62; Adj D.: MU = 19.82 spikes/s ± 2.20, P < 0.0005; NonA D.: MU = 28.19 spikes/s ± 3.60, P = 0.876; Adj Ph.: MU = 10.98 spikes/s ± 1.27, P < 0.0005; NonA Ph.: MU = 3.71 spikes/s ± 0.86, P < 0.0005), with the greatest suppression when stimuli were presented to nonadjacent phalanges. See Figure S3-3A for combined SU and MU results. The slight shortening of multi-unit latencies when adjacent digits were stimulated (Adj D.: MU = 17.62 ms ± 0.29) compared to single-site stimulation (Single-site: MU = 20.37 ± 0.32, P < 0.0005) was present in single-unit data (see Figure S3-3B for combined SU and MU data).

Response Field relationship category. Like results for single units, the peak firing rates of multi-unit data were significantly lower when both stimuli were outside of the Response Field (OUT_OUT: MU = 3.51 spikes/s ± 0.77) compared to other conditions when one or both stimuli were inside the Response Field, as follows: IN_OUT: MU = 20.93 spikes/s ± 3.32, P < 0.0005; CN_OUT: MU = 11.68 spikes/s ± 2.00, P = 0.001; IN_BOTH: MU = 14.26 spikes/s ± 2.57, P = 0.001; and CN_IN: MU = 28.49 spikes/s ± 2.20, P < 0.0005. Overall, peak firing rates were lowest when both stimuli were outside the Response Field and highest when both stimuli were within the Response Field, and

presenting one stimulus outside the Response Field reduced peak firing rates approximately 50%, like our results for single-units (see Figure S3-4A for combined SU and MU results). When both stimuli were outside of the Response Field, the latencies were slightly longer (OUT_OUT: MU = 21.89 ms ± 0.60) than when both stimuli were inside the Response Field (IN_BOTH: MU = 18.52 ms ± 0.63, P = 0.002; CN_IN: MU = 17.80 ms ± 0.30, P < 0.0005). This effect was not significantly different when single unit data were analyzed separately. See Figure S3-4B for combined SU and MU results.

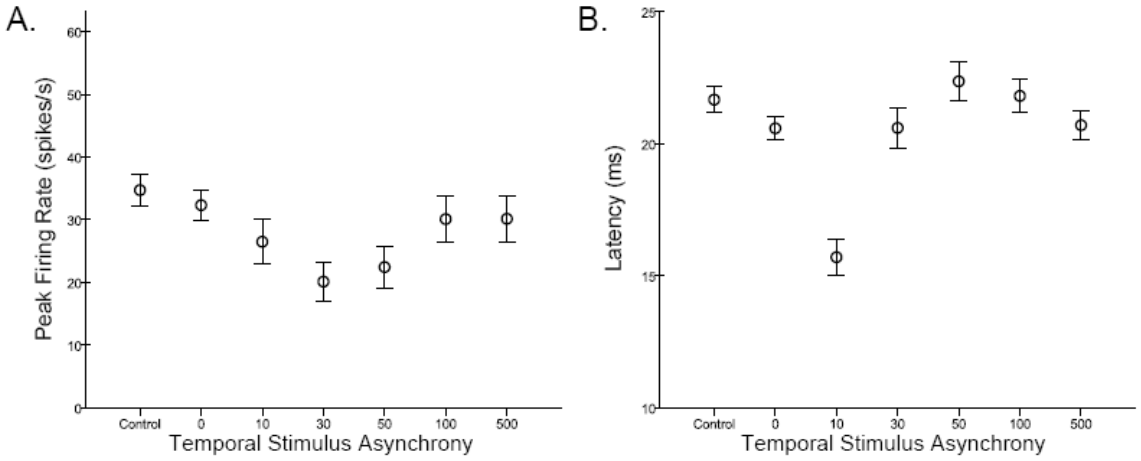

Figure S3-2. Effects of temporal stimulation conditions for peak firing rate and response latency measures from single- and multi-units. Observed mean values from 309 single units and 392 multi-units are shown with error bars representing 95% confidence intervals. A. Means of peak firing rate values (spikes/s) are plotted for each temporal stimulation category comparing the preferred control stimulation (Single) to paired stimulation at 0, 10, 30, 50, 100, and 500 ms stimulus onset asynchronies. Dual-site stimulation suppressed peak firing rates relative to single-site stimulation. A stimulus onset asynchrony of 30 ms resulted in the greatest suppression of peak firing rate, and this suppression was significantly different from all other stimulus categories (P < 0.0005 for all comparisons) except from the 50 ms delay category (P = 0.605). B. Means of response latencies (ms) plotted for each temporal stimulation condition show that 10 ms stimulus onset delays resulted in faster latencies than single-site control stimulation (P < 0.0005).

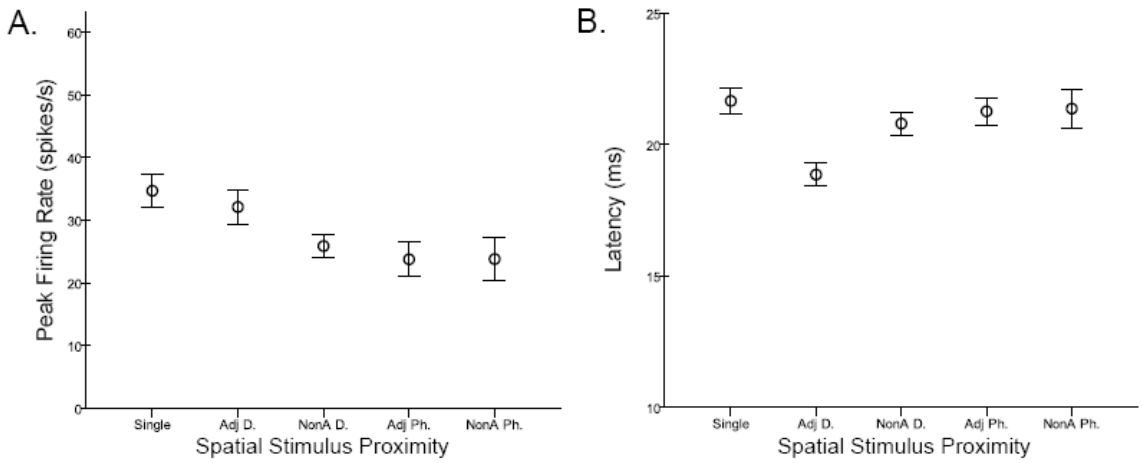

Figure S3-3. Effects of spatial stimulation conditions for peak firing rate and response latency measures from single- and multi-units. Observed mean values from 309 single units and 392 multi-units are shown with error bars representing 95% confidence intervals. A. Means of peak firing rates are plotted for each spatial proximity condition in which the stimuli were presented on separate adjacent digit sites (Adj D.), separate nonadjacent digit sites (NonA D.), within a single digit on adjacent phalanges (Adj Ph.), or within a single digit on nonadjacent phalanges (NonA Ph.). Dual-site stimulation suppressed peak firing rates compared to single-site stimulation for all conditions ($P < 0.0005$) except when nonadjacent phalanges were stimulated ($P = 0.184$). B. Latencies did not vary greatly with spatial stimulus proximity, but latencies were slightly faster in response to stimulation on Adj D. and NonA Ph. compared to single-site stimulation ($P < 0.0005$ and $P = 0.043$, respectively).

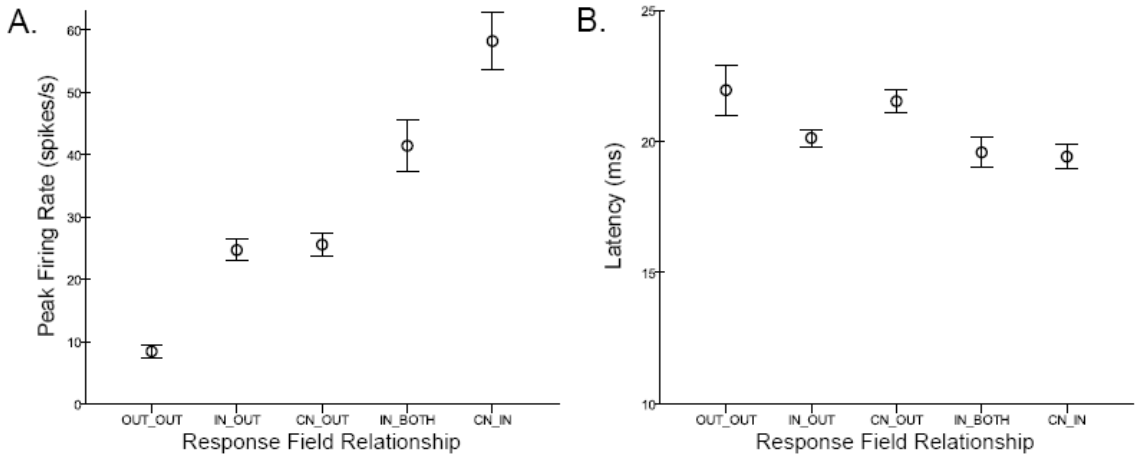

Figure S3-4. Effects of Response Field relationships for peak firing rate and response latency measures from single- and multi-units. Observed mean values from 309 single units and 392 multi-units are shown with error bars representing 95% confidence intervals. A. Means of peak firing rate values are plotted for each type of relationship of the Response Field to the stimulus location. Peak firing rates were lower when the stimuli were outside of the Response Field (OUT_OUT) compared to all other conditions ($P < 0.0005$ for all comparisons). B. Latencies were slightly, but not significantly longer when both stimuli were presented outside of the neuron's Response Field (OUT_OUT) compared to all other Response Field stimulus relationships.

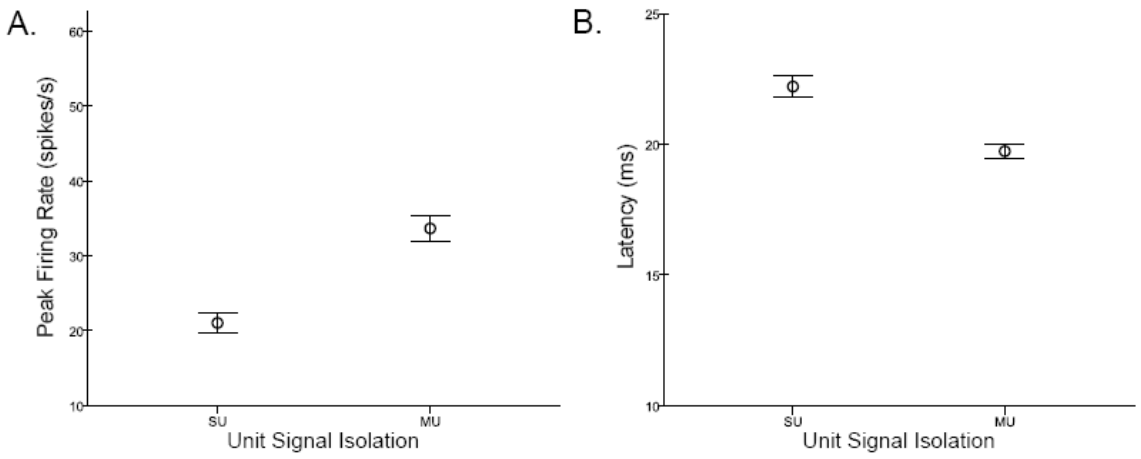

Figure S3-5. Effect of signal isolation for peak firing rate and response latency measures. Observed mean values from 309 single units and 392 multi-units are shown with error bars representing 95% confidence intervals. A. Means of peak firing rates were significantly different between single units (SU) and multi-units (MU), P = 0.004. B. Means of latencies were significantly different between SUs and MUs, P < 0.0005.

Spatiotemporal interactions. To display how peak firing rate responses were affected by presenting the two stimuli at varying spatiotemporal relationships, we normalized the firing rate values by the preferred site stimulation values. Once normalized, firing rate values in SU and MU categories were not significantly different (P = 0.542), therefore, we plotted the normalized values together (Figure S3-6). Peak firing rates were reduced when stimuli were presented at 30 and 50 ms delays at sites both within the neuron's Response Field. Co-stimulating nonadjacent digits resulted in less suppression overall, particularly when one stimulus was inside and the other was outside the Response Field. Stimulation on adjacent phalanges within a digit resulted in strong suppression across all Response Field relationships when the preferred stimulus was presented at 30 and 50 ms delays after the non-preferred stimulus onset. Table S3-5 provides the significant differences for the 3-way interactions between temporal stimulation condition, spatial proximity, and Response Field relationship for the data

normalized to the control condition for individual units. We were interested in the 3- and 4-way interactions in our analysis that take into account all of the tested factors that influence response latencies. To display how response latencies were affected by the paired stimuli presented with varying spatiotemporal relationships compared to the control stimulation for each condition, we normalized the latency values by the control stimulation. Once normalized, latency values in SUs and MUs were not significantly different ($P = 0.438$); therefore, we plotted the normalized values together (Figure S3-7). Since latencies did not vary greatly among units (SD 6.31 ms), the changes in latency due to the stimulus conditions were slight. The shortest latencies occurred in response to the presentation of the preferred stimulus 10 ms after the non-preferred stimulus within the same digit, regardless of Response Field relationship. Short latencies occurred as well as when the preferred stimulus was presented 10 ms after the non-preferred stimulus on adjacent digits when the locations were both within the neuron's Response Field. Table S3-6 provides the results for the significant differences for the 3-way interactions between temporal stimulation condition, spatial proximity, and Response Field relationship after the data for individual units were normalized to the control condition.

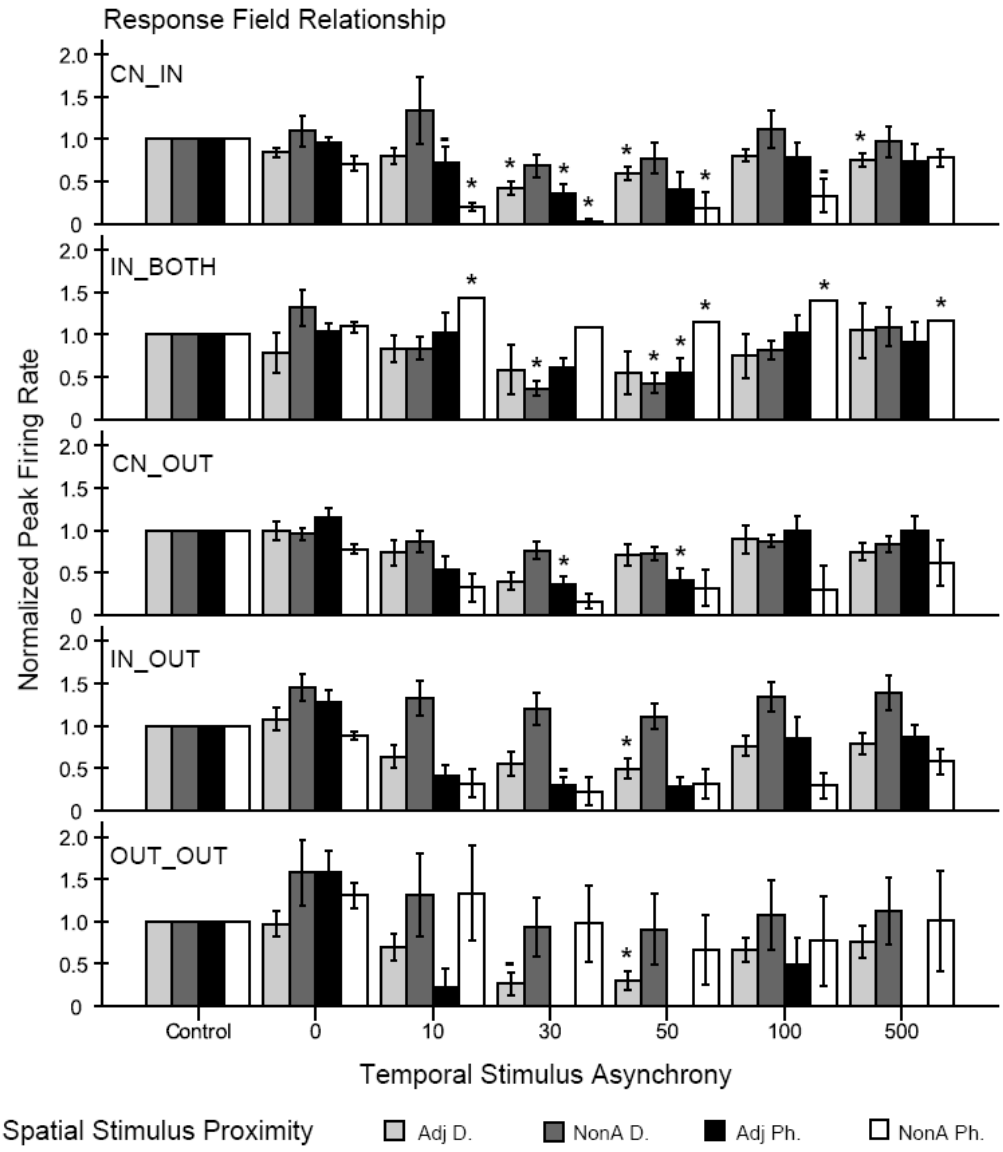

Figure S3-6. Means of peak firing rate values normalized to single-site stimulation across spatial and temporal stimulus conditions. Bar graphs show the mean peak firing rate after the value for each neuron unit was divided by the value during the single-site stimulation on the preferred location in the stimulus pair. Thus, the control values are all equal to 1 and deviations from the control are greater than or less than 1. (See *Methods*.) The temporal stimulation conditions are shown on the x-axis to group the values. Shaded bars indicate the spatial proximity of the tested stimulation: gray, Adj D. = adjacent digits; dark gray, NonA D. = nonadjacent digits; black, Adj Ph. = within 1 digit, adjacent phalanges; white, NonA Ph. = within 1 digit, nonadjacent phalanges or palm pads. When a bar is not shown, there were zero units with significant responses in that category. Separate panels designate the relationship of the stimulation to the Response Field of the reference unit as: CN_IN = 1 probe in the center of the Response Field, 1 probe inside the Response Field; IN_BOTH = 2 probes inside the Response Field, but not in the center; CN_OUT = 1 probe in the center of the Response Field, 1 probe outside the Response Field; IN_OUT = 1 probe inside the Response Field, but not in the center, 1 probe outside the Response Field; and OUT_OUT = 2 probes outside the Response Field. Error bars are ± 1 SEM. Asterisks (*) indicate significant differences $P \leq 0.05$. Dashes (–) indicate differences from control that did not reach the *a priori* significance level, but are $0.100 \geq P > 0.05$. Data are shown for single units and multi-units combined because normalized values were not significantly different ($P = 0.542$).

Table S3-5. Comparisons of peak firing rates normalized to single-site stimulation on the preferred location for 3-way interaction conditions with significant and near significant differences from control values

Temporal Stimulation	Spatial Proximity	Response Field	Mean Difference	P value
10ms	Adj Ph.	CN_IN	0.4679 ± 0.10497	0.081
10ms	NonA Ph.	IN_BOTH	-0.8722 ± 0.1233	< 0.0005
10ms	NonA Ph.	CN_IN	0.5823 ± 0.08341	< 0.0005
30ms	Adj D.	OUT_OUT	0.7200 ± 0.15922	0.060
30ms	Adj D.	CN_IN	0.6769 ± 0.06752	< 0.0005
30ms	NonA D.	IN_BOTH	0.6747 ± 0.07264	< 0.0005
30ms	Adj Ph.	CN_OUT	0.9588 ± 0.16985	< 0.0005
30ms	Adj Ph.	CN_IN	0.8329 ± 0.15228	< 0.0005
30ms	NonA Ph.	IN_OUT	0.5275 ± 0.11836	0.081
30ms	NonA Ph.	CN_IN	0.7479 ± 0.08376	< 0.0005
50ms	Adj D.	OUT_OUT	0.7254 ± 0.09978	< 0.0005
50ms	Adj D.	IN_OUT	0.5606 ± 0.10369	0.001
50ms	Adj D.	CN_IN	0.5701 ± 0.05643	< 0.0005
50ms	NonA D.	IN_BOTH	0.5827 ± 0.11375	0.003
50ms	Adj Ph.	CN_OUT	0.8318 ± 0.13642	< 0.0005
50ms	Adj Ph.	IN_BOTH	1.0229 ± 0.22227	0.041
50ms	NonA Ph.	IN_BOTH	-0.5780 ± 0.12325	0.027
50ms	NonA Ph.	CN_IN	0.5101 ± 0.08376	< 0.0005
100ms	NonA Ph.	IN_BOTH	-0.8299 ± 0.12325	< 0.0005
100ms	NonA Ph.	CN_IN	0.3667 ± 0.08315	0.100
500ms	Adj D.	CN_IN	0.4146 ± 0.07994	0.002
500ms	NonA Ph.	IN_BOTH	-0.6060 ± 0.12325	0.009

Values are means ± SE. Mean difference values (single-site – paired stimulation) are shown for peak firing rate values (spikes/s) normalized so that the single-site stimulation value is always equal to 1 (see *Methods*). P values reported from Bonferroni correction for multiple comparisons in SPSS. (See *Methods* for detailed description of Response Field and for abbreviations).

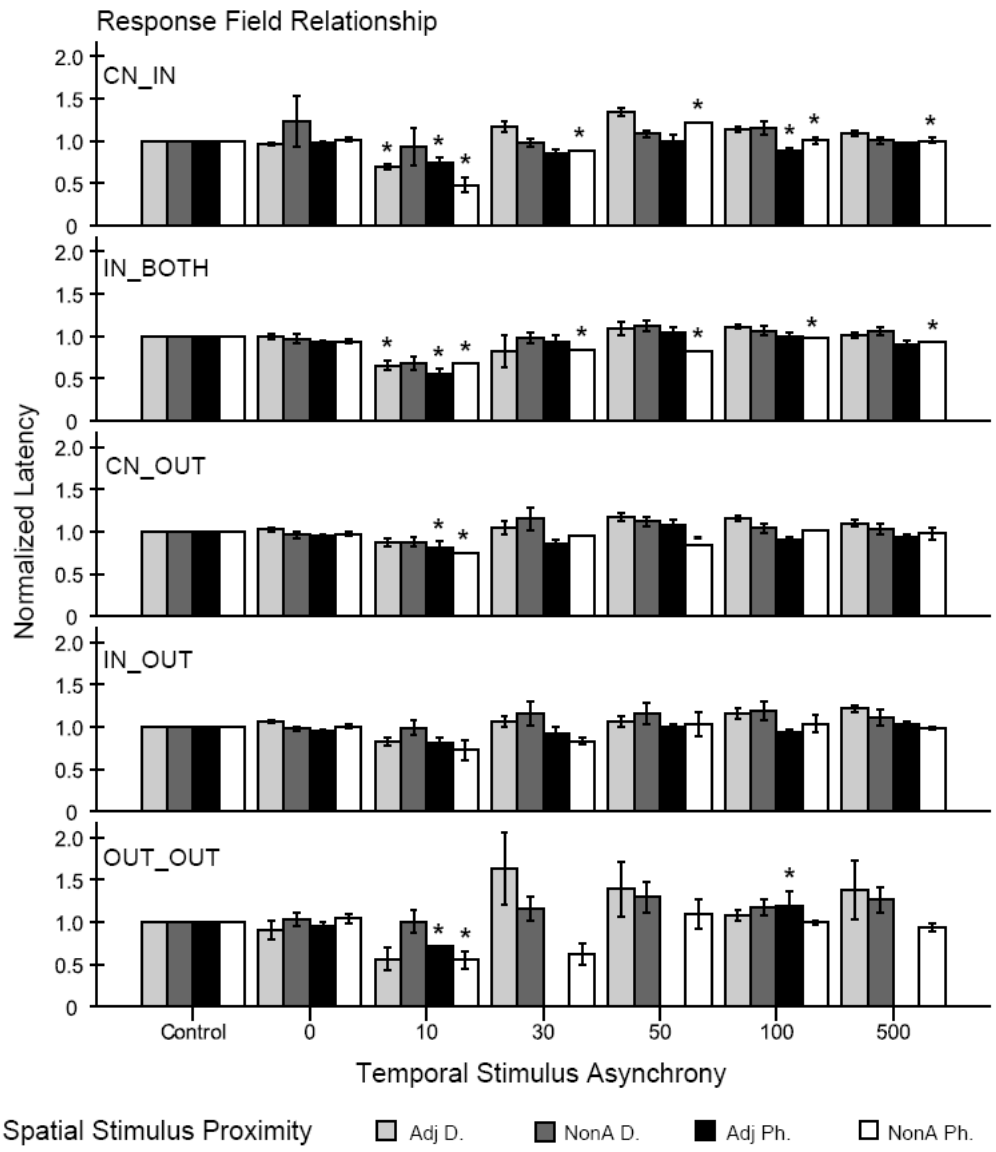

Figure S3-7. Mean latency normalized to control stimulation across spatial and temporal stimulus conditions. Bar graphs show the mean excitatory latency after the value for each neuron unit was divided by the value during the control stimulation, with the conventions as in Figure S3-6. Error bars are ± 1 SEM. Asterisks (*) indicate significant differences $P \leq 0.05$. The dash (–) indicates difference from control that did not reach the *a priori* significance level, but is $0.100 \geq P > 0.05$. Data are shown for single units and multi-units combined because normalized values were not significantly different ($P = 0.438$). While effects were present, the latency differences were small and less systematic than the effects on peak firing rate (Figure S3-6).

Table S3-6. Comparisons of latencies normalized to single-site stimulation on the preferred location for 3-way interaction conditions with significant and near significant differences from control values

Temporal Asynchrony	Spatial Proximity	Response Field	Mean Difference	P value
10ms	Adj D.	IN_BOTH	0.3439 ± 0.05286	< 0.0005
10ms	Adj D.	CN_IN	0.2826 ± 0.05760	0.009
10ms	Adj Ph.	OUT_OUT	0.2690 ± 0.01272	< 0.0005
10ms	Adj Ph.	CN_OUT	0.2826 ± 0.05628	0.005
10ms	Adj Ph.	IN_BOTH	0.4049 ± 0.03779	< 0.0005
10ms	Adj Ph.	CN_IN	0.2706 ± 0.04725	< 0.0005
10ms	NonA Ph.	OUT_OUT	0.3113 ± 0.06509	0.016
10ms	NonA Ph.	CN_OUT	0.3243 ± 0.03720	< 0.0005
10ms	NonA Ph.	IN_BOTH	0.5029 ± 0.03106	< 0.0005
10ms	NonA Ph.	CN_IN	0.4906 ± 0.05652	< 0.0005
30ms	NonA Ph.	IN_BOTH	0.3088 ± 0.02563	< 0.0005
30ms	NonA Ph.	CN_IN	0.1749 ± 0.01466	< 0.0005
50ms	NonA Ph.	CN_OUT	0.2170 ± 0.04802	0.058
50ms	NonA Ph.	IN_BOTH	0.3355 ± 0.02720	< 0.0005
50ms	NonA Ph.	CN_IN	-0.1616 ± 0.01488	< 0.0005
100ms	Adj Ph.	OUT_OUT	-0.2020 ± 0.00397	< 0.0005
100ms	Adj Ph.	CN_IN	0.1198 ± 0.01756	< 0.0005
100ms	NonA Ph.	IN_BOTH	0.1769 ± 0.02503	< 0.0005
100ms	NonA Ph.	CN_IN	-0.0525 ± 0.01016	0.002
500ms	NonA Ph.	IN_BOTH	0.2151 ± 0.02542	< 0.0005
500ms	NonA Ph.	CN_IN	-0.0505 ± 0.01014	0.006

Values are means ± SE. Mean difference values (single-site – paired stimulation) are shown for latency values (ms) normalized so that the single-site stimulation value is always equal to 1 (see *Methods*). P values reported from Bonferroni correction for multiple comparisons in SPSS. (See *Methods* for detailed description of Response Field and for abbreviations).

CHAPTER IV

EFFECTS OF SPATIOTEMPORAL STIMULUS PROPERTIES ON SPIKE TIMING CORRELATIONS IN OWL MONKEY PRIMARY SOMATOSENSORY CORTEX HAND REPRESENTATION

Abstract

Neuronal spike timing correlations may be one way in which stimulus properties are encoded in primary somatosensory cortex. One aspect of neuronal correlations that has not been well studied is how the spatiotemporal properties of tactile stimuli may affect the presence and magnitude of correlations. We presented single- and dual-site stimuli with varying spatiotemporal relationships to the hands of three anesthetized owl monkeys (*Aotus trivirgatus)* and recorded neuronal activity from 100-electrode arrays implanted in primary somatosensory cortex. We examined the correlation magnitudes derived from joint peristimulus time histogram (JPSTH) analysis of single neuron pairs to determine how spike timing correlations may be related to spatiotemporal stimulus properties. As expected, we found that the *proportions* of correlated pairs tended to decrease as the distance between the electrodes increased. Additionally, correlations were related to the stimuli such that when paired stimulus sites were closer spatially, the proportions of correlated pairs were greater (~24%, adjacent phalanges) than when the paired stimuli were distant (~15%, nonadjacent digits). Presenting paired stimuli at stimulus onset asynchronies had small but significant effects on the correlation *magnitude*. The spatial proximity of the paired stimuli also affected the correlation magnitude, but the relationship did not precisely follow that expected based on cortical

connectivity between stimulus sites. These results provide evidence that spatiotemporal integration occurs at the level of area 3b in monkeys in unexpected ways.

Introduction

In daily life, tactile stimulation occurs at multiple points simultaneously (such as when one is seated at a desk, typing), and the tactile sensations we experience may be suppressed or utilized in our behavior. In a highly simplified version of the real-life situation, we stimulated two points simultaneously or asynchronously on adjacent and nonadjacent hand sites to examine the spatiotemporal stimulus effects on cortical populations in primary somatosensory cortex, area 3b, in three anesthetized owl monkeys. We hypothesized that spike timing correlations would be related to the spatiotemporal properties of tactile stimulation in predictable ways based on anatomical connectivity. Our goal was to extend the existing studies on the properties of correlations in primary somatosensory cortex of primates to determine if spatial and temporal stimulus manipulations affect the presence and magnitude of spike timing correlations. As discussed in our previous paper (Reed et al., 2008), we focus on correlated firing that may reflect a common input arriving nearly simultaneously to the neurons, or lateral connections within cortex, or may reflect both types of connections. The properties and possible roles of neuronal correlations are actively studied in multiple brain areas and are reviewed elsewhere (e.g., Salinas and Sejnowski, 2001; Jermakowicz and Casagrande, 2007), but the existing information on the correlations in primate primary somatosensory cortex is perhaps less extensive than data from primate primary visual cortex. We briefly

review studies of primary somatosensory cortex from which we inferred that spatiotemporal stimulus parameters may affect neuron correlations.

We are particularly interested in the hand representation of the primate somatosensory cortex, and while spatiotemporal contributions to changes in correlated activity have not been completely specified, we draw from previous work in this model. Spike timing correlations have been shown to change in the 3b hand representations of two owl monkeys following long-term behavioral training to detect taps presented to adjacent digits (Blake et al., 2005). Receptive fields expanded, often to include sites on the two adjacent digits stimulated; and correlations between neuron pairs emerged across distances ≤ 1.4 mm (Blake et al., 2005). Thus, it has been established that providing asynchronous taps on adjacent digits in a behaviorally relevant context affects the presence of correlations between neuron pairs. Our study tests if similar stimuli affect the presence and magnitude of correlations in anesthetized monkeys.

Area 3b in primates is the homologue of S1 in other mammals (Kaas, 1983); and correlated spiking activity in S1 of anesthetized cats has been shown to relate to features of stationary and moving air jet stimuli, including location preference and directional selectivity based on the correlation magnitudes (Roy and Alloway, 1999). For example, some neuron pairs were more strongly correlated when stationary air jets stimulated one site over another, and some neuron pairs were more strongly correlated when the air jet moved in one direction versus the opposite (Roy and Alloway, 1999). In anesthetized rats, whiskers were stimulated at different frequencies and the correlations in S1 neuron pairs were compared to determine if particular stimuli were more likely to cause correlations (Zhang and Alloway, 2004). While neurons in layer 4 did not show clear

selectivity for stimulus frequency, neuron pairs in other layers showed evidence for selectivity for high or low frequencies (Zhang and Alloway, 2004). In an extension of this study, Zhang and Alloway (2006) used air jets moving along the rows and arcs of the rat whiskers to examine directional selectivity of the correlated activity. They found that correlation magnitudes were strongest for pairs in the same row of barrel cortex and strongest for stimulation moving along a row rather than an arc. Thus, they concluded that the strength of correlations varied with the density of intracortical connections. (Zhang and Alloway, 2006) Therefore, a basis for spatial and temporal stimulus parameters to affect pairwise correlations in S1 has been generally established by studies in anesthetized cats and rats.

We had the following expectations of our results. As the density of intrinsic connections has been implicated in affecting the strength of neuronal correlations (e.g., Roy and Alloway, 1999; Blake et al., 2005; Zhang and Alloway, 2006), we expected that neurons close in spatial proximity cortically would tend to have higher correlation magnitudes than distant neurons we recorded in anesthetized owl monkeys. Further, we expected that simultaneous stimulation of paired locations would result in higher correlations between neuron pairs with common input (compared to asynchronous stimulation), since the synchronization of the stimuli would be reflected in the neuron firing. Spatial and temporal parameters might interact, such that the strongest correlations might occur for neuron pairs closest in cortical space, representing the closest locations on the hand, when the stimuli were presented closest in time. Then, we expected interactions to vary as a function of spatial and temporal proximity in a predictable pattern. Thus, we expected our results to yield probable explanations for the properties of

correlations in area 3b in the primate hand representation. To test our predictions, the current study examined the effects of both spatial and temporal stimulus features by presenting paired stimuli simultaneously and at selected stimulus onset asynchronies on locations that varied in spatial proximity on the hand (from sites within a single digit to sites across digits). We published an initial report from two of the three monkeys described here in which we compared the correlation magnitudes between stimulation on a single digit site with simultaneous stimulation on nonadjacent digit sites to examine the occurrence and magnitudes of correlations across the 3b hand representation (Reed et al., 2008). Here we extend those studies to describe the spatiotemporal stimulus effects on the occurrence and magnitude of correlations.

Materials and Methods

Preparation

All procedures followed the guidelines established by the National Institutes of Health and the Animal Care and Use Committee at Vanderbilt University. Three adult owl monkeys (*Aotus trivirgatus*) were prepared for electrophysiological recordings in primary somatosensory cortex as previously described (Reed et al., 2008). Cases 1 and 2 were males, each weighing1 kg, and case 3 was a female, weighing 1.2 kg. The same three monkeys were part of a study on neuron response properties (Chapter 3), and cases 1 and 2 were part of a previous study related to spike timing correlations (Reed et al., 2008). A ketamine injection (10-30 mg/kg, intramuscular) was administered to each monkey for sedation during surgical preparations. Anesthesia was induced with 2-4%

halothane gas and intravenous propofol (10 mg/kg/hr) was used to maintain anesthesia during surgery. A servo-controlled heating pad was used to maintain body temperature (measured rectally) between 37-39°C. The monkey was secured in a stereotaxic device throughout the surgery and experiment. Paralysis was maintained by intravenous vecuronium bromide (0.1-0.3 mg/kg/hr) mixed with 5% dextrose and Lactated Ringer's solution after the initial induction dose of 1-3 ml vecuronium bromide. Animals were then artificially ventilated with a mixture of N_2O: O_2: CO_2 (75: 23.5: 1.5) at a rate sufficient to maintain peak end tidal CO_2 at ~ 4%. Electrocardiograms and electroencephalograms aided our assessment of anesthetic depth. A craniotomy and duratomy were performed overlying the area of interest in primary somatosensory cortex. The pneumatic array inserter was set to 600 µm depth to aim for placement of the electrode tips within layer 3 of cortex. The opening was covered with 1% agar mixed with Ringer's solution to prevent desiccation and provide electrode stability. Supplemental anesthesia during recordings was provided by 0.3 mg/kg/hr propofol following the completion of surgical procedures. In monkey 3, 1.2 mg/kg sufentanil was added to the Lactated Ringer's solution for infusion during the surgical procedures in order to stabilize anesthetic depth. Following delivery of this sufentanil dose, monkey 3 was maintained under propofol anesthesia and vecuronium bromide paralysis without supplemental sufentanil for the remainder of the recording experiment.

Stimulation Procedures

We collected responses to paired stimulation on adjacent and nonadjacent digits, as well as on adjacent and nonadjacent phalanges within a single digit. Two independent

force- and position-feedback controlled motor systems (300B, Aurora Scientific Inc., Aurora, ON, CA) provided the paired stimulation via a custom-designed Visual Basic program. Round Teflon probes 1 mm in diameter were secured to the lever arms of the motors to provide a small contact surface of stimulation. Stimulus probes indented the skin 0.5 mm for 0.5 s, followed by 2.0 s off of the skin, for 100 to 120 trials (255-300 s). (Data were analyzed from 100 trials.) The long indentation allowed us to record transient and sustained responses (Sur et al., 1984). Indentations were delivered to selected skin sites simultaneously (0 ms) and at stimulus onset asynchronies of 10, 30, 50, 100, and 500 ms to study the effects of varying the temporal proximity of stimuli on correlations in spike timing between neuron pairs. Each site in the stimulus pair was also stimulated individually for 100-120 trials and considered "control stimulation". We mapped receptive fields during the experiment to help reconstruct the electrode array location. We used minimal receptive field mapping to aid our placement of the stimulus probes. We followed standard mapping procedures as published elsewhere (Merzenich et al., 1978; Nelson et al., 1980), and our procedures for mapping and tactile stimulation have been published (Reed et al., 2008).

Data Acquisition

Recordings were made using the 100-electrode "Utah" array and the Bionics Data Acquisition System (now Blackrock Microsystems, Salt Lake City, UT). Signals were amplified by 5000 and band-pass filtered between 250 Hz and 7.5 kHz. Each electrode threshold was automatically set for 3.25 times the mean activity. The waveforms were sampled at 30 kHz for 1.5 ms windows (Samonds et al., 2003).

Histology

Following data collection, animals were given an overdose of sodium pentobarbital and perfused transcardially with saline followed by fixative. The brains were removed and prepared for histological analysis as described previously (Jain et al., 2001). The cortex was separated from the thalamus, flattened, and cut frozen at 40 µm. We processed sections for myelin to aid in reconstructing the electrode sites. (See Reed et al., 2008; Figure SI 4) The appearance and disappearance of electrode tracks across serial sections was used to estimate electrode depth.

Data Analysis

Spike Sorting and Data Selection

Details regarding the spike sorting procedures are reported fully in Reed et al., 2008. Recording files were opened in Matlab (The Mathworks, Inc., Natick, MA) and signals for a given stimulus block were sorted together offline with an automatic spike classification program based on the t-distribution Expectation Maximization algorithm (Shoham et al., 2003) which is made available with the data acquisition system. A second spike sorter program, Plexon Offline Sorter (Plexon Inc., Dallas, TX), was then used to verify the quality of unit isolation such that single units had refractory periods ≥ 1.2 ms; p values ≤ 0.05 for multivariate ANOVA related to cluster separation; and distinct waveform amplitudes and shapes when compared with other activity on the same electrode (Nicolelis et al., 2003). Only single units were included in this analysis and only one single unit per electrode was included in the analysis to avoid possible spurious

correlations between units on the same electrode if our unit isolation was imperfect. When more than one single unit was collected on an electrode, we selected the single unit with the best waveform isolation and the best responsiveness over multiple stimulation conditions. In addition to selecting only single units to include in the analysis, we included only those units that met the following conditions: 1) the unit should respond to at least one of the conditions in a stimulus series or 2) should have mean firing rates greater than 2 spikes/s during the sustained portion of the stimulation between 100 and 500 ms after stimulus onset and 3) if the unit did not respond to any of the conditions in a stimulus series, at least half of the conditions should produce firing rates that meet condition #2. These criteria reduced the number of units that would have too few spikes for a valid calculation of the spike timing correlations (e.g., Aertsen et al., 1989; Gerstein et al., 1989; Gerstein, 2000). From the selected single units, we generated all of the possible pairs for cross-correlation analysis.

Spike Timing Correlations

While there are many aspects of the JPSTH and cross-correlation histogram to examine, our measure of interest in this study was the magnitude of the peak correlation. We followed the same methods for obtaining the peak correlations between neurons pairs that we published previously (Reed et al., 2008) in which the cross-correlation histogram is derived from the conventional joint peristimulus time histogram (JPSTH) analysis (e.g., Aertsen et al., 1989; Gerstein et al., 1989; Ventura et al., 2005) with all the spike trains aligned on the onset of skin indentation, similar to other studies in somatosensory cortex (S. Roy et al., 1999, 2001; Zhang and Alloway, 2004, 2006; Blake et al., 2005; A.

Roy et al., 2007). To measure precise spike timing synchrony, small bin sizes between 1-5 ms are often used to ensure that each bin contains 1 spike or less (e.g., Aertsen et al., 1989; Gerstein et al., 1989; Oram et al., 2001; Alloway et al., 2002; Roy et al., 2007). We chose an intermediate bin size of 10 ms due to the low spontaneous firing rates in the cortex under anesthesia. Bin sizes greater than 5 ms have been used by others (e.g., Vaadia et al., 1995; Oram et al., 2001) and this resolution is finer than the coarse temporal synchrony found using bin sizes larger than 20 ms (Oram et al., 2001). For our data, the 10 ms bins still allow most bins to contain 1 spike or less, as only the occasional transient response reaching 100 spikes/s or more will violate this assumption, and this bin size allows us to measure the correlation during the sustained portion of the stimulus in which firing rates were relatively low and often did not reach an appropriate number of spikes for use in the JPSTH calculation (Aertsen et al., 1989; Gerstein et al., 1989; Gerstein, 2000) without this binning adjustment. The JPSTH was measured in windows from 0 to 700 ms after stimulus onset (70 bins) and was normalized by the standard method of subtracting the shift-predictor to correct for the effects of firing rate on the coincidence of spike occurrences. We then tested the reliability of the normalized JPSTH to determine which of the peak correlations derived from the normalized JPSTHs could be considered a significant correlation value among the population that we collected. The JPSTHs were grouped based on the spatial and temporal stimulus conditions and the relationship of the neuron pairs to the stimulus sites. Then, for one of each pair of neurons, the order of the trials was shuffled and the "shuffled correlation" value was derived from this JPSTH. These shuffled correlations were obtained for all of the pairs in each spatiotemporal group, and we used a bootstrapping procedure (5000 iterations) to

test the normalized peak correlation values from each neuron pair against the distribution of the population of shuffled correlation values. Correlation values which exceeded two times the standard deviation over the mean of the bootstrapped distribution were considered significant. Our standard corrections in the correlation calculations reduce the impact of responses in unconnected neurons to a common stimulus and statistical coincidence due to firing rate. Like others, we acknowledge that "uncorrected correlations" likely have roles in stimulus processing (e.g., Gerstein et al., 1989), but our goal was to relate correlations to functional connectivity. Figure 4-1 shows a normalized JPSTH and a shuffled JPSTH from two neurons recorded in area 3b of monkey 1 to demonstrate the method. We compared the significant peak correlation values across stimulus conditions to determine how spatiotemporal stimulus properties may affect the correlation strength in the summary analysis described in a later subsection.

To represent the relationship of the electrode distance between the correlated neurons with the magnitude of the spike timing correlations, we measured the distance between electrodes and the correlation strength when the dual-site stimuli were presented simultaneously. We examined these paired values of distance and spike timing correlation magnitude in a scatter plot categorized by the proximity between the stimulus locations, and for each obtained the linear correlation coefficient using Matlab ("corrcoef" command). For visualization purposes, we developed a spatial representation of the 100-electrode array as published previously (Reed et al., 2008). In these schematics, dots signify the location of each neuron in the array, and the dot sizes indicate the mean correlation strength for the neuron at that electrode location, averaged

across all of the neuron pairings. We graphed connecting lines between pairs of correlated neurons and depicted the strength of the correlation by the line thickness.

Firing Rate Responses

We performed two types of firing rate measures. The first measure was used to determine the relationship between average firing rates and correlation magnitudes. The geometric mean spike rate is commonly used for this purpose to average the firing rates of the two neurons in the correlated pair (e.g., Bair et al., 2001; de la Rocha et al., 2007; Greenberg, 2008; Jermakowicz et al., 2009). For this measure, we took the average firing rate of each neuron during the period for which the correlation was determined, 0 to 700 ms from stimulus onset. The geometric mean firing rate (GMFR) was calculated as the square root of the product of the two neurons' firing rates.

The second measure was used to determine the relationship of the responsiveness of the individual neurons in the correlated pair to the stimulus location. We collected information about the receptive fields of each neuron with the intention of grouping the data based on the relationship of the neurons in the pair to each other and to the stimulus sites using a "Response Field" calculation we described in a companion study (Chapter 3). However, the relationship of the receptive fields of both neurons in each correlated pair with the locations of each stimulus probe was complex and had too many levels to analyze meaningfully (44 levels that could be grouped to a minimum of 9 levels). To include an assessment of the firing rate responses of each neuron in a correlated pair may affect the magnitude of correlation, we used a factor based on firing rate that is similar to measuring receptive field overlap, but is simplified to a calculation of the presence or

absence of a response to stimulation. We termed our variable "pair response" to relate the responses of the neurons in the correlated pair. If both neurons in the pair responded to the given stimulation, pair response = 2; if only one of the neurons in pair responded to stimulation, pair response = 1; and if neither neuron responded to the stimulation, pair response = 0.

Neuron responsiveness was determined based on the peak firing rate meeting criteria as follows. First, spike data were smoothed by convolving spike trains with a function resembling a postsynaptic potential using Matlab (The Mathworks, Inc., Natick, MA), as described in Reed et al., 2008. Next, the peak firing rate was calculated from 100 trials as the maximum of the spike density function within a response time window (50 ms after stimulation onset) and corrected by subtracting the average baseline firing rate calculated over 500 ms prior to stimulation onset. The threshold value for excitatory responses was determined as the average baseline firing rate plus two standard deviations of this baseline, with a minimum value of 5 spikes/s. If the peak firing rate exceeded the threshold value, it was considered a significant response. The response designation for each neuron in a correlated pair was combined to result in the final value for the "pair response" measure. The variable is not equivalent to a measure of receptive field overlap, but actually relates to the relationship of the two neurons' receptive fields with the stimulus locations. Pair response = 0 does not mean the pair has 0% receptive field overlap, but it means that the stimuli were outside of the receptive fields of both neurons in the correlated pair.

Summary Statistics

Data from Matlab calculations for neuron correlation measures were compiled and summarized in Excel to determine which normalized correlations were statistically significant out of the total recorded pairs and to import only the information from neuron pairs with significant correlations into SPSS 17.0 (SPSS, Inc., Chicago, IL) for further analysis. The information associated with each significant correlation included: 1) the temporal stimulation type of single- or dual-site stimulation at 0, 10, 30, 50, 100, or 500 ms stimulus onset delays; 2) the spatial proximity of the stimulus probes in the stimulus series of adjacent digits (Adj D.), nonadjacent digits (NonA D.), adjacent phalanges within a digit (Adj Ph.), or nonadjacent phalanges within a digit (NonA Ph.); and 3) a variable we termed "pair response" related to the firing rate response to stimulation of each neuron in the pair. (See above for determination of the pair response variable.)

We performed a form of analysis of variance on the factors related to the stimulus onset asynchrony, the proximity of the stimuli, and the pair response relationship of the neuron pairs. The data had several properties that led us to use Generalized Estimating Equations, an extension of Generalized Linear Models (for review, Tuerlinckx et al., 2006), to analyze the factors contributing to the variance in correlation magnitudes. The data were imbalanced by group, and most importantly, the data were likely to be correlated rather than best considered independent observations (e.g., Hardin and Hilbe, 2003, p. 3-5) since some of the same neuron pairs had been recorded across several temporal stimulation conditions. This analysis has fewer assumptions regarding the data distribution than a parametric repeated measures analysis of variance and accounts for the possibility of correlated (non-independent) data across the stimulus measures (e.g., Liang

and Zeger, 1986; Zeger and Liang, 1986). We used this approach to estimate the sources of variance in the data set of correlation values related to the factors of the temporal stimulus condition, the spatial proximity of the stimuli, and the pair response relationship of the neuron pairs. The Bonferroni correction for multiple comparisons was applied within the analysis. The Generalized Estimating Equations analysis provides estimates of the population averages of the correlation magnitude (our dependent variable) based on the values of the predictor variables and estimates for the significance of the effects.

To compare correlation magnitudes with other measures, we performed linear regression using SPSS. These measures included cortical distance between correlated neurons and geometric mean firing rate (GMFR) between correlated neurons.

Results

The majority of the electrodes were located in the area 3b hand representation (see Figure 4-1 for case 1; Figure 4-3 for case 3; Figure 4-4 for case 2). The neurons included in the analysis were drawn primarily from area 3b as neurons in areas 3a and 1 did not respond well under the anesthetic conditions. We obtained the fewest single unit pairs from monkey 1, at 2,921 pairs, since this experiment was our first and shortest in recording duration. We obtained 58,571 single unit pairs across the experiment duration from monkey 2, and 25,420 pairs from monkey 3.

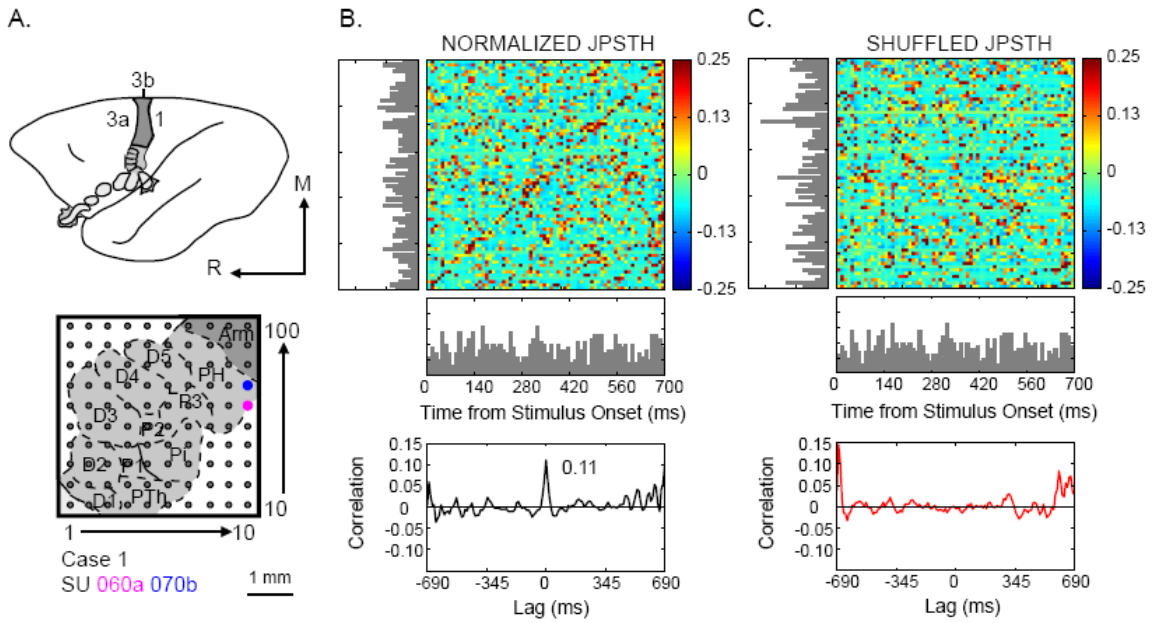

Figure 4-1. Example of a normalized and a shuffled JPSTH reveal significant correlations in spike timing between two neurons. A. The estimated array location for case 1 within the area 3b hand representation is shown with the approximate representations of the digits (D1-5) and the palm including the digital (P1-3), thenar (PTh), hypothenar (PH) and insular (Pi) pads are outlined. The pink and blue dots mark the electrodes where the two neurons "060a" and "070b" were recorded for the analysis shown. These two single units recorded from the hypothenar palm pad representation (PH) showed strong spike timing correlations revealed in the normalized JPSTH and the correlation histogram derived from the JPSTH during single-site stimulation on P1 (B). B, top. Spike timing synchrony between the two neurons is shown in the normalized JPSTH matrix for 10 ms bins. The color code represents the magnitude of the normalized correlation at lag times over a poststimulus time of 700 ms, with the 0 ms lag time at the diagonal. The PSTHs from the two neurons in response to 100 repetitions of 0.5 s skin indentations on P1 are shown to the left and below the matrix. The red and blue lines overlying the PSTHs indicate that matched trials were analyzed (i.e., spikes in trial 1 from unit 060a were binned with spikes in trial 1 from unit 070b). B, bottom. The cross-correlation histogram derived from the normalized JPSTH is computed by summing the JPSTH bins parallel to the main diagonal to show the average correlation magnitude. In this case, spike times were correlated at the 0 ms lag with a peak magnitude of 0.11. The peak magnitude of the correlation is our measure of interest, and we determine if this peak magnitude exceeds that determined when the precise spike timing is disrupted by shuffling the trials. C, top. The shuffled JPSTH is determined by shuffling the trials with respect to each other to disrupt spike timing without changing the average firing rate. The trial shuffling is indicated by the blue dashes overlying the PSTHs of each neuron such that the trials of neuron 2 do not match the trials of neuron 1 (i.e., spikes in trial 1 from unit 060a were binned with spikes in trial 25 from unit 070b). C, bottom. The correlation derived from the shuffled JPSTH is compared to the correlation from the normalized JPSTH to determine if the peak in the normalized correlation exceeds two times the standard deviation over the mean of the shuffled correlation. Additionally, to determine whether peak correlation magnitudes represented significant correlations within the population, we compared each peak correlation to a distribution of shuffled correlations obtained for a population of neuron pairs as described in the *Methods*. In subsequent figures of JPSTH-derived correlations, the normalized correlations are shown as a black line and the shuffled correlations are overlaid as a red line.

To evaluate the spatiotemporal factors contributing to differences in correlation magnitude, we selected only those pairs which were determined to be significantly correlated within the population (see *Methods*). Thus, we analyzed 16,011 normalized peak correlations from 4,938 single unit pairs, as some pairs were recorded across multiple stimulus conditions. The mean of the observed correlation magnitudes for the dataset was 0.0335 (SD 0.0149), and the median and mode were both 0.0300. The maximum correlation observed in the data set was 0.22 and the minimum for significant correlation values was 0.01. We used Generalized Estimating Equations to determine the significant sources of variance between correlated pairs, using a factorial model of temporal stimulus asynchrony, spatial stimulus proximity, and the (firing rate) responses of both units in the pair to the stimulation. The distribution of the correlation magnitudes across these spatial and temporal conditions is shown in Figure 4-2. The estimated mean correlation magnitude was 0.034, which was close to the observed mean. All main effects, two-way interactions, and three-way interactions tested were highly significant as determined through the Generalized Estimating Equations analysis (Table 4-1). All figures plot the observed data, while significance values of the statistical effects were determined based on the estimates of the data from the statistical analysis. Figure 4-3 shows the main effects on correlation magnitudes for temporal asynchrony, spatial proximity, and responsiveness categories for the observed correlation values.

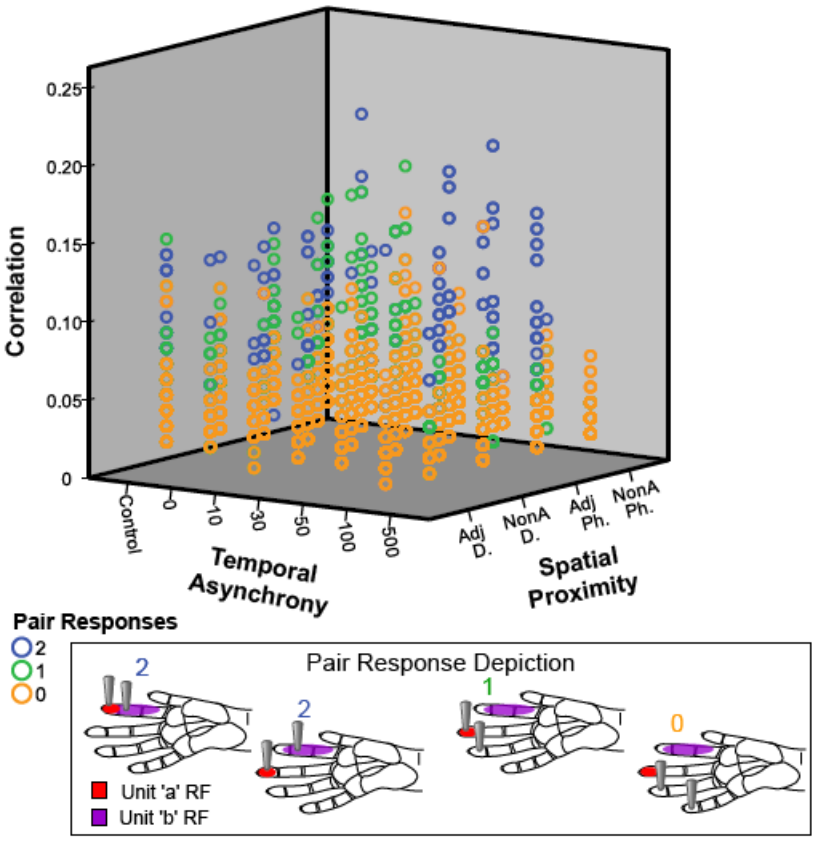

Figure 4-2. Peak correlations between single units plotted in three dimensions show distributions across spatiotemporal parameters. Peak correlations significantly greater than the shuffled correlations are shown in the 3-D scatter plot with the temporal stimulation condition plotted on the x-axis, and the spatial proximity of the paired stimulus sites plotted on the z-axis, versus correlation magnitude on the y-axis. The marker color indicates the pair response condition, which refers to whether both, one, or neither unit in the pair responded with significant firing rate increases to stimulation. When neither unit responded to stimulation, correlation magnitudes tended to be lowest across all other conditions. The schematic depicts the configurations of the stimulation probes in relation to receptive fields (RFs) for hypothetical units in a correlated pair, unit "a" and unit "b". When the pair response value is 2, two types of relationships are possible. The RFs of the two units can be close in proximity and the stimulation can be close in proximity (within the same digit) so that both units in the pair respond to stimulation. Alternatively, the RFs of the units could be distant (on adjacent or nonadjacent digits) and one stimulus probe is within the RF of one unit, while the second probe is within the RF of the second unit. Thus, this categorization does not directly relate to RF overlap, but rather relates to mutual firing rate increases due to stimulation inside the RF.

Table 4-1. Tests of model effects for variance in correlation magnitude classified by spatiotemporal stimulus characteristics and interactions

Variance Source	Wald Chi-Square	df	P value
(Intercept)	6141.513	1	< 0.0005
Temporal Asynchrony	151.236	5	< 0.0005
Spatial Proximity	46.048	3	< 0.0005
Pair Response	74.818	2	< 0.0005
Temporal x Spatial	131.679	15	< 0.0005
Temporal x Response	66.337	10	0.001
Spatial x Response	43.344	6	< 0.0005
Temporal x Spatial x Response	135.125	30	< 0.0005

Tests of model effects using Generalized Linear Modeling with Generalized Estimating Equations on the dependent variable correlation. N = 16011 observations from single neuron pairs.

Temporal Stimulus Asynchrony

Presenting the stimulation alone or in pairs simultaneously and at delays from 10-500 ms had small but significant effects on the correlation magnitudes. The variations in correlation magnitudes did not follow predictable patterns, as shown in Figure 4-3A. The estimated mean correlation when a single location was stimulated (0.0341 ± 0.00034)

was greater than the mean correlation when two locations were stimulated simultaneously (0.0319 ± 0.00040; P < 0.0005) and was less than the correlation when stimuli were presented at the following onset delays: 10 ms (0.0363 ± 0.00053; P < 0.0005) and 100 ms (0.0373 ± 0.00063; P < 0.0005). When stimuli were presented at the other tested delays, the correlation magnitudes were not significantly different from single-site stimulation (30 ms = 0.0341 ± 0.00074, P = 1.000; 50 ms = 0.0356 ± 0.00093, P = 1.000; 500 ms = 0.0333 ± 0.00062, P = 1.000). These correlation magnitudes varied within a small range, but the differences were statistically significant. In contrast to our predictions, correlation magnitudes did not decrease as the paired stimuli were separated by longer time delays.

Spatial Stimulus Proximity

The effects of spatial proximity on correlation magnitudes differed slightly from those expected. We expected that the strongest correlations would occur when adjacent phalanges within a digit were stimulated because these locations are close in proximity and densely connected in area 3b, while the weakest correlations would occur when nonadjacent digits were stimulated., The correlation magnitudes we observed are shown in Figure 4-3B. The estimated correlation magnitude when a single site was stimulated was 0.0341 ± 0.00034, which was significantly less than the correlation magnitude when adjacent digits were stimulated (Adj D. = 0.0370 ± 0.00088, P = 0.003) and when adjacent phalanges were stimulated (Adj Ph. = 0.0381 ± 0.00116; P = 0.004); and was significant greater than when nonadjacent phalanges were stimulated (NonA Ph. = 0.0301 ± 0.00083; P < 0.0005). Stimulation on nonadjacent digits did not result in significant

differences from single-site stimulation (NonA D. = 0.0339 ± 0.00077, P = 1.000). Stimulation on adjacent digits resulted in similar correlation magnitudes as stimulation on adjacent phalanges within a digit (P = 1.000), and greater correlation magnitudes than stimulation on nonadjacent phalanges (P < 0.0005) and stimulation on nonadjacent digits (P = 0.047). Generally, a spatial gradient existed such that correlation magnitudes showed dependence on the proximity between the paired stimulus sites.

Pair Response Relationships

We also examined the relationship between the correlation magnitude and the neuron responsiveness to stimulation, and the results were consistent with our expectations. When both neurons in the pair responded to the stimulation the correlation magnitude was higher than when only one neuron in the pair responded and when neither responded (Figure 4-3C). The JPSTH procedure we used to obtain the correlation magnitudes is designed to correct for the correlations expected based on firing rate. (The more spikes each neuron fires, the more chances there are for the spike timings to be correlated between the two reference neurons. The correlation magnitudes we report are those beyond what is expected based on firing rate alone.) The categorization of the responsiveness in this case does not directly reflect the receptive field relationships of the neurons in the pair to the stimulation locations (see Figure 4-2, Inset). The trends in the observed correlation magnitudes are shown in Figure 4-3C. When *both* neurons in the pair responded to the stimulation, the mean correlation was the highest (0.0406 ± 0.00121) and greater than when only *one* neuron in the pair responded to stimulation (0.0328 ± 0.00029; P < 0.0005) and when *neither* neuron responded (0.0308 ± 0.00031; P

< 0.0005). The mean correlation when one neuron in the pair responded to stimulation was greater than when neither neuron responded ($P < 0.0005$). Thus, as expected, two neurons that were stimulated within their receptive fields were more strongly correlated than other neurons.

Spatiotemporal Interactions

The interactions of spatial and temporal stimulus characteristics were also factors in our analysis since temporal and spatial stimulus parameters did not occur in isolation, but in combination. We illustrate examples from two monkey cases. Figure 4-4 shows an example from a pair of neurons recorded from monkey 3 in which the correlation magnitude during single-site stimulation was greater than correlation when two sites were stimulated simultaneously within one digit. These neurons had overlapping minimal receptive fields, but the stimulation did not occur in the region of overlap. Figure 4-5 shows an example from a pair of neurons recorded from monkey 2 in which the minimal receptive fields did not overlap and the stimulation did not take place within the minimal receptive fields, but a high correlation magnitude was maintained during single-site stimulation and simultaneous stimulation within one digit.

For the population, all of the spatiotemporal interaction effects included in our model were significant effects. We focused on the 3-way interaction ($P < 0.0005$) between the temporal stimulus relationship, the proximity of the stimuli on the hand, and the "pair response" to relate the responses of the two neurons in the pair to the

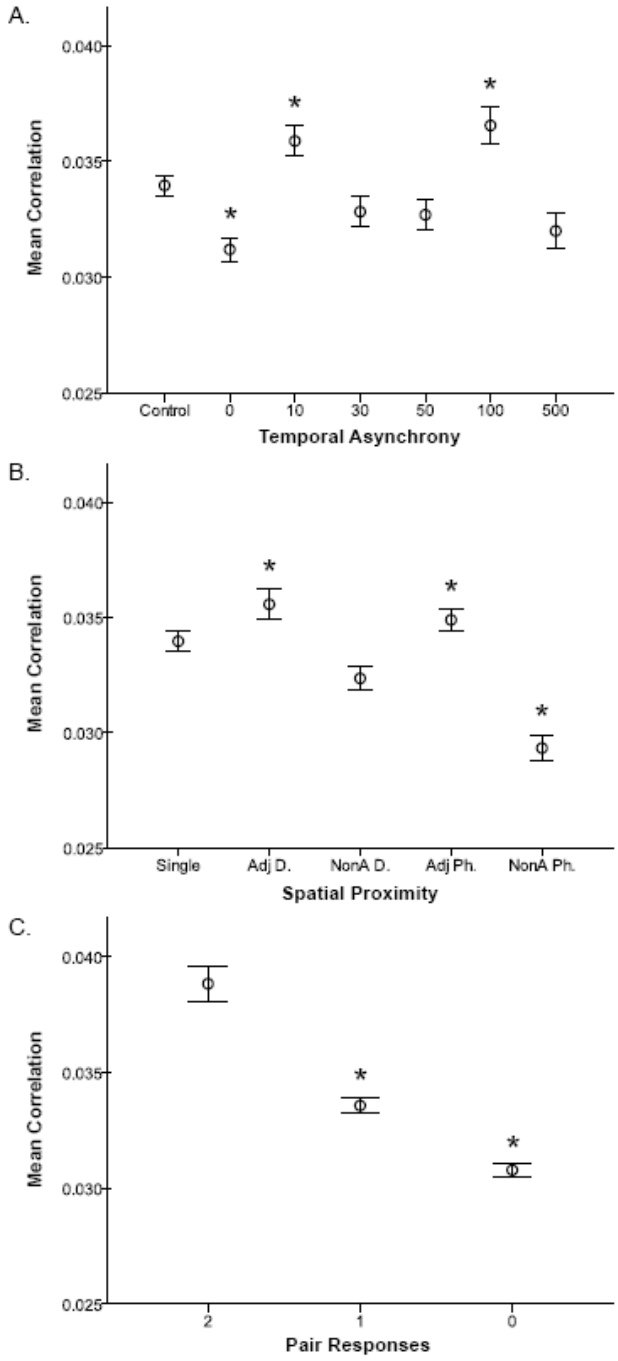

Figure 4-3. Correlation magnitude variations across spatiotemporal stimulus parameters. Asterisks (*) indicate significant differences from the first group in each panel. See Figure 4-2 for abbreviations and category descriptions. A. The mean correlation when a single control location was stimulated was significantly higher than when two locations were stimulated simultaneously, and lower than when one site was stimulated 10 ms or 100 ms before the second location; however, the correlation values only varied slightly. B. The mean correlations were higher for dual-site stimulation compared to single-site stimulation for all cases except when nonadjacent digits (NonA D.) were stimulated. C. When both neurons in the pair responded to the stimulation (2), the correlation magnitude was higher than when only one neuron in the pair responded and when neither responded. When only one neuron in the pair responded (1), the correlation magnitude was higher than when neither responded.

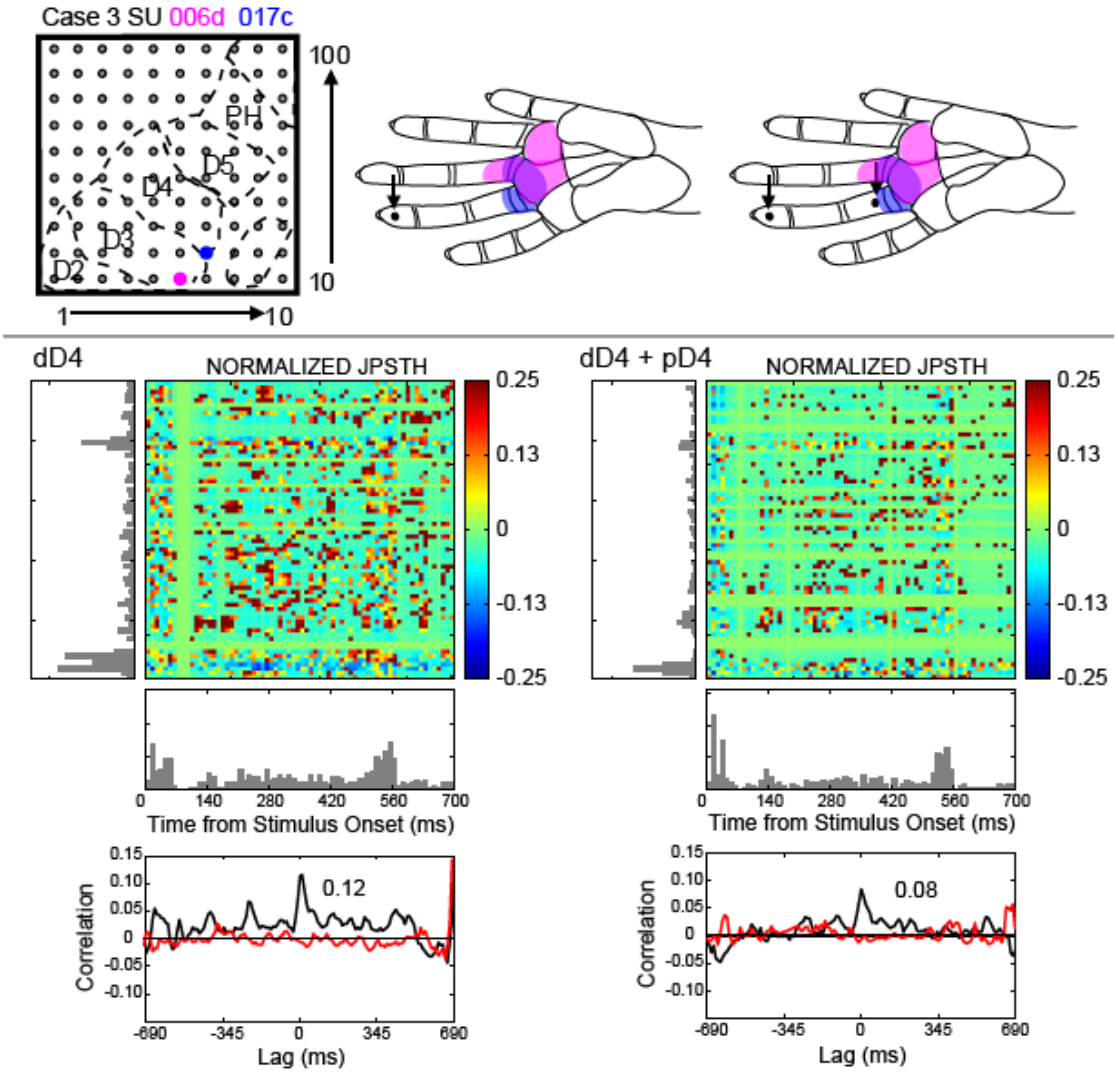

Figure 4-4. Example of correlations between a neuron pair during single-site and simultaneous dual-site stimulation that follows the population trends. Upper panel. The location of the array relative to the area 3b hand representation is depicted for monkey 3, following conventions in Figure 4-1. The electrode locations for the single neurons are represented by a pink dot (006d) and a blue dot (017c), and the receptive fields from these electrodes are indicated on the hand diagrams in corresponding colors. Overlap of receptive fields is indicated by violet shading. Black dots on hand schematics represent the stimulation locations on distal digit 4 alone (left) and on paired sites, distal and proximal D4 (right). Lower panel. The normalized JPSTHs and correlation histograms show spike timing correlations between units 006d and 017c when dD4 was stimulated alone (left) or stimulated with pD4 simultaneously (right). The spike timing correlation at the 0 ms lag was strong at 0.12 when dD4 was stimulated alone, despite the distance of the stimulation location from the region of receptive field overlap. When a simultaneous stimulus was added on pD4, close to the receptive field from electrode 17, the correlation magnitude decreased.

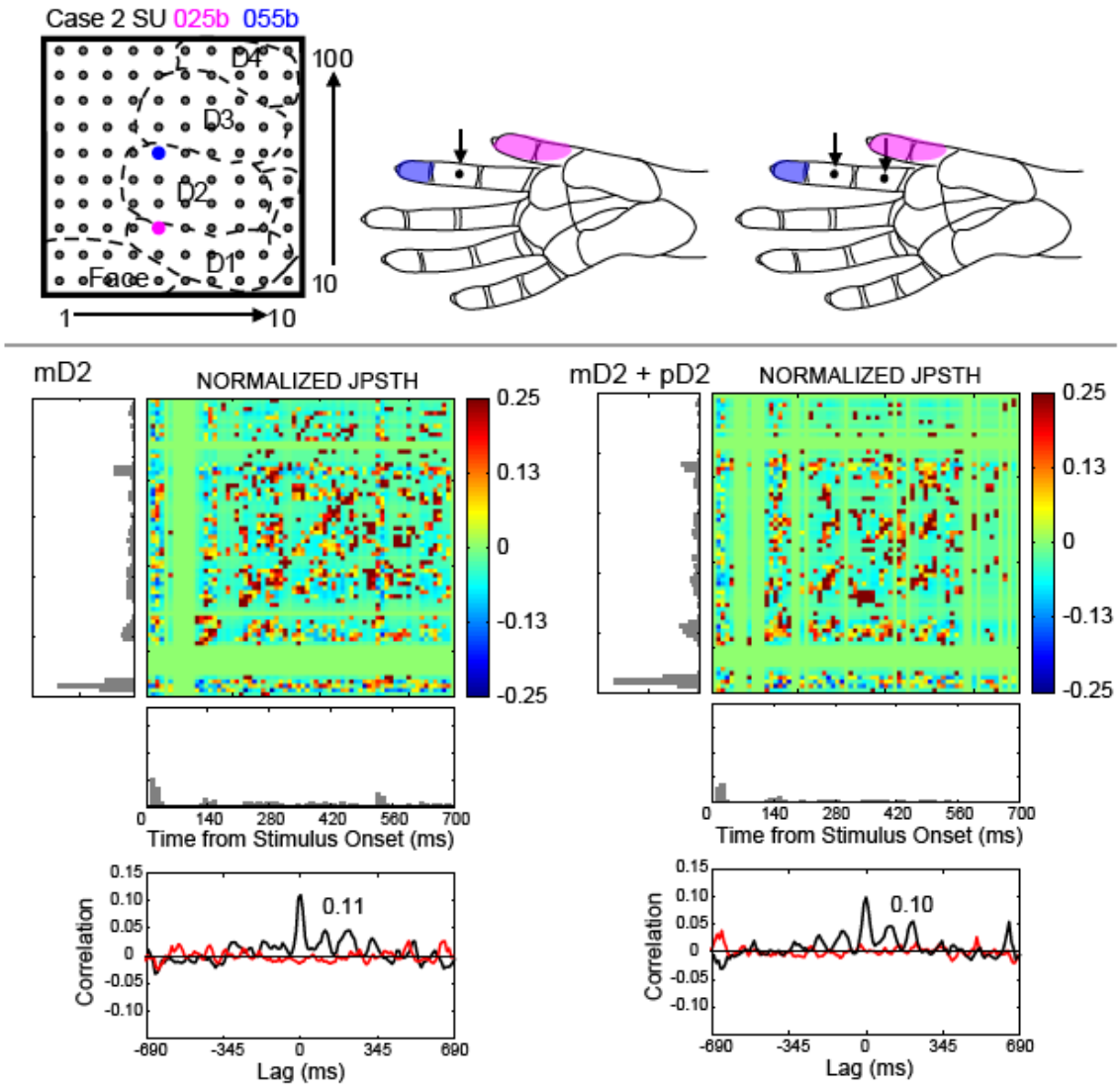

Figure 4-5. Example of correlations between a neuron pair during single-site and simultaneous dual-site stimulation that violates the population trends. Upper panel. The location of the array relative to the area 3b hand representation is depicted for monkey 2. The electrode locations for the single neurons in this example are represented by a pink dot (025b) and a blue dot (055b), and receptive fields from these electrodes are indicated on the hand diagrams in corresponding colors. Black dots on hand schematics represent the stimulation locations on middle digit 2 alone (left) and on paired sites, middle and proximal D2 (right). Lower panel. The normalized JPSTHs and correlation histograms show spike timing correlations between units 025b and 055b when mD2 was stimulated alone (left) or stimulated with pD2 simultaneously (right). The spike timing correlation at the 0 ms lag was strong at 0.11 when mD2 was stimulated alone, despite the distance of the stimulation location from the receptive fields. When a simultaneous stimulus was added on pD2, the correlation remained nearly the same, with the peak magnitude decreasing slightly to 0.10.

stimulation in Figure 4-6. Correlation magnitudes were consistently highest when both neurons in the pair responded to stimulation (pair response = 2). Correlation magnitudes tended to increase more when both neurons in the pair responded to stimulation (pair response = 2) when that stimulation was presented at longer stimulus onset delays, except when stimuli were presented to adjacent digits. Instead, when adjacent digits were stimulated, correlation magnitudes were relatively stable across temporal stimulation conditions. The correlation magnitudes were lowest in general when nonadjacent phalanges within a digit were stimulated and the trends were variable, in part due to large variability in the mean correlation in some categories. The interaction effects were not as clear as we had predicted, but the main effects were recapitulated across temporal and spatial stimulus conditions.

The 100-electrode array allows us to study multiple neuron pairs simultaneously, and allows us to examine patterns of correlations across cortical space. Figure 4-7 shows an example of the correlation patterns of single neurons from selected spatiotemporal stimulus conditions in monkey 3. These patterns show overall similarities when single sites were stimulated, despite the difference in location of the two single controls (digits 2 and 5). In other words, the basic network structure did not shift much across the recorded locations based on the stimulus parameters. The numbers of significant correlations decreased when these two sites were stimulated simultaneously, but some correlations between specific pairs appeared that were not present in either of the single-site stimulation conditions. The correlations in the remaining dual-site stimulation conditions shown in Figure 4-7 increase in number and magnitude compared to simultaneous

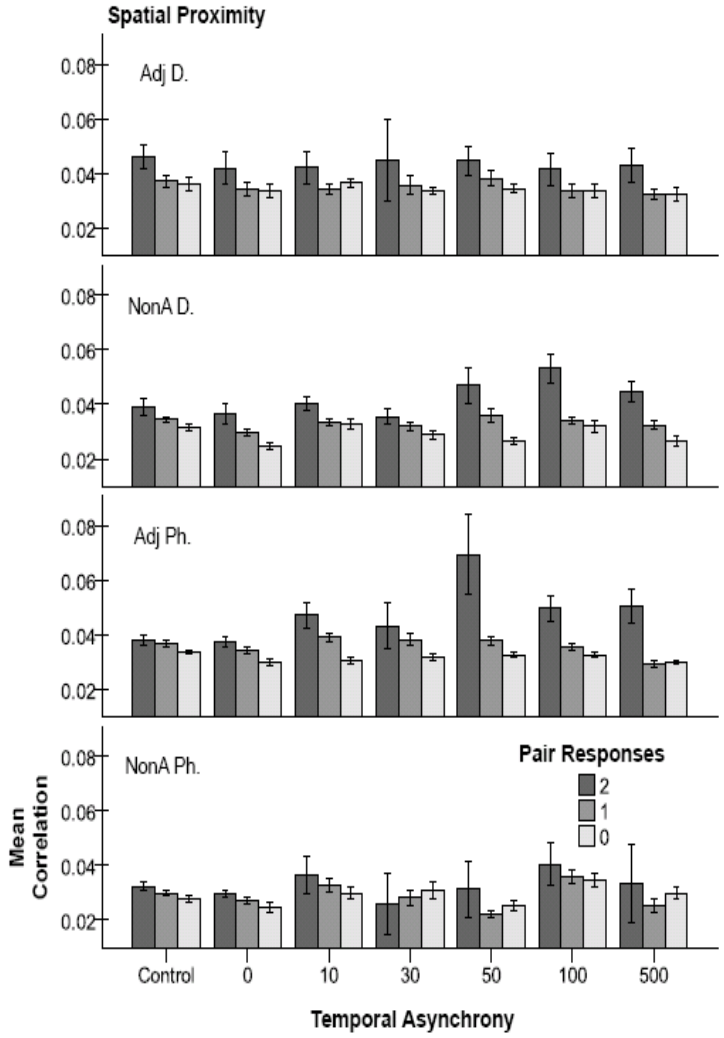

Figure 4-6. Mean correlation magnitudes across spatiotemporal stimulation conditions. Bar graphs of mean correlation magnitudes are shown with error bars representing 95% confidence intervals. The conditions of single site control stimulation, simultaneous stimulation (0), and asynchronous stimulation at 10, 30, 50, 100, and 500 ms delays are shown on the x-axis to group the values. Shaded bars indicate the firing rate responses of the two neurons in the correlated pair relative to the stimulation: 2 = both neurons responded to stimulation; 1 = only one neuron responded; 0 = neither neuron responded. Separate panels designate the spatial proximity of the stimulation sites in a stimulus block. Adj D. = adjacent digits or palm pads; NonA D. = nonadjacent digits or palm pads; Adj Ph. = adjacent phalanges within a digit; NonA Ph. = nonadjacent phalanges or pads within a digit or digit to adjacent palm pad.

stimulation, which is similar to the trends in the population (Figure 4-3A). Single-site stimulation can result in significant correlations between neurons separated by large distances across the hand (Figure 4-7), but we sought to determine if the distance between paired stimuli would affect the strength of the correlations relative to the distance between the two neurons, as described in the following section.

Electrode Distance Effects on Correlation Magnitude and Proportions

We examined the relationship of the magnitude of the correlation derived from the JPSTH and the distance between the electrode pairs from which the correlated neurons were recorded, as has been done in other studies within somatosensory cortex (Roy et al., 1999; Alloway et al., 2002; Reed et al., 2008). The overall results were somewhat unexpected, as the distance between stimulation locations did not greatly affect the distance between correlated neurons. Since the temporal stimulation condition had variable effects, we selected only the condition in which stimuli were presented simultaneously, and then analyzed only the pairs with significant spike timing correlations. The Pearson correlation between the electrode distance and the magnitude of the correlated activity was -0.083 ($P < 0.0005$; $N = 2529$), and the correlation between stimulus proximity and correlation magnitude was -0.077 ($P < 0.0005$; $N = 2529$). The data are shown in a scatter plot divided by the proximity category (Figure 4-8). Weak but significant correlations were found between neuron pairs across all electrode distances, from 400 to 4800 μm, while stronger correlation magnitudes tended to occur between neurons recorded from nearby electrodes. However, relatively strong correlations were found between neuron pairs separated by more than 4 mm, particularly when locations

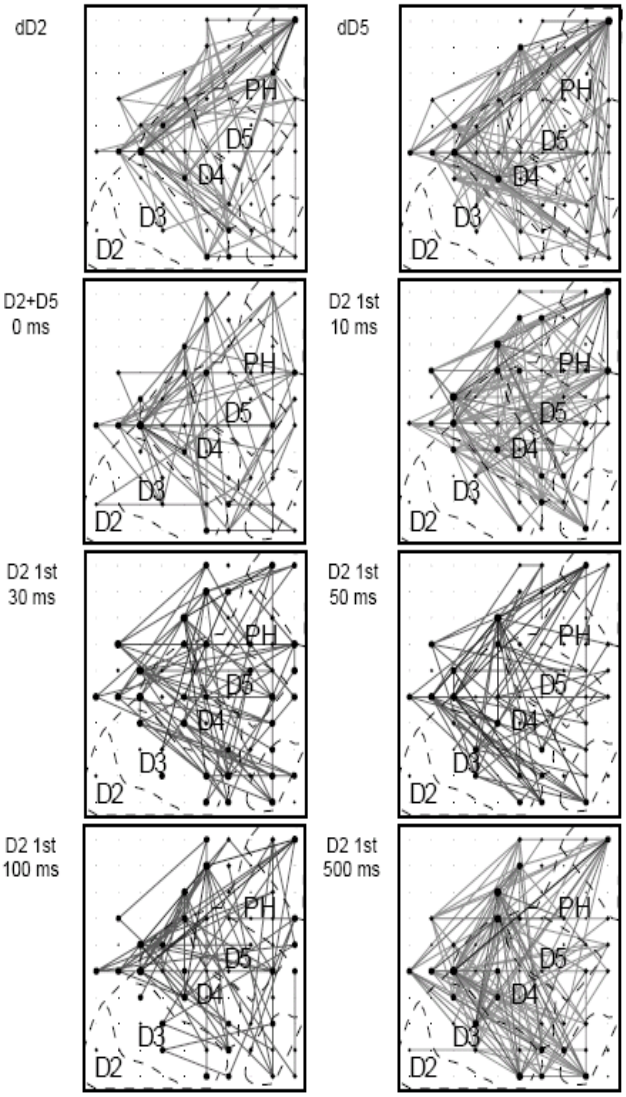

Figure 4-7. Depiction of correlations between neuron pairs during spatiotemporal stimulation blocks. Stimuli were presented to distal digit 2 (dD2) and distal digit 5 (dD5) individually in monkey 3 in blocks of 100 trials. These locations were stimulated simultaneously and then asynchronously with dD2 stimulation preceding dD5. Black dots indicate electrode sites from which single neurons were recorded and significant correlations between neurons are represented by the lines connecting the dots. The size of the dots and the thickness of the connecting lines represent the magnitude of the correlations. When correlations are not statistically significant, no lines are shown, but the sizes of the dots increase accordingly. Each panel includes an overlay of the approximate location of the electrode array within the hand representation of area 3b. Note, electrodes represented outside of the 3b hand representation may be located in area 3a or in area 3b, as the boundary drawn is approximate.

within a single digit were stimulated. The proportions of correlated pairs compared to the total recorded pairs for each proximity classification during simultaneous stimulation are listed in Table 4-2. Stimulation on adjacent phalanges resulted in the greatest proportion of correlated pairs at 27.1%, followed by stimulation on adjacent digits (24.6%) and stimulation on nonadjacent phalanges (24.1%), with fewer pairs correlated when nonadjacent digits were stimulated (17.2%). These total proportions determined for the simultaneous stimulation condition matched our expectations and resembled the values determined by summarizing over all of the stimulation conditions, described to follow.

Stimulus Proximity Effects on Proportions of Correlations

Based on the proximity of the stimulation on the hand, we determined the proportions of single units that were significantly correlated out of the total recorded pairs. Summarizing over all stimulation conditions for the data from the three monkeys combined, the proportions of correlated pairs appeared to decrease when the stimulation sites were distant, as we expected. When stimulus sites were presented to adjacent phalanges within a single digit, the proportion of correlated pairs was greatest at 23.5% (6,148/26,148 pairs). When nonadjacent phalanges within a single digit were stimulated 19.2% of the pairs were correlated (3,027/15,738 pairs). When adjacent digits (or palm pads) were stimulated 16.2% of the pairs were correlated (1,995/12,296 pairs). 14.8% of the pairs were correlated when nonadjacent digits (or palm pads) were stimulated (4,842/32,730 pairs). Therefore, the proportions of correlated pairs were highest when sites within a single digit were stimulated and lowest when sites across separate digits were stimulated.

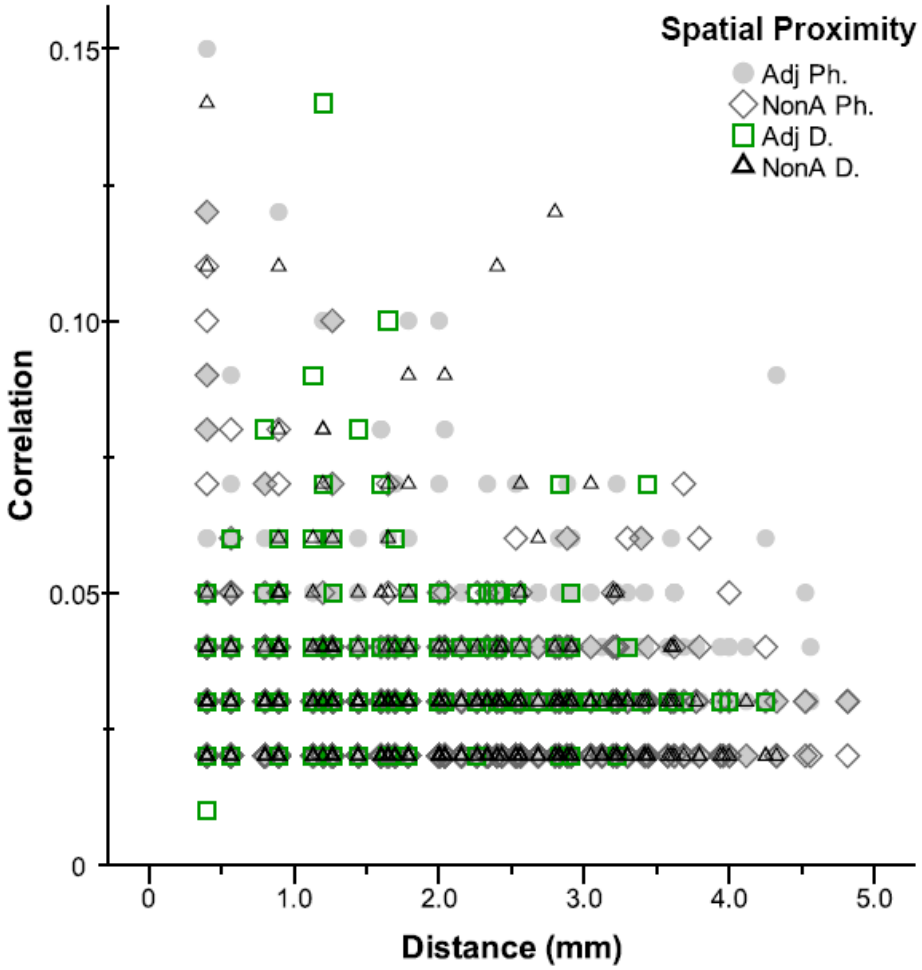

Figure 4-8. The relationship between correlation magnitude and distance between electrode pairs. The magnitudes of statistically significant correlations are plotted (y-axis) based on the geometric distance between the electrode pairs from which the activity was recorded (x-axis). Data are plotted only for the stimulus conditions in which two sites were stimulated simultaneously. Locations of the stimuli varied based on proximity measures and these proximity measures are shown such that gray filled circles represent stimulation on adjacent phalanges within a digit (Adj Ph.); gray open diamonds represent stimulation on nonadjacent phalanges within a digit (NonA Ph.); green open squares represent stimulation on separate, adjacent digits (Adj D.); and black open triangles represent stimulation on separate, nonadjacent digits (NonA D.).

Table 4-2. Proportions of correlated neuron pairs across electrode distances when two hand sites were stimulated simultaneously

	Electrode distance, mm						
	0-1	1-2	2-3	3-4	4-5	5-6	Total
				Adjacent Phalanges			
Recorded pairs, n	631	1061	1267	530	68	1	3558
Correlated pairs, n	196	263	344	141	20	0	964
Proportion, %	31.1	24.8	27.2	26.6	29.4	0	27.1
				Nonadjacent Phalanges			
Recorded pairs, n	120	140	260	60	0	0	580
Correlated pairs, n	20	20	100	0	0	0	140
Proportion, %	16.7	14.3	38.5	0	_	_	24.1
				Adjacent Digits			
Recorded pairs, n	918	1452	1624	680	94	1	4769
Correlated pairs, n	262	327	402	158	22	0	1171
Proportion, %	28.5	22.5	24.8	23.2	23.4	0	24.6
				Nonadjacent Digits			
Recorded pairs, n	599	966	1123	425	35	0	3148
Correlated pairs, n	110	173	181	74	5	0	543
Proportion, %	18.4	17.9	16.1	17.4	14.3	_	17.2
				Totals			
Recorded pairs, n	2268	3619	4274	1695	197	2	12055
Correlated pairs, n	588	783	1027	373	47	0	2818
Proportion, %	25.9	21.6	24.0	22.0	23.9	0	23.4

Blank (_) is undefined.

Relationship of Correlation Magnitude and Firing Rate by Spatiotemporal Conditions

We examined the relationship between correlation magnitudes and the average firing rates of neurons in the correlated pair as a way to assess how neuron responsiveness to the stimulus conditions affected the correlation strength. Additionally, if correlations are important for relaying stimulus information, we would expect correlation magnitudes to show some independence from firing rates. Across all temporal stimulation conditions, spatial proximity of the stimuli affected the relationships between correlation magnitude and average firing rate. Figure 4-9A presents the entire data set of significant correlation magnitudes plotted against the geometric mean firing rate (GMFR, spikes/s), in which the temporal stimulation condition is plotted on the z-axis and the spatial proximity of the stimuli is shown by the color of the data markers.

Linear regression analysis on the data without accounting for different spatial proximity factors showed that correlation magnitudes tended to increase with larger mean firing rates (Pearson $r = 0.452$, $P < 0.0005$, $N = 16{,}011$). However, inspection revealed that the relationship was strongest when nonadjacent digit locations were stimulated (Pearson $r = 0.639$, $P < 0.0005$, $N = 4842$) and weakest found when adjacent phalanges within a single digit were stimulated (Pearson $r = 0.311$, $P < 0.0005$, $N = 6148$). When nonadjacent digits were stimulated, correlation magnitudes were relatively low, but the average firing rates were relatively high (mean correlation = 0.0335, SD = 0.0170; mean GMFR = 4.716 spikes/s, SD = 6.614). When adjacent phalanges within a single digit were stimulated, firing rates remained low overall, while correlations between neuron pairs reached their highest magnitudes (mean correlation = 0.0356, SD = 0.0165; mean GMFR = 2.257 spikes/s, SD = 1.935). When adjacent digits were stimulated, the

relationship between correlation magnitude and average firing rate was weakly positive (Pearson r = 0.0464, P < 0.0005, N = 1994), as was the relationship when nonadjacent phalanges within a single digit were stimulated (Pearson r = 0.515, P < 0.0005, N = 3027). However, different effects led to these similar weak linear relationships. When adjacent digits were stimulated the average correlations and average firing rates were relatively high (mean correlation = 0.0367, SD = 0.0148; mean GMFR = 3.494 spikes/s, SD = 2.915). When nonadjacent phalanges within a digit were stimulated, the average correlations and average firing rates were low (mean correlation = 0.0297, SD = 0.0121; mean GMFR = 2.130 spikes/s, SD = 1.516). The trends can be seen clearly in Figure 4-9B, in which the data are shown for only a single temporal stimulation condition. Thus, when stimulation locations were close in proximity, correlation magnitudes did not vary strongly with firing rate, while correlation magnitude varied with firing rate more strongly when nonadjacent digits were stimulated.

We expected some dissociation between correlation magnitude and average firing rate. While the average firing rates for the neuron pairs with significant correlations varied within the control condition, the average firing rates tended to be reduced by paired stimulation, with the maximal reductions occurring when paired stimuli were presented within 30 and 50 ms of each other (Figure 4-10A). The exception to this trend occurred when stimuli were presented on nonadjacent digit locations. Correlation magnitudes did not follow the firing rate trends under these spatiotemporal stimulation conditions (Figure 4-10B).

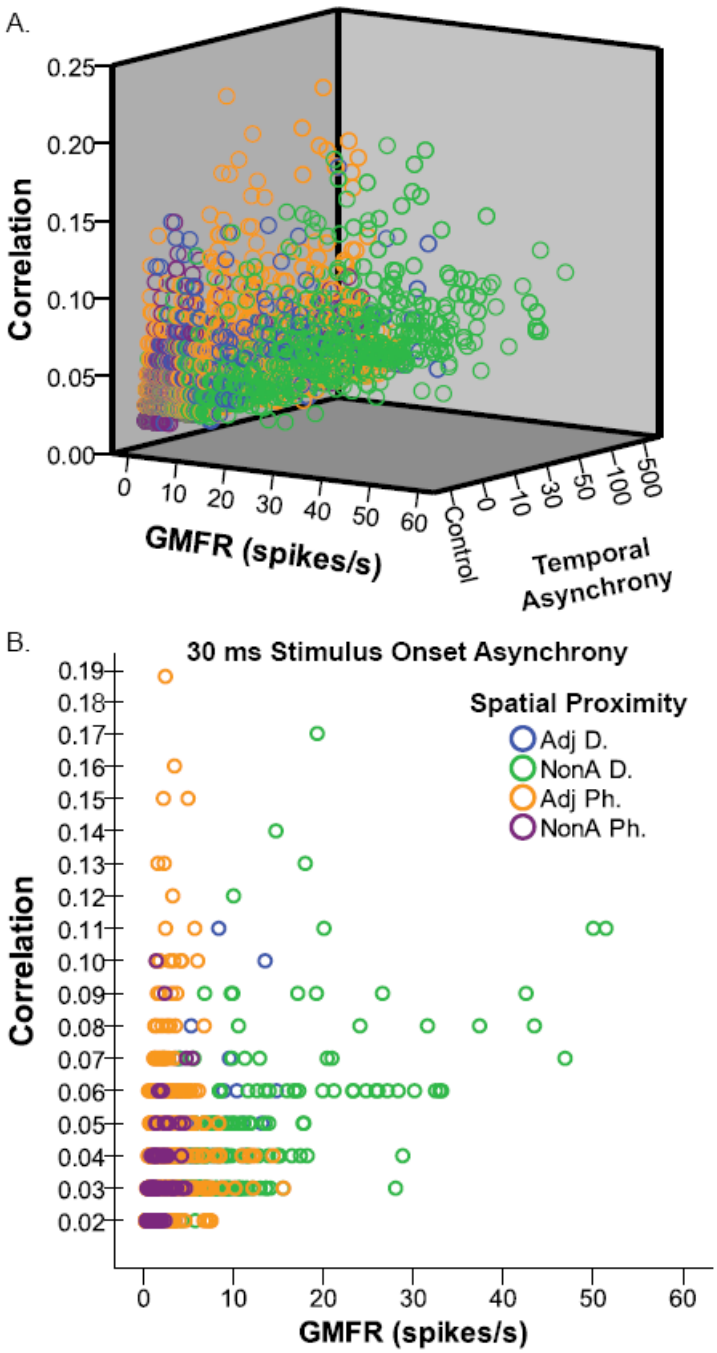

Figure 4-9. Spatiotemporal stimulus effects on the relationship between correlation and firing rate magnitudes. A. Peak correlation magnitudes versus the geometric mean firing rate (GMFR, spikes/s) of the neurons in the correlated pair are shown in the 3-D scatter plot with the temporal stimulation condition plotted on the z-axis. Marker color indicates the spatial proximity of the dual probe stimulation on adjacent digits (Adj D.), nonadjacent digits (NonA D.), adjacent phalanges within a digit (Adj Ph.), and nonadjacent phalanges within a digit (NonA Ph.). B. A 2-D scatter plot is shown by selecting only the data points within the temporal stimulation condition in which one probe contact preceded the other by 30 ms. This view helps reveal that the relationship of correlation magnitudes increasing with increasing firing rates occurs primarily when nonadjacent digit locations were stimulated, as the average firing rate was not strongly suppressed by the paired stimulation under these conditions.

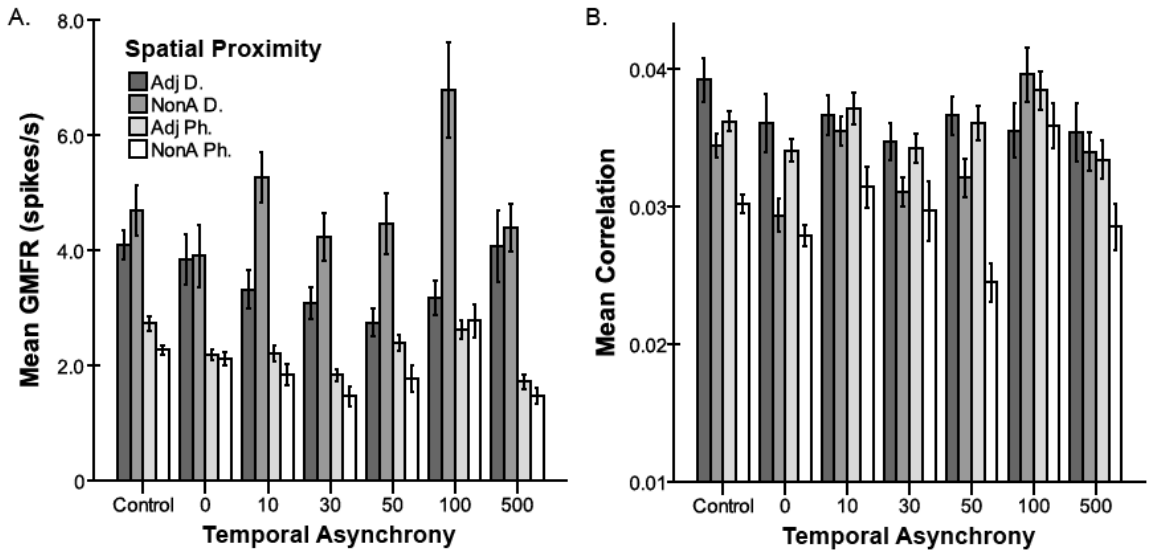

Figure 4-10. Spatiotemporal stimulus effects on average firing rates compared to correlations. A. The geometric mean firing rates (GMFR, spikes/s) for the correlated neuron pairs in the dataset were averaged within temporal stimulation conditions (x-axis) and spatial proximity conditions (each bar series). Error bars represent 95% confidence intervals. The control condition refers to single-site stimulation on the individual hand locations that were stimulated in pairs. While the GMFRs for the neuron pairs with significant correlations varied within the control condition, the GMFR was reduced by paired stimulation, with the maximal reductions occurring when paired stimuli were presented within 30 and 50 ms of each other. Note, when stimuli were presented on nonadjacent digit locations this trend was not found. B. The correlation magnitudes were averaged within temporal stimulation conditions (x-axis) and spatial proximity conditions (each bar series). Spatial and temporal stimulation conditions resulted in variable changes in correlation magnitudes. The changes in correlation magnitudes do not follow the trends shown by the average firing rate magnitudes of the correlated neuron pairs in A.

Discussion

The presence of spike timing correlations suggests that neuron pairs are linked in some way, by common input or synaptic connections, for example. It is becoming widely accepted that the functional connections measured through spike timing correlations are dynamic and have been shown to change in area 3b neurons after tactile behavioral training in owl monkeys (Blake et al., 2005). We found that a general network of correlated pairs existed in our simultaneous recordings from 100-electrode arrays in area 3b; and stimuli varying in spatiotemporal properties resulted in small changes to the magnitude of correlations and the identities of correlated pairs (Figure 4-7), perhaps illustrating the short-term dynamics in the population related to stimulus properties. We did not find the precise patterns of spatiotemporal interactions we expected to obtain based on anatomical connectivity within area 3b; however, we can compare our results to those of others to make some assertions regarding how spatiotemporal stimulus parameters affect spike timing correlations in primary somatosensory cortex.

Effects of Spatial and Temporal Stimulus Properties on Correlation Magnitudes

In accordance with the hypothesis that the correlations in primary somatosensory cortex are useful for signaling objects that are grouped in time and space, we expected that simultaneous stimulation of two locations might increase the magnitude or numbers of correlations between neuron pairs due to common synaptic input; and that the farther apart in time two paired stimuli were presented, the lower the correlation magnitudes would be. Our results did not match this expectation, as dual-site simultaneous

stimulation reduced the overall correlation magnitude compared to stimulation on a single site, as well as compared to paired stimulation presented farther apart in time (Figure 4-3A). A possible explanation for this finding is that simultaneous stimulation on different and discontinuous parts of the hand is more disruptive to the existing correlations occurring in a given network and may be closely related to the effects of lateral inhibition and activating projections in the cortex. We did not calculate correlations during periods of spontaneous activity as a comparison condition because spontaneous firing rates tended to be very low in our anesthetized monkeys; however, for our conditions, correlations obtained during driven activity tended to reflect correlations present during spontaneous activity when spike rates are high enough to perform the calculation (Reed et al., 2008, Chapter 2 see SI Figure 2-6).

Summarizing over the entire set of temporal stimulus conditions, the proximity of the paired stimuli on the hand affected the magnitude of significant correlations (Figure 4-3B); although again the effect did not precisely follow expectations. We expected that the closer the stimulus locations were in space, the higher the correlation magnitude would be, assuming that correlation magnitude reflected aspects of common input and density of intrinsic connections, and theoretically, object similarity. We found that stimulation on adjacent digits resulted in the highest correlation magnitudes, followed by stimulation on adjacent phalanges within a digit. It is possible that the two stimuli presented on adjacent digits could be more readily perceived as a possible common object than two small and distinct stimuli presented on adjacent phalanges within a digit. This idea may also help explain why stimulation on nonadjacent digit sites resulted in greater correlation magnitudes than stimulation on nonadjacent phalanges. These

perception-based explanations are speculative, but anatomical connections within the area 3b hand representation appear denser in the distal to proximal axis within a digit than across digit representations (Fang et al., 2002); thus, there is an anatomical basis to expect differences in the functional connections of these regions. However, we expected correlations to be higher in the distal to proximal axis within a digit than across digits.

The final main effect we examined to explain the variance in the correlations was a factor we termed "pair responses", which represents the number of units in the correlated pair that responded to the presented stimulus with significant increases in firing rate above baseline. Thus, "pair responses" gives a simplified measure of the overlap between neuron receptive fields with the stimulus locations. We selected this measure after determining that the relationship of the receptive fields of both neurons in each pair with the locations of each stimulus probe was too complex to analyze (44 levels that could be combined to a minimum of 9 levels). As may be expected, we found that when both neurons in the pair responded to the stimulation, the correlation magnitude was highest, and when neither neuron responded to stimulation, significant correlations were still present, but the correlation magnitude was lowest (Figure 4-3C). With this indirect relation that takes the responses of both neurons in the pair into account, our results are similar to others (e.g., de la Rocha et al., 2007 [*in vitro* and model neurons]; Greenberg et al., 2008 [rat visual cortex]; Jermakowicz et al., 2009 [primate visual cortex]) who reported trends for correlation magnitude to increase with increasing firing rates, averaged over both neurons in the correlated pair.

Spatiotemporal Stimulus Interactions

We made basic predictions regarding the existence of spatiotemporal interactions affecting the magnitude of correlations. While our model predicted significant interactions, the 3-way interactions between temporal stimulus onset asynchronies, spatial proximity of the stimuli, and the pair response relationships (Figure 4-6) deviated from the trends we expected. Our results corroborated the expectation that the pair responses would play a role in the magnitude of the correlations across all stimulus parameters. But our results did not satisfy the following two expectations: 1) that stimulation on distant locations (nonadjacent digits) would result in decreases in correlation magnitudes compared to paired stimulation within a single digit, and 2) that stimulation at longer stimulus onset delays would result in decreases in correlation magnitudes compared to near-simultaneous stimulation. If such effects exist, they were not detectable in our experiments and analysis. An example of the correlations in the recorded single units from one monkey during a specific stimulation series presented in Figure 4-7 reflects the complexity of the interactions occurring across the hand representation under the selected spatiotemporal stimulation conditions. The general localization of the correlated pairs remained qualitatively the same, spanning most of the hand representation, throughout the stimulation series. Single site stimulation on digit 5 did not result in increased correlation numbers or magnitudes localized within the representation of that digit. The example in this figure illustrates the surprising result that simultaneous stimulation, regardless of stimulation proximity, resulted in decreased correlation magnitudes on average. We use these figures for illustration purposes, but we currently do not have a way to analyze these patterns for individual examples to

determine if there are significant differences. We rely on our statistical analysis of the population to extract the importance of spatial and temporal stimulus parameters on the overall patterns we obtain from the population.

Relationship of Correlations and Cortical Distance

Although the variation in the *magnitude* of correlations did not match all of our predictions, the variation in the *proportion* of correlations across cortical distance and stimulus proximity followed our expectations. Generally, the proportions of correlated neurons decreased with increasing distance between neuron pairs; and when sites closer in spatial proximity were stimulated simultaneously, greater proportions of neurons were correlated (Table 4-2). These data extend our report on nonadjacent digit stimulation in a previous paper (Reed et al., 2008). Alloway and colleagues (1999, 2002) examined cross-correlations between neuron pairs in cat somatosensory cortex (S1 and S2) and also found a tendency for the proportion of correlated pairs to decrease with increasing distance between electrode pairs recording single unit and multi-unit activity; however, they examined smaller electrode spacing to a total distance of about 0.9 mm, while our array allowed us to examine 0.4 mm electrode spacing up to a total distance of 4.8 mm. We also found a tendency for correlation magnitudes to decrease when the electrode distance increased, but significant correlations were found even at distances beyond 4 mm (Figure 4-8). The presence of low magnitude correlations across all distances recorded resulted in a linear correlation coefficient that was low and weak (Pearson $r = -0.083$; $P < 0.0005$; $N = 2529$). This trend resembles that found by Greenberg et al. (2008) in their calcium imaging study in visual cortex of awake and anesthetized rats.

They reported weak relationships between the correlation magnitude and distance between electrode sites (awake: r = 0.004, P = 0.94; anesthetized r = -0.07, P = 0.023). When we examined the correlation magnitudes based on proximity of stimulation sites, there was a tendency for simultaneous stimulation on adjacent phalanges to result in the highest magnitude correlations overall; however, low magnitude correlations were present across all stimulus types (Figure 4-2) and all electrode distances (Figure 4-8).

Relationship of Correlation Magnitude and Average Firing Rate by Spatiotemporal Conditions

Several reports describe significant relationships between correlation magnitudes and average firing rates, such that higher correlation magnitudes tend to occur when the two neurons in the pair have higher average firing rates (e.g., de la Rocha et al., 2007; Greenberg et al., 2008; Jermakowicz et al., 2009); though others have reported only very weak relationships (Samonds and Bonds, 2005). We examined this trend in our data and found weak, positive relationships overall. However, when we analyzed the linear relationship of correlation and average firing rate based on the spatial proximity of the paired stimulation, we found that the relationship of correlation magnitudes increasing with increasing firing rates appeared primarily when nonadjacent digit locations were stimulated (Figure 4-9). This effect occurred because the average firing rates were not greatly suppressed by the paired stimulation on nonadjacent digit locations, while firing rates tended to be reduced (compared to single-site control stimulation) when paired stimuli were presented on locations in closer proximity (Figure 4-10A). This difference in suppression may result from weaker lateral inhibition when nonadjacent digits were stimulated compared to when sites closer in proximity were stimulated. We found some

potential sampling bias such that geometric mean firing rates were lowest for correlated pairs collected during single-site stimulation of locations that were later part of dual-site stimulation on phalanges within the same digit (Figure 4-10A). This sampling effect may have occurred because only two of the three monkeys were tested with stimuli presented within the same digit; while all three monkeys were tested with stimuli presented to locations on adjacent and nonadjacent digit or palm sites. Nevertheless, similar trends in average firing rate were found when stimuli were presented on adjacent digits, adjacent phalanges, and nonadjacent phalanges within a digit; thus, the low magnitudes of the average firing rates during stimulation within a digit did not change the trends we found when the paired stimuli were presented with stimulus onset delays.

Figure 4-11 summarizes the magnitudes of correlations and average firing rates of the correlated neurons when paired stimuli were presented to sites across the hand, averaged over all temporal stimulation conditions. The correlation magnitudes did not strictly decrease with decreasing average firing rates when different parts of the hand were stimulated. Stimulation on adjacent phalanges within a digit representation resulted in the highest proportion of correlated pairs and nearly the highest correlation magnitudes; thus, Figure 4-11 depicts the relationship between these locations as the strongest based on correlations, followed by a nearly equivalent strength between locations on adjacent digits. This reflects the lower proportion of correlated pairs and the higher correlation magnitudes found when adjacent digit sites were stimulated. Stimulation on nonadjacent phalanges resulted in the second largest proportion of correlated pairs, but the magnitudes were low, reflected by the thin line. The line between nonadjacent digits was similar in thickness, as this group had the lowest proportion of

correlated pairs by far, but the magnitudes of those correlations were high. In some ways, the results correspond to the density of intrinsic connections along the distal-proximal axis of the digit representation (Fang et al., 2002), with unexpectedly high correlation strength between adjacent digit representations. When nonadjacent digits were stimulated, average firing rates showed the largest magnitudes and least suppression. Analysis of average firing rates indicated suppressive interactions of similar strength when adjacent and nonadjacent phalanges were stimulated; however, the correlations did not show the same relationships across these areas. Thus, our findings indicate that correlation magnitudes do not necessarily increase with firing rate under all stimulus conditions (Figure 4-10).

Similar to our results, Roy and Alloway (1999) found that 17% of the neuron pairs they recorded in cat S1 showed changes in correlations related to directional preferences to moving air jet stimulation without corresponding changes in the firing rate. But in general, they found that when firing rate increased (comparing spontaneous and driven activity as well as comparing stationary and moving stimuli), correlation magnitudes tended to increase (Roy and Alloway, 1999). Interestingly, Greenberg et al. (2008) confirmed that firing rates decreased during anesthesia; however, they found that spike timing correlations increased during anesthesia compared to awake periods. Vaadia et al. (1995), studying sensorimotor frontal cortex neurons in behaving macaque monkeys, and deCharms and Merzenich (1996), studying auditory cortex neurons in anesthetized marmoset monkeys, both found that spike timing correlations can change without corresponding changes in mean firing rate. Roelfsema et al. (2004), studying primary visual cortex neurons in behaving macaques, found that firing rates covaried

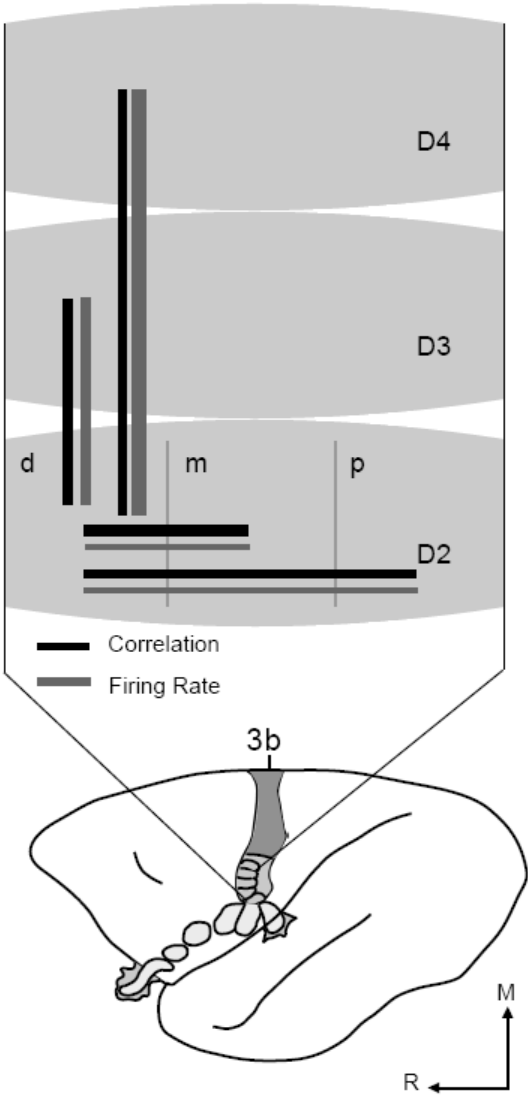

Figure 4-11. Summary schematic of interactions within the hand representation based on correlations and average firing rate responses. A schematic of the owl monkey brain shows the organization of area 3b. The orientation of the brain is indicated by arrows. M = medial and R = rostral. Part of the hand representation is schematized and enlarged to illustrate a summary of correlation and firing rate response results. Solid black lines represent relationships between parts of the area 3b hand representation based on the magnitudes of spike timing correlations. Solid gray lines between parts of the digit representations indicate relationships based on magnitudes of average firing rate based on the geometric mean firing rate of the correlated pairs. Line thickness approximates the relative magnitudes within each line category for the spatial proximity of paired stimuli, averaged over the temporal stimulation conditions. The relative strength of correlations between neurons did not strictly follow the magnitudes of average firing rates of those neurons when different parts of the hand were stimulated. (See Discussion for details.)

with perceptual grouping of stimuli, but correlation magnitudes varied instead with general task difficulty. Our findings, in conjunction with those of others, indicate that correlation magnitudes do not strictly follow firing rate modulations and thus reveal a different type of modulation compared to the firing rate responses.

Firing rates are affected by stimulus properties and can be suppressed by effects such as lateral inhibition. If spike timings are correlated, spikes from presynaptic neurons may be able to activate postsynaptic neurons even when spike rates are low. In our study, we found conditions when firing rates tended to decrease while the correlation strength was maintained near control levels, such as when stimuli were presented with their onsets 30 ms apart (Figures 4-9, 4-10). In instances in which firing rates decrease and correlations do not follow, additional stimulus information may potentially be conveyed via correlated activity to drive postsynaptic neurons. These results indicate that the spatiotemporal stimulus influences on correlation magnitudes are not directly tied to the influences on firing rate magnitudes, and correlations between neurons may play additional roles in integrating tactile information.

Overall, these correlations between neurons spanning across the hand representation in primary somatosensory cortex indicate that widespread interactions occur within area 3b of primates, and the magnitude and presence of correlated activity is affected by the spatial and temporal configurations of tactile stimuli in some unexpected ways that do not mirror changes in firing rate. While the influence of the temporal stimulus relationships on the magnitude of spike timing correlations is unclear, the average strength of correlations suggests that adjacent phalanges and adjacent digits have stronger functional connections than nonadjacent phalanges and nonadjacent digits in the

area 3b hand representation of owl monkeys. These findings may be relevant to tactile object perception, as stimuli that contact adjacent skin locations may be more likely to be part of the same object. Our results support the hypothesis that sensory stimulus information affects correlations between neurons, and these correlations may play a different role in the brain than firing rate alone.

Acknowledgements

Each of the following will be co-authors on the published manuscript from this work: Drs. Hui-Xin Qi, Pierre Pouget, Zhiyi Zhou, Melanie Bernard, Mark J. Burish, A.B. Bonds, and Jon H. Kaas. This work was supported by the James S. McDonnell Foundation (JHK) and NIH grants NS16446 (JHK), F31-NS053231 (JLR), EY014680-03 (ABB), and T32-GM07347 (MJB). Matlab scripts were written primarily by P. Pouget and John Haitas in collaboration with J.L. Reed and Jurnell Cockhren. We thank Dr. Omar Gharbawie and Corrie Camalier for help collecting data from 2 of the 3 monkeys.

References

Aertsen AMHJ, Gerstein GL, Habib M, Palm G. 1989. Dynamics of neuronal firing correlation: modulation of "effective connectivity". *J Neurophysiol* 61: 900-917.

Alloway KD, Zhang M, Dick SH, Roy SA. 2002. Pervasive synchronization of local neural networks in the secondary somatosensory cortex of cats during focal cutaneous stimulation. *Exp Brain Res* 147: 227–242.

Bair W, Zohary E, Newsome WT. 2001.Correlated firing in macaque visual area MT: time scales and relationship to behavior. *J Neurosci* 21: 1676-1697.

Blake DT, Strata F, Kempter R, Merzenich MM. 2005. Experience-dependent plasticity in S1 caused by noncoincident inputs. *J Neurophysiol* 94: 2239-2250.

DeCharms RC, Merzenich MM. 1996. Primary cortical representation of sounds by the coordination of action-potential timing. *Nature* 381: 610-613.

De la Rocha J, Doiron B, Shea-Brown E, Josić K, Reyes A. 2007. Correlation between neural spike trains increases with firing rate. *Nature* 448: 802-807.

Fang P-C, Jain N, Kaas JH. 2002. Few intrinsic connections cross the hand-face border of area 3b of new world monkeys. *J Comp Neurol* 454: 310-319.

Gerstein GL. 2000. Cross-correlation measures of unresolved multi-neuron recordings. *J Neurosci Methods* 100: 41–51.

Gerstein GL, Bedenbaugh P, Aertsen AMHJ. 1989. Neuronal assemblies. *IEEE Trans Biomed Eng* 36: 4-14.

Greenberg DS, Houweling AR, Kerr JND. 2008. Population imaging of ongoing neuronal activity in the visual cortex of awake rats. *Nat Neurosci* 11: 749-751.

Hardin JW, Hilbe JM. 2003. Generalized estimating equations. Boca Raton: Chapman and Hall/CRC.

Jain N, Qi H-X, Kaas JH. 2001. Long-term chronic multichannel recordings from sensorimotor cortex and thalamus of primates. Chapter 5 In *Progress in Brain Research*, ed. MAL Nicolelis, 130: 1-10. Amsterdam: Elsevier Science B.V.

Jermakowicz WJ, Casagrande VA. 2007. Neural networks a century after Cajal. *Brain Res Rev* 55: 264-284.

Jermakowicz WJ, Chen X, Khaytin I, Bonds AB, Casagrande VA. 2009. Relationship between spontaneous and evoked spike-time correlations in primate visual cortex. *J Neurophysiol* 101: 2279-2289.

Kaas JH. What, if anything, is SI? 1983. Organization of first somatosensory area of cortex. *Physiol Rev* 63: 206-231.

Liang K-Y, Zeger SL. 1986. Longitudinal data analysis using generalized linear models. *Biometrika* 73: 13-22.

Merzenich MM, Kaas JH, Sur M, Lin CS. 1978. Double representations of the body surface within cytoarchitectonic areas 3b and 1 in "SI" in the owl monkey (*Aotus trivirgatus*). *J Comp Neurol* 181: 41-74.

Nelson RJ, Sur M, Felleman DJ, Kaas JH. 1980. Representations of the body surface in postcentral parietal cortex of *Macaca fascicularis*. *J Comp Neurol* 192: 611-643.

Nicolelis MAL, Dimitrov D, Carmena JM, Crist R, Lehew G, Kralik JD, Wise SP. 2003. Chronic, multisite, multielectrode recordings in macaque monkeys. *Proc Natl Acad Sci USA* 100: 11041-11046.

Oram MW, Hatsopoulos NG, Richmond BJ, Donoghue JP. 2001. Excess synchrony in motor cortical neurons provides redundant direction information with that from coarse temporal measures. *J Neurophysiol* 86: 1700-1716.

Reed JL, Pouget P, Qi H-X, Zhou Z, Bernard MR, Burish MJ, Haitas J, Bonds AB, Kaas JH. 2008. Widespread spatial integration in primary somatosensory cortex. *Proc Natl Acad Sci USA* 105: 10233-10237.

Roelfsema PR, Lamme VA, Spekreijse H. 2004. Synchrony and covariation of firing rates in the primary visual cortex during contour grouping. *Nat Neurosci* 7: 982-991.

Roy A, Steinmetz PN, Hsiao SS, Johnson KO, Niebur E. 2007. Synchrony: a neural correlate of somatosensory attention. *J Neurophysiol* 98: 1645-1661.

Roy S, Alloway KD. 1999. Synchronization of local neural networks in the somatosensory cortex: a comparison of stationary and moving stimuli. *J Neurophysiol* 81: 999–1013.

Roy SA, Dear SP, Alloway KD. 2001. Long-range cortical synchronization without concomitant oscillations in the somatosensory system of anesthetized cats. *J Neurosci* 21: 1795-1808.

Salinas E, Sejnowski TJ. 2001. Correlated neuronal activity and the flow of neural information. *Nat Rev Neurosci* 2: 539-550.

Samonds JM, Allison JD, Brown HA, Bonds AB. 2003. Cooperation between area 17 neuron pairs enhances fine discrimination of orientation. *J Neurosci* 23: 2416-2425.

Samonds JM, Bonds AB. 2005. Gamma oscillation maintains stimulus structure-dependent synchronization in cat visual cortex. *J Neurophysiol* 93: 223-236.

Shoham S, Fellows MR, Normann RA. 2003. Robust, automatic spike sorting using mixtures of multivariate t-distributions. *J Neurosci Methods* 127:111-122.

Sur M, Wall, JT, Kaas JH. 1984. Modular distribution of neurons with slowly adapting and rapidly adapting responses in area 3b of somatosensory cortex in monkeys. *J Neurophysiol* 51: 724-744.

Tuerlinckx F, Rijmen F, Verbeke G, De Boeck P. 2006. Statistical inference in generalized linear mixed models: A review. *Br J Math Stat Psychol* 59: 225-255.

Vaadia E, Haalman I, Abeles M, Bergman H, Prut Y, Slovin H, Aertsen A. 1995. Dynamics of neuronal interactions in monkey cortex in relation to behavioural events. *Nature* 373: 515-518.

Ventura V, Cai C, Kass RE. 2005. Statistical assessment of time-varying dependency between two neurons. *J Neurophysiol* 94: 2940-2947.

Zeger SL, Liang K-Y. 1986. Longitudinal data analysis for discrete and continuous outcomes. *Biometrics* 42: 121-130.

Zhang M, Alloway KD. 2004. Stimulus-induced intercolumnar synchronization of neuronal activity in rat barrel cortex: A laminar analysis. *J Neurophysiol* 92: 1464-1478.

Zhang M, Alloway KD. 2006. Intercolumnar synchronization of neuronal activity in rat barrel cortex during patterned airjet stimulation: A laminar analysis. *Exp Brain Res* 169: 311-325.

CHAPTER V

SPATIOTEMPORAL PROPERTIES OF NEURON RESPONSE SUPPRESSION IN OWL MONKEY PRIMARY SOMATOSENSORY CORTEX BY STIMULI PRESENTED TO BOTH HANDS

Abstract

Despite the lack of ipsilateral receptive fields (RFs) in area 3b of primary somatosensory cortex, interhemispheric interactions have been reported to varying degrees. We investigated the spatiotemporal properties of these interactions to determine: 1) the types of responses; 2) timing between bimanual stimuli to evoke the strongest interactions; 3) topographical distribution of effects; and 4) their dependence on the similarity of stimulus locations on the two hands. We examined response magnitudes and latencies of single neurons and multi-neuron clusters recorded from 100-electrode arrays implanted in one hemisphere of two anesthetized owl monkeys. Skin indentations were delivered to the two hands simultaneously and asynchronously at mirror locations (matched sites on the same digit on each hand) and nonmirror locations. Since multiple neurons were recorded simultaneously, stimuli on the contralateral hand could be within or outside of the classical RFs. For most neurons, stimulation on the ipsilateral hand suppressed responses to stimuli on the contralateral hand. Maximum suppression occurred when the ipsilateral stimulus was presented 100 ms before the contralateral stimulus onset ($P < 0.0005$). The longest stimulus onset delay of 500 ms allowed contralateral responses to recover to control levels ($P = 0.428$). Stimulation on mirror digits did not differ from stimulation on nonmirror locations ($P = 1.000$). Response

latencies changed little with stimulation parameters; latencies for all categories averaging 23.74 ms (SD = 6.91). These results indicate that interhemispheric interactions are common in area 3b, somewhat topographically diffuse, and maximal when the suppressing ipsilateral stimulus preceded the activating contralateral stimulus.

Introduction

Receptive fields for monkey area 3b neurons have been exclusively localized to the contralateral hand (for review, see Kaas, 1983), and 3b has few callosal connections to directly mediate hand-hand interactions (Killackey et al., 1983). Bilateral receptive fields have been found in the hand representations of higher-level cortical areas, including areas 1, 2, and the secondary somatosensory area, S2 (for review, see Iwamura, 2002). While it may seem unlikely that stimuli on the two hands interact to influence responses in area 3b, there are reasons to postulate that such interactions exist. Several studies have reported evidence for interhemispheric interactions in anterior parietal cortex during bimanual stimulation in humans (e.g., Schnitzler et al., 1995; Hoechstetter et al., 2001; Braun et al., 2005; Zhu et al., 2007) and nonhuman primates (Burton et al., 1998; Tommerdahl et al., 2006). Thus, our purpose is not to prove that such interactions exist; rather, our purpose is to focus on neuron response properties in area 3b in order to quantify the spatial and temporal properties of these interhemispheric interactions. Specifically, we investigated the distribution of response types (suppression, facilitation), the topographic specificity of the effects (mirror versus nonmirror hand sites), and the

timing between stimulus presentation on the two hands that evoked the strongest effects in area 3b of anesthetized owl monkeys.

In the primary somatosensory cortex of monkeys, interhemispheric interactions have been described as primarily suppressive, such that simultaneous tactile stimulation on both hands suppresses neural activity in the contralateral hemisphere as measured through optical imaging (Tommerdahl et al., 2006). Interhemispheric effects are likely to involve intrahemispheric feedback projections to area 3b from higher-order cortical areas which contain bilateral receptive fields (for review, Calford, 2002). The topographic extent of these suppressive effects has not been well-established, but the effects are expected to be somewhat widely distributed topographically based on the diffuse nature of feedback projections (e.g., Cusick et al., 1989; Darian-Smith et al., 1993; Burton and Fabri, 1995; Burton et al., 1995).

Additionally, the temporal properties of interhemispheric effects have not been well studied in area 3b. When tactile stimuli are presented to the two hands asynchronously, how do neurons respond? Because the interhemispheric interactions likely require multi-synaptic processing, we expected that when contralateral stimuli were presented with increasing onset delays relative to ipsilateral stimuli, the suppressive effects would increase to reach a maximum. Burton et al. (1998) presented vibratory tactile stimuli to matching sites on the two hands in awake macaque monkeys, and the stimuli had asynchronous onset delays of 150 or 300 ms. (In their study, ipsilateral stimuli could precede or follow the contralateral stimuli.) They did not report changes in firing rate in area 3b neurons during asynchronous bimanual stimulation; however, Burton et al. (1998) reported mostly suppression in neurons in areas 1, 2, and S2.

Therefore, we presented 500 ms skin indentations on matching and non-matching locations on the two hands, as long duration indentations drive area 3b neurons well, and presented the paired stimuli simultaneously or at onset delays of 10, 30, 50, 100, and 500 ms to characterize the spatiotemporal stimulation effects on interhemispheric interactions.

Materials and Methods

Preparation

All procedures followed the guidelines established by the National Institutes of Health and the Animal Care and Use Committee at Vanderbilt University. Two adult owl monkeys (*Aotus trivirgatus*) were prepared for electrophysiological recordings in the left hemisphere of primary somatosensory cortex following procedures detailed previously (Reed et al., 2008). These monkeys (case 2, male, 1 kg and case 3, female, 1.2 kg) were both part of studies related to processing stimuli on the contralateral hand (Reed et al., 2008; Chapter 3). Monkeys were anesthetized with propofol during surgery (10 mg/kg/hr, intravenous) and electrophysiological recording (0.3 mg/kg/hr). During surgery and recording sessions monkeys were paralyzed via vecuronium bromide (0.1-0.3 mg/kg/hr, intravenous) mixed with 5% dextrose and Lactated Ringer's solution and were artificially ventilated with a mixture of N2O: O2: CO2 (75: 23.5: 1.5) at a rate sufficient to maintain peak end tidal CO2 at ~ 4%. In monkey 3, 1.2 mg/kg sufentanil was added to the Lactated Ringer's solution during the surgical procedures in order to stabilize anesthetic depth. Following delivery of this amount of sufentanil, the monkey was maintained under anesthesia without supplemental sufentanil during extracellular recordings. As described

previously (Reed et al., 2008), the 100-electrode array (now Blackrock Microsystems, Salt Lake City, UT) was inserted to a depth of 600 μm using a pneumatic inserter so that the electrode tips were expected to be located within cortical layer 3.

Tactile Stimulation and Recording Procedures

We compared responses to paired stimulation on mirror digits versus nonmirror digits. Our equipment and stimulus parameters have been described previously (Reed et al., 2008; Chapter 3). Briefly, stimuli were provided by two independent force- and position-feedback controlled motor systems (300B, Aurora Scientific Inc., Aurora, ON, CA), with contact made by round Teflon probes 1 mm in diameter. Stimuli consisted of pulses that indented the skin 0.5 mm for 0.5 s, followed by 2.0 s off of the skin, repeated for 255 s (100 trials). Indentations were delivered to paired skin sites simultaneously (0 ms) and at selected stimulus onset delays of 10, 30, 50, 100, and 500 ms. Single-site control stimuli were delivered to the ipsilateral and contralateral sites prior to paired stimulation while recordings were made from the left hemisphere. The fingernails were glued (cyanoacrylic) to Teflon screws fixed in plasticine to keep the hand stable during stimulus blocks.

In addition to controlled mechanical stimulation, we used light tactile stimulation to map the minimal receptive fields (mRFs) of selected electrodes. Receptive field mapping aided our reconstruction of the electrode locations as within and outside of area 3b, to complement our subsequent histological identification of area 3b. As we have published previously (Reed et al., 2008), the mRF was defined as the region of skin where a near-threshold light touch with a probe reliably evoked spikes from the recorded

neurons. Typical procedures for mRF mapping have been published (e.g., Merzenich et al., 1978; Nelson et al., 1980).

Recordings were made using the 100-electrode array and the Bionics Data Acquisition System (now Blackrock Microsystems). The signals on each channel were amplified by 5000 and band-pass filtered between 250 Hz and 7.5 kHz. The threshold for each electrode was automatically set for 3.25 times the mean activity and the waveforms were sampled at 30 kHz for 1.5 ms windows (Samonds et al., 2003).

Histology

Upon experiment completion, animals were perfused with saline followed by fixative, and the brains were prepared for histological analysis as previously described (Jain et al., 2001). The cortex was flattened, frozen, and cut parallel to the surface at 40 µm. Sections were processed for myelin to aid in determining the electrode locations relative to the area 3b hand representation (see Reed et al., 2008). Electrode depth was estimated by identifying the appearance and disappearance of electrode tracks across serial sections.

Data Analysis

Spike Sorting

The details of the spike sorting procedures have been described previously (Reed et al., 2008). Briefly, spike signals were sorted offline with an automatic spike classification program based on the t-distribution Expectation Maximization algorithm

(Shoham et al. 2003) which is part of the data acquisition system. A second spike sorter program, Plexon Offline Sorter (Plexon Inc., Dallas, TX), was used to verify the quality of unit isolation such that single units had refractory periods ≥ 1.2 ms; P values ≤ 0.05 for multivariate ANOVA related to cluster separation; and distinct waveform amplitudes and shapes when compared with other activity on the same electrode (Nicolelis et al., 2003). Single- and multi-units were categorized separately but grouped together for factor analysis. Multiple single units collected from one electrode were included in the analysis, but at most only one multi-unit per electrode was included in the analysis.

Peak Firing Rate

As described in Reed et al. (2008), to determine peak firing rate, spike trains were smoothed with a spike density function using Matlab (The Mathworks, Inc., Natick, MA). A spike density function was produced by convolving the spike train from each trial with a function resembling a postsynaptic potential specified by τg, the time constant for the growth phase, and τd, the time constant for the decay phase as:

$R(t) = (1 - \exp(-t/\tau d)*\exp(-t/\tau d)$.

Based on physiological data from excitatory synapses, τg was set to 1 ms (e.g., Mason et al., 1991; Moore and Nelson, 1998). We set τd to 5 ms (Mason et al., 1991; Moore and Nelson, 1998; Veredas et al., 2005) because the transient nature of the on and off responses in primary somatosensory neurons was excessively smoothed at larger values, particularly when stimuli were presented at stimulus onset asynchronies of 10 and 30 ms. We examined onset responses within a 50 ms response time window from the onset of the stimulus of interest. When stimuli were presented with onset asynchronies,

the window began from the onset of the second (contralateral) stimulus; thus, the first (ipsilateral) stimulus acted as a "conditioning stimulus" as described by others (e.g., Chowdhury and Rasumusson, 2003; Gardner and Costanzo, 1980b; Greek et al., 2003).

The excitatory peak firing rate was determined as the maximum of the spike density function within the response time window, and the average baseline firing rate (calculated over a 500 ms window prior to stimulation onset) was subtracted from this value. This peak firing rate value was required to be greater than a threshold value, which was the average baseline firing rate plus two standard deviations of this baseline with a minimum value of 5 spikes/s. To determine if this value was significant, the nonparametric Mann-Whitney U test and the parametric Student's t-test were performed and results compared. The U test and t test resulted in the same categorizations of significance ($\alpha = 0.05$). When no excitatory response was detected in the response window, responses were examined for possible suppressive effects. However, the current study does not include inhibitory responses.

Response Latency

Response latencies were calculated using Matlab and determined from spike density function histograms as the initial time when the rate meets the half-height over the threshold value of the peak firing rate within the response time window (see *Peak Firing Rate*). Briefly, the peak latency was calculated using polynomial fitting of the spike density function. The firing rate values of the half-height and the threshold value were compared. The greater of the half-height or the threshold value was selected, and the time was designated as the response latency. This method of determining excitatory

response latency is similar to measures that determine the width or duration of peaks in histograms (e.g., Tutunculer et al., 2006; Davidson et al., 2007). Results were checked manually for proper assignments.

Firing Rate Modulation Index

We developed a modulation index based on methods used to describe multisensory integration (Stanford et al., 2005; Alvarado et al., 2007). The observed average firing rate response within the 50 ms response window during a given bimanual stimulation condition was compared with the distribution of expected average responses based on summation of the unit's response to the two stimuli presented individually. The expected distribution was based on the sum of two control values computed for every combination of trials, for 100 trials (100 x 100). 100 trials were randomly selected (without replacement) from the distribution and averaged to give the predicted average response to bimanual stimulation. This was repeated 10,000 times to build a reference distribution of predicted responses and compare the observed response to this distribution, following the methods of Alvarado et al. (2007). The Kolmogorov-Smirnov test of normality was used for the observed responses (100 trials each) and the predicted responses (100 trials selected from 10,000 bootstrapped samples). When normality assumptions were met, paired t tests for matched samples were used; otherwise, nonparametric Wilcoxon signed rank tests were used. The modulation categories were "superadditive", "subadditive", "additive", "suppressive", or "no difference" from the response to the contralateral stimulus, similar to the methods of Stanford et al. (2005). "Superadditive" responses were greater than the predicted distribution by 2 times the

standard deviation of the distribution, and "subadditive" responses were less than the predicted distribution by 2 times the standard deviation of the distribution.

As an additional quantifier, a percent modulation calculation was also performed similar to the multisensory integration index (Meredith and Stein, 1983; Alvarado et al., 2007) and suppression index (Jiang and Stein, 2003) using the following equation:

$\%\ \text{modulation} = ((FR_{\text{bimanual stimuli}} - FR_{\text{contralateral control}}) / FR_{\text{contralateral control}})*100.$

These calculations incorporated a correction to subtract the average baseline firing rate from the observed average firing rate, and the overall calculation is a subtraction of the response to the contralateral stimulus from the response to the 2-site stimulation, with the result divided by the response to the contralateral stimulus and multiplied by 100.

Response Field

Since we recorded from multiple neurons simultaneously using a 100-electrode array, the stimulus locations did not always coincide with the receptive fields of each neuron. We defined excitatory "Response Fields" based on the neuron unit firing rates in response to above-threshold skin indentations with our stimulus probes. When a single site on the hand was stimulated, that site was classified as inside that unit's excitatory Response Field if the peak firing rate after subtracting the average baseline firing rate was greater than or equal to 3 times the standard deviation of the average firing rate for the population of neurons (see Chapter 3). For a given neuron, responses for all of the locations that were stimulated for a given experiment were compared. The maximum value for firing rate was found, and that stimulation location was designated as in the

center of that unit's Response Field. When the unit firing rate did not meet the criteria to be categorized as *inside*, the location was considered *outside* of the Response Field. This Response Field is a firing-rate-based estimate similar to the concept of the receptive field (as measured by suprathreshold stimulation) and was used to examine and classify spatial integration. When both hands were stimulated together, the Response Field designations during stimulation of the two single sites were combined.

Data Classification

Data were classified based on several conditions that were used in a statistical model to estimate the contributions of those factors to the observed latencies and firing rates. These factors were the temporal relationship of the stimuli, the spatial relationship of the stimuli, and the neuron's Response Field relationship to the stimuli (Figure 5-1).

For the temporal stimulation condition, the preferred control was the contralateral location in a stimulus pairing, and the paired stimulus conditions included presentations of the ipsilateral stimulus with the contralateral stimulus simultaneously (0 ms) or preceding the contralateral stimulus by 10, 30, 50, 100, or 500 ms. The spatial relationship of the stimuli refers to the stimulus probe placement on mirror or nonmirror locations on the two hands. The paired hand locations stimulated included "mirror locations" for monkey 2 on left and right distal digit 2 (dD2) and left and right distal digit 3 (dD3); and for monkey 3 on left and right distal digit 4 (dD4), left and right palm pad 3 (P3), and left and right palm pad 4 (P4). Stimulation on "nonmirror locations" included for monkey 2 left middle D3 with right dD2, left middle D4 with right dD2, left dD2 with right dD3, left middle D4 with right dD3, and left dD4 with right dD3; and for monkey 3

left distal digit 5 (dD5) with right dD4 and left dD5 with right palm pad 3 (monkey 3). The relationship of the paired stimuli to the Response Field of the reference unit was included as a factor that could influence the firing rate and latency. Although we allowed for the possibility that units would respond to the ipsilateral stimulus, the ipsilateral stimulus was outside of the Response Fields of all the units collected and included in this analysis. As such, the combined categories were outside-outside (OUT_OUT), inside-outside (IN_OUT), and center-outside (CN_OUT). Finally, we classified the data into single units (SU) and multi-units (MU) and tested this factor for influence on response latency and peak firing rate.

Summary Analysis

The values we obtained for excitatory response latency and peak firing rate from Matlab were summarized in Excel and imported into SPSS 17.0 (SPSS, Inc., Chicago, IL) for further analysis. The data distributions differed from the normal and Poisson distributions (Kolmogorov-Smirnov 1-sample test); therefore, we employed Generalized Estimating Equations (for correlations in data due to repeated measures) in SPSS to analyze this complex dataset. (For detailed information regarding Generalized Estimating Equations analysis, refer to Liang and Zeger, 1986; Zeger and Liang, 1986; Hardin and Hilbe, 2003.) We tested several parameters, and the final statistical model parameters for both latency and firing rate results were based on a gamma probability distribution with the log link function, a first-order autoregressive correlation matrix, and a robust model estimator. See Chapter 3 and Appendix A for detailed descriptions of use of the Generalized Estimating Equations method. In these models, latency or peak firing rate

acted as the dependent variable and the predictor variables included: the temporal stimulus relationship, the spatial relationship of stimuli, the relationship of the stimulus to the Response Field of the neuron unit, and the classification of the unit as a single- or muli-unit. (See depictions of the predictor variable categories in Figure 5-1.) The Bonferroni correction for multiple comparisons was applied, and the Wald Chi-Square statistic was used to test the significance of the effects of the statistical model. The Generalized Estimating Equations analysis provides estimates of the population averages of the dependent variable based on the values of the predictor variables and provides estimates for the significance of the effects.

Results

We obtained single- and multi-unit recordings from 100-electrode arrays implanted in cortical layer 3, primarily from area 3b, of two owl monkeys during stimulation on selected locations on the ipsilateral and contralateral hand. Figure 5-2 depicts the placement of the electrode arrays in the left hemispheres of each of the monkey cases, as determined from receptive field mapping during the recording procedures and myelin staining patterns in sections of flattened cortex. The numbers of units meeting the criteria for analysis were as follows: 117 single units (SUs) and 152 multi-units (MUs) from case 2; and 132 SUs and 121 MUs from case 3. Data were collapsed across the two monkeys for summary analysis. The numbers of SUs and MUs in the summary analysis were based on unique combinations of units and stimulus conditions.

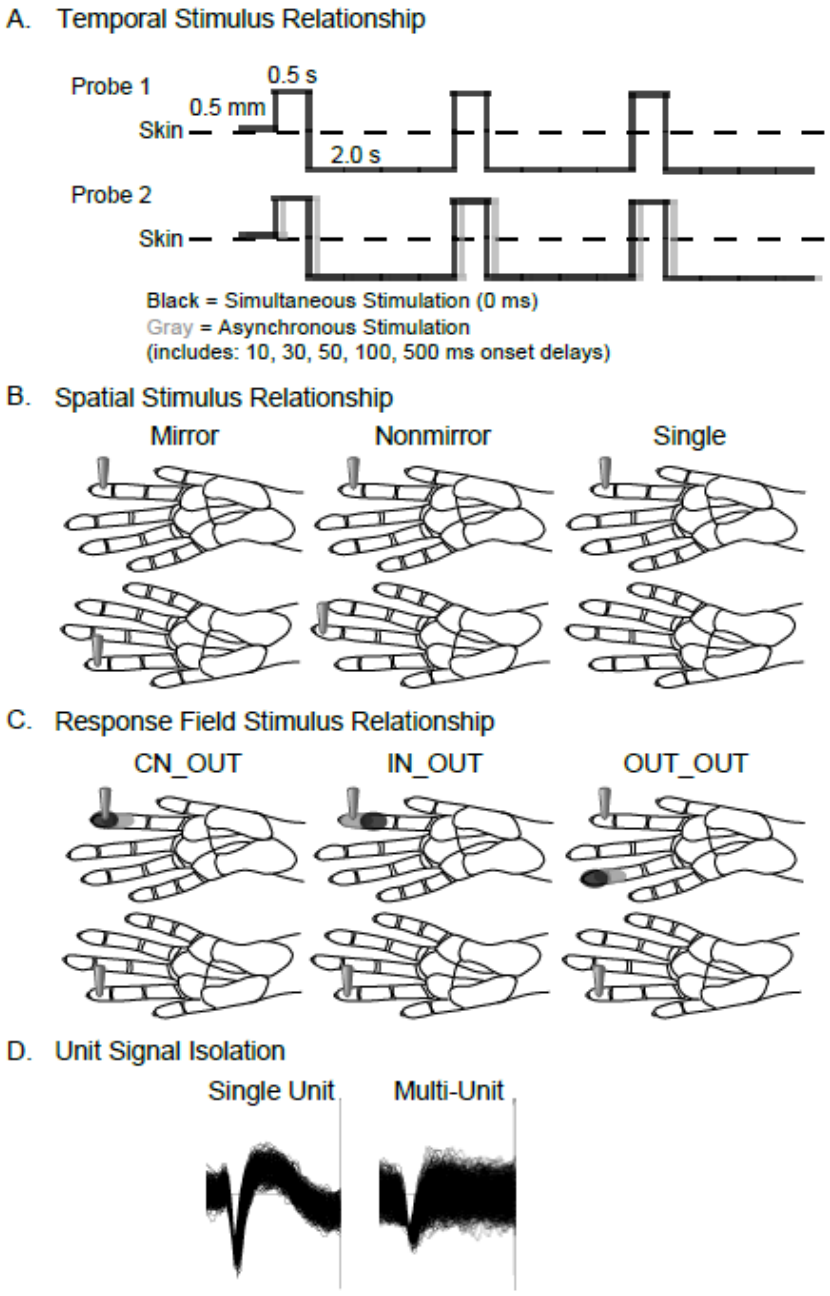

Figure 5-1. Schematics depict data categories used for summary analysis. A. Temporal stimulation is depicted by solid lines indicating the duration the stimulus probe indents the skin (0.5 s), indentation depth (0.5 mm), and duration the probe is off of the skin per stimulus cycle (2.0 s). Paired stimulation, indicated by Probe 1 and Probe 2, may be simultaneous or asynchronous. To depict overlap in contact time of the asynchronous stimulation, the gray line is shifted relative to the black line. B. Locations of the two stimulus probes on schematics of the owl monkey hand illustrate the spatial proximity category on matching sites on the two hands (Mirror), on non-matching sites (Nonmirror), or on the contralateral hand alone (Single). C. Black shading on schematics of the owl monkey hand indicates the center of the Response Field for a hypothetical neuron. Gray shading on the hand indicates locations inside the Response Field, but outside the center "hotspot" for the hypothetical reference neuron. The locations of the two probes indicate the stimulus location relative to the Response Field. D. Data were also classified by the quality of the signal isolation into single units (SU) or multi-units (MU). Examples of each unit type are shown from monkey case 3. The trace window for each unit type shown spanned 128 μV and 1.6 ms.

A series of example rasters and histograms in Figure 5-3 shows one neuron's responses to ipsilateral, contralateral, and bimanual stimulation on matching, mirror locations. Figure 5-4 shows the responses of the same neuron when the paired stimulation sites were located on non-matching, nonmirror locations. The effects in this example neuron resemble the population results; such that ipsilateral stimulation suppressed responses to contralateral stimuli, and this effect was slightly more pronounced when the stimuli were presented on mirror locations instead of nonmirror locations. We examined changes in the response latency and peak firing rate compared to those during contra-lateral stimulation under these varying spatial and temporal conditions.

Contributions to the Variance of Peak Firing Rate and Response Latency

We collected 1743 SU firing rate observations and 1911 MU firing rate observations that met the inclusion criteria under the spatiotemporal stimulus conditions. The mean peak firing rate for the observed values in the dataset was 19.37 spikes/s (SD 25.14) and the median peak firing rate was 11.32 spikes/s. We obtained fewer response latencies than firing rate observations because not all firing rates were significantly greater than the baseline in response to stimulation. We collected 1322 SU response latencies and 1558 MU response latencies that met our inclusion criteria under the spatiotemporal stimulus conditions. The mean response latency for the observed values in the dataset over all conditions was 23.74 ms (SD 6.91) and the median response latency was 22.20 ms. The modeling analysis predicted that several factors influenced the peak firing rate values; and these spatiotemporal stimulus conditions affected peak firing rate more than latency.

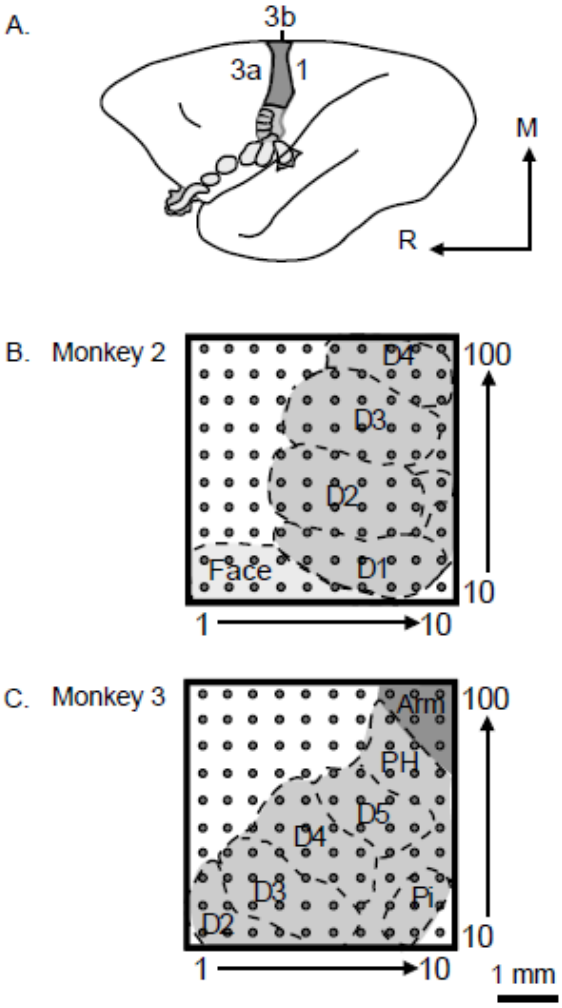

Figure 5-2. Schematic reconstructions show 100-electrode array placement in two owl monkey cases. A. A schematic of the owl monkey brain is shown with area 3b highlighted. The orientation of the brain is indicated by the arrows. R = rostral and M = medial. B-C. The placements of the 100-electrode array in each case tended to cover a large part of the area 3b hand representation. The 1 mm scale bar refers to the array size for both monkey cases.

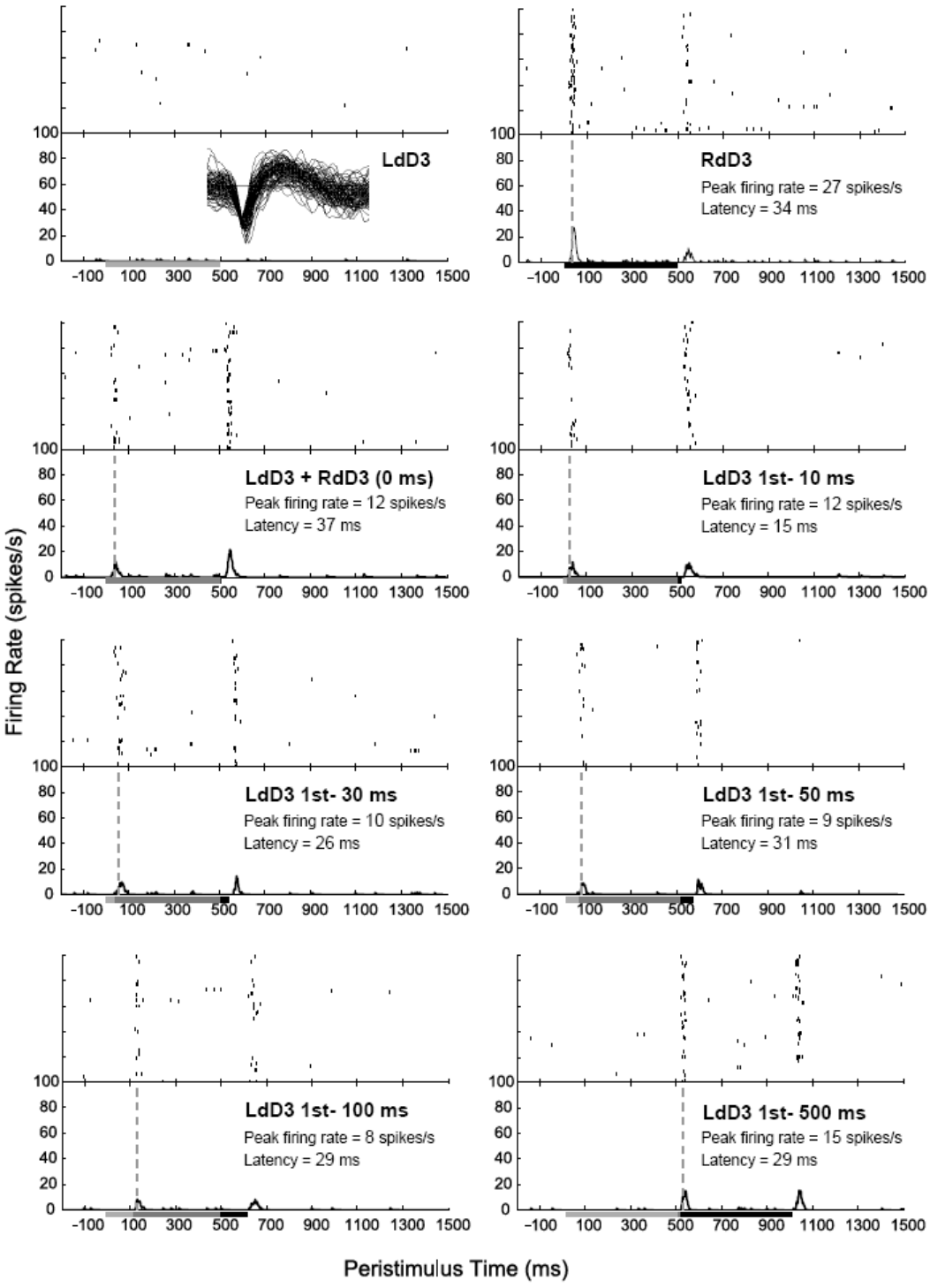

Figure 5-3. Example histograms depict changes in response to bimanual stimulation on mirror locations. Traces of the unit waveforms are inset (unit 074a from case 2). Histograms smoothed by a spike density function over 100 trials are shown: when each hand was stimulated individually; then for both locations simultaneously; and for trials when the ipsilateral (left) stimulus was presented at intervals before the onset of the contralateral (right) stimulus. Each stimulus duration was 500 ms, indicated by the line on the x-axis. Vertical dashed lines indicate latency. Generally, peak firing rates were suppressed by bimanual stimulation.

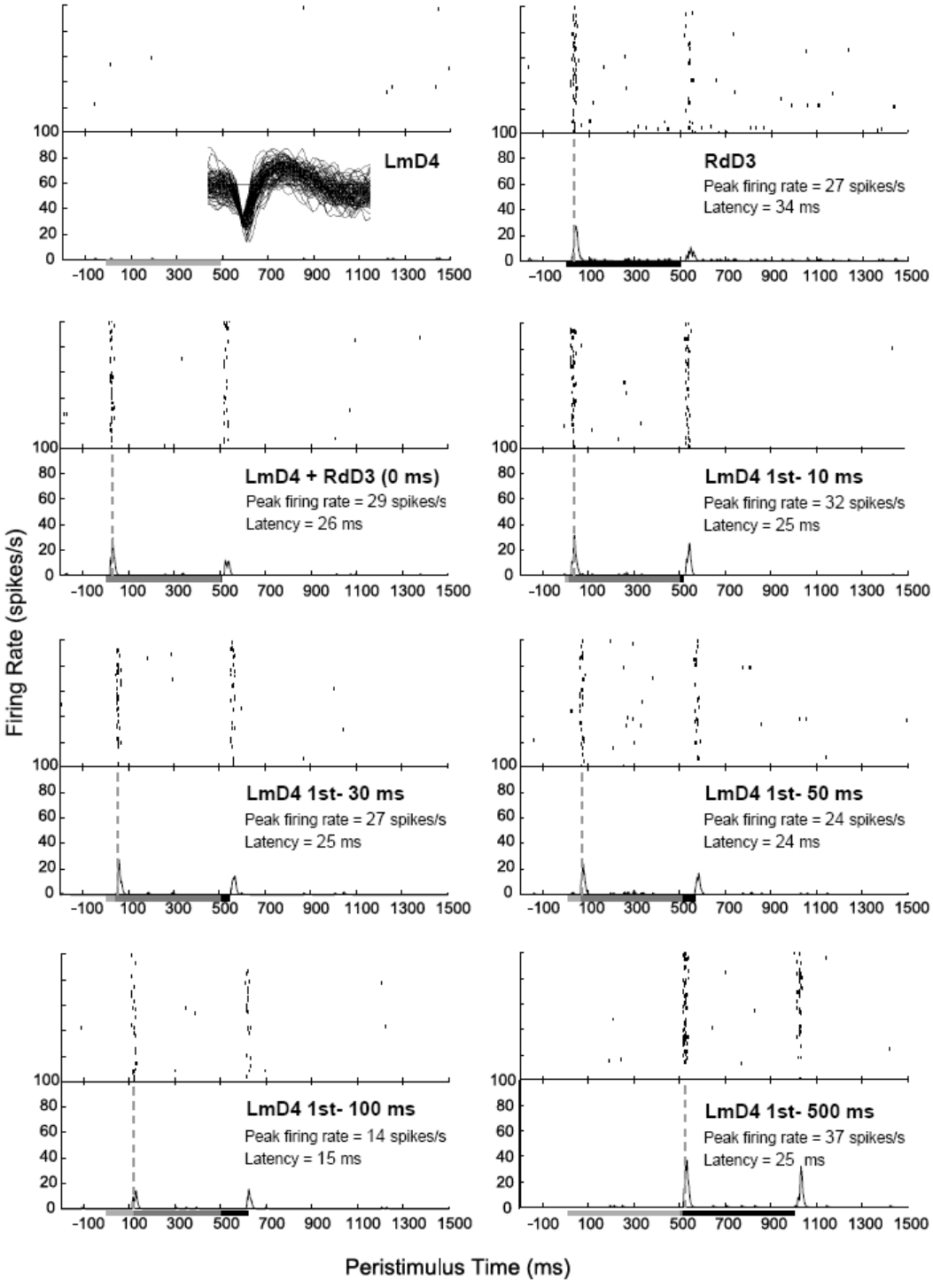

Figure 5-4. Example histograms from a single unit depict peak firing rate and latency changes in response to bimanual stimulation on nonmirror locations. The traces of the unit waveforms recorded for the given stimulation series are inset in the upper left histogram (unit 074a from case 2, same as Figure 5-3). Stimulation on nonmirror locations resulted in less suppression in the same unit shown in Figure 5-3 compared to responses during stimulation on mirror locations. In both cases, the firing rate response dropped to its lowest level when the ipsilateral stimulus preceded the contralateral stimulus by 100 ms.

Tests of the model effects were performed using the Wald Chi-Square statistic for significance of main effects and selected 2-, 3-, and 4-way interactions (Tables 5-1, 5-2). The results for which significance calculations are reported are estimates of the peak firing rate and latency values based on the analysis (rather than the observed data values). Deviations between the observed data values and the predicted estimates were slight, and the estimates from the analysis followed the trends in the data. Plots in Figures 5-5 and 5-6 are observed values.

Table 5-1. Tests of model effects for variance in peak firing rate classified by spatial and temporal stimulus characteristics, unit type, and interactions

Variance Source	Wald Chi-Square	df	P value
(Intercept)	3542.320	1	< 0.0005
Temporal Relationship	41.450	5	< 0.0005
Spatial Relationship	0.140	1	0.709
Response Field (RF)	173.406	2	< 0.0005
Unit Type	4.354	1	0.037
Temporal x Spatial	21.475	5	0.001
Temporal x RF	41.138	12	< 0.0005
Temporal x Unit	5.259	6	0.511
Temporal x Spatial x RF	12.228	12	0.428
Temporal x Spatial x RF x Unit	41.858	32	0.114

Tests of model effects using Type III analysis from Generalized Linear Modeling with General Estimating Equations on the dependent variable peak firing rate. N = 522 units with correlated measures from the 7 levels of the variable "Temporal Relationship" (observations = 3654).

Table 5-2. Tests of model effects for variance in latency classified by spatial and temporal stimulus characteristics, unit type, and interactions

Variance Source	Wald Chi-Square	df	P value
(Intercept)	86865.269	1	< 0.0005
Temporal Relationship	9.401	5	0.094
Spatial Relationship	0.000	1	0.983
Response Field (RF)	5.089	2	0.079
Unit Type	35.201	1	< 0.0005
Temporal x Spatial	18.025	5	0.003
Temporal x RF	11.380	12	0.497
Temporal x Unit	2.548	6	0.863
Temporal x Spatial x RF	18.678	12	0.097
Temporal x Spatial x RF x Unit	28.147	32	0.662

Tests of model effects using Type III analysis from Generalized Linear Modeling with General Estimating Equations on the dependent variable latency. N = 522 unit subjects with correlated measures from the 7 levels of the variable "Temporal Relationship" (included observations = 2875, missing observations = 779).

Temporal Stimulation Relationship

As expected based on the work of others, we found decreases in peak response magnitudes compared to contralateral stimulation (17.44 spikes/s ± 0.59) for all of the temporal stimulation conditions in which the ipsilateral stimulus was presented simultaneously with or preceding the contralateral stimulus. As shown in Figure 5-5A, maximum suppression was found when the ipsilateral stimulus was presented 100 ms before the onset of the contralateral stimulus (12.67 spikes/s ± 0.71, $P < 0.0005$). The longest stimulus onset delay of 500 ms allowed the contralateral response to recover nearly to control levels (15.93 spikes/s ± 0.81, $P = 0.428$). The remaining pairwise comparisons with contralateral control stimulation are as follows: 0 ms = 14.00 spikes/s ± 0.76, $P < 0.0005$; 10 ms = 15.02 spikes/s ± 0.80, $P = 0.003$; 30 ms = 14.43 spikes/s ± 0.80, $P < 0.0005$; and 50 ms = 14.22 spikes/s ± 0.80, $P < 0.0005$. Thus, the inter-hemispheric effects on the responses to contralateral stimulation occurred not only when stimuli were presented simultaneously, but they had a maximum suppressive effect when the onset of the ipsilateral stimulus preceded the contralateral stimulus by 100 ms.

Unlike peak firing rate, the response latency to the contralateral stimulus was not significantly affected by the presentation of the ipsilateral stimulus ($P = 0.094$, Figure 5-5B). Thus, ipsilateral stimulation in conjuction with contralateral stimulation did not affect the latency of responses, but did affect the peak response magnitude.

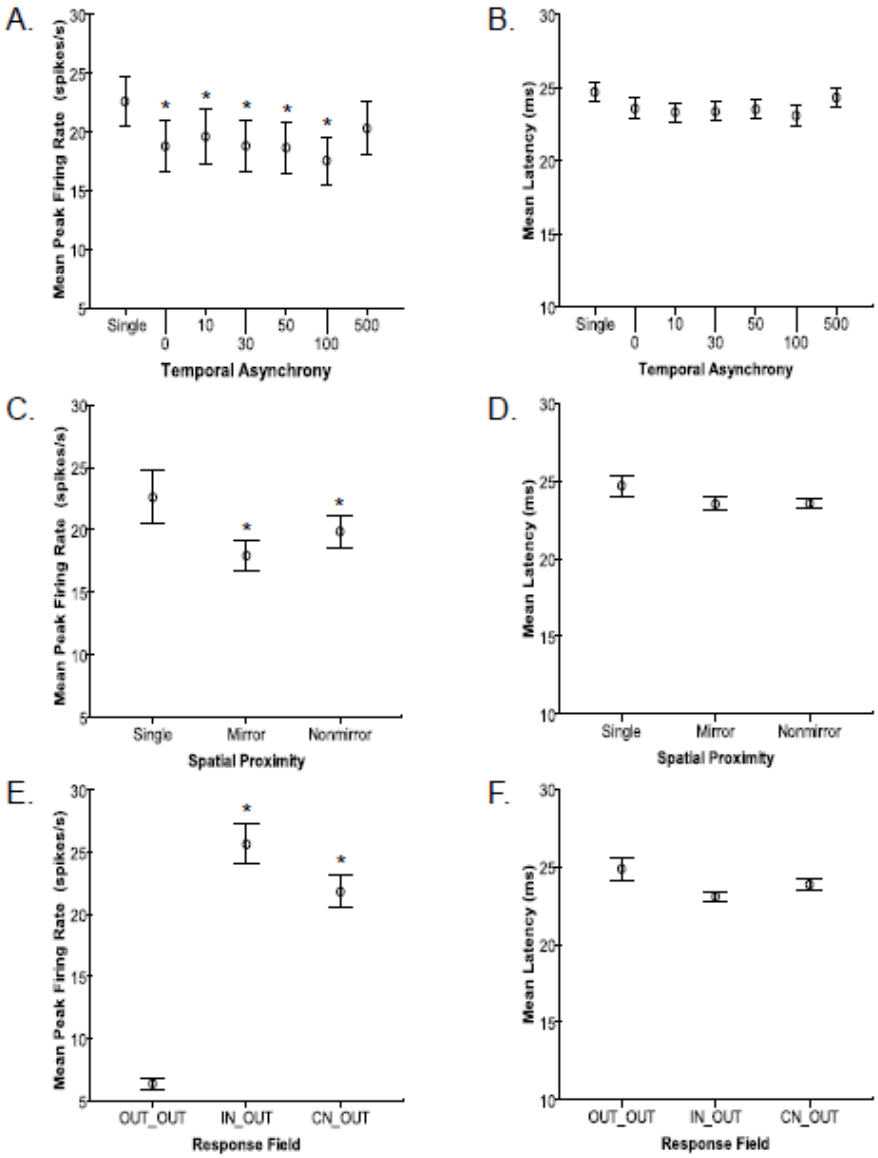

Figure 5-5. Peak firing rates and response latencies differ across spatial and temporal stimulus factors. Error bars represent 95% confidence intervals. Asterisks (*) indicate significant differences relative to the first category in each panel. A. Means of peak firing rates (spikes/s) are plotted for each temporal stimulation category. On the x-axis, "Single" refers to the contralateral stimulus, and numbers refer to the delay between the onset of the ipsilateral stimulus and the onset of the contralateral stimulus. Contralateral stimulation resulted in differences from all groups except the 500 ms onset delay group. B. Means of latencies (ms) were not significantly different for temporal stimulation conditions. C. Means of peak firing rate values are plotted for the spatial proximity conditions in which the stimuli were on matched locations on the two hands (Mirror), when the stimuli were on different digits of the hands (Nonmirror), and when a single site on the contralateral hand was stimulated (Single). Peak firing rates were suppressed by mirror and nonmirror bimanual stimulation compared to single-site contralateral stimulation, but mirror and nonmirror groups were not significantly different from each other. D. Mean latencies were not significantly different for the spatial proximity categories. E. Means of peak firing rates for each type of Response Field relationship show that peak firing rates were lower when the stimuli were outside of the Response Field (OUT_OUT) compared to when the contralateral stimulus was inside the Response Field (IN_OUT, CN_OUT). IN_OUT and CN_OUT groups were not significantly different from each other. F. Differences in mean response latencies for the Response Field relationships were not statistically significant.

Spatial Stimulation Relationship

Bimanual stimulation resulted in suppression of peak firing rates compared to contralateral stimulation alone (Contralateral = 17.44 spikes/s ± 0.58; Mirror = 14.62 spikes/s ± 1.03, P = 0.010; Nonmirror = 14.08 spikes/s ± 0.80, P < 0.0005; Figure 5-5C). Stimulation on mirror digits was not different from stimulation on nonmirror digits (P = 1.000). Also, presenting paired stimuli on mirror or nonmirror hand locations did not impact the latency of the response to contralateral stimulation (P = 0.983, Figure 5-5D). Therefore, the interhemispheric effects were not strongly topographically matched.

Response Field Relationship

Shown in Figure 5-5E, when both stimuli were outside of the Response Field (OUT_OUT, 6.08 spikes/s ±0.51), the peak firing rates were significantly lower than other conditions when the contralateral stimulus was inside the Response Field (IN_OUT, 25.01 spikes/s ± 2.08; P < 0.0005; CN_OUT, 20.29 spikes/s ± 1.66; P < 0.0005). The highest firing rates were found when the contralateral stimulus was within the Response Field of the reference unit, and the responses in these two categories were not significantly different (IN_OUT and CN_OUT, P = 0.229). Thus, the location of the contralateral stimulus in relation to the Response Field of the reference unit had a large effect on the firing rate; and the interaction of Response Field with the temporal stimulus relationship was a significant source of the variance in firing rates (P < 0.0005, Table 5-1).

While the Response Field relationship may exhibit a weak tendency to affect the latency of the response to the contralateral stimulus (P = 0.079, Table 5-2) such that

latencies are longer when the paired stimuli are both outside the Response Field, none of the pairwise comparisons between the Response Field categories were significantly different from each other (Figure 5-5F). Thus, the Response Field categorization affected the variance in peak firing rates but had little effect on latencies.

Unit Isolation

Peak firing rate responses of MUs were slightly but significantly higher than those of SUs (MU = 16.05 spikes/s ± 1.06; SU = 13.22 spikes/s ± 0.92; P = 0.043; Figure 5-6A). Similarly, excitatory response latencies of MUs were slightly, but significantly faster than those of SUs (MU = 22.37 ms ± 0.33; SU = 25.44 ms ± 0.42; P < 0.0005; Figure 5-6B).

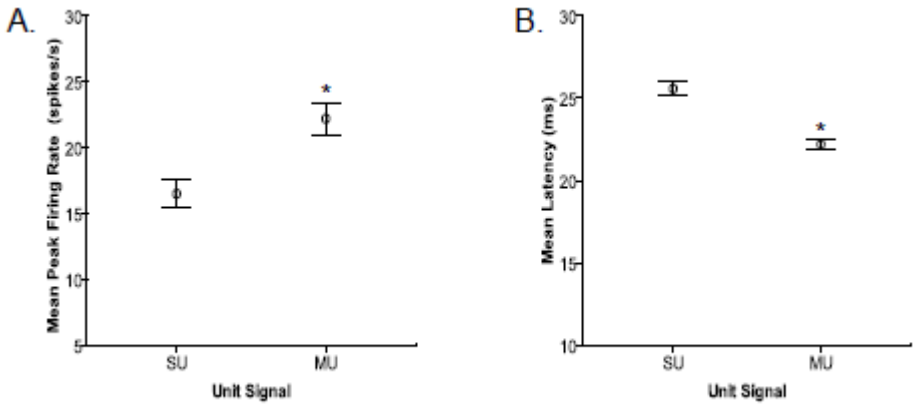

Figure 5-6. Peak firing rates and response latencies differ between single units and multi-units. Error bars represent 95% confidence intervals for both panels. Asterisks (*) indicate significant differences relative to the single unit category. A. On average, multi-units (MU) had higher peak firing rates than single units (SU). B. Multi-units had shorter latencies than single units, on average.

Interactions and Summary

Although the effect of the spatial stimulus relationship was not a significant source of variance in the statistical model, the interaction of temporal stimulus relationship with spatial stimulus relationship was significant for peak firing rate (P = 0.001; Table 5-1) and for latencies (P = 0.003, Table 5-2). This interaction effect resulted from the suppression relative to contralateral stimulation (17.44 spikes/s ± 0.59) that was stronger during simultaneous stimulation of mirror locations (13.40 spikes/s ± 1.02; P = 0.002) than simultaneous stimulation on nonmirror locations (14.63 spikes/s ± 1.13, P = 0.328), and the suppression when stimuli were applied asynchronously at 10 ms delays was weaker for stimulation on mirror locations (15.99 spikes/s ± 1.16, P = 1.000) than for nonmirror locations (14.11 spikes/s ± 0.42, P = 0.039). In contrast, latencies in response to bimanual stimulation differed most from latencies in response to contralateral stimulation alone (24.76 ms ± 0.37) when the stimulation sites were on nonmirror locations and the ipsilateral stimulus preceded the contralateral stimulus by 30 ms (22.89 ms ± 0.46, P = 0.026). However, this latency difference and all other pairwise differences in latency were very small (1-2 ms differences), and were thus not convincing contributions to the variance in latencies.

Notably, the interaction between the temporal stimulation category and the unit isolation was not significant for peak firing rate (P = 0.511, Table 5-1) or latency (P = 0.863, Table 5-2). This indicates that single units and multiunits behave similarly rather than differently in response to the temporal stimulation. The 3- and 4-way interactions tested were not significant sources of variance and are not displayed graphically. Since the interaction of all four factors, including the signal isolation, did not contribute to the

variance in the peak firing rates (P = 0.114, Table 5-1) and latencies (P = 0.662, Table 5-2), our results provided further indications that single- and multi-units appeared to behave in similar ways in response to the spatiotemporal stimulation conditions.

In summary, the peak firing rate in response to contralateral stimulation was affected by the temporal relationship of the onsets of the contralateral and ipsilateral stimuli. While there was little difference on average between peak firing rates when the paired stimuli were presented to mirror or nonmirror locations on the hand, there was a significant spatiotemporal interaction effect on peak firing rate. In contrast, the latency in response to the contralateral stimulus was affected little by the spatiotemporal relationship with the ipsilateral stimulus.

To depict population responses from recordings across the 100-electrode array, we plotted the peak firing responses in a color map of the array for a subset of stimulus parameters in each of the two monkeys during stimulation on mirror (Figure 5-7A) and nonmirror locations (Figure 5-7B). Individual neuron units (represented by colored squares) sometimes showed different changes in firing rate under the same stimulation parameters, but the color map plots are not easily quantified. Therefore, we calculated a trial-by-trial modulation index for each unit to determine whether paired bimanual stimulation affected the response to the contralateral stimulus.

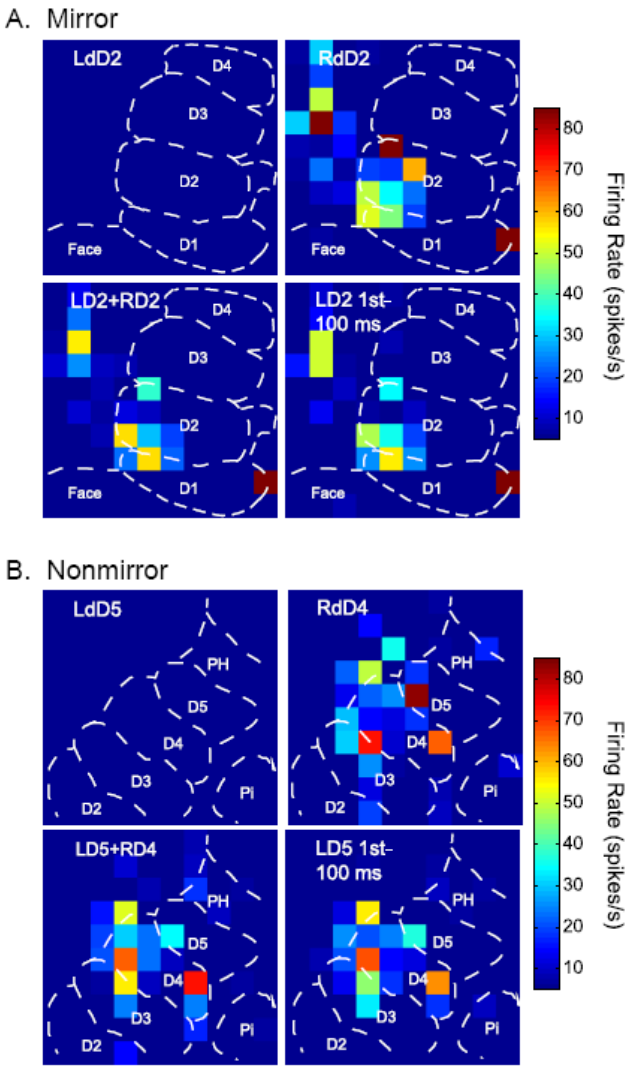

Figure 5-7. Peak firing rates represented as color maps across the 100-electrode array during bimanual stimulation on mirror and nonmirror locations. Each square represents an electrode in the array and the peak firing rate value averaged over 100 trials during the 50 ms response window. The color scale ranges from 5 to 85 spikes/s with hot colors representing higher peak firing rates. Electrodes from which no significant responses were obtained during the stimulation are indicated in dark blue (no squares). The dashed lines indicate approximate locations of the representations within area 3b. A. Peak firing rates in case 2 during a stimulation series on mirror locations on distal digit 2 (dD2) show that no driven activity (> 5 spikes/s) was found when a single site on the ipsilateral digit was stimulated (top left). As expected, activity was evoked when the contralateral digit was stimulated (top right). When the two mirror sites were stimulated simultaneously (lower left), peak firing rates decreased on average across the recording area. When the ipsilateral digit was stimulated 100 ms before the onset of the contralateral stimulus, the overall suppression was maintained and some units were further suppressed (lower right). B. Peak firing rates in case 3 during a stimulation series on nonmirror locations show similar trends to those found during stimulation on mirror locations. No driven activity was found when a single site on the ipsilateral distal digit 5 (LdD5) was stimulated (top left), and driven activity was found when the contralateral distal digit 4 (RdD4) was stimulated (top right). When both locations were stimulated simultaneously (lower left), the activity across most electrodes decreased, but activity on some electrodes increased. When the ipsilateral site was stimulated 100 ms before the onset of the contralateral stimulation (lower right), most units were suppressed or unchanged compared to simultaneous bimanual stimulation.

Firing Rate Modulation Index

We analyzed the single unit and multi-unit data together for firing rate modulation calculations because single units were not significantly different from multi-units (P = 0.261). Summarizing over the stimulation parameters, we found that the majority of unit responses were suppressed by paired ipsilateral stimulation (1865/2994, 62.3%). About one third (1005/2994, 33.6%) of the unit responses to contralateral stimulation were not significantly changed by ipsilateral stimulation. Only about 4% of unit responses (124/2994) were facilitated by ipsilateral stimulation. The presence of response facilitation is somewhat unexpected, but only a small proportion of responses showed this form of modulation during bimanual stimulation.

When we tallied the response modulation types based on the spatial and temporal stimulus characteristics, we found that stimulation on mirror and nonmirror locations in which the stimulus probes were within or outside of the neuron's Response Field resulted in the same basic trends (Figures 5-8, 5-9). Facilitation occurred rarely, but when facilitation was found, the ipsilateral stimulus was presented at short onset delays (0, 10, or 30 ms) before the contralateral stimulus. Suppression occurred with increasing frequency as the stimulus onset delays increased. Particularly when mirror locations were stimulated, the most instances of suppression were found when the ipsilateral stimulus preceded the contralateral stimulus by 100 ms. When the contralateral (and ipsilateral) stimulus location was outside the neuron's Response Field, the proportion of suppressive responses was nearly equivalent to the proportion of responses that did not change during bimanual stimulation compared to contralateral stimulation alone. Overall, the dominant

effect of a preceding ipsilateral stimulus was to suppress the response to the contralateral stimulus at long onset delays (50, 100, or 500 ms).

In addition to the increased number of suppressed responses with increasing stimulus onset delays, the magnitude of the suppression increased as well (Figure 5-10). The greatest percentage of suppression occurred when the ipsilateral stimulus preceded the contralateral stimulus by 100 ms. The magnitude of facilitation changed in an opposing manner. The magnitude of facilitation was very low when the stimuli were presented at long onset delays, and reached 10% or greater when the stimuli were presented within 10 ms of each other. The magnitude of suppression was low, but still around 20% when stimuli were presented at short onset delays, and increased in magnitude when stimuli were presented at long onset delays. In general, both mirror and nonmirror stimulation resulted in the same trends; however, the effects on modulation magnitude were more pronounced when mirror locations were stimulated.

Discussion

The goal of this study was to quantify the contributions of spatial and temporal stimulus properties to the response properties of neurons in primary somatosensory cortex when tactile stimuli were applied to both hands. To address this goal, we recorded the activity of single neurons and multi-neuron clusters in owl monkeys using a 100-electrode array implanted in the left hemisphere of primary somatosensory cortex and presented stimuli on mirror and nonmirror locations on the hands with selected stimulus onset delays. Overall, stimulation on the two hands had weak effects on the latency of responses to contralateral stimuli (Table 5-2, Figure 5-5). However, the spatiotemporal

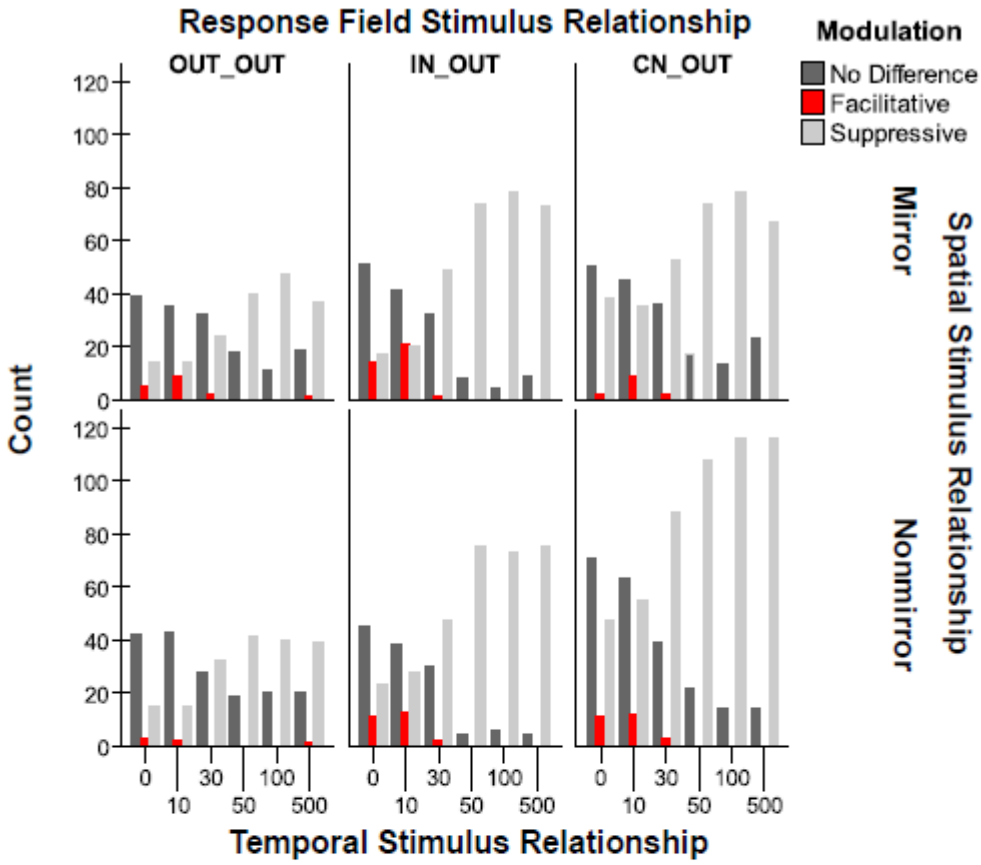

Figure 5-8. Suppression dominates observations of firing rate modulation across spatiotemporal stimulus conditions at longer stimulus onset asynchronies. Comparing the expected sum of the responses to ipsilateral and contralateral stimulation to the actual responses resulted in modulation categories of: "No Difference" compared to the response to the contralateral stimulus alone, "Facilitative" compared to the summation of the responses of the controls, and "Suppressive" compared to the response to the contralateral control. Shaded bars represent the modulation categories. The types of paired stimulation conditions are grouped on the x-axis referring to the stimulus onset delays from 0 to 500 ms, in which the contralateral stimulus was always presented after the ipsilateral stimulus. The row panels show the total counts of these categories for the two spatial stimulus proximity categories, "Mirror" and "Nonmirror". The column panels divide the data based on the Response Field category: "OUT_OUT", "IN_OUT", and "CN_OUT". As expected, we collected fewer responses to stimulation when both stimulation sites were outside the Response Field of the neuron, and the counts reflect this, but the trends were the same across the categories. Suppression dominated the modulation types, particularly at longer stimulus onset delays (50-500 ms); whereas many responses were classified as "no difference" for short stimulus onset delays (0-30 ms). Facilitation occurred rarely, but was predominantly found when the stimulus onset delays were short (0-30 ms).

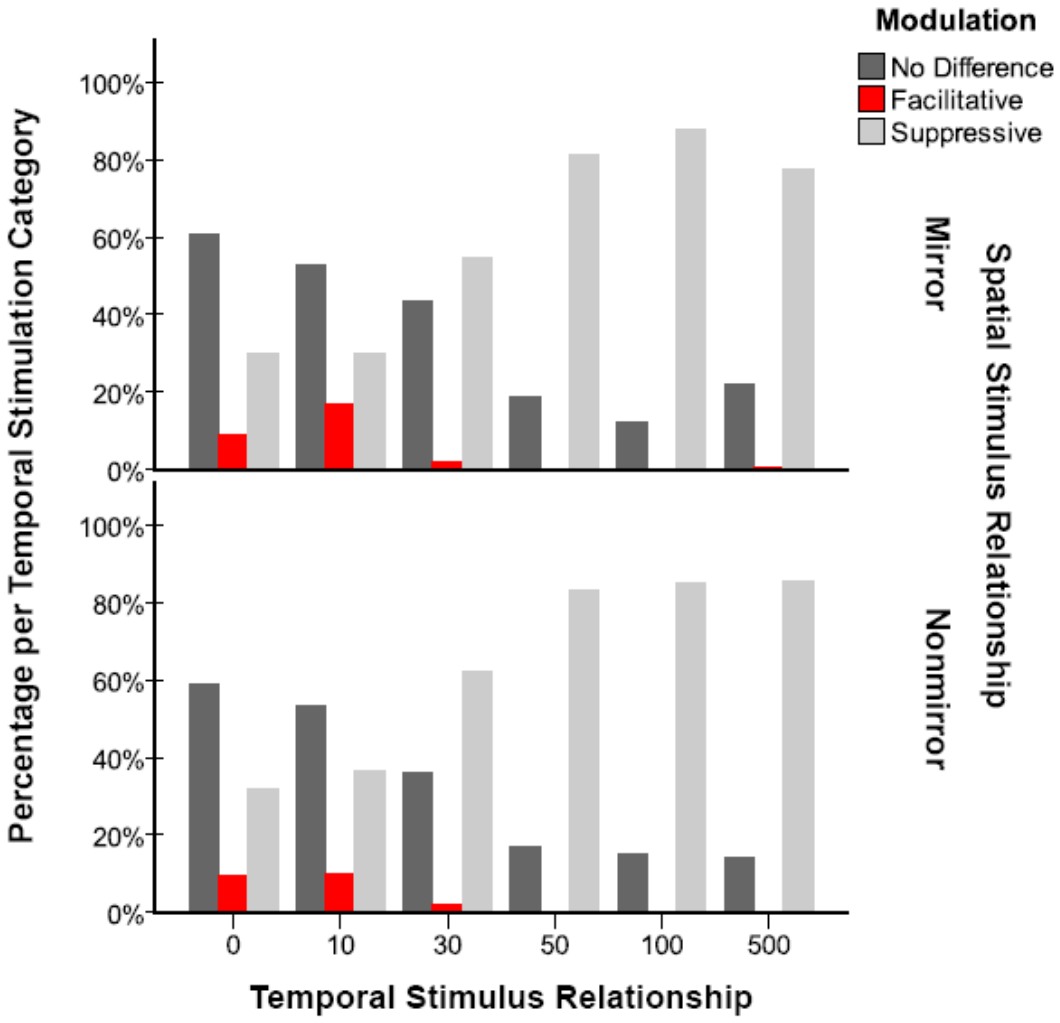

Figure 5-9. Percentage of responses per temporal stimulation category provides the proportions of responses which were facilitated, suppressed, or unchanged relative to the sum of the responses to ipsilateral and contralateral stimulation. These data are the same as those in Figure 5-8; however, instead of showing the counts of observations, the percentage of responses exhibiting each modulation type were calculated within each temporal stimulus relationship category on the x-axis. Additionally, the data were summarized across all of the Response Field relationships because similar trends were found across these categories. For stimulation on mirror and nonmirror locations, at short temporal stimulus asynchronies, fewer responses differed from the expected sum of the ipsilateral and contralateral responses. As the delay between stimulus onsets increased, the proportion of responses that were suppressed increased. The greatest proportion of responses were suppressed when the ipsilateral stimulus preceded the contralateral stimulus by 100 ms (88% of responses were suppressed during mirror stimulation, and 85% were suppressed during nonmirror stimulation). Facilitation was rare, but occurred primarily when the two hands were stimulated nearly simultaneously (17% of responses were facilitated when mirror locations were stimulated with the 10 ms onset delay, and 10% were facilitated when nonmirror locations were stimulated with the 10 ms onset delay).

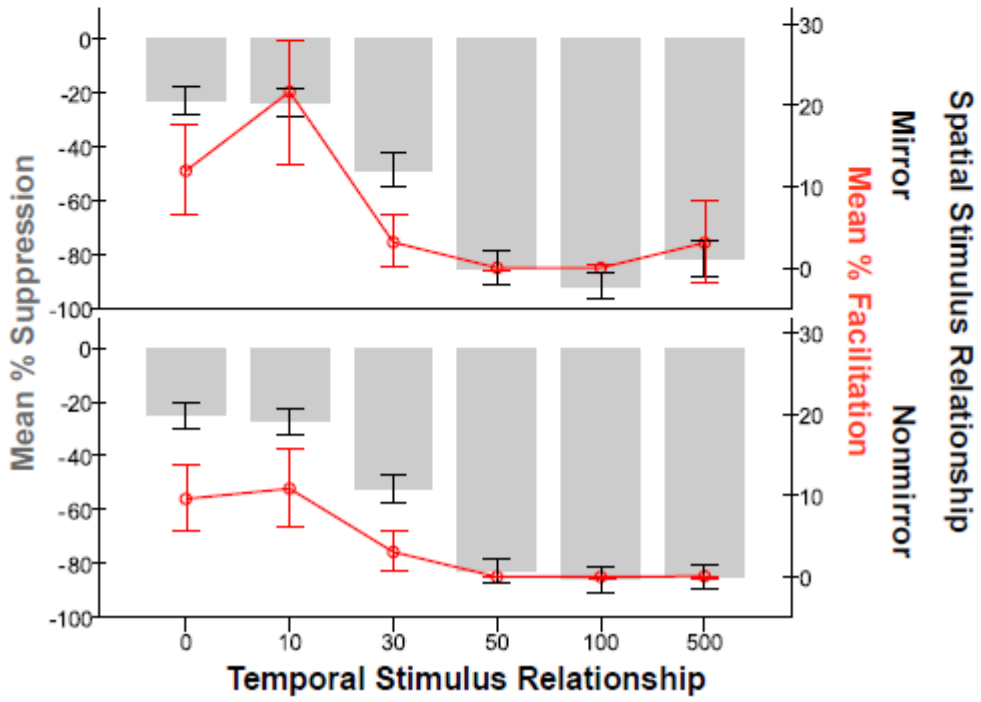

Figure 5-10. The percentage of facilitation and suppression was quantified to provide an index for how much the peak firing rates during paired stimulation differed from expected across the temporal stimulation conditions (x-axis). The values are collapsed across the Response Field categories, but separate panels show the effects for stimulation on Mirror locations and Nonmirror locations. The plots have dual y-axes such that the mean percentage of suppression in each category is shown by the gray bars and the values follow the left axis. The mean percentage of facilitation is shown by the red line and data markers and the values follow the right axis. Error bars are 95% confidence intervals. Using this index, when the response to paired stimulation does not differ from the contralateral response, the value is zero. The average percentages for suppression and facilitation include the zero values. The magnitude of facilitation dropped near zero when stimulus onsets were separated by 50–500 ms and hovered around a 10% difference when stimulus onsets were closer in time. The average magnitude of suppression was low when the stimulus onsets were close in time, and increased when the stimulus onsets were separated by longer delays. Responses were suppressed the most on average, by 92%, when mirror locations were stimulated with a 100 ms delay in stimulus onsets.

relationships of the bimanual stimuli significantly affected the peak firing rates in response to contralateral stimuli (Table 5-1, Figures 5-5, 5-8). Although SUs and MUs had significantly different estimated mean values for peak firing rate and latency, they appeared to behave similarly in response to the spatiotemporal stimulation conditions since the interaction factors in the statistical analysis were not significant (Tables 5-1, 5-2). In other words, the mean values of the peak firing rate differed between these groups, but when single units decreased in peak firing rate, multi-units decreased in peak firing rate as well. Since latency was little changed by the spatiotemporal stimulus properties, we discuss latency first, and then discuss the effects on measures of firing rate.

Response Latency Is Influenced Little by Bimanual Stimulation

The response latencies in our data set did not vary much with the spatiotemporal properties of bimanual stimulation (Figure 5-5). Although we found a statistical interaction between the temporal stimulus relationship and the spatial stimulus relationship ($P = 0.003$, Table 5-1), the latency differences were only about 1-2 ms, and thus were not convincing. While the main spatiotemporal effects analyzed in this study were not statistically convincing contributors to the variance in response latencies, we found a trend that response latencies were longer when the stimulus was located outside the Response Field of the neuron unit (Figure 5-5F). This result is consistent with the finding that latencies tend to increase (lengthen) when firing rates decrease (e.g., Boloori and Stanley, 2006), as peak firing rates were low when the stimulus was outside the Response Field (by definition). Both of these results correspond to our findings on the

effects of spatiotemporal bimanual stimulation parameters on firing rate (see next section on Peak Firing Rate).

Overall, the effects of bimanual stimulation on response latencies of area 3b neurons in primates have not been well-described. However, the effects of unilateral stimulation of the ipsilateral and contralateral hands alone have been described in area 3b neurons in macaque monkeys (Lipton et al., 2006). In current source density analysis of the field potentials, the onset latency of the ipsilateral response (mean ~ 23 ms) was longer than the contralateral response (mean ~ 6.4 ms) and the activity began in the extragranular layers rather than the granular layers. This suggests a feedback process is responsible for the cortical activity in response to ipsilateral median nerve stimulation. (Lipton et al., 2006) Our electrode recordings were taken only from the supragranular layers; however, we expect that our stimulation conditions would evoke laminar profiles similar to those found in macaque monkeys. There is evidence that findings in monkeys may be similar to findings in humans. In subsets of patients in evoked potential studies (Noachtar et al., 1997) and magnetoencephalography (MEG) studies (Zhu et al., 2007), ipsilateral primary somatosensory cortex responded to unilateral median nerve stimulation or tactile stimulation, and these ipsilateral responses occurred with longer latency than the contralateral responses (1.2-17.8 ms delay for evoked potentials, 3.5-24 ms delay for MEG signals). Rather than finding ipsilateral activation in subsets of human subjects, reliable detection (10/10 subjects) has been reported recently for evoked potentials in response to unilateral median nerve stimulation (Sutherland and Tang, 2006); thus, we do not expect that ipsilateral activation is found only in monkeys and subsets of humans. We did not observe significant changes in firing rate of neurons to

stimulation on the ipsilateral hand alone; therefore, we did not have latency values to compare between ipsilateral and contralateral stimulation alone. The responses to bimanual stimulation occurred after the ipsilateral information was integrated within the individual neurons, and our average response latency value was ~ was 24 ms (SD 6.91).

Although we did not find striking changes in response latency based on the spatiotemporal parameters of bimanual stimulation, these results provide new information regarding the response latency in area 3b neurons during bimanual stimulation and are consistent with hypothesis that the effects in area 3b are mediated by feedback connections with diffuse projection patterns (e.g., Cusick et al., 1989; Darian-Smith et al., 1993; Burton and Fabri, 1995; Burton et al., 1995; Angelucci et al., 2002; Shmuel et al., 2005), such that stimulation on mirror versus nonmirror locations does not have a large influence on the neuron response properties.

Peak Firing Rate Is Influenced by Bimanual Stimulation

As expected, firing rates were primarily suppressed by bimanual stimulation (Figure 5-5A, C). These results coincide with the predominance of suppressive modulation reported by others for primary somatosensory neurons in monkeys (Burton et al., 1998; Tommerdahl et al., 2006). We found the maximal suppression occurred when the ipsilateral stimulus preceded the contralateral stimulus onset by 100 ms (Figures 5-5A, 5-8). To our knowledge, similar studies using the same stimulus onset asynchronies have not been published. However, using similar stimulation parameters, Greek et al. (2003) found that stimulation on adjacent digits on the contralateral hand of raccoons resulted in maximum response suppression of primary somatosensory cortex neurons at

interstimulus intervals between 20-40 ms. Under our stimulation conditions, we have found that maximum response suppression occurs in area 3b of owl monkeys at interstimulus intervals between 30-50 ms (see Chapter 3). Thus, maximum response suppression for bimanual stimuli occurs at longer stimulus onset delays than for paired unilateral stimuli.

Burton et al. (1998) did not find strong effects of paired ipsilateral and contralateral vibratory stimulation on area 3b neurons in awake, behaving macaque monkeys; however, in area 2 and S2 they found primarily response suppression when an ipsilateral stimulus preceded the contralateral stimulus. The authors reasoned that the neurons they studied in areas 3b and 1 may not have received subthreshold input from the ipsilateral hand (Burton et al., 1998). In contrast, we found suppressive effects in area 3b of anesthetized monkeys receiving passive pulse indentation stimulation. There may be differences between macaque and owl monkeys or the neurons sampled to account for the differences between our current findings with those of Burton et al. (1998). Nevertheless, we do not find our results to be at odds with other studies. In fact, from their discussion it appeared that Burton et al. (1998) expected to find suppressive effects in area 3b: "And we might have seen onset order effects in anterior parts of S1 with even smaller receptive fields because in-field inhibition is also found in this part of S1 (Alloway and Burton, 1991). Failure to see stimulus order effects in all of the area 3b and most area 1 cells studied simply may be because none of these cells received even subthreshold excitatory drive from the ipsilateral hand."

Like Burton et al. (1998), Calford and Tweedale (1990) indicated that bimanual stimulation of single neurons in primary somatosensory cortex of macaque monkeys and

flying foxes resulted in no differences from contralateral stimulation alone. They did, however, find evidence that interhemispheric interactions do occur and were revealed when a digit ipsilateral to the recorded neurons was amputated or anesthetized (Calford and Tweedale, 1990, 1991a,b). While Calford and Tweedale (1990, 1991a,b) did not quantify changes in peristimulus time histograms, they did report that receptive field sizes of neurons contralateral to the amputated or anesthetized digit increased.

Our results of firing rate suppression in area 3b neurons during bimanual stimulation are consistent with imaging studies in squirrel monkeys (Tommerdahl et al., 2006). Using optical imaging of areas 3b and 1, Tommerdahl et al. (2006) found that simultaneous stimulation of the two hands resulted in suppression of the cortical activity compared to contralateral stimulation alone. Optical imaging revealed a small increase in activity in the contralateral cortex following stimulation of the ipsilateral hand alone that we did not observe in our extracellular recordings (Tommerdahl et al., 2006), and together these results are consistent with subthreshold activation of contralateral primary somatosensory cortex by ipsilateral input.

While the effects of bimanual stimulation have not been well-described for area 3b neurons in primates, our findings relate to studies by others of unilateral stimulation. In fMRI and field potential analyses in macaque monkeys, Lipton et al. (2006) found that electrical stimulation of the ipsilateral median nerve resulted in the expected excitatory contralateral response as well as an ipsilateral response dominated by inhibition. Similarly, in subsets of human subjects, Hlushchuk and Hari (2006) found negative BOLD responses during tactile stimulation of the ipsilateral hand. These examples

illustrate that ipsilateral input is expected to provide subthreshold input to the contralateral hemisphere that is mostly suppressive.

Suppression by the presence of an ipsilateral stimulus was not a universal effect in our study, as some responses were facilitated or unchanged relative to contralateral stimulation alone (Figures 5-8, 5-9). Many neurons showed no effect of bimanual stimulation, but a subset showed facilitation of response magnitudes, and when these facilitations occurred, they were at short stimulus onset delays (Figures 5-8, 5-9). Facilitative response modulation during bimanual stimulation was unexpected based on the reports by others (Burton et al., 1998; Tommerdahl et al., 2006); however, the proportion of facilitation was low (4%) and was likely revealed based on our large sample of simultaneous electrophysiological recordings and our spatiotemporal stimulation parameters (Figure 5-10).

The effects on firing rate were not very topographically specific within the hand representation (Figures 5-5B, 5-8), as may be expected for effects mediated by diffusely distributed feedback connections (e.g., Cusick et al., 1989; Darian-Smith et al., 1993; Burton and Fabri, 1995; Burton et al., 1995; Angelucci et al., 2002; Shmuel et al., 2005). However, the statistical analysis revealed spatiotemporal interactions such that the most firing rate suppression (92%) occurred when the ipsilateral stimulus preceded the contralateral stimulus by 100 ms, particularly when mirror locations were stimulated (Table 5-1, Figure 5-10). In their optical imaging studies, Tommerdahl et al. (2006) found no difference between stimulating on mirror and nonmirror hand locations simultaneously; however, stimulating the contralateral hand and ipsilateral foot simultaneously did not differ from stimulating the contralateral hand alone. Like

Tommerdahl et al. (2006), we did not find significant differences between simultaneous stimulation on mirror and nonmirror locations, and only when we stimulated the sites asynchronously did we uncover topographic specificity related to interhemispheric interactions.

Possible Significance

These results contribute to the understanding of spatiotemporal response properties that may relate to tactile discrimination and learning. As these studies were performed in anesthetized animals, the effects reflect the basic responses to passive stimulation without the influence of attention or task-relevance.

Suppression has roles in information transmission and is likely related to the "interference" effects revealed in psychophysical studies in humans. For example, Braun et al. (2005) found that suprathreshold stimuli applied to the left hand 200 or 500 ms before a near-threshold test stimulus on the right hand resulted in increased numbers of subject responses incorrectly identifying the location of the test stimulus. Thus, the presentation of the ipsilateral stimulus "interfered" with the ability of subjects to correctly localize the contralateral stimulus. Our findings that suprathreshold ipsilateral stimuli suppressed responses to suprathreshold contralateral stimuli in many neurons sampled from area 3b (~ 62% of the responses) correspond well with human psychophysical studies such as from Braun et al. (2005). However, human neurophysiological studies do not consistently find that primary somatosensory cortex is suppressed by bimanual stimulation. For example, in a magnetoencephalographic (MEG) study, Hoechstetter et al. (2001) stimulated the two hands simultaneously and found that significant suppressive

interactions occurred in secondary somatosensory cortex, but not primary somatosensory cortex. Disbrow et al. (2001) found no significant differences in the latency and magnitude of the MEG response between stimulation on one hand versus two hands for primary somatosensory cortex. The fact that we found substantial numbers of neurons that were not affected by bimanual stimulation (~ 34% of the responses) may relate in part to the reasons why human studies have not found suppressive interactions between bimanual stimulation in primary somatosensory cortex.

Our results indicate that an underlying perceptual bias exists when locations on the two hands are stimulated so that in most cases, the presence of the ipsilateral stimulus interferes with and suppresses the response to the contralateral stimulus. However, in order to successfully perceive tactile stimulation, some neurons should be unchanged or even facilitated by the presence of an ipsilateral stimulation, as we found. Training of a contralateral finger on tactile pressure discrimination has been shown to transfer to the mirror ipsilateral finger (as well as to the adjacent contralateral finger) in humans; thus, learning of some tactile discriminations on the hands has been shown to have topographical organization (Harris et al., 2001). Firing rate suppression due to bimanual stimulation does not appear to be the best mechanism to result in such learning transfer. Thus, the 4% of neuron responses in our sample which were facilitative may relate to the subset of neurons in primary somatosensory cortex that mediate the accurate perception of tactile stimuli presented to both hands and transfer of tactile learning.

Acknowledgements

Drs. Hui-Xin Qi, Zhiyi Zhou, Melanie Bernard, Mark J. Burish, A.B. Bonds, and Jon H. Kaas participated in these experiments or their design and will be co-authors on the published manuscript. Matlab scripts were written primarily by Dr. Pierre Pouget and John Haitas in collaboration with JLR and Jurnell Cockhren. Dr. Omar Gharbawie and Corrie Camalier helped collect data. This work was supported by the James S. McDonnell Foundation (JHK) and NIH grants NS16446 (JHK), F31-NS053231 (JLR), EY014680-03 (ABB), and T32-GM07347 (MJB).

References

Alenda A, Nuñez A. 2004. Sensory-interference in rat primary somatosensory cortical neurons. *Eur J Neurosci* 19: 766-770.

Alloway KD, Burton H. 1991. Differential effects of GABA and bicuculline on rapidly- and slowly-adapting neurons in primary somatosensory cortex of primates. *Exp Brain Res* 85: 598-610.

Alvarado JC, Vaughan JW, Stanford TR, Stein BE. 2007. Multisensory versus unisensory integration: contrasting modes in the superior colliculus. *J Neurophysiol* 97: 3193-3205.

Angelucci A, Levitt JB, Lund JS. 2002. Anatomical origins of the classical receptive field and modulatory surround field of single neurons in macaque visual cortical area V1. Chapter 29 In *Progress in Brain Research*, ed. EC Azmita, J DeFelipe, EG Jones, P Rakic, and CE Ribak, 136: 373-388. Amsterdam: Elsevier Science B.V.

Berwick J, Redgrave P, Jones M, Hewson-Stoate N, Martindale J, Johnston D, Mayhew JEW. 2004. Integration of neural responses originating from different regions of the cortical somatosensory map. *Brain Res* 1030: 284-293.

Blankenburg F, Ruff CC, Bestman Sven, Bjoertornt O, Eshel N, Josephs O, Weiskopf N,

Driver J. 2008. Interhemispheric effect of parietal TMS on somatosensory response confirmed directly with concurrent TMS-fMRI. *J Neurosci* 28: 13202-13208.

Boloori AR, Stanley GB. 2006. The dynamics of spatiotemporal response integration in the somatosensory cortex of the vibrissa system. *J Neurosci* 26: 3767-3782.

Braun C, Hess H, Burkhardt M, Wühle A, Preissl H. 2005. The right hand knows what the left hand is feeling. *Exp Brain Res* 162: 366-373.

Burton H, Fabri M. 1995. Ipsilateral intracortical connections of physiologically defined cutaneous representations in area 3b and 1 of macaque monkeys: projections in the vicinity of the central sulcus. *J Comp Neurol* 355: 508-538.

Burton H, Fabri M, Alloway K. 1995. Cortical areas within the lateral sulcus connected to cutaneous representations in areas 3b and 1: a revised interpretation of the second somatosensory area in macaque monkeys. *J Comp Neurol* 355: 539-562.

Burton H, Sinclair RJ, Whang K. 1998. Vibrotactile stimulus order effects in somatosensory cortical areas of rhesus monkeys. *Somatosens Mot Res* 15: 316-324.

Calford MB. 2002. Dynamic representational plasticity in sensory cortex. *Neuroscience* 111: 709-738.

Calford MB, Tweedale R. 1990. Interhemispheric transfer of plasticity in the cerebral cortex. *Science* 249: 805-807.

Calford MB, Tweedale R. 1991a. Acute changes in cutaneous receptive fields in primary somatosensory cortex after digit denervation in adult flying fox. *J Neurophysiol* 65: 178-187.

Calford MB, Tweedale R. 1991b. Immediate expansion of receptive fields of neurons in area 3b of macaque monkeys after digit denervation. *Somatosens Mot Res* 8: 249-260.

Conti F, Manzoni T. 1994. The neurotransmitters and postsynaptic action of callosally projecting neurons. *Behav Brain Res* 64: 37-53.

Cusick CG, Wall JT, Felleman DJ, Kaas JH. 1989. Somatotopic organization of the lateral sulcus of owl monkeys: area 3b, S-II, and a ventral somatosensory area. *J Comp Neurol* 282: 169-190.

Darian-Smith C, Darian-Smith I, Burman K, Ratcliffe N. 1993. Ipsilateral cortical projections to areas 3a, 3b, and 4 in the macaque monkey. *J Comp Neurol* 335: 200-213.

Davidson AG, O'Dell R, Chan V, Schieber MH. 2007. Comparing effects in spike-triggered averages of rectified EMG across different behaviors. *J Neurosci Methods* 163: 283-294.

Disbrow E, Roberts T, Poeppel D, Krubitzer L. 2001. Evidence for interhemispheric processing of inputs from the hands in human S2 and PV. *J Neurophysiol* 85: 2236-2244.

Greek KA, Chowdhury SA, Rasmusson DD. 2003. Interactions between inputs from adjacent digits in somatosensory thalamus and cortex of the raccoon. *Exp Brain Res* 151: 364-371.

Hansson T, Brismar T. 1999. Tactile stimulation of the hand causes bilateral cortical activation: a functional magnetic resonance study in humans. *Neurosci Lett* 271: 29-32.

Hardin JW, Hilbe JM. 2003. *Generalized estimating equations*. Boca Raton, FL: Chapman and Hall/CRC.

Harris JA, Harris IM, Diamond ME. 2001. The topography of tactile learning in humans. *J Neurosci* 21: 1056-1061.

Hoechstetter K, Rupp A, Stančák A, Meinck H-M, Stippich C, Berg P, Scherg M. 2001. Interaction of tactile input in the human primary and secondary somatosensory cortex—A magnetoencephalographic study. *Neuroimage* 14: 759-767.

Hlushchuk Y, Hari R. 2006. Transient suppression of ipsilateral primary somatosensory cortex during tactile finger stimulation. *J Neurosci* 26: 5819-5824.

Iwamura Y, Tanaka M, Iriki A, Taoka M, Toda T. 2002. Processing of tactile and kinesthetic signals from bilateral sides of the body in the postcentral gyrus of awake monkeys. *Behav Brain Res* 135: 185-190.

Iwamura Y, Tanaka M, Sakamoto M, Hikosaka O. 1983. Functional subdivisions representing different finger regions in area 3b or the first somatosensory cortex of the conscious monkey. *Exp Brain Res* 51: 315-326.

Jain N, Qi H-X, Kaas JH. 2001. Long-term chronic multichannel recordings from sensorimotor cortex and thalamus of primates. Chapter 5 In *Progress in Brain Research*, ed. MAL Nicolelis, 130: 1-10. Amsterdam: Elsevier Science B.V.

Kaas JH. 1983. What, if anything, is SI? Organization of first somatosensory area of cortex. *Physiol Rev* 63: 206-231.

Killackey HP, Gould HJ, III, Cusick CG, Pons TP, and Kaas JH. 1983. The relation of

corpus callosum connections to architectonic fields and body surface maps in sensorimotor cortex of new and old world monkeys. *J Comp Neurol* 219: 328-419.

Kurth R, Villringer K, Mackert B-M, Schwiemann J, Braun J, Curio G, Villringer A, Wolf K-J. 1998. fMRI assessment of somatotopy in human Brodmann area 3b by electrical finger stimulation. *Neuroreport* 9: 207-212.

Liang K-Y, Zeger SL. 1986. Longitudinal data analysis using generalized linear models. *Biometrika* 73: 13-22.

Lipton ML, Fu K-MG, Branch CA, Schroeder CE. 2006. Ipsilateral hand input to area 3b revealed by converging hemodynamic and electrophysiological analyses in macaque monkeys. *J Neurosci* 26: 180-185.

Mason A, Nicoll A, Stratford K. 1991. Synaptic transmission between individual pyramidal neurons of the rat visual cortex in vitro. *J Neurosci* 11: 72-84.

Merzenich MM, Kaas JH, Sur M, Lin CS. 1978. Double representations of the body surface within cytoarchitectonic areas 3b and 1 in "SI" in the owl monkey (*Aotus trivirgatus*). *J Comp Neurol* 181: 41-74.

Merzenich MM, Kaas JH, Wall J, Nelson RJ, Sur M, and Felleman D. 1983. Topographic reorganization of somatosensory cortical areas 3b and 1 in adult monkeys following restricted deafferentation. *Neuroscience* 8: 33-55.

Moore CI, Nelson SB. 1998. Spatio-temporal subthreshold receptive fields in the vibrissa representation of rat primary somatosensory cortex. *J Neurophysiol* 80: 2882-2892.

Mountcastle VB, Powell TPS. 1959. Neural mechanisms subserving cutaneous sensibility, with special reference to the role of afferent inhibition in sensory perception and discrimination. *Bull Johns Hopkins Hosp* 105: 201-232.

Nelson RJ, Sur M, Felleman DJ, Kaas JH. 1980. Representations of the body surface in postcentral parietal cortex of *Macaca fascicularis*. *J Comp Neurol* 192: 611-643.

Nicolelis MAL, Dimitrov D, Carmena JM, Crist R, Lehew G, Kralik JD, Wise SP. 2003. Chronic, multisite, multielectrode recordings in macaque monkeys. *Proc Natl Acad Sci USA* 100: 11041-11046.

Noachtar S, Lüders HO, Dinner DS, Klem G. 1997. Ipsilateral median somatosensory evoked potentials recorded from human somatosensory cortex. *Electroencephalogr Clin Neurophysiol* 104: 189-198.

Ogawa S, Lee T-M, Stepnoski R, Chen W, Zhu X-H, Ugurbil K. 2000. An approach to

probe some neural systems interaction by functional MRI at neural time scale down to milliseconds. *Proc Natl Acad Sci USA* 97: 11026-11031.

Reed JL, Pouget P, Qi H-X, Zhou Z, Bernard MR, Burish MJ, Haitas J, Bonds AB, Kaas JH. 2008. Widespread spatial integration in primary somatosensory cortex. *Proc Natl Acad Sci USA* 105: 10233-10237.

Rema V, Ebner FF. 2003. Lesions of mature barrel field cortex interfere with sensory processing and plasticity in connected areas of the contralateral hemisphere. *J Neurosci* 23: 10378-10387.

Samonds JM, Allison JD, Brown HA, Bonds AB. 2003. Cooperation between area 17 neuron pairs enhances fine discrimination of orientation. *J Neurosci* 23: 2416-2425.

Schnitzler A, Salmelin R, Salenius S, Jousmäki V, Hari R. 1995. Tactile information from the human hand reaches the ipsilateral primary somatosensory cortex. *Neurosci Lett* 200: 25-28.

Shin H-C, Won C-K, Jung S-C, Oh S, Park S, Sohn J-H. 1997. Interhemispheric modulation of sensory transmission in the primary somatosensory cortex of rats. *Neuroscience Letters* 230: 137-139.

Shmuel A, Korman M, Sterkin A, Harel M, Ullman A, Malach R, Grinvald A. 2005. Retinotopic axis specificity and selective clustering of feedback projections from V2 to V1 in the owl monkey. *J Neurosci* 25: 2117-2131.

Shoham S, Fellows MR, Normann RA. 2003. Robust, automatic spike sorting using mixtures of multivariate t-distributions. *J Neurosci Methods* 127: 111-122.

Shuler MG, Krupa DJ, Nicolelis MAL. 2001. Bilateral integration of whisker information in the primary somatosensory cortex of rats. *J Neurosci* 21: 5251-5261.

Stanford TR, Quessy S, Stein BE. 2005. Evaluating the operations underlying multisensory integration in the cat superior colliculus. *J Neurosci* 25: 6499-6508.

Sur M. 1980. Receptive fields of neurons in areas 3b and 1 of somatosensory cortex in monkeys. *Brain Res* 198: 465-471.

Sur M, Wall, JT, Kaas JH. 1984. Modular distribution of neurons with slowly adapting and rapidly adapting responses in area 3b of somatosensory cortex in monkeys. *J Neurophysiol* 51: 724-744.

Sutherland MT, Tang AC. 2006. Reliable detection of bilateral activation in human primary somatosensory cortex by unilateral median nerve stimulation. *Neuroimage* 33: 1042-1054.

Tanosaki M, Suzuki A, Takino R, Kimura T, Iguchi Y, Kurobe Y, Haruta Y, Hoshi Y, Hashimoto I. 2002. Neural mechanisms for generation of tactile interference effects on somatosensory evoked magnetic fields in humans. *Clin Neurophysiol* 113: 672-680.

Tommerdahl M, Simons SB, Chiu JS, Favorov O, Whitsel BL. 2006. Ipsilateral input modifies the primary somatosensory cortex response to contralateral skin flutter. *J Neurosci* 26: 5970-5977.

Tuerlinckx F, Rijmen F, Verbeke G, De Boeck P. 2006. Statistical inference in generalized linear mixed models: A review. *Br J Math Stat Psychol* 59: 225-255.

Tutunculer B, Foffani G, Himes BT, Moxon KA. 2006. Structure of the excitatory receptive fields of infragranular forelimb neurons in the rate primary somatosensory cortex responding to touch. *Cereb Cortex* 16: 791-810.

Veredas FJ, Vico FJ, Alonso JM. 2005. Factors determining the precision of the correlated firing generated by a monosynaptic connection in the cat visual pathway. *J Physiol* 567.3: 1057-1078.

Zeger SL, Liang K-Y. 1986. Longitudinal data analysis for discrete and continuous outcomes. *Biometrics* 42: 121-130.

Zhu Z, Disbrow EA, Zumer JM, McGonigle DJ, Nagarajan SS. 2007. Spatiotemporal integration of tactile information in human somatosensory cortex. *BMC Neurosci* 14: 8-21.

CHAPTER VI

DIGITAL NERVE BLOCK ON ONE HAND AFFECTS RESPONSES TO STIMULATION ON THE OPPOSITE HAND IN OWL MONKEY PRIMARY SOMATOSENSORY CORTEX NEURONS

Abstract

When a single finger is anesthetized with local anesthetic, humans perceive increases in the size of that digit, and neurons recorded from primary somatosensory cortex of non-human primates expand their receptive field sizes associated with that digit. Additionally, receptive field sizes of neurons recorded in the cortex ipsilateral to the anesthetized digit expand. We focused on quantifying interhemispheric interactions in area 3b (primary somatosensory cortex) that correspond to these receptive field expansions. To accomplish this goal, we implanted a 100-electrode array in the left hemisphere of three owl monkeys to record neuron response magnitudes and latencies to stimulation on the right hand before and after blocking the nerves from one digit on the left hand with local anesthetic. We sought to determine how the location of the contralateral stimulus affected the neuron responses after the ipsilateral digit block. We expected that locations that were outside the neuron's receptive field before the digit block might respond to stimulation after the block, and neurons with receptive fields on the contralateral digit that matched the anesthetized digit might show facilitated responses to stimulation. The changes we found in peak firing rates and latencies were complementary, but did not precisely match these expectations, as stimulation did not

result in overall peak firing rate increases that we expected based on receptive field expansion. Thus, the electrophysiological responses are more complex than the homogeneous effect of receptive field expansion suggests. These quantitative results reveal both the heterogeneity of responses in primate area 3b and the relationship of the response types to the spatial location of the stimulation.

Introduction

Temporary digit denervations by local anesthetic injections induce short-term plasticity in primary somatosensory cortex and reveal sources of input to a region that are normally suppressed. Several studies on this phenomenon have been conducted to characterize changes in receptive field sizes in animal subjects (e.g., Calford and Tweedale, 1990, 1991a,b) and changes in perception (e.g., Gandevia and Phegan, 1999; Werhahn et al., 2002) or cortical activity (e.g., Werhahn et al., 2002; Waberski et al., 2003, 2007) in humans. Studies by Calford and Tweedale (e.g., 1990, 1991a,b) reported that within a few minutes after a single digit is denervated by local anesthetic injections (or amputation in some studies), receptive fields of neurons representing that digit in the contralateral primary somatosensory cortex expand. In addition, receptive fields of neurons representing that digit (on the opposite hand) in the ipsilateral primary somatosensory cortex expand. The results of these denervation studies indicate that neuron responses are influenced by the spontaneous activity of neurons with receptive fields outside the recorded neuron's receptive field, even across the hemispheres. These interhemispheric effects were particularly surprising because while bilateral receptive

fields have been reported for higher somatosensory areas (for review, Iwamura, 2002), none have been reported for the 3b hand area (for review, Kaas, 1983); and area 3b has few to no callosal connections between the hand representations (Killackey et al., 1983). These studies did not characterize neuron response properties beyond mapping the receptive fields of neurons and did not completely describe the effects of denervation on heterotopic digits (i.e., when digit 1 was denervated, neurons which originally responded to contralateral or ipsilateral digit 1 and some neighboring skin sites were mapped). Therefore, in the current study we focused on quantifying the neuronal response properties of firing rate and latency rather than receptive field mapping, and we stimulated matching (homotopic) digits and nonmatching (heterotopic) sites relative to the injected digit.

To focus our efforts on quantifying the surprising interhemispheric effects, we blocked input from one digit and characterized the changes in responses to stimulation on the opposite hand in owl monkeys. Our aim was to reduce some of the spontaneous activity from the opposite hand to deduce the effects of normal levels of spontaneous activity and quantify the changes in neuron response properties, rather than to repeat studies which characterized receptive fields. One aspect missing from previous studies is an analysis of the spatial topography of the interhemispheric effects and the response property changes due to the location of the stimulus relative to the receptive field of the neuron. Since the presence of expanded receptive fields on the opposite hand suggests that tonic interhemispheric inhibition was removed after denervation (e.g., Calford and Tweedale, 1990, 1991a,b; Calford, 2002), we predicted that response properties of neurons in area 3b would reflect this disinhibition by increasing peak firing rate and

possibly shortening response latency. Some neurons that did not respond to stimulation at a particular location before denervation should respond to stimulation after denervation, if receptive field expansion corresponds to disinhibiting latent inputs to cortical neurons. In order to test these predictions, we measured neuron activity before and after a local anesthetic block of input from the ipsilateral hand to determine if neurons become more or less responsive to stimulation on the contralateral hand. Additionally, we sought to determine if the effects of local anesthetic blocking were specific to matched sites on the two hands or if the effects occurred diffusely across the hand representation. Since the area 3b hand representation receives few callosal projections from the homotopic area, feedback projections that area 3b receives from higher order somatosensory areas that do have callosal projections likely mediate some of the interhemispheric effects (Calford, 2002, review). Feedback projections are somewhat diffusely somatotopically organized (e.g., Cusick et al., 1989; Darian-Smith et al., 1993; Burton and Fabri, 1995; Burton et al., 1995); therefore, the effects on neuron response properties may reflect such somatotopy. We also expected some variability in the response properties that may relate to the location of the stimulus inside or outside the receptive field of the neuron.

Materials and Methods

Three adult owl monkeys (*Aotus trivirgatus*), weighing between 1-1.5 kg, were subjects in these experiments. One of these monkeys (case 3, female, 1.2 kg) was used in studies related to normal tactile processing without local anesthetic injections (Chapters 3 and 4). After beginning the experiment in case 5 (male, 1 kg), we discovered the distal

part of right digit 3 had been damaged (in an incident that was not included in medical records and must have occurred several years prior). This animal was wild-caught by another facility and the full medical history was unknown. The results of the experiment in case 5 are included as a comparison with the results from case 3 and case 4 (female, 1.5 kg). Results from case 5 can be considered a case study on the effects of acute deafferentation of an ipsilateral digit following chronic deafferentation of part of a contralateral digit.

Preparation

All procedures followed the guidelines established by the National Institutes of Health and the Animal Care and Use Committee at Vanderbilt University. Owl monkeys were prepared for electrophysiological recordings in the left hemisphere of primary somatosensory cortex as described previously (Reed et al., 2008). To briefly summarize, monkeys were anesthetized with propofol during surgery (10 mg/kg/hr, intravenous) and electrophysiological recording (0.3 mg/kg/hr). Monkeys were paralyzed with vecuronium bromide (0.1-0.3 mg/kg/hr, intravenous) mixed with 5% dextrose and Lactated Ringer's solution and were artificially ventilated with a mixture of N2O: O2: CO2 (75: 23.5: 1.5) at a rate sufficient to maintain peak end tidal CO2 at ~ 4%. For monkey 3 only, 1.2 mg/kg sufentanil was added to the Lactated Ringer's solution during the surgical procedures in order to stabilize anesthetic depth. Following delivery of this amount of sufentanil, the monkey was maintained under anesthesia without supplemental sufentanil during recording experiments. The 100-electrode array (Blackrock Microsystems, Salt Lake City, UT) was inserted to a depth of 600 μm using a pneumatic inserter so that the

electrode tips were expected to be located within layer 3 of the left hemisphere of anterior parietal cortex.

Local Bupivacaine Injections

We administered local anesthetic, 0.25% bupivacaine hydrochloride, from here on referred to as bupivacaine, to a single digit ipsilateral to the recording electrodes in each monkey. In case 5 we administered 0.1 cc to each side of the base of the digit (digit 5). In cases 3 and 4, we administered 0.05 cc to each side of the base of the digit (digits 4 and 5, respectively). The total volumes of 0.25% bupivacaine (0.1 and 0.2 mL) we used for digital nerve block in owl monkeys were adapted from values commonly used in humans (~0.03 mg/kg). In each monkey, only one digit was injected with bupivacaine and the responses to stimulation before and after bupivacaine injection were recorded in one day. Other studies exploring the effects of local anesthesia on receptive field size used lidocaine rather than bupivacaine (e.g., Calford and Tweedale, 1990, 1991a,b). A recent study (Alhelail et al., 2009) comparing bupivacaine (0.5%) and lidocaine (1%) with epinephrine for digital nerve blocks in humans confirmed that the duration of anesthesia induced by bupivacaine tends to be longer than that induced by lidocaine (median = 701 min and 321 min, respectively; $P < 0.05$). We chose bupivacaine for its longer duration of action compared to lidocaine. Alhelail et al. (2009) also found no difference in the onset of anesthesia (tested by pin pricks) between bupivacaine (median = 3.30 min) and lidocaine with epinephrine (median = 3.45 min; $P = 0.84$). Additionally, digital injections of 0.25% bupivacaine induced local anesthesia within the same period of time as a 1:1 mixture of 1% lidocaine and 0.25% bupivacaine (Valvano and Leffler, 1996); therefore,

we do not expect that our use of bupivacaine resulted in qualitatively different effects from the use of lidocaine in other studies beyond the increased duration of anesthesia.

We emulated traditional digital block methods used in patients (for brief review, Scarff and Scarff, 2007). When properly performed, pin prick tests confirm that the entire digit becomes anesthetized following this procedure. While we had no confirmation of the anesthetic effect from our owl monkey subjects, we inferred the onset and approximate duration of the neural effects based on receptive field mapping. Recordings of neuron responses to mechanical stimulation were made beginning a few minutes after bupivacaine injection and continued until the effects of the bupivacaine appeared to wane (~2.5-6 hours) based on receptive field mapping of a selected electrode channel.

Tactile Stimulation and Recording Procedures

Our equipment and stimulus parameters have been described previously (Reed et al., 2008; Chapter 3). Briefly, stimuli were provided by two independent force- and position-feedback controlled motor systems (300B, Aurora Scientific Inc., Aurora, ON, CA), with contact made by round Teflon probes 1 mm in diameter. Stimuli consisted of pulses that indented the skin 0.5 mm for 0.5 s, followed by 2.0 s off of the skin, repeated for at least 255 s (100 trials). In one owl monkey, case 4, the stimuli were delivered using a Chubbuck stimulator (Chubbuck, 1966) with a 1 mm diameter probe (because the primary stimulator was undergoing hardware servicing). Stimuli were applied before and after injecting bupivacaine into one digit on the left (ipsilateral) hand while recordings were made from the left hemisphere. The fingernails were glued (cyanoacrylic) to Teflon screws fixed in plasticine to keep the hand stable during stimulus blocks. We marked

stimulus locations on the skin with permanent marker as well as on a drawing of the hand in order to place the stimulus probe as close as possible to the same locations before and after bupivacaine injections. Recordings after bupivacaine began after receptive field mapping of a selected electrode channel revealed receptive field expansion. This occurred within the first 7-20 minutes after bupivacaine injection. All of the recordings after bupivacaine included in the analysis were made before the receptive mapping of the selected channel indicated that the receptive field size had returned to the original size before bupivacaine injection. For both cases 4 and 5, all recordings included in the analysis were made within 2.5 hours after bupivacaine injection. For case 3, most of the recordings were made within 2.5 hours, but 3 recordings were made up to 4.5 hours after the bupivacaine injection.

In addition to controlled stimulation, we manually applied light tactile stimulation to map the minimal receptive fields (mRFs) of selected electrodes. As we have previously described (Reed et al., 2008), the mRF was defined as the region of skin where a near-threshold light touch with a probe reliably evoked spikes from the recorded neurons. We followed typical procedures for mRF mapping (e.g., Merzenich et al., 1978; Nelson et al., 1980). We determined mRFs for each responsive electrode in the array at least one time during the experiment. We then focused on selected electrodes to map before and after bupivacaine injection. Mapping mRFs served two purposes: 1) to indicate the effect of local anesthetic by receptive field expansion and 2) to aid our reconstruction of the electrode locations as within and outside of area 3b.

We used the 100-electrode array and the Bionics Data Acquisition System (now Blackrock Microsystems, Salt Lake City, UT) to record signals from single neurons and

multi-neuron clusters. The signals on each channel were amplified by 5000 and band-pass filtered between 250 Hz and 7.5 kHz. The threshold for each electrode was automatically set for 3.25 times the mean activity and the waveforms were sampled at 30 kHz for 1.5 ms windows (Samonds et al., 2003).

Histology

Upon experiment completion, animals were perfused with saline followed by fixative, and the brains were prepared for histological analysis as previously described (Jain et al., 2001). The cortex was flattened, frozen, and cut parallel to the surface at 40 μm. Sections were processed for myelin to aid in determining the electrode locations relative to the area 3b hand representation (see Reed et al., 2008), along with minimal receptive field maps.

Data Analysis

Spike Sorting

The details of the spike sorting procedures have been described previously (Reed et al., 2008). To summarize briefly, spike signals were sorted offline with an automatic spike classification program (Shoham et al., 2003) which is part of the data acquisition system. We used a second spike sorter program, Plexon Offline Sorter (Plexon Inc., Dallas, TX), to verify the quality of unit isolation such that single units had refractory periods ≥ 1.2 ms; P values ≤ 0.05 for multivariate ANOVA related to cluster separation; and distinct waveform amplitudes and shapes when compared with other activity on the

same electrode (Nicolelis et al., 2003). Single- and multi-units were categorized separately but grouped together for factor analysis in the statistical model. Multiple single units collected from one electrode were included in the analysis, but at most only one multi-unit per electrode was included in the analysis.

Peak Firing Rate

As described in Reed et al. (2008), spike trains were smoothed with a spike density function using Matlab (The Mathworks, Inc., Natick, MA) before peak firing rate was determined. A spike density function was produced by convolving the spike train from each trial with a function resembling a postsynaptic potential specified by τg, the time constant for the growth phase, and τd, the time constant for the decay phase as: $R(t) = (1 - \exp(-t/\tau d)*\exp(-t/\tau d)$.

Based on physiological data from excitatory synapses, τg was set to 1 ms (e.g., Mason et al., 1991; Moore and Nelson, 1998). We set τd to 5 ms (Mason et al., 1991; Moore and Nelson, 1998; Veredas et al., 2005) because the transient nature of the on and off responses in primary somatosensory neurons was excessively smoothed at larger values. We examined onset responses within a 50 ms window from the stimulus onset.

The excitatory peak firing rate was determined as the maximum of the spike density function within the 50 ms response time window, and the average baseline firing rate (calculated over a 500 ms window prior to stimulation onset) was subtracted from this value. This peak firing rate value was required to be greater than a threshold value, which was the average baseline firing rate plus two standard deviations of this baseline, with a minimum value of 5 spikes/s. To determine if this value was significant, the

nonparametric Mann-Whitney U test and the parametric Student's t-test were performed and results compared. The U test and t test resulted in the same categorizations of significance ($\alpha = 0.05$). When no excitatory response was detected in the response window, responses were examined for possible suppressive effects. Suppressive responses had average firing rates less than the average baseline firing rate by at least 1.65 times below the standard deviation of the baseline, and this low firing had to be sustained for 10 ms or longer.

Response Latency

We calculated response latencies from spike density function histograms as the initial time when the firing rate meets the half-height over the threshold value of the peak firing rate within the response time window (see *Peak Firing Rate*). Briefly, the peak latency was calculated using polynomial fitting of the spike density function in Matlab to determine the time of the greater of the half-height or the threshold value (see Chapters 3 and 4). This method of determining excitatory response latency is similar to measures that determine the width or duration of peaks in histograms (e.g., Davidson et al., 2007). Suppressive response latencies were not included in the statistical analysis. Results were checked manually for proper assignments.

Response Field

Receptive field mapping across the 100-electrode array takes time, and we needed a quick measure of how the stimulus location related to the receptive fields of each neuron across the recording time. We defined excitatory "Response Fields" based on the

neuron unit firing rates in response to above-threshold skin indentations with our stimulus probes. Thus, the Response Field is a firing-rate-based estimate similar to the concept of the receptive field measured by suprathreshold stimulation. When a single site on the hand was stimulated, that site was classified as *inside* that unit's excitatory Response Field if the peak firing rate after subtracting the average baseline firing rate was greater than or equal to 3 times the standard deviation of the average firing rate for the population of neurons recorded from the 100-electrode array. For a given neuron, responses for all of the locations that were stimulated for a given experiment were compared. The maximum value for firing rate was found, and that stimulation location was designated as in the *center* of that unit's Response Field. When the unit firing rate did not meet the criteria to be categorized as *inside*, the location was considered to be *outside* of the Response Field.

Data Classification

Data were classified based on several conditions that were used in a statistical model to estimate the contributions of those factors to the observed response properties. These factors were the 1) the recording period before (pre) or after (post) the local bupivacaine injection; 2) the spatial relationship of the contralateral stimulus to the ipsilateral injection site (match or non-match); 3) the relationship of the neuron's Response Field to the stimuli (out, in, or center); 4) the quality of the signal isolation into single units (SUs) or multi-units (MUs); and 5) the identity of the monkey case from which the neurons were recorded (case 3, 4, or 5).

Summary Analysis

The values we obtained for excitatory peak firing rates and latencies from Matlab were summarized in Excel and imported into SPSS 17.0 (SPSS, Inc., Chicago, IL) for further analysis, along with the associated classifications (described above). Although we included one measure before bupivacaine injection and one measure after bupivacaine injection, we did not perform a nonparametric 2-sample test (like the Wilcoxon signed rank test) because we wanted to assess the contributions of the selected factors to the variance in the firing rates and latencies. Two measures, one before bupivacaine and one after bupivacaine injection, were selected for each stimulation location since not all locations were stimulated more than once before the apparent effects of bupivacaine ended in each monkey. All of the recordings included in the analysis were made before the receptive field sizes of selected channels had returned to their original sizes; therefore, the time after injection was not included as a variable in this analysis.

We employed Generalized Estimating Equations (e.g., Liang and Zeger, 1986; Zeger and Liang, 1986) in SPSS to analyze this complex dataset, using the normal distribution with the identity link function and a first-order autoregressive correlation matrix structure (e.g., Hardin and Hilbe, 2003, p. 66) for repeated measures on each neuron observation. See Appendix A for detailed information regarding Generalized Estimating Equations. Thus, in these models, latency or firing rate acted as the dependent variable and the predictor variables included: the bupivacaine injection period (pre or post), the spatial relationship of the stimulus to the injected digit (matched or non-matched), the relationship of the stimulus to the Response Field of the neuron unit (out, in, or center), and the classification of the unit as a single- or muli-unit, and the monkey

case. We first examined the data for each monkey separately since we knew that monkey 5 could potentially have different results from the other two monkeys due to the unreported injury. Including the data from monkey 5 in the statistical analysis prevented the Generalized Estimating Equations routine from reaching convergence to fit the data. Thus, we included only the data from monkeys 3 and 4 in our statistical analysis to examine the normal effects on contralateral area 3b neurons of anesthetizing an ipsilateral digit. Similarly, selecting the alternative distribution and link function for continuously distributed data, namely the gamma distribution with the log link function, to analyze these data prevented the model from converging on a solution. Therefore, we did not employ the comparison of goodness-of-fit statistics between solutions based on the normal distribution and the gamma distribution described in Appendix A. The data from latency measures resembled the normal distribution; however, data from firing rate measures were skewed due to the presence of unresponsive neurons which were assigned values of 0 spikes/s for peak firing rate responses. The analysis only used neurons which had non-zero values before and after bupivacaine administration; thus, the data used in the statistical analysis resembled the normal distribution.

We performed the Generalized Estimating Equations analysis for the full factorial model, and then performed subsequent modeling analyses to select the combination of main effects and interactions that best represented the hypothesis and the data (based on model goodness-of–fit statistics). The criterion for statistical significance of all tests was alpha = 0.05. The Bonferroni correction for multiple comparisons was applied. The Generalized Estimating Equations analysis provides estimates of the population averages

of the dependent variable (peak firing rate and response latency) based on the values of the predictor variables and estimates the significance of the effects.

Results

We recorded single- (SUs) and mult-units (MUs) from a 100-electrode array implanted in cortical layer 3 of the left anterior parietal cortex of three owl monkeys. Recordings were made mostly from area 3b of each owl monkey, as depicted in Figure 6-1. Since the array placements varied somewhat in each owl monkey, we tallied the numbers of electrodes that were likely located in area 3b and in area 3a. The proportions of electrodes located in area 3b were similar in each case: Case 3 = 68 electrodes in 3b, 32 electrodes in 3a; Case 4 = 62 electrodes in 3b, 38 in 3a; Case 5 = 66 in 3b, 34 in 3a. The recordings after bupivacaine injections that were included in the analysis were made after minimal receptive field mapping revealed that receptive fields of selected electrodes had expanded, as shown in Figure 6-2, indicating that the local anesthetic had taken effect to expand receptive field sizes (e.g., Calford and Tweedale, 1990, 1991a,b). As mentioned, we discovered that monkey 5 had been recovered from an injury to the right distal digit 3 (see Figure 6-1D). Due to the possibility of plasticity in the somatosensory hand representation following injury, data were summarized from monkeys 3 and 4 for statistical analysis, while the data from monkey 5 was separated and compared with data from monkeys 3 and 4. In fact, including the data from monkey 5 in the statistical analysis prevented the modeling routine from fitting the data; therefore, data from monkey 5 were omitted from the final statistical models and were considered separately.

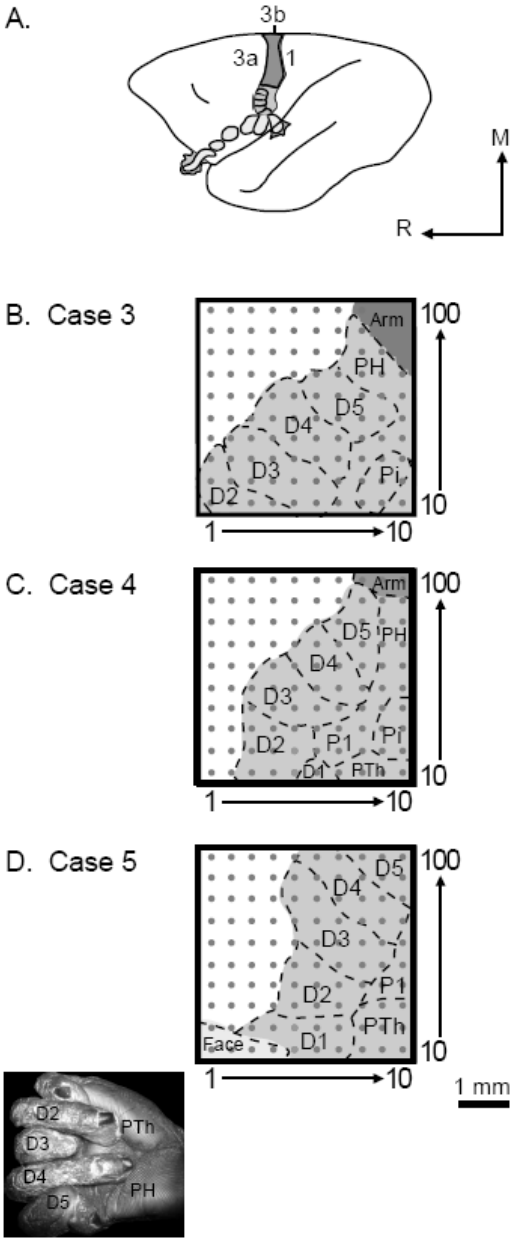

Figure 6-1. Schematic reconstructions of 100-electrode array placement in primary somatosensory cortex of three owl monkey cases. A. Area 3b is highlighted in a schematic of the owl monkey brain. Areas 3a and 1 flank 3b, but neurons in these areas tend not to respond well to light tactile stimulation under the general anesthetic conditions of these experiments. The brain orientation is indicated by arrows. M = medial, R = rostral. B-C. The placements of the 100-electrode array in monkeys 3 and 4 covered much of the area 3b hand representation but excluded part or all of digit 1 (D1) and part of the palm. D. The placement of the 100-electrode array in case 5 included most of the digit representations, but excluded part of digit 5 and part of the palm. Inset is a post-mortem photograph of the right hand in case 5, revealing the abnormal digit 3. In all cases, electrode locations were approximated based on examination of myelin-stained sections of flattened cortex and the results of receptive field mapping during recording experiments to estimate the digit and palm pad representations in area 3b. The scale bar refers to the electrode schematics, as electrodes were spaced 0.4 mm apart.

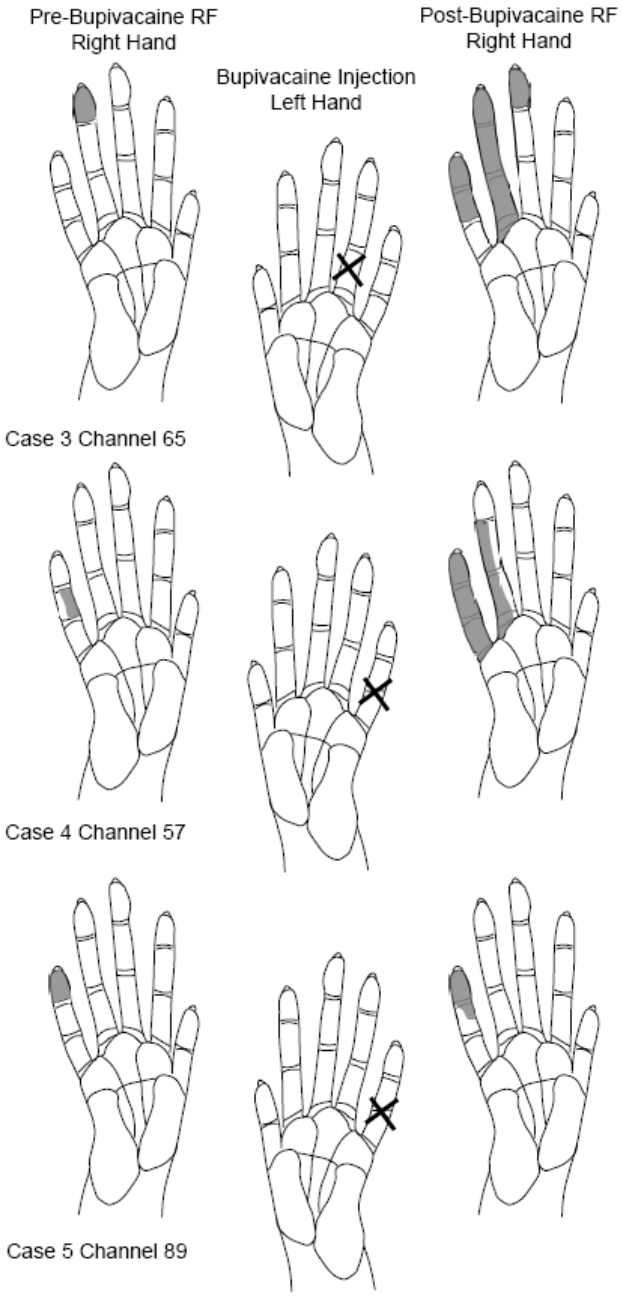

Figure 6-2. Sample receptive field maps before and after bupivacaine injection in one digit of the ipsilateral (left) hand from three different owl monkeys. Left. Minimal receptive fields (mRFs) were mapped for a selected electrode channel from each of the three monkeys. Middle. Bupivacaine was injected into each side of the base of the digit indicated with an "X". Right. Between 5-20 minutes after bupivacaine injection, mRFs were mapped again for the same channels, revealing some expansion consistent with previous studies (Calford and Tweedale, 1990, 1991a,b).

Across all recordings, we obtained single- and multi-unit activity in response to contralateral stimulation before and after bupivacaine injection in an ipsilateral digit: from case 3 we obtained 490 SU response pairs and 401 MU response pairs; from case 4 we obtained 667 SU response pairs and 440 MU response pairs; and from case 5 we obtained 305 SU response pairs and 394 MU response pairs. Not all of these responses before and after bupivacaine injection were significantly greater than baseline firing rates; therefore, from case 3 we analyzed 120 SUs and 127 MUs; from case 4 we analyzed 80 SUs and 49 MUs; and from case 5 we analyzed 21 SUs and 38 MUs. (Fewer responsive electrodes were found in case 5, and this case was used as a comparison due to the digit injury.) Only units that responded with firing rates significantly greater than baseline firing before and after bupivacaine injection could be analyzed using the statistical models; therefore, we tallied the numbers of units that did not respond significantly as well in order to determine the overall responsiveness that may not be reflected in the statistical analysis.

From case 3, 38% (339/891) of the units recorded did not show an excitatory response to stimulation before and after bupivacaine injection; and 5 of these units were inhibited before and after bupivacaine, 3 were inhibited before bupivacaine but showed no excitatory or inhibitory response after injection, and 3 showed no response before bupivacaine but were inhibited after injection. Nearly 18% (158/891) of the units did not respond to stimulation before bupivacaine, but responded significantly to stimulation after injection, and of these units, 9 were inhibited before bupivacaine. About 16% (147/891) of the units responded to stimulation before bupivacaine but not after injection, and of these units, 2 were inhibited after injection. About 28% (247/891) units responded

to stimulation before and after bupivacaine injection and were included in the further statistical analysis.

From case 4, nearly 60% (664/1107) of the units did not respond to stimulation before and after bupivacaine injection; and of these units, 1 unit was inhibited before and after bupivacaine, 1 was inhibited before bupivacaine but did showed no excitatory or inhibitory response after injection, and 10 units showed no response before bupivacaine but were inhibited after injection. Nearly 20% (221/1107) of the units did not respond before bupivacaine, but responded after injection. About 8.4% (93/1107) of the units responded to stimulation before bupivacaine but did not respond after injection, and of these units, 3 were inhibited after injection. Nearly 11.7% (129/1107) of the units responded to stimulation before and after bupivacaine injection and were included in further analysis.

From case 5, nearly 73% of the units recorded did not respond to stimulation before and after bupivacaine injection (508/699 units); and of these units, 2 were inhibited before bupivacaine but did not respond after injection, and 4 did not respond before bupivacaine but were inhibited after injection. Less than 10% of the units were responsive after bupivacaine but not before injection (67/699 units), and of these units, 2 were inhibited before injection. About 9% of the units were responsive before bupivacaine but not after injection (65/699 units). The 8.4% (59/699) of the units remaining were responsive before and after bupivacaine injection and were able to be further analyzed. Thus, recordings from case 5 were the least responsive.

The mean of the peak firing rate values from all three monkeys before bupivacaine injection was 24.51 spikes/s (SD 27.95), and the median was 13.90 spikes/s.

The mean of the response latency values from all three monkeys before bupivacaine injection was 26.84 ms (SD 9.67), and the median was 25.28 ms. When monkey 5 was excluded from the summary, the mean of the peak firing rate values was 24.77 spikes/s (SD 27.43), and the median was 14.24 spikes/s. The mean of the response latency values was 25.88 ms (SD 8.42), and the median was 25.10 ms. The results of the statistical analysis (of the data from monkeys 3 and 4) of peak firing rate and latency are found in Tables 6-1 and 6-2, respectively. All figures plot the observed data, while the significance values of the statistical effects were determined based on the predicted data values estimated from the statistical analysis. Examples of units responsive to contralateral

Table 6-1. Tests of model effects for variance in firing rate classified by bupivacaine period, spatial stimulus characteristics, unit type, monkey case, and selected interactions

Variance Source	Wald Chi-Square	df	P value
(Intercept)	769.568	1	< 0.0005
Bupivacaine	0.110	1	0.740
Stimulation Site	8.477	1	0.004
Response Field	845.775	2	< 0.0005
Unit Signal	33.983	1	< 0.0005
Monkey Case	29.376	1	< 0.0005
Bupivacaine x Site	4.242	1	0.039
Bupivacaine x Response Field	2.028	2	0.363
Bupivacaine x Unit Signal	0.008	1	0.930
Bupivacaine x Site x RF	12.404	4	0.015

Tests of model effects from Generalized Linear Modeling with Generalized Estimating Equations on the dependent variable peak firing rate. N = 1994 unit subjects with repeated measures before and after bupivacaine injection.

Table 6-2. Tests of model effects for variance in latency classified by bupivacaine period, spatial stimulus characteristics, unit type, monkey case, and selected interactions

Variance Source	Wald Chi-Square	df	P value
(Intercept)	10830.048	1	< 0.0005
Bupivacaine	0.728	1	0.383
Stimulation Site	2.855	1	0.091
Response Field	8.665	2	0.013
Unit Signal	32.579	1	< 0.0005
Monkey Case	45.891	1	< 0.0005
Bupivacaine x Site	3.414	1	0.065
Bupivacaine x Response Field	2.674	2	0.263
Bupivacaine x Unit Signal	1.128	1	0.288
Bupivacaine x Site x RF	3.869	4	0.424

Tests of model effects from Generalized Linear Modeling with Generalized Estimating Equations on the dependent variable latency. N = 1369 unit subjects with repeated measures before and after bupivacaine injection.

stimulation before bupivacaine injection are shown for cases 3 and 4 in Figure 6-3 and in Figure 6-4 for case 5. These example units followed the overall trends we found in the population for response property changes after ipsilateral bupivacaine injection.

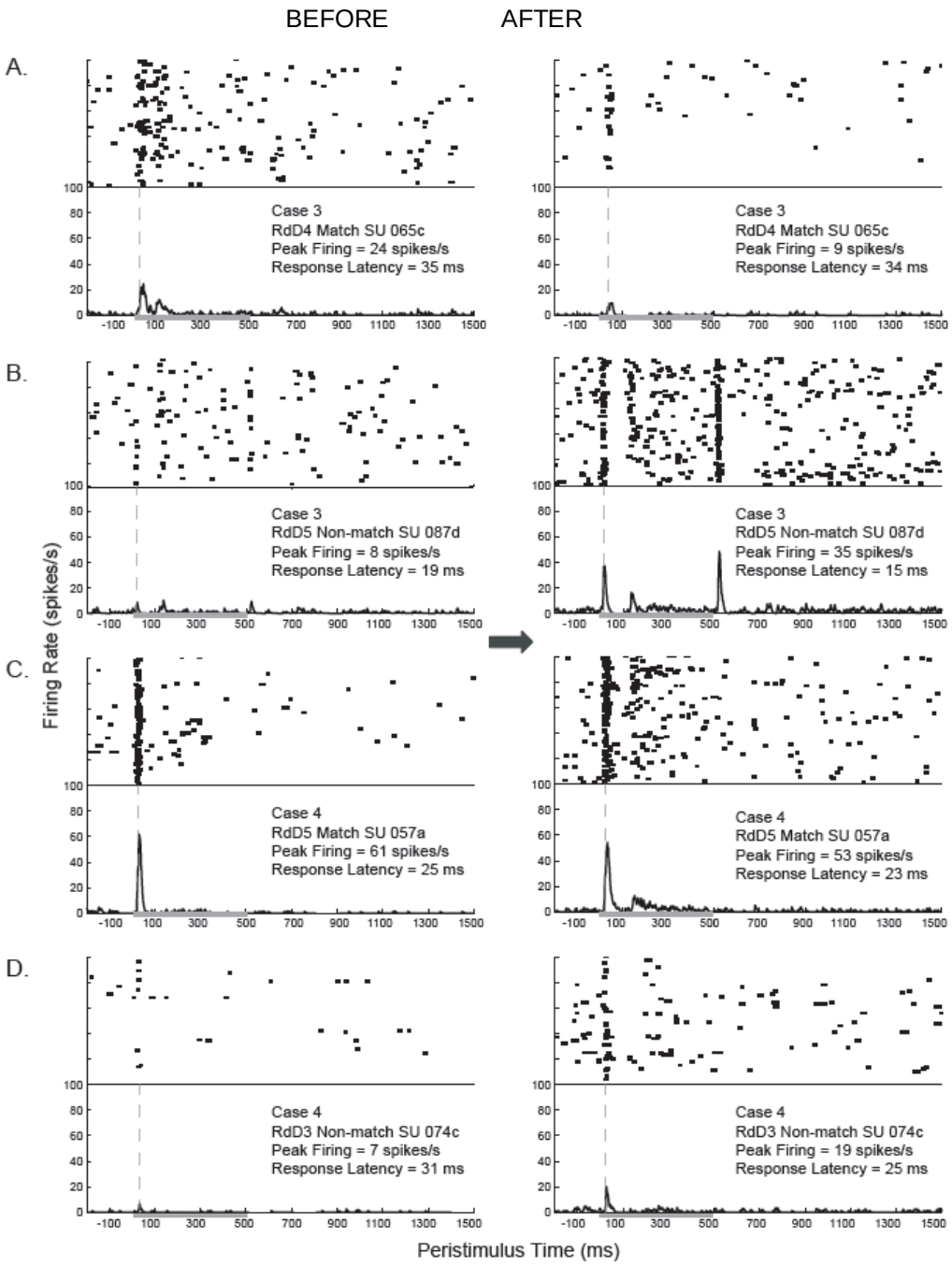

Figure 6-3. Peristimulus time histograms (PSTHs) and rasters before and after bupivacaine injection in two monkeys. PSTHs left of the arrow occurred before bupivacaine injection, and those right of the arrow occurred after injection. PSTHs show 100 trials of 500 ms indentations (indicated by horizontal gray line). Vertical dashed lines indicate response latency. Examples reflect trends in the data. A. Neuron 065c from monkey 3 was more responsive before bupivacaine injection than after. Stimulation occurred on right distal digit 4 (RdD4), inside the Response Field of the neuron. Bupivacaine was administered to left D4, indicated by the label "Match". B. When a non-matching digit, right distal digit 5 (RdD5), was stimulated neuron 087d from case 3 showed the opposite pattern. C. The peak response of neuron 057a from monkey 4 decreased slightly, while the activity during sustained stimulation increased when RdD5 was stimulated after left D5 was injected with bupivacaine. D. Neuron 074c from case 4 responded weakly to stimulation on RdD3 before bupivacaine injection, but increased responsiveness after the injection on left D5.

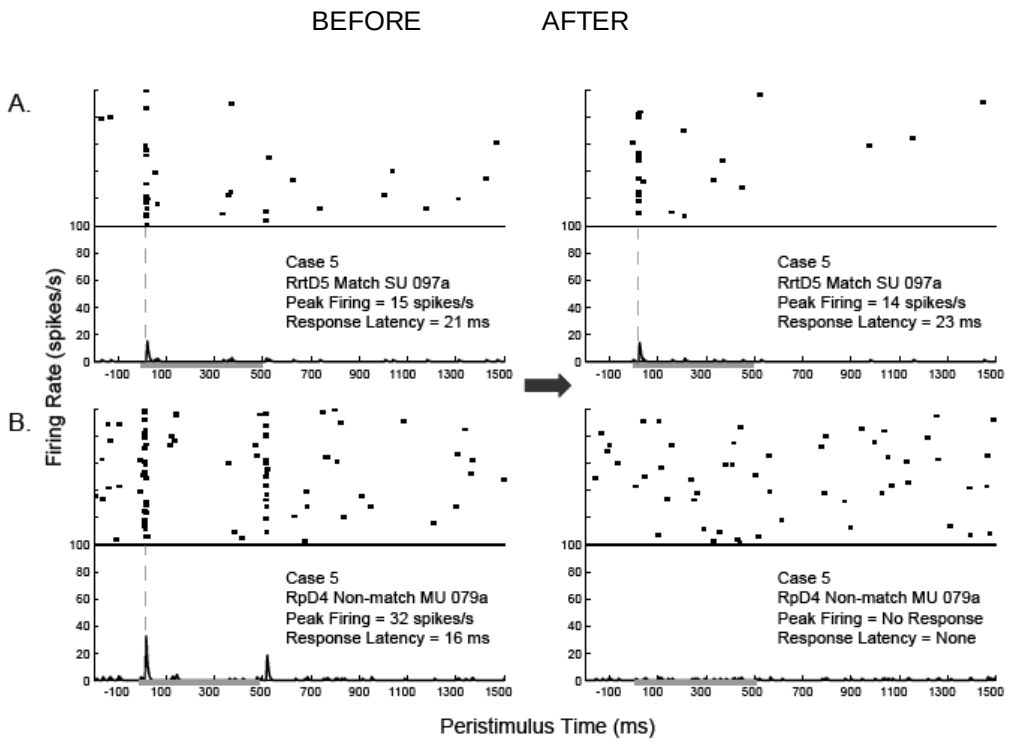

Figure 6-4. Example peristimulus time histograms (PSTHs) and rasters before and after bupivacaine injection in monkey 5. PSTHs left of the arrow show neuron activity before bupivacaine injection, and PSTHs right of the arrow show activity after bupivacaine injection. Conventions are the same as Figure 6-3. Case 5 had a long-standing injury that was not described in the medical records, and since the responses to bupivacaine injection did not follow the trends from the other two cases, this monkey was examined separately. A. An example neuron (097a) recorded from monkey 5 was nearly equally responsive to stimulation on the right radial tip of digit 5 (RrtD5) before and after the bupivacaine injection in the left D5. B. An example neuron cluster (079a) from monkey 5 responded well to stimulation on right proximal digit 4 (RpD4) before bupivacaine was injected into a non-matching digit (left D5), but did not respond to stimulation following the injection. These individual examples reflect the trends in the population from monkey 5.

Effects of Ipsilateral Bupivacaine Injection on Peak Firing Rate and Response Latency

The peak firing rates and response latencies of units before and after bupivacaine injection were analyzed for cases 3 and 4 in order to estimate the sources of variance in the responses to ipsilateral bupivacaine injection. Averaged over both monkeys, the mean response latency before bupivacaine was 25.88 ± 0.34 ms (N = 615), and the mean response latency after bupivacaine was 26.72 ± 0.32 ms (N = 754; Figure 6-5A). This small difference in response latency after bupivacaine injection was not statistically significant (P = 0.383). The mean peak firing rate before bupivacaine was 15.30 ± 0.78 spikes/s (N = 997), and the mean peak firing rate after bupivacaine was 17.31 ± 0.74 spikes/s (N = 997; Figure 6-5B); however, this small increase in firing rate was not statistically significant (P = 0.740). Overall, bupivacaine injection in an ipsilateral digit had little effect on response latency, and slightly increased peak firing rates in response to stimulation on the contralateral hand. Although the effect of local bupivacaine anesthesia was not significant when averaged across neurons, we examined interactions between the bupivacaine injection and the other predictor variables.

Effects of Stimulation Location Compared to Bupivacaine Injection Location

As expected, the stimulation location itself did not affect the response latency when the effect of bupivacaine is not considered. The effect of the stimulation location is best considered as the interaction effect between the bupivacaine injection and the stimulation location (an interaction term in the statistical model instead of a main effect term). When the contralateral stimulation location matched the ipsilateral digit injected with bupivacaine, response latency tended to lengthen following the injection (26.33 ±

0.47 ms and 27.54 ± 0.51 ms, P = 0.362). Response latency tended to shorten slightly following bupivacaine injection when the contralateral stimulation location did not match the ipsilateral digit injected with bupivacaine (26.30 ± 0.52 ms and 25.87 ± 0.40 ms, P = 1.000). The interaction of the bupivacaine injection and the relationship of the stimulus location to the injection location approached significance due to the difference between the direction of the effects on latency (P = 0.069).

Peak firing rate tended to decrease slightly after bupivacaine injection when the contralateral stimulation location matched the ipsilateral digit injected (25.96 ± 1.72 spikes/s and 23.30 ± 1.44 spikes/s, P = 0.766). Peak firing rate tended to increase slightly after bupivacaine injection when the contralateral stimulation location did not match the ipsilateral digit injected (19.12 ± 1.19 spikes/s and 21.03 ± 1.03 spikes/s, P = 1.000). The interaction of the bupivacaine injection and the relationship of the stimulus location to the injection location was significant due to the difference between the direction of the effects (P = 0.012).

Thus, both peak firing rate and latency showed complementary patterns of effects of bupivacaine when the relationship of the stimulus location to the injection site was taken into account.

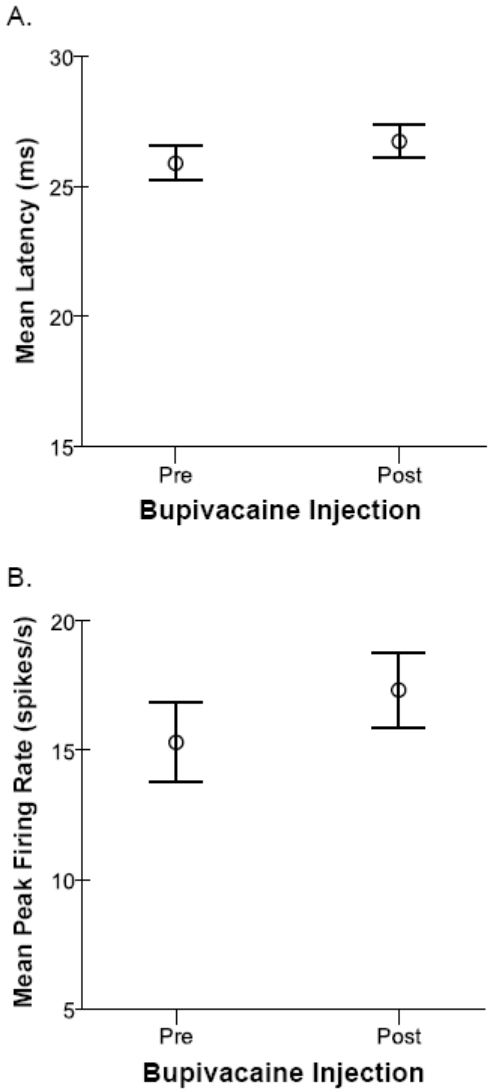

Figure 6-5. Averaged over all conditions, latencies and peak firing rates changed little after bupivacaine injection. Averages are plotted with error bars representing 95% confidence intervals. A. Response latencies averaged over all conditions across cases 3 and 4 did not differ before and after bupivacaine injection into an ipsilateral digit (P = 0.383). Examined individually, cases 3 and 4 showed similarly small differences in response latencies (~2 ms; not plotted). B. Peak firing rates averaged over all conditions across cases 3 and 4 revealed a slight increase in peak firing rate occurred after bupivacaine injection, but this was not statistically convincing (P = 0.740). We found similar trends for individual monkeys (not plotted), which did not reach statistical significance (case 3: P = 0.400; case 4: P = 0.493).

Effects of Response Field Relationship to Stimulation Before and After Bupivacaine

By definition, the Response Field categorization varied with firing rate; therefore, the effects of interest included how the Response Field categorization may affect the firing rate and latency following ipsilateral bupivacaine injection. Since some receptive fields are known to expand in size following ipsilateral digit denervation, we expected that after bupivacaine, fewer neurons would be categorized as outside the Response Field, and this categorization would relate to increases in firing rate and perhaps shortening of response latencies.

The interaction of the bupivacaine injection with the Response Field categorization affected response latencies ($P = 0.006$). Latency shortened slightly after bupivacaine injection when neurons were stimulated in the center of the Response Field (CENTER = 26.51 ± 0.68 ms and 25.76 ± 0.63 ms, $P = 1.000$). Latency lengthened slightly when neurons were stimulated inside (but not in the center) of the Response Field (IN = 25.45 ± 0.35 ms and 26.34 ± 0.36 ms, $P = 0.556$) and when neurons were stimulated outside of the Response Field (OUT = 26.99 ± 0.71 ms and 28.03 ± 0.63 ms, $P = 1.000$). Thus, while the differences in response latency before and after bupivacaine were not significantly different based on Response Field classifications, the interaction effect was significant overall because the latencies tended to shorten when the stimulus was in the center of the Response Field and the latencies tended to lengthen when the stimulus was located elsewhere in relation to the Response Field.

The interaction between the bupivacaine injection with the Response Field categorization affected the peak firing rates ($P < 0.0005$), but not in the precise way expected. Following bupivacaine injection, peak firing rates increased when the neurons

were stimulated outside of the Response Field (OUT = 5.64 ± 0.49 spikes/s and 7.02 ± 0.45 spikes/s, P = 0.029). However, this trend was not found when neurons were stimulated in the center of the Response Field (CENTER = 34.85 ± 2.59 spikes/s and 31.98 ± 2.12 spikes/s, P = 1.000) or inside (but not in the center) of the Response Field (IN = 27.13 ± 1.24 spikes/s and 27.50 ± 1.13 spikes/s, P = 1.000). Because the Response Field was determined based on the characteristics of the population firing rates (see METHODS), the observed firing rate increase when locations outside the Response Field were stimulated following bupivacaine suggests that the firing rates within the population increased, despite the lack of effects when the stimulus was located inside the Response Field. The neurons responding to stimuli inside their Response Fields may have already been firing near their maximum rate.

Differences Between Single- and Multi-Units

As may be expected, there were slight but significant differences in response latency and peak firing rate between single- and multi-units. The latencies of single units were slightly longer in general than latencies of multi-units (27.91 ± 0.32 ms and 25.12 ± 0.38 ms, respectively, P < 0.0005). Bupivacaine did not differentially affect latencies of single- and multi-units after injection, as bupivacaine slightly lengthened the latencies of single units (27.51 ± 0.44 ms and 28.31 ± 0.41 ms, P = 0.902) and multi-units (25.13 ± 0.51 ms and 25.10 ± 0.47 ms, P = 1.000). Correspondingly, the firing rates of single units were lower than firing rates of multi-units (18.73 ± 0.62 spikes/s and 25.98 ± 1.30 spikes/s, respectively, P < 0.0005). Bupivacaine did not differentially affect peak firing rates of single units (18.94 ± 0.89 spikes/s and 18.52 ± 0.79 spikes/s, P = 1.000) and

multi-units (26.14 ± 1.56 spikes/s and 25.82 ± 1.38 spikes/s, P = 1.000). Thus, although the magnitudes of response latencies and firing rates differed between single- and multi-units, bupivacaine did not act on single- units differently than multi-units.

Contributions of Multiple Stimulus Variables on the Effects of Bupivacaine

We expected that the combined influences of the stimulus location relative to the Response Field of the neuron and relative to the bupivacaine injection on the ipsilateral digit would affect neuron response properties following bupivacaine injection. Latency was not significantly affected by the interaction of these three conditions (P = 0.424), but the trends are shown in Figure 6-6A. When the contralateral stimulation location matched the location of the ipsilateral bupivacaine injection the latency tended to lengthen following the injection when the stimulus was outside (OUT = 26.41 ± 1.00 ms and 29.47 ± 0.96 ms, P = 1.000) or inside (IN = 25.80 ± 0.39 ms and 26.71 ± 0.47 ms, P = 1.000) the neuron's Response Field, but changed little when the stimulus was in the center of the Response Field (CENTER = 26.79 ± 0.87 ms and 26.45 ± 1.05 ms, P = 1.000). In contrast, when the contralateral stimulation location did not match the location of the ipsilateral bupivacaine injection, the latencies tended to shorten after injection when the stimulus was outside (OUT = 27.57 ± 0.98 ms and 26.58 ± 0.81 ms, P = 1.000) the neuron's Response Field, while latencies changed little when the stimulus was in the center of the neuron's Response Field (CENTER = 26.24 ± 1.05 ms and 25.06 ± 0.69 ms, P = 1.000) or inside (IN = 25.11 ± 0.57 ms and 25.96 ± 0.55 ms, P = 1.000) the Response Field. Thus, the interaction of bupivacaine with the relationships of the stimulus location to the injected digit and to the neuron's Response Field was not significant, but trends

emerged such that bupivacaine had some differential influence on response latencies depending on the stimulus location.

Unlike latency, peak firing rate was affected by the interaction of bupivacaine injection with the relationships of the stimulus location to the injection site and to the Response Field of the neuron ($P = 0.015$), as shown in Figure 6-6B. When the contralateral stimulation location matched the location of the bupivacaine injection and the stimulus was located outside the neuron's Response Field, firing rate increased after injection (OUT = 6.49 ± 0.72 spikes/s and 8.55 ± 0.70 spikes/s, $P = 0.048$). When the stimulus was inside the Response Field or in the center of the Response Field, firing rates tended to decrease following bupivacaine, but the differences were not significant (IN = 30.73 ± 1.84 spikes/s and 27.52 ± 1.63 spikes/s, $P = 1.000$; CENTER = 40.66 ± 4.19 spikes/s and 33.84 ± 3.45 spikes/s, $P = 1.000$). When the stimulation location did not match the location of the bupivacaine injection, firing rates tended to increase after injection within all of the Response Field categories (OUT = 4.78 ± 0.57 spikes/s and 5.49 ± 0.49 spikes/s, $P = 1.000$; IN = 23.53 ± 1.72 spikes/s and 27.48 ± 1.57 spikes/s, $P = 1.000$; CENTER = 29.04 ± 2.99 spikes/s and 30.12 ± 2.42 spikes/s, $P = 1.000$). Therefore, even though not all of the pairwise comparisons were significantly different, the overall interaction effect was a significant contributor to the variance in peak firing rates because the bupivacaine injection tended to have differential effects on firing rate depending on the stimulation location.

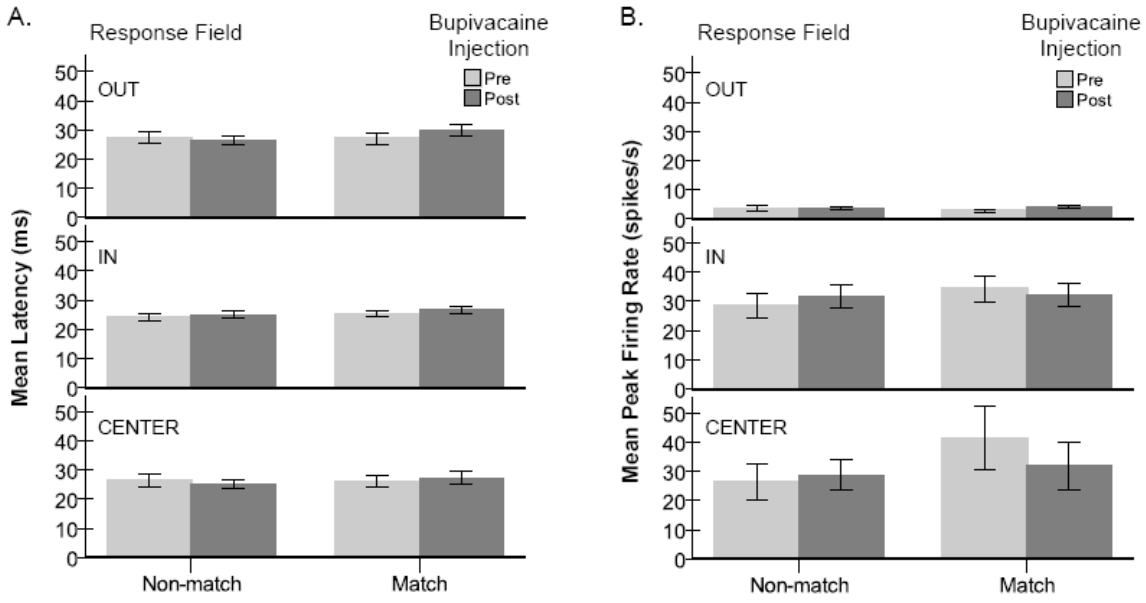

Figure 6-6. Bupivacaine effects on latencies and peak firing rates differ depending on stimulus relationships. Data from monkeys 3 and 4 were categorized based on the relationship of the stimulus location to the neuron Response Field (OUT, IN, or CENTER). Data in the left columns were collected when the stimulation site on the right hand was located on a non-matching digit relative to the bupivacaine injection on the left hand (Non-match). Data in the right column were collected when the stimulation site on the right hand was located on the digit that matched the bupivacaine injection location on the left hand (Match). Light gray bars indicate data collected before the bupivacaine injection (Pre), and dark gray bars indicate data after the bupivacaine injection (Post). Error bars are 95% confidence intervals. A. When a non-matching digit was stimulated, latencies tended to shorten after bupivacaine injection, but when the matching digit was stimulated, latencies tended to lengthen after bupivacaine injection. B. The changes in firing rate tend to oppose the changes in latency. Firing rates tend to increase after bupivacaine injection when a non-matching digit was stimulated relative to the ipsilateral bupivacaine injection. When the stimulated digit on the right hand matched the digit on the left hand that was anesthetized, the firing rate tended to decrease. When the stimulus location was outside the Response Field of the neuron, firing rates remained low before and after bupivacaine injection.

Comparisons Between Normal Monkeys and an Injured Monkey

The latency and peak firing rate data varied somewhat across all three monkeys, but the data from monkey 5 were treated separately due to the injury monkey 5 suffered on right digit 3 that could result in plasticity in the somatosensory cortex. In the statistical model, we found that the data from monkeys 3 and 4 also varied from each other in response latency ($P < 0.0005$) and peak firing rate ($P < 0.0005$), with samples from monkey 3 showing shorter latencies (case 3 = 24.86 ± 0.34 ms; case 4 = 28.17 ± 0.37 ms) and higher firing rates (case 3 = 25.09 ± 1.13 spikes/s; case 4 = 19.62 ± 0.74 spikes/s) than monkey 4. However, the data from these two monkeys combined yielded similar trends and a working statistical model. (Recall, including the data from monkey 5 in the statistical analysis prevented the modeling analysis from fitting the data.) Generally the latency and peak firing rate data from monkey 5 were more variable (Figure 6-7A, B), the latencies tended to be longer (32.29 ± 0.83 ms), and the peak firing rates tended to be lower (3.64 ± 0.35 spikes/s) than those we obtained from monkeys 3 and 4. However, we found receptive field expansion in all three cases following ipsilateral bupivacaine injection (Figure 6-2).

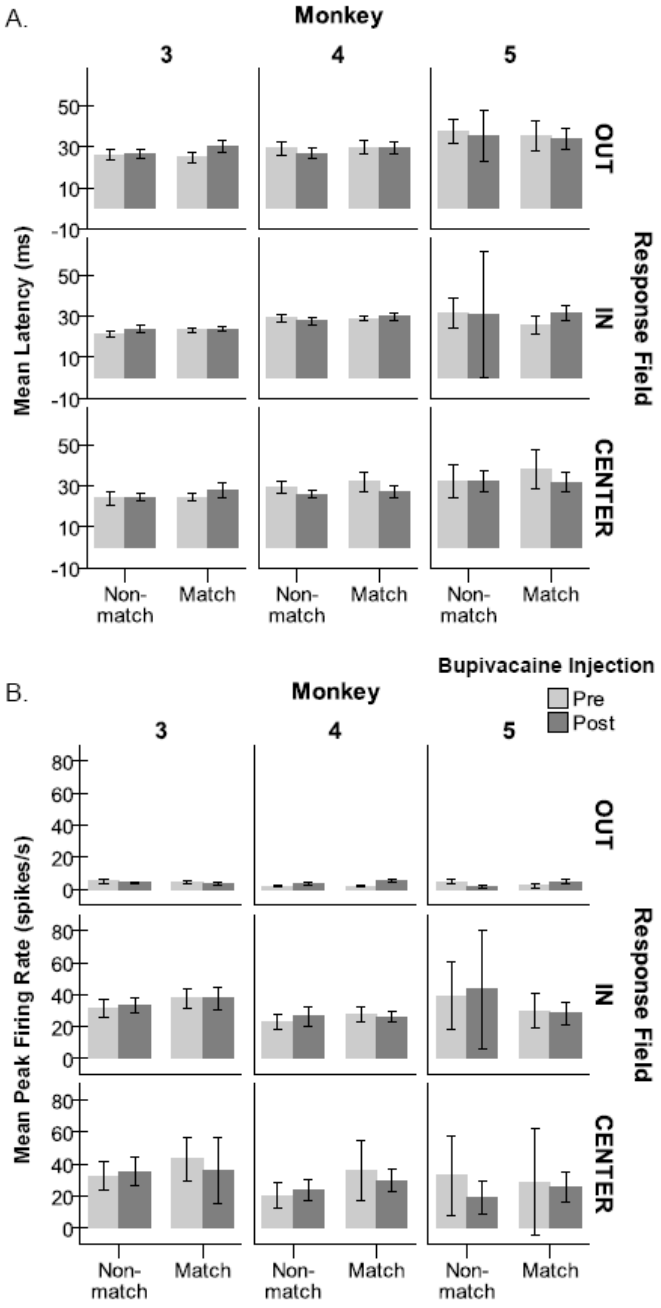

Figure 6-7. Comparison of bupivacaine effects on latencies and peak firing rates across cases. Data shown in Figure 6-6 (monkeys 3 and 4 combined) are divided to show the effects of bupivacaine in all three monkey cases. Light gray bars indicate responses before bupivacaine injection (Pre), and dark gray bars indicate responses after bupivacaine injection (Post). Error bars are 95% confidence intervals. Data were divided into categories based on monkey case (columns), stimulus relationship to the Response Field (rows), and stimulus relationship to the bupivacaine injection site (column subdivisions). A. Latencies were categorized to indicate how bupivacaine injection in an ipsilateral digit affected response latencies to contralateral stimulation within each monkey. Data from monkey 5 were more variable than data from the other two monkeys. B. Peak firing rates were categorized to indicate how bupivacaine injection affected responses within each monkey. Peak firing rates were more variable from monkey 5 than other monkeys, and the effects of bupivacaine appeared to show opposite trends in monkey 5 compared to the data from monkeys 3 and 4.

Additionally, the classification of the relationship of the stimulus to the Response Field changed as expected for all monkey cases. Figure 6-8 shows the tallies of the Response Field categorizations for cases 3 and 4 combined, and for monkey 5 separately (inset). As expected if the primary effect of bupivacaine injection in an ipsilateral digit is to expand affected receptive fields (rather than shrink their sizes), we found that after bupivacaine injection, fewer stimulus locations were classified as outside of the Response Field (OUT) and more locations were classified as inside of the Response Field (IN, CENTER). This effect generally occurred across stimulus locations and across all three monkey cases. Despite the similarities of the effects of bupivacaine on the Response Field tallies, the counts of the locations classified as outside of the Response Field (OUT) were higher relative to the counts of the locations classified as inside of the Response Field (IN, CENTER) in monkey 5 compared to monkeys 3 and 4 combined (Figure 6-8). Cortical activity appeared to be more depressed in monkey 5, and examining the topography of the responses (Figure 6-9), we found that the electrodes that responded to stimulation were more scattered across the representations rather than mostly concentrated within the expected representations compared to the uninjured monkeys.

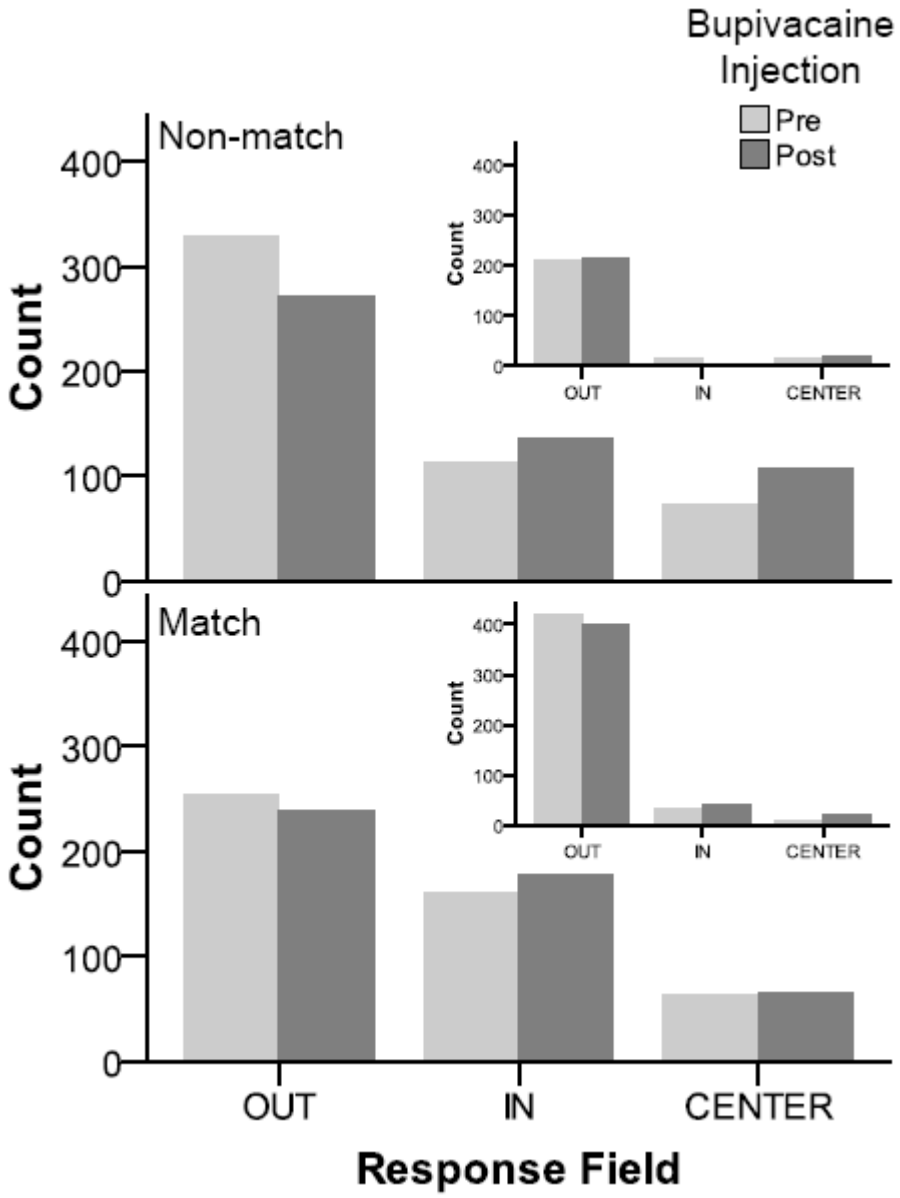

Figure 6-8. Bupivacaine effects on the tallies of Response Field properties. The effects of bupivacaine injection in an ipsilateral digit on the relationship of the stimulus to the neuron Response Field are shown for the conditions in which a non-matching digit was stimulated relative to the ipsilateral bupivacaine injection (Non-match) and when the matching digit was stimulated (Match). Data are summarized across monkeys 3 and 4. Light gray bars indicate the counts before bupivacaine was administered and dark gray bars indicate the counts after the injection. The trend shows that the stimulus locations classified as outside the Response Field (OUT) decreased after bupivacaine injection, while the locations classified as inside the Response Field (IN, CENTER) increased. Inset shows the data for monkey 5, which resembles the data from the other monkeys, but we obtained fewer instances in which the stimulus was inside the Response Field in monkey 5 and more instances in which the stimulus was outside the Response Field compared to the results from the other two monkeys.

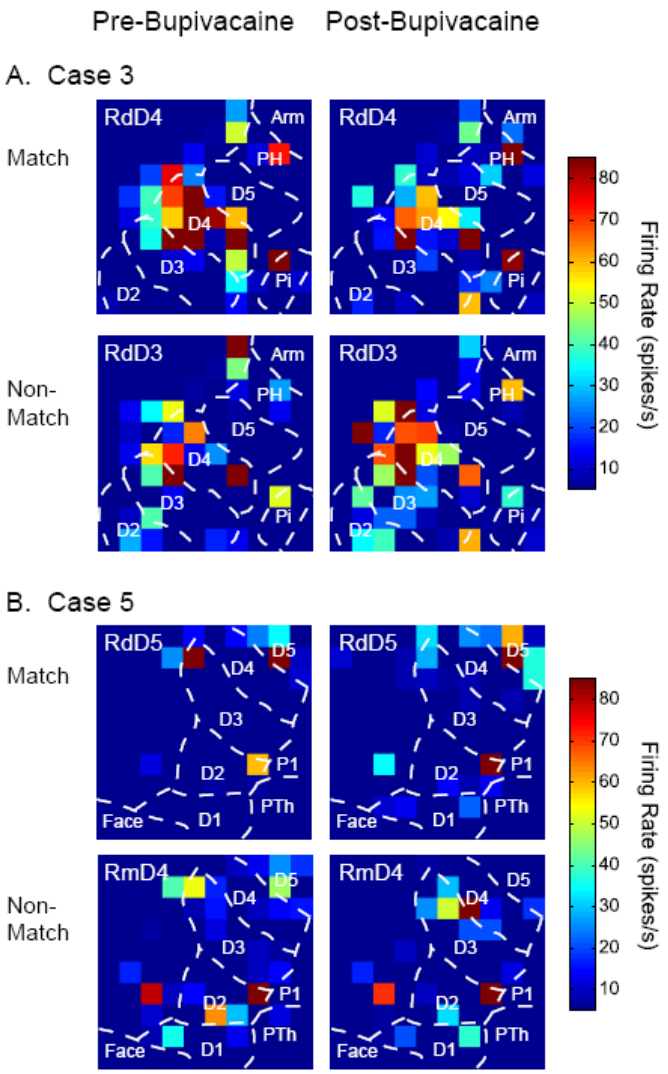

Figure 6-9. Comparison of neuron activity across the 100-electrode array between two monkeys. Peak firing rates of single neurons and multi-units are shown in a color map with dashed lines overlaid to indicate the approximate sites of activity within cortex. The color scale ranges from 5 to 85 spikes/s. Dark blue (no squares) indicates that activity over 5 spikes/s did not occur within 50 ms from stimulus onset. Left column shows peak firing rates averaged over 100 trials before the bupivacaine injection in an ipsilateral digit. Right column shows peak firing rates after the bupivacaine injection. A. Recordings from a normal monkey, case 3, are shown before and after bupivacaine injection in left digit 4 (D4). Upper panel shows responses when a site on right distal D4 (RdD4) was stimulated (Match). After bupivacaine, peak firing rates within the D4 representation decreased on average. A subset of electrodes showed increases and no changes in peak firing rates after bupivacaine injection. Lower panel shows responses when RdD3 was stimulated (Non-Match) before and after bupivacaine injection into left D4. Many peak firing rates increased after bupivacaine injection, while a few decreased or showed no change. B. Monkey 5 had recovered from an unknown injury on right digit 3, and the number of responsive electrodes were fewer and more scattered than those in monkeys 3 and 4. Upper panel shows the peak firing rates when RdD5 was stimulated before and after bupivacaine was injected into the matching ipsilateral digit, left D5 (Match). Several electrodes within the D5 representation increased firing rates following bupivacaine. A few electrodes outside the approximated D5 representation decreased firing rates after bupivacaine. Lower panel shows activity when right middle digit 4 (RmD4) was stimulated before after bupivacaine injection into left D5 (Non-Match). Peak firing rates tended to decrease after bupivacaine, but a few electrodes, notably near the D3 and D4 representations, increased peak firing rates after the local anesthetic.

Discussion

We measured neuron activity following local anesthetic injection to block afferent input from the ipsilateral hand in order to determine what modulation occurs in units responding to stimulation on the contralateral hand. This quantitative study expands previous electrophysiological studies and applies to the functional effects of spontaneous activity outside the minimal receptive field on response modulation, specifically for interactions between the two hand representations. We found changes in peak firing rates and latencies following local anesthetic injections that were complementary and largely corresponded to focal receptive field expansions, but the response properties did not follow expectations precisely. The majority of Response Fields (or receptive fields) may not be changed by bupivacaine injection, but those that changed expanded rather than shrank. Here we discuss the results found in two normal monkeys and discuss how these results compare to those found in the injured monkey and to previous studies. We conclude with the implications for interhemispheric interactions that can be gained from quantitative study.

Effects of Bupivacaine on the Sample Responses

The recordings from all three monkeys included large proportions of neurons that were not responsive to the stimulation conditions tested before and after bupivacaine injection: Case 3 ~ 38%, Case 4 ~ 60%, Case 5 ~ 73%. These proportions likely differed due to the placement of the electrode arrays and the stimulus conditions tested in each monkey. In all three cases, we focused on stimulating right digits 4 and 5 because we

anesthetized left digit 4 (monkey 3) or digit 5 (monkeys 4 and 5). The placement of the electrode array in monkey 5 missed a portion of the representation of digit 5; therefore, we may have obtained more responses from monkey 5 if the array placement had been shifted slightly. In all cases, few neurons sampled were inhibited before or after bupivacaine injection: Case 3 = 22 units, Case 4 = 15 units, Case 5 = 8 units. Units that were not responsive before bupivacaine became responsive after bupivacaine may reflect expanding receptive fields: Case 3 ~ 16%, Case 4 ~ 20%, Case 5 ~ 10%. However, we did not include these units in the statistical analysis because it was not always clear that the units were comparable before and after bupivacaine injection (as over the course of the experiments, new signals can be spontaneously recorded). Thus, the tallies of unit responses indicate that few neurons were inhibited under any stimulus condition and that between 10-20% of the sampled units may have gained new responsiveness following bupivacaine injection corresponding to receptive field expansion. We further analyzed the subset of units which responded to stimulation before and after bupivacaine injection to determine if the response properties changed and if the spatial location of the stimulus (relative to the anesthetized digit) contributed to the variance in the response properties.

Spatial Stimulus Influences on Effects of Bupivacaine on Neuron Response Properties

The effects of bupivacaine on peak firing rate and response latency were not statistically significant when averaged over the stimulus conditions (Tables 6-1, 6-2). Our interest was in the topographic specificity of the effects of bupivacaine to infer the underlying somatotopy of interhemispheric interactions. In addition, we asked whether the relationship of the stimulus location to the neuron's Response Field influenced the

direction of the interhemispheric interactions. We found trends for changes following bupivacaine injection in latency ($P = 0.069$; Table 6-2) which complemented the significant changes in peak firing rate ($P = 0.012$; Table 6-1) that were associated with the relationship of the stimulus location to the injection location (Match or Non-match; Figure 6-6). This finding that peak firing rate increased after bupivacaine when locations were stimulated that did not match the ipsilateral injection location appears to relate well with observed receptive field expansion described in previous studies (e.g., Calford and Tweedale, 1990, 1991a,b). In other words, neurons responded more strongly to stimulation after bupivacaine than before bupivacaine when the stimulus was located on a non-matching digit site; and this situation may be expected to occur when receptive fields associated with the matched digit expand to the non-matched digit.

Perhaps it is surprising that firing rates decreased when the stimulation locations were within the digit that matched the ipsilateral injection location since the small receptive fields on the digit generally first expand within the same digit, and then may expand to adjacent digit or palm sites. We expected that the receptive field expansions would correspond to response facilitation within the site of the original receptive field. This contradictory finding indicates that the firing rate decreased or did not change for neurons that responded to stimulation on the matched digit. The effect of bupivacaine injection thus has a topographic distribution that is not uniformly excitatory. One possible explanation for the unexpected firing rate decreases (and trend for latency lengthening) is related to lateral inhibition. Before the local anesthetic block, a neuron responds to stimulation on the matched digit with a high peak firing rate. Following the block, activation spreads across the digit, which also evokes more lateral inhibition. The average

decrease in peak firing rate resembles the effect of cortical cooling of area 3b was tested in one macaque monkey and 14 bats (Clarey et al., 1996). In their study, Clarey et al. (1996) found that initially following cortical cooling of the foot representation in area 3b in one hemisphere, receptive fields of neurons in the opposite hemisphere expanded, and initially, responses to mechanical (brush) stimulation increased and new responses emerged. However, during the plateau of the cortical cooling (about 42 to 52 minutes after the start of the cooling procedure), the neuron responses to mechanical stimulation decreased even below original levels before returning to the approximate pre-cooling levels (Clarey et al., 1996). The data from this study were summarized by comparing the pre-cooling responses to the maximum increase or decrease in response magnitude of all neurons in each animal; thus, the initial response increases following the cooling dominated the final data summary. Our data were all collected during this "plateau period" rather than the initial onset of the anesthetic effect, and we divided the data based on the relationship of the stimulus location to the anesthetic injection and to the Response Field of the reference neuron. Therefore, our data are consistent with, but expand, those of previous studies.

Some electrophysiological properties of neurons in primary somatosensory cortex have been described in raccoons after digit amputation or nerve transaction (Turnbull and Rasmusson, 1990); however, the findings appear to be slightly different from those reported in monkeys following local anesthetic injections or amputation. When digital nerves innervating the glaborous skin were transected in digit 4 of raccoons and recordings were made in the contralateral primary somatosensory cortex, Turnbull and Rasmusson (1990) found that the receptive fields were most abnormal within the digit 4

representation and less likely to be abnormal near the representations of digits 3 and 4, while the overall responsiveness of the cortex was reduced compared to normal animals. Amputation resulted in neurons that responded only to the offset of stimulation, rather than to the onset, and these off responses had more variable latencies and large receptive fields than those found in normal cortical neurons (Turnbull and Rasmusson, 1990). The effects in raccoons were studied only in the contralateral cortex; therefore, the electrophysiological properties of response latency and amplitude in the primary somatosensory cortex have not been studied following local anesthetic injection into an ipsilateral digit. A study in which topographic maps were determined before and immediately after median nerve section and ligation in an adult owl monkey and 3 squirrel monkeys found that inputs to areas 3b and 1 from the radial and dorsal hand were "unmasked" and area 3b receptive fields were much larger (Merzenich et al., 1983b). Similar to the nerve section studies in raccoons (Turnbull and Rasmusson, 1990), Merzenich et al. (1983b) found large unresponsive zones that corresponded to the normal territory of the median nerve input in contralateral cortex immediately following median nerve section.

Since our results and those of Calford and Tweedale (e.g., 1990, 1991a,b) did not include large unresponsive territories in the cortex ipsilateral to the digit blocked with local anesthetic, we expect that acute deafferentation by local anesthetic injections may have different effects on neuron response properties in the ipsilateral cortex than nerve transection and amputation have on the contralateral cortex. Deafferentation induces rapid changes in cortex thought to result from the unmasking of connections, particularly horizontal connections. This rapid plasticity likely involves inhibitory processes based on

evidence that receptor damage leads to loss of inhibitory inputs (Rajan, 1998) and studies that reveal unmasking of normally silent inputs in deprived cortex (Wall et al., 2002, review). Specifically regarding interhemispheric interactions, evidence indicates that tonic inhibition in the somatosensory pathways is released by deafferentation, and activity is transferred between hemispheres to area 3b via the callosal connections of the areas 1 and 2 representations (Killackey, 1983; Calford, 2002, review). The majority of callosal projections appear to release excitatory neurotransmitters; however, a subset of callosal projections (10-32%) may have inhibitory effects (Cont and Manzoni, 1994, review). It is possible that the topographic differences in the effects of the local anesthetic injections could be mediated by subsets of callosal connections.

Comparison of Normal Monkeys with a Monkey After Unknown Digit Injury

As shown in Figure 6-1, case 5 had sustained an injury to the right distal digit 3 at some point prior to his acquisition, presumably sustained in his natural habitat at least 4 years before the experiment. The injury was not included in the medical records and was unnoticed when monkeys were selected for the experiment. Given that the medical history of this monkey included two years within our facility and two years within another facility, this monkey had recovered from the injury for several years before our experiment. Despite the injury, the cortical organization in area 3b of monkey 5 did not appear to differ greatly from that of the other two cases (Figure 6-1, Figure 6-9). Qualitative examination of the area representing the digits in monkey 5 did not reveal dramatic changes in the sizes of the digit representations (Figure 6-1) or minimal receptive fields (see Figure 6-2 for an example) to compensate for the abnormal D3.

These findings are consistent with previous research showing that individual animals are known to have substantial variability of the area 3b hand representation (Merzenich et al., 1987), and receptive field size and organization has been shown to resemble those of normal animals after long survival times after peripheral nerve injury (Churchill et al., 1998). The overall topography of the hand representation of area 3b in monkey 5 appeared to be nearly normal, which differs somewhat from reorganization following complete digit amputations (e.g, Merzenich et al., 1984; Jain et al., 1998, review); however, only the distal portion of digit 3 was missing in monkey 5. The comparably normal topography in monkey 5 is consistent with findings in owl and squirrel monkeys 2-9 months following median nerve sections (e.g., Merzenich et al., 1983a; Garraghty and Kaas, 1991) and other peripheral nerve injury studies (for review, Kaas, 2000). The remaining portions of digit 3 appeared to take up the region normally occupied by the intact digit 3, and this phenomenon was also found in a macaque monkey after partial amputation of digit 2 (Manger et al., 1996).

The quantitative examination of the responses revealed differences between the abnormal case and normal monkeys. The differences between the data obtained from monkey 5 and cases 3 and 4 prevented these data from being included in a statistical model of the effects of bupivacaine and the relationship of stimulus location to the effects (the model using Generalized Estimating Equations would not come to a convergence to fit the data). The proportions of electrodes placed within area 3b versus area 3a were similar across all 3 monkeys; therefore, we do not expect that the differences between monkey 5 and the other monkeys were due in large part to the placement of the array. If more electrodes had been placed in area 3a in monkey 5, then we would expect lower

numbers of neurons responsive to light tactile stimulation. Rather, the differences between the two normal monkeys and monkey 5 were related in part to the low firing rates and long latencies in the injured monkey before and after bupivacaine injection. However, the maximum peak firing rate in response to stimulation in monkey 5 was still high (~158 spikes/s) and comparable to the maximum peak firing rates we recorded in monkeys 3 and 4 (~229 spikes/s and ~141 spikes/s, respectively). Over all, the variances in the peak firing rates were similar as well. The standard deviation of the peak firing rates before bupivacaine injection was 24.8 spikes/s for Case 3, 11.1 spikes/s for Case 4, and 14.8 spikes/s for Case 5 (N = 891, N = 1159, N = 699, respectively). However, the variability of the firing rates and latencies recorded when the stimulation was inside the Response Field (IN, CENTER) was very large, and the effects of bupivacaine injection in the ipsilateral digit tended to follow opposite patterns compared to those found in the normal monkeys (Figure 6-7). Since the cortical organization and neuron properties of monkey 5 were largely similar to those of the normal monkeys, it is possible that the variability in the data that prevented analysis of the data from monkey 5 with monkeys 3 and 4. Some of this variability may have arisen from differences in anesthetic depth across the cases, although we tried to maintain anesthetic depth at similar levels. Thus, the responsiveness of neurons sampled from monkey 5 was largely similar to normal monkeys, but the interhemispheric interactions due to acute deafferentation of an ipsilateral digit may have been altered, possibly due at least in part to the partial loss of a contralateral digit.

The effects of bupivacaine in the two normal monkeys can be considered to reveal acute interhemispheric plasticity. In monkey 5, loss of the right distal digit 3 at least 4

years prior to experimentation had resulted in a chronic change of the sensory surface; therefore the acute effects of bupivacaine injection in the left hand occurred within the context of chronic changes following injury. To our knowledge, no studies have examined the interhemispheric effects of local anesthetic injections into an ipsilateral digit following partial amputation (or any form of deafferentation) of a contralateral digit. The findings from this case indicate that despite generally normal properties in the cortex contralateral to the amputation, the injury may have changed the system enough so that interhemispheric connections produce responses that would be unexpected in normal monkeys.

Functional Relevance of Interhemispheric Interactions

A primary inspiration for this work came from the receptive field mapping studies of Calford and Tweedale (e.g., 1990, 1991a,b). Receptive field expansions of contralateral neurons following ipsilateral digit denervation by local anesthesia or amputation suggests that a source of tonic inhibition was removed by denervation that affected both the contralateral and ipsilateral cortex (Calford and Tweedale, 1990, 1991a,b; Calford, 2002, review). Studies have investigated this effect in humans. After lidocaine was injected into the thumb (Gandevia and Phegan, 1999), subjects reported that the perceived size of the anesthetized thumb and the unanesthetized lips increased. The perceived sizes of the digits adjacent to the thumb did not change, nor were changes reported for the digits contralateral to the injected thumb. Non-painful electrical stimulation and painful cooling of the thumb both increased the perceived thumb size, but to a lesser extent than did lidocaine injection. These perceptual changes may be

consistent with a psychophysical and evoked potential study in which the right hand was anesthetized and the subjects performed a grating orientation task with the left index finger or lower lip (Werhahn et al., 2002). Werhahn et al. (2002) reported enhanced tactile spatial acuity specific to the hand and not found on the lip when the hand was anesthetized, and this behavioral effect was associated with cortical processing enhancement.

These human studies confirm a large-scale topographic specificity of the interhemispheric interactions; while our study shows evidence of additional fine-scale topography which resulted in differences between the effects of local anesthesia on matched and non-matched hand locations. These effects were not expected based on the previous studies of receptive field expansion and await confirmation in humans.

Acknowledgements

Each of the following will be co-authors on the published manuscript from this work: Drs. Hui-Xin Qi, Zhiyi Zhou, Melanie Bernard, Mark J. Burish, A.B. Bonds, and Jon H. Kaas. In addition, we acknowledge the following contributions. Dr. Omar Gharbawie and Corrie Camalier helped collect data. Matlab scripts were written primarily by Dr. Pierre Pouget and John Haitas in collaboration with JLR and Jurnell Cockhren. This work was supported by the James S. McDonnell Foundation (JHK) and NIH grants NS16446 (JHK), F31-NS053231 (JLR), EY014680-03 (ABB), and T32-GM07347 (MJB).

References

Alhelail M, Al-Salamah M, Al-Mulhim M, Al-Hamid S. 2009. Comparison of bupivacaine and lidocaine with epinephrine for digital nerve blocks. *Emerg Med J* 26: 347-350.

Burton H, Fabri M. 1995. Ipsilateral intracortical connections of physiologically defined cutaneous representations in area 3b and 1 of macaque monkeys: projections in the vicinity of the central sulcus. *J Comp Neurol* 355: 508-538.

Burton H, Fabri M, Alloway K. 1995. Cortical areas within the lateral sulcus connected to cutaneous representations in areas 3b and 1: a revised interpretation of the second somatosensory area in macaque monkeys. *J Comp Neurol* 355: 539-562.

Calford MB. 2002. Dynamic representational plasticity in sensory cortex. *Neuroscience* 111: 709-738.

Calford MB, Tweedale R. 1990. Interhemispheric transfer of plasticity in the cerebral cortex. *Science* 249: 805-807.

Calford MB, Tweedale R. 1991a. Acute changes in cutaneous receptive fields in primary somatosensory cortex after digit denervation in adult flying fox. *J Neurophysiol* 65: 178-187.

Calford MB, Tweedale R. 1991b. Immediate expansion of receptive fields of neurons in area 3b of macaque monkeys after digit denervation. *Somatosens Mot Res* 8: 249-260.

Chubbuck JG. 1966. Small motion biological stimulator. *Appl Phys Lab Tech Digest* 5: 18-23.

Churchill JD, Muja N, Myers WA, Besheer J, Garraghty PE. 1998. Somatotopic consolidation: a third phase of reorganization after peripheral nerve injury in adult squirrel monkeys. *Exp Brain Res* 118: 189-196.

Clarey JC, Tweedale R, Calford MB. 1996. Interhemispheric modulation of somatosensory receptive fields: evidence for plasticity in primary somatosensory cortex. *Cereb Cortex* 6: 196-206.

Conti F, Manzoni T. 1994. The neurotransmitters and postsynaptic action of callosally projecting neurons. *Behav Brain Res* 64: 37-53.

Cusick CG, Wall JT, Felleman DJ, Kaas JH. 1989. Somatotopic organization of the

lateral sulcus of owl monkeys: area 3b, S-II, and a ventral somatosensory area. *J Comp Neurol* 282: 169-190.

Darian-Smith C, Darian-Smith I, Burman K, Ratcliffe N. 1993. Ipsilateral cortical projections to areas 3a, 3b, and 4 in the macaque monkey. *J Comp Neurol* 335: 200-213.

Davidson AG, O'Dell R, Chan V, Schieber MH. 2007. Comparing effects in spike-triggered averages of rectified EMG across different behaviors. *J Neurosci Methods* 163: 283-294.

Gandevia SC, Phegan CML. 1999. Perceptual distortions of the human body image produced by local anaesthesia, pain and cutaneous stimulation. *J Physiol* 514: 609-616.

Garraghty PE, Kaas JH. 1991. Large-scale functional reorganization in adult monkey cortex after peripheral nerve injury. *Proc Natl Acad Sci USA* 88: 6979-6980.

Hardin JW, Hilbe JM. 2003. *Generalized estimating equations*. Boca Raton: Chapman and Hall/CRC.

Iwamura Y, Tanaka M, Iriki A, Taoka M, Toda T. 2002. Processing of tactile and kinesthetic signals from bilateral sides of the body in the postcentral gyrus of awake monkeys. *Behav Brain Res* 135: 185-190.

Jain N, Florence SL, Kaas JH. 1998. Reorganization of somatosensory cortex after nerve and spinal cord injury. *News Physiol Sci* 13: 143-149.

Jain N, Qi H-X, Kaas JH. 2001. Long-term chronic multichannel recordings from sensorimotor cortex and thalamus of primates. Chapter 5 In *Progress in Brain Research*, ed. MAL Nicolelis, 130: 1-10. Amsterdam: Elsevier Science B.V.

Kaas JH. 1983. What, if anything, is SI? Organization of first somatosensory area of cortex. *Physiol Rev* 63: 206-231.

Kaas JH. 2000. The reorganization of somatosensory and motor cortex after peripheral nerve or spinal cord injury in primates. Chapter 14 In *Progress in Brain Research*, ed. FJ Seil, 128: 173-179. Amsterdam: Elsevier Science B.V.

Killackey HP, Gould HJ, III, Cusick CG, Pons TP, Kaas JH. 1983. The relation of corpus callosum connections to architectonic fields and body surface maps in sensorimotor cortex of new and old world monkeys. *J Comp Neurol* 219: 328-419.

Liang K-Y, Zeger SL. 1986. Longitudinal data analysis using generalized linear models. *Biometrika* 73: 13-22.

Manger PR, Woods, TM, Jones EG. 1996. Plasticity of the somatosensory cortical map in macaque monkeys after chronic partial amputation of a digit. *Proc R Soc Lond B* 263: 933-939.

Mason A, Nicoll A, Stratford K. 1991. Synaptic transmission between individual pyramidal neurons of the rat visual cortex in vitro. *J Neurosci* 11: 72-84.

Merzenich MM, Kaas JH, Sur M, Lin CS. 1978. Double representations of the body surface within cytoarchitectonic areas 3b and 1 in "SI" in the owl monkey (*Aotus trivirgatus*). *J Comp Neurol* 181: 41-74.

Merzenich MM, Kaas JH, Wall J, Nelson RJ, Sur M, Felleman D. 1983a. Topographic reorganization of somatosensory cortical areas 3b and 1 in adult monkeys following restricted deafferentation. *Neuroscience* 8: 33-55.

Merzenich MM, Kaas JH, Wall J, Sur M, Nelson RJ, Felleman D. 1983b. Progression of change following median nerve section in the cortical representation of the hand in areas 3b and 1 in adult owl and squirrel monkeys. *Neuroscience* 10: 639-665.

Merzenich MM, Nelson RJ, Stryker MP, Cynader MS, Schoppmann A, Zook JM. 1984. Somatosensory cortical map changes following digit amputation in adult monkeys. *J Comp Neurol* 224: 591-605.

Merzenich MM, Nelson RJ, Kaas JH, Stryker MP, Jenkins WM, Zook JM, Cynader MS, Schoppmann A. 1987. Variability in hand surface representations in areas 3b and 1 in adult owl and squirrel monkeys. *J Comp Neurol* 258: 281-296.

Moore CI, Nelson SB. 1998. Spatio-temporal subthreshold receptive fields in the vibrissa representation of rat primary somatosensory cortex. *J Neurophysiol* 80: 2882-2892.

Nelson RJ, Sur M, Felleman DJ, Kaas JH. 1980. Representations of the body surface in postcentral parietal cortex of *Macaca fascicularis*. *J Comp Neurol* 192: 611-643.

Nicolelis MAL, Dimitrov D, Carmena JM, Crist R, Lehew G, Kralik JD, Wise SP. 2003. Chronic, multisite, multielectrode recordings in macaque monkeys. *Proc Natl Acad Sci USA* 100: 11041-11046.

Rajan R. 1998. Receptor organ damage causes loss of cortical surround inhibition without topographic map plasticity. *Nat Neurosci* 1: 138-143.

Reed JL, Pouget P, Qi H-X, Zhou Z, Bernard MR, Burish MJ, Haitas J, Bonds AB, Kaas JH. 2008. Widespread spatial integration in primary somatosensory cortex. *Proc Natl Acad Sci USA* 105: 10233-10237.

Samonds JM, Allison JD, Brown HA, Bonds AB. 2003. Cooperation between Area 17 neuron pairs enhances fine discrimination of orientation. *J Neurosci* 23: 2416-2425.

Scarff CE, Scarff CW. 2007. Digital nerve blocks: more gain with less pain. *Australas J Dermatol* 48: 60-61.

Shoham S, Fellows MR, Normann RA. 2003. Robust, automatic spike sorting using mixtures of multivariate t-distributions. *J Neurosci Methods* 127: 111-122.

Turnbull BG, Rasmusson DD. 1990. Acute effects of total or partial digit denervation on raccoon somatosensory cortex. *Somatosens Mot Res* 7: 365-389.

Valvano MN, Leffler S. 1996. Comparison of bupivacaine and lidocaine/bupivacaine for local anesthesia/digital nerve block. *Ann Emerg Med* 27: 490-492.

Veredas FJ, Vico FJ, Alonso JM. 2005. Factors determining the precision of the correlated firing generated by a monosynaptic connection in the cat visual pathway. *J Physiol* 567.3: 1057-1078.

Waberski TD, Dieckhöfer A, Reminghorst U, Buchner H, Gobbelé R. 2007. Short-term cortical reorganization by deafferentation of the contralateral sensory cortex. *Neuroreport* 18: 1199-1203.

Waberski TD, Gobbelé R, Kawohl W, Cordes C, Buchner H. 2003. Immediate cortical reorganization after local anesthetic block of the thumb: source localization of somatosensory evoked potentials in human subjects. *Neurosci Lett* 347: 151-154.

Wall JT, Xu J, Wang X. 2002. Human brain plasticity: an emerging view of the multiple substrates and mechanisms that cause cortical changes and related sensory dysfunctions after injuries of sensory inputs from the body. *Brain Res Rev* 39: 181-215.

Werhahn KJ, Mortensen J, Van Boven RW, Zeuner KE, Cohen LG. 2002. Enhanced tactile spatial acuity and cortical processing during acute hand deafferentation. *Nat Neurosci* 5: 936-938.

Zeger SL, Liang K-Y. 1986. Longitudinal data analysis for discrete and continuous outcomes. *Biometrics* 42: 121-130.

CHAPTER VII

DISCUSSION

Although each chapter of this dissertation stands alone, this section integrates information across the chapters and specific aims. A summary of the main findings from each chapter is provided here, followed by an examination of how these results can be integrated into an overall view of spatiotemporal stimulus processing in the primate primary somatosensory cortex. Also included is a justification of the use of the common methods throughout the body of work, and a discussion of the research limitations. Finally, applications and future directions of this research are discussed.

Main Findings and Conclusions

Our main findings from our recordings of area 3b neuronal responses can be divided into three main categories: 1) results of single-site stimulation on the hand; 2) results of dual-site stimulation within one hand; and 3) how input from the two hands affects area 3b. For each chapter of the dissertation, we obtained responses to single-site stimulation, which were compared with responses to dual-site stimuli presented within the contralateral hand or were used to examine interhemispheric interactions.

Results of Single-Site Stimulation on the Contralateral Hand

To summarize the findings from single-site stimulation, responses of area 3b neurons to the 500 ms skin indentations within the minimal receptive field included transient excitatory onset responses, which could be followed by some response depression, a variable level of maintained activity, and often an offset response, depression, and a return to pre-stimulus levels of spontaneous activity. Many of the neurons we recorded appeared to have rapidly adapting-like characteristics and did not maintain high levels of activity throughout the skin indentation. When single-site stimulation occurred outside the minimal receptive field of a reference neuron, we found that responses could be absent or weakly excitatory, and in very rare occasions, could suppress spontaneous firing rates. The responses to single-site stimulation inside and outside the minimal receptive field were similar to those reported previously from area 3b neurons in anesthetized owl monkeys and macaque monkeys (Sur et al., 1984) and awake macaque monkeys (e.g., Towe and Amassian, 1958; Mountcastle et al., 1969; Gardner and Costanzo, 1980a,b; Burton et al., 1998; DiCarlo et al., 1998; Sripati et al., 2006). While there have been fewer studies of pairwise correlations between neurons in primary somatosensory cortex of monkeys, our correlation magnitudes during single-site stimulation were similar to those reported previously in anesthetized squirrel monkeys (Jain et al., 2001) and to those in primary somatosensory cortex of anesthetized cats (e.g., Alloway et al., 2002). When a single site on the contralateral hand was stimulated, we found that pairs of neurons had correlated spike times even when the distance between the electrodes exceeded 2 mm. Overall, the proportions of correlated pairs tended to decrease as the distance between the electrodes increased. (Chapter 2, Reed et al., 2008)

Results of Dual-Site Stimulation within the Contralateral Hand

The dual-site stimulus conditions used in these studies were selected to investigate temporal and spatial stimulus influences on neuron responses. As reported in Chapter 2 (Reed et al., 2008), we found that when nonadjacent digit or palm locations were stimulated simultaneously, pairs of neurons had correlated spike times across distances that covered nearly the entire length of the hand representation in owl monkeys. These results suggested that neuronal interactions can extend across nonadjacent digit representations, despite the lack of receptive fields that encompass nonadjacent digits in area 3b (e.g., Merzenich et al., 1978). This chapter provided initial evidence that intrahemispheric processing of stimuli likely involves integrating sensory input from across multiple digits or palm pad representations.

To extend our investigations beyond simultaneous dual-site stimulation, we adapted traditional condition-test paradigms to our stimulus parameters such that the onset of a conditioning stimulus occurred before the onset of a test stimulus. Typically, the stimuli used in these studies are short duration pulses so that the stimuli are not affecting the skin at the same time (e.g., Gardner and Costanzo, 1980b, Greek et al., 2003). We used a 500 ms duration stimulus and stimulus onset asynchronies of 0, 10, 30, 50, 100, and 500 ms. These onset asynchronies were chosen from previous studies (e.g., Gardner and Costanzo, 1980b, Greek et al., 2003) to determine what intervals might cause maximal interactions across the stimuli. To examine spatial stimulus influences on response properties, we selected paired stimulation locations on adjacent and nonadjacent digit or palm locations, as well as paired sites within a digit on adjacent and nonadjacent phalanges. These sites were selected to encompass paired sites on the hand and to

compare the effects of stimulation *within* digits to effects *across* digits to determine any spatial topography of the effects.

In Chapter 3, we investigated the spatiotemporal stimulus effects on the neuron properties of peak firing rate and response latency. Compatible with our initial study in Chapter 2 on spike timing correlations, we found that paired stimulation across nonadjacent digits can affect neuron responses, thus, we confirmed that spatial interactions were revealed by firing rate and latency measures. Additionally, we found a temporal gradient for stimulus interactions such that a preceding, non-preferred stimulus suppressed the response to the second, preferred stimulus when separated by a stimulus onset asynchrony of 30-50 ms. For the effects of spatial locations, we found that paired stimulation on adjacent digits resulted in greater peak firing rates than stimulation on adjacent phalanges within a digit, which was somewhat surprising considering that the density of intrinsic connections within the hand representation is particularly strong within a digit (Fang et al., 2002). This comparison of responses to stimulation presented within and across digits is new to the literature. Another addition we contributed to the literature was that of the "Response Field", which we used to characterize the relationship of the stimulus location to the response of a given neuron. We also introduced an adaptation of a modulation index that is typically used in multisensory research (e.g., Stanford et al., 2005; Alvarado et al., 2007) to categorize how the responses of neurons to paired stimuli compared to the response expected from the sum of the responses to the single sites alone. From this index, we determined that stimuli presented at onset asynchronies produced different response types in subsets of neurons across all four spatial stimulation categories, with suppressive modulation dominating when the onset

asynchronies were 30 ms or greater. Facilitative modulation was rare, but when it occurred, it occurred when stimulus onset asynchronies were between 0 and 30 ms. Thus, in this chapter we quantified spatiotemporal stimulus influences on neuron response properties when sites on one hand were stimulated.

Chapter 4 returned to correlations as the measure of interest, but expanded on Chapter 2 by including the spatiotemporal stimulus conditions described in Chapter 3. Correlations did not follow our predictions, but they were somewhat affected by spatiotemporal stimulus properties and still supported the hypothesis that widespread spatiotemporal interactions occur in area 3b. When paired stimulus sites were closer in spatial proximity, the proportions of correlated pairs were greater than when the paired stimuli were distant. However, correlation magnitudes did not follow predictable patterns in response to temporal onset asynchronies. The spatial proximity of the paired stimuli affected the correlation magnitude, but the relationship did not precisely follow that expected based on cortical connectivity between stimulus sites, as stimulation on separate, adjacent digit sites resulted in similar correlation magnitudes as stimulation on adjacent phalanges within one digit and greater correlation magnitudes than stimulation on nonadjacent phalanges within one digit and stimulation on nonadjacent digits. These results provided evidence that spatiotemporal integration in the form of spike timing correlations occurs at the level of area 3b in monkeys in ways which differed from patterns of firing rates.

How Input from the Two Hands Affected Area 3b

The first chapter to address interhemispheric interactions was Chapter 5, which described the effects on neuron firing rate and latency in response to bimanual stimulation. The temporal stimulation parameters matched those we used in experiments to stimulate the contralateral hand, but the spatial stimulation conditions were reduced in complexity because paired stimulation was applied to mirror sites or nonmirror sites on the two hands. The majority of responses in the primary somatosensory cortex were suppressed by paired stimulation. Maximal suppression occurred when the ipsilateral stimulus preceded the contralateral stimulus by 100 ms, and this was particularly strong when mirror locations were stimulated. We found a tendency for the effects of paired stimulation to be stronger when mirror locations were stimulated instead of nonmirror sites, but differences between stimulation on mirror and nonmirror locations were small. Our studies added temporal stimulus onset asynchronies and spatial stimulus categories not present in the literature previously. Previous studies reported primarily suppressive effects of ipsilateral stimulation on the response to contralateral stimulation (Burton et al., 1998; Tommerdahl et al., 2006), while our study revealed proportions of responses that were facilitated (~4%) or unchanged (~34%) relative to contralateral stimulation alone.

Chapter 6 addressed interhemispheric interactions with a study of acute de-afferentation of one digit and tactile stimulation on the opposite hand. This study was initiated based on reports of receptive field expansions in cortex following local anesthetic injections or digit amputation on the ipsilateral hand (e.g., Calford and Tweedale, 1990; Calford and Tweedale, 1991a,b). We sought to quantify the response properties that underlie the receptive field expansions, and.we found unexpected

heterogeneity of responses. This study included a comparison between normal animals and one monkey (case 5) that had experienced a partial digit amputation at least 4 years prior to the experiment. Despite the long-term injury, several aspects of the responses in case 5 resembled normal responses. Thus, this study provided quantitative analysis from three monkeys regarding the emergence of responses to contralateral stimulation following local anesthetic injections into an ipsilateral digit. The variations in the responses when the contralateral stimulation location matched the site of the ipsilateral injection compared to when the contralateral stimulation location did not match the ipsilateral injection site supported the findings of coarse somatotopy in other studies of interhemispheric interactions (e.g., Werhahn et al., 2002).

Synthesis

Intrahemispheric Processing in Primary Somatosensory Cortex

In this dissertation we have employed several methods to better understand tactile stimulus processing when only one hand is stimulated, with the focus on how neurons within the contralateral primary somatosensory cortex respond. Our studies on response properties of firing rate and latency can give us general information about stimulus interactions in cortex, which must have underlying anatomical substrates; and our studies on spike timing correlations between pairs of neurons relate to the underlying functional connections within the primary somatosensory cortex. Shorter latencies tended to occur in neurons with higher firing rates (Chapter 3). To simplify the discussion, we focused on comparing results from spike timing correlations and individual neuron firing rate

measures. Correlation magnitude is generally believed to be related to the firing rate (e.g., de la Rocha et al., 2007), since the more spikes two neurons fire, the more likely it will be that spikes will occur at the same time. However, correlations in spike timing could occur independently of firing rate, as we and others have found (for review, see Salinas and Sejnowski, 2001). The normalized JPSTH procedure that we used to determine the cross-correlations between neuron pairs took firing rate into account to determine the correlation magnitudes beyond those expected based on firing rates. Thus, when we examined our firing rate results (either the geometric mean firing rate of neuron pairs or individual neuron firing rates) we found that they did not precisely follow the same trends that we found for correlation magnitudes.

Even though firing rate suppression increased when the stimuli were separated in time, correlations did not decrease in magnitude and did not follow consistent patterns that matched the patterns in firing rates (Figure 7-1). Note that the correlations are measured across pairs of neurons, and these values are averaged across all correlated pairs (which could have any spatial locations within the area of cortex sampled by the 100-electrode array), while the population means of peak firing rates calculated from individual neurons are shown in Figure 7-1. For a more direct relationship between correlations of neuron pairs with firing rate, we calculated the geometric mean firing rate between the two correlated neurons. For geometric mean firing rate, the firing rate when adjacent phalanges were stimulated was less than when nonadjacent digits were stimulated across temporal stimulation conditions; however, the correlation magnitudes were slightly higher on average when adjacent phalanges were stimulated compared to when nonadjacent digits were stimulated (see Figure 4-9). This example shows that the

correlation magnitudes did not reflect simply the geometric mean firing rate of the two neurons in the pair. It appears that despite the magnitude of the geometric mean firing rate of neurons in the pair, correlation magnitudes were highest when adjacent digits were stimulated, followed by when adjacent phalanges were stimulated. Peak firing rates of individual single neurons did not show the same trend (Figure 7-1C, D). This pattern is not exactly what we would have predicted for effects mediated largely by intrinsic connections, based on the report that intrinsic connections are very dense within the digit representations and slightly less dense across digit representations (Fang et al., 2002). In accordance with these intrinsic connection patterns, we expected correlations would be stronger when sites within a single digit were stimulated and weakest when nonadjacent digits were stimulated. Similarly, we expected that paired stimuli would have the strongest effects on peak firing rate when the stimuli were presented within the same finger and would have weak to no effects when presented on nonadjacent digits. However, intrinsic connections are still likely substrates for these effects due to the gradient of the effects. It is possible that the dense connections within the digits also mediate lateral inhibition that reduces the firing rate and correlations when those two sites are stimulated together, similar to "in-field inhibition" described by Gardner and Costanzo (1980a,b) when multiple air puffs were presented to the forearm in unanesthetized macaque monkeys.

In summary, we applied three different measures to examine intrahemispheric processing of spatiotemporal stimulus information in primary somatosensory cortex. These measures quantify different properties of neurons, and here we discuss what the

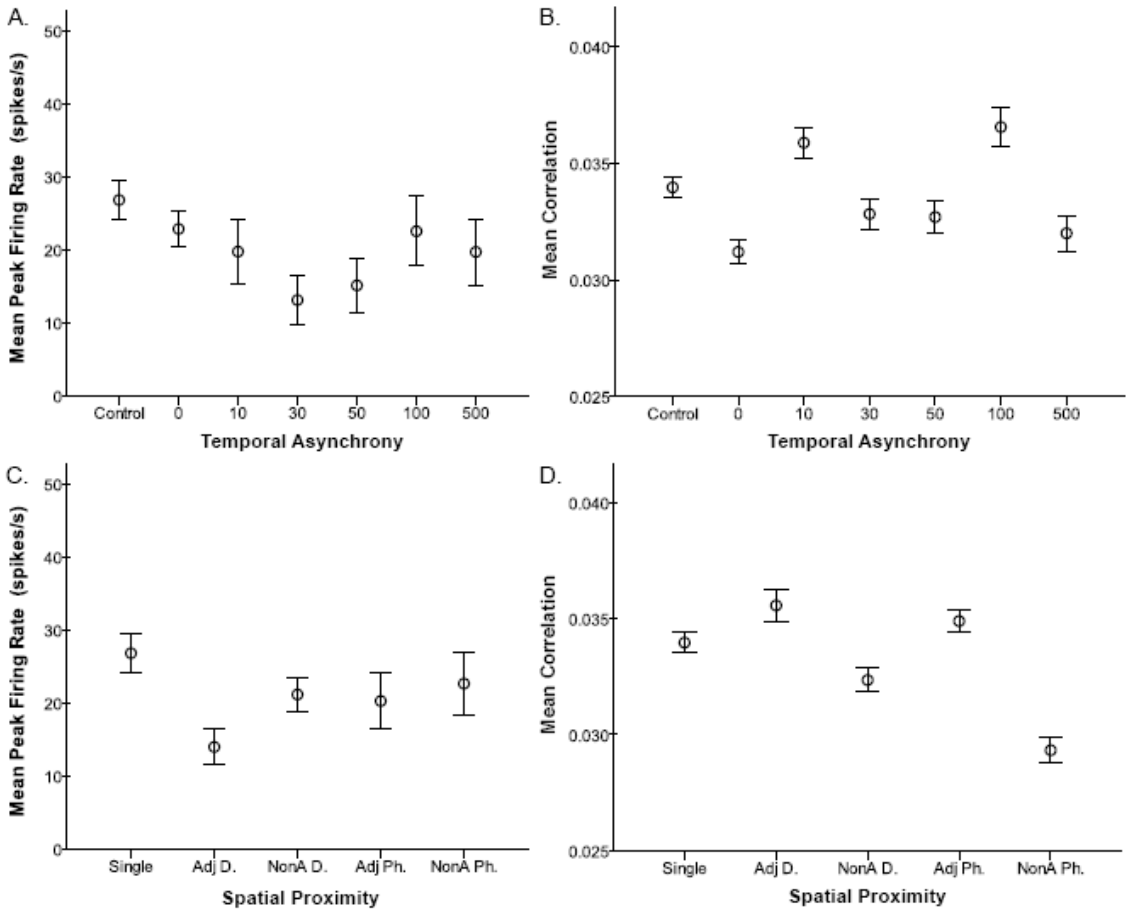

Figure 7-1. Comparison of trends in peak firing rates of single units and correlation magnitudes between pairs of single neurons for temporal and spatial stimulus relationships. Error bars are 95% confidence intervals for all panels. Markers indicate the means of the observed datasets (not statistical predicted values). A. Peak firing rates showed a clear decreasing trend when a non-preferred stimulus was presented before the preferred stimulus, with firing rates suppressed the most when the onset delays occurred at 30 and 50 ms. B. Correlation magnitudes did not follow the firing rate trends and varied within a small range in inconsistent patterns when stimuli were presented with selected stimulus onset delays. C. Peak firing rates of single neurons were suppressed when dual-site stimuli were presented compared to single-site stimuli. D. Correlation magnitudes did not follow the trends in firing rate due to the spatial relationship of stimuli. Stimulation on adjacent digits (Adj D.) and adjacent phalanges (Adj Ph.) resulted in slightly higher correlations than single-site stimulation (Single) and stimulation on nonadjacent digits (NonA D.) and nonadjacent phalanges within a digit (NonA Ph.).

combined information can reveal. The individual neuron measures of firing rate and latency are thought to be related, such that when firing rate increases, latencies tend to shorten (e.g., Boloori and Stanley, 2006). We have found that this relationship was not always strong, as firing rate and latency did not change together in many of the instances in our large sample, and we found a weak negative correlation between latency and peak firing rate ($\rho = -0.141$, $P < 0.0005$; see Chapter 3). Measures of firing rate and latency are associated with stimulus preferences of neurons and preference changes. Spike timing correlations are believed to be related to functional connectivity between neurons, how reliably information may be transmitted (for reviews, see Salinas and Sejnowski, 2001; Niebur et al., 2002), and may be related to stimulus properties in the somatosensory system (e.g., Zhang and Alloway, 2004, 2006).

What do the differences between the patterns in firing rate and the patterns in the correlation magnitudes tell us? Perhaps these differences could mean that firing rate and correlations can provide different information or serve different functions. Salinas and Sejnowski (2001) suggested that spike timing correlations (and oscillations) may control the strength of the neuronal signal rather than providing different information than the spike rate. Since the state of oscillatory activity in the brain is related to the likelihood of a neuron firing an action potential (e.g., Fetz et al., 2000), this role for correlations seems highly plausible. In addition, Samonds and Bonds (2005) found that gamma oscillation contributes to the maintenance of spike timing synchrony in cat primary visual cortex cells, and similar to Salinas and Sejnowski (2001), they suggested that maintained synchrony could aid in reliable transmission of the spiking information. There is also evidence that spike timing correlations may be related to encoding information from

complex stimuli, such as visual cocircular contours (Samonds et al., 2006 [cat]) and airjet motion (Zhang and Alloway, 2004, 2006 [rat whiskers]). Our study used relatively simple stimuli (single or paired skin indentations), rather than complex tactile stimuli resembling contours or movement arcs. However, correlation magnitudes appeared to relate to the spatial relationships of the paired stimuli (rather than the temporal relationships of the indentations). Thus, we suggest that our results examining the firing rates and latencies of single neurons and multi-unit clusters may be closely related to how stimuli affect individual neurons (or small groups of neurons), while the strength of the correlations may relate to how reliably that information is transmitted and provide some stimulus-related spatial information.

Interhemispheric Processing Compared to Intrahemispheric Processing in Primary Somatosensory Cortex

Integrating the results from our studies of intrahemispheric processing and inter-hemispheric processing produce a more complete picture of how area 3b functions. While we did not record neuron responses in two hemispheres simultaneously, we analyzed response magnitudes and response latencies under conditions in which one or both hemispheres were expected to contribute to the neuron response properties observed. Two main aspects of the intra- and interhemispheric studies were interesting to compare: the stimulus onset asynchrony that resulted in the maximum suppression of peak firing rate; and the distributions of response facilitation, suppression, and no change during dual-site stimulation.

Maximum Response Suppression

Our investigations of the temporal interaction effects were based on condition-test paradigms in animal studies, but also resemble "temporal masking" experiments performed in psychophysical studies in humans. Using temporal masking terminology, the first, conditioning stimulus in our experiments is the "masker" and the second, test stimulus is called the "target" stimulus. Temporal masking is greatest when the masker and the target are presented to the same location on the hand; however, masking is found when the two stimuli are presented to different locations on the same hand and on opposite hands (for review, see Craig, 2009). Human studies more often use vibratory stimuli rather than the pulse stimuli used in this dissertation, and these studies tend to find that when stimuli are presented on opposite hands, the greatest masking effect occurs when the stimuli are presented simultaneously (e.g., Craig, 2009, review). In contrast, our method using 0.5 s indentations that overlapped in time allowed us to determine differences between intrahemispheric and interhemispheric processing that are likely to relate to the underlying functional connectivity mediating the temporal masking effects at the level of neurons in primary somatosensory cortex.

The peak firing rate was suppressed most when the non-preferred stimulus on the contralateral hand preceded the preferred stimulus by 30 ms and 50 ms (Figure 3-4A). When the non-preferred stimulus was presented to the ipsilateral hand, the peak firing rate was suppressed most when the preferred contralateral stimulus was presented at 100 ms onset delay (Figure 5-5A). The difference in the onset delay resulting in maximal suppression for contralateral and bilateral stimuli implies that the full strength of the

suppression occurs when the delay of the second stimulus accounts for the time for the signals to travel to reach the reference neuron.

Distribution of Modulation Types

Dual-site stimulation within the contralateral hand and dual-site stimulation on the ipsilateral and contralateral hand resulted in large proportions of suppression, but also responses that were unchanged by the presence of the non-preferred stimulus. Somewhat surprisingly, both types of experiments resulted in small proportions of facilitated responses and these facilitations occurred primarily when the two stimuli were presented closely in time, between 0-30 ms (see Figures 3-6, 3-7, 5-8). The occurrence of facilitations during bimanual stimuli was surprising, based on the predominance of suppression reported under similar stimulus conditions (e.g., Burton et al., 1998; Tommerdahl et al., 2006), as discussed in Chapter 5. Additionally, the observation that facilitation occurred within the same stimulus onset asynchronies (0-30 ms) when paired stimuli were presented within one hand and when paired stimuli were presented to the two hands was unexpected. Instead, we expected that when the stimuli presented to the two hands, longer stimulation onset asynchronies would be required for facilitation to occur than when stimuli were presented within one hand. These findings for facilitation when bimanual stimuli were presented simultaneously and near-simultaneously indicate a relatively fast pathway is able to modulate the responses of area 3b neurons despite the sparse callosal connections between the hand representations of area 3b (Killackey et al., 1983).

Bimanual stimulation resulted in mostly response suppressions, while digital nerve block on the ipsilateral hand was associated with expanded receptive field sizes on the contralateral hand and stimulation on the contralateral hand resulted in increases in peak firing rates on average (although this effect was weak and variable). Nevertheless, these complementary effects of bimanual stimulation versus removal of a subset of ipsilateral inputs supports the idea that the local anesthetic injection results in disinhibition to allow receptive field expansion (for review, see Calford, 2002). A problem with the disinhibition theory to explain receptive field expansion and changes in responsiveness is that the possible source of tonic inhibition is unknown. C-fibers have been suggested as sources of tonic inhibition, but no C-fibers with tonic activity have been found (Calford, 2002, review).

Even without knowing the precise mechanism through which the two hemispheres interact to affect area 3b neurons, our studies revealed topographic effects that have not been described previously. Experiments using bimanual stimulation revealed slight differences in response properties between stimulating mirror locations on the two hands compared to nonmirror locations (Tables 5-1, 5-2; Figure 5-8). Local anesthetic injections revealed that contralateral stimulation on the digit that matched the ipsilateral anesthetized digit resulted in opposite effects compared to contralateral stimulation on a non-matching digit (Table 6-1; Figure 6-6). Since weakly somatotopic interhemispheric interactions were found under both experiment types, these results provide additional support to the prevailing theories that feedback projections mediate interhemispheric

interactions in area 3b rather than homotopic callosal connections (Calford, 2002, review).

Overall Integration

The series of studies included in this dissertation examined intrahemispheric and interhemispheric processing of tactile stimuli in primary somatosensory cortex of owl monkeys. The effects of surround modulation were studied in all experiments. In most experiments, at least one stimulus probe was placed in the surround of a given neuron's receptive field. In the experiments in which local anesthetic was delivered to an ipsilateral digit and single-site stimulation was provided to a contralateral location, we considered that anesthetic revealed the surround effects of the ipsilateral hand. All of these studies have shown that surround modulation of neurons in primary somatosensory cortex is extensive in time (stimulus onset asynchronies over 100 ms can suppress responses) and in space (stimulation on nonadjacent digits within one hand and even the opposite hand can affect responses). While these studies were not the first to suggest the presence of widespread spatiotemporal interactions in primary somatosensory cortex, this dissertation offers more quantification of these effects across additional stimulus parameters and categories beyond what has been previously reported.

Common Measures, Methods, Analyses, and Their Validities

Measures

Our primary measures included the individual neuron measures of response latency and response magnitude (peak firing rate) as well as the pairwise measure of spike timing correlations. We selected peak firing rate as our primary measure of firing rate (compared to average firing rate over a given time window) because this measure would provide common results for all types of excitatory responses. In particular, peak firing rate values were similar between rapidly-adapting (RA) responses and slowly-adapting (SA) responses, while average firing rates measured across the stimulus duration would have differed between the two response types. We originally categorized unit responses as RA- and SA-like based on methods by Leiser and Moxon (2006), but the units were not consistently categorized, as different stimuli caused responses of the same neuron to be RA- or SA-like. Average firing rate over a given response window would be greater for SA- than RA-like responses, and the firing patterns could change differentially due to different stimulation parameters. For universality and simplicity, we chose to investigate peak firing rate as the unit of the response magnitude. However, we collected average firing rates in addition to peak firing rates. Further analysis would be required to characterize the firing patterns and average firing rates over longer time windows and compare RA-like responses with SA-like responses.

Latency is a standard measurement; however, there is no single standard method for calculating latency in the literature. The method used depends on the brain region studied (e.g., low baseline activity versus high baseline activity) and the experimental

questions and methods. Therefore we selected a method to calculate latency that was similar to other methods (e.g., Tutunculer et al., 2006; Davidson et al., 2007) and produced appropriate results empirically. All of the latency calculations described in this dissertation followed the same methods involving the selection of firing-rate-based criteria to determine the response latency. We also compared our method to another method and found similar latency values, described as follows. On a subset of data (all of the recordings from monkey 1 and half of the recordings from monkey 2), we used a "Poisson surprise index" to determine latency based on the average time when bursts of spikes occurred that deviated from expectations based on Poisson processes. This routine was written for Matlab and provided by Dr. Pierre Pouget (then at Vanderbilt University) and was based on Poisson spike train analysis from Hanes et al. (1995). The original Matlab code was written by Dr. Chenchal Subraveti, then P. Pouget provided modifications, and final modifications were made by the dissertation author. When the maximum response occurred within our window of interest, these two latency measures were well-correlated. However, because the Poisson surprise latency measure was not able to restrict the burst analysis to a small time window, this measure would identify responses that were outside our region of interest (e.g., the "off" response instead of the "on" response). The latency measure used in this dissertation coincided with the response latencies determined by visual inspection, was usually similar to the values determined by the Poisson surprise index, and resulted in numerical values within normal latency ranges reported in monkey primary somatosensory cortex (e.g., Hsiao et al., 2009, review). Additionally, we used the same latency calculation consistently throughout this body of work; therefore, we have confidence that the summary analyses from latency

calculations are reasonable indicators of the effects of spatiotemporal stimulus conditions on excitatory response latency.

Multiple methods exist to calculate spike timing synchrony; however, the cross-correlation derived from the JPSTH is well-established (e.g., Aertsen et al., 1989; Gerstein and Kirkland, 2001). We included only single units in our analysis of the changes in the correlation magnitudes due to varying spatio-temporal stimulation (Chapter 4); thus, we eliminated the difficulty of interpreting multi-unit correlations (e.g., Bedenbaugh and Gerstein, 1997; Gerstein, 2000). We focused on the presence of correlations and changes in the magnitude of the peak of the cross-correlation histogram. While our correlation magnitudes were low, they were within the ranges commonly reported (e.g., Roy and Alloway, 1999; Steinmetz et al., 2000; Alloway et al., 2002). There are several additional aspects of neuronal synchrony that may be analyzed using these data, including: the lag times of the peak in the correlations; the patterns in the coincidence histograms; and effects beyond the 0 ms diagonal, such as the presence of oscillations. We found that significant peaks in the cross-correlation histograms occurred at 0 ms lag times with 10 ms bins for our data, which may not be surprising given that the majority of the electrodes were recording from the same cortical area and the same cortical layer. Additional analyses and improved methods for examining correlated firing between two or more neurons could be applied to this data set in the future.

Experimental Methods and Data Classification

We performed common methods throughout the experiments of this dissertation which helped to examine spatiotemporal interactions and classify the data. In a typical

experiment, we stimulated single locations on the hand, and we stimulated paired locations simultaneously and at stimulus onset asynchronies. When we used stimulus onset asynchronies, our experiments resembled condition-test paradigms in which the conditioning stimulus is presented prior to the test stimulus. This condition provided our examination of how temporal stimulus relationships influenced neurons in the contralateral primary somatosensory cortex. We selected specific values for stimulus onset asynchronies based on those used by Gardner and Costanzo (1980b) and Greek, Chowdhury, and Rasmusson (2003) to examine a range of temporal intervals. We included the 500 ms onset delay, which was a longer delay than other studies had tested, so that we would include a wide range of intervals and to use the same parameters to explore intra- and interhemispheric interactions.

To examine how spatial stimulus relationships influenced neurons, we stimulated paired sites on the hand that varied in their proximity within digits and across digits. Other studies have investigated the effects of stimulation on adjacent digits and nonadjacent digits (e.g., Friedman et al., 2008), but this work extended to stimulation on adjacent and nonadjacent phalanges within a single digit. We also classified the relationship of the stimulus to the Response Field, a category that we developed that is similar to the receptive field as determined by firing rate. This measure was similar to the qualitative measure of receptive fields described by Tutunculer et al. (2006).

We classified units as single units and multi-units, based on waveform isolation using offline spike sorting tools. In most experiments, we included single units and multi-units in the statistical analysis to determine if these categories of units were different from each other. Across all of the experiments, we found that the means of the multi-unit

measures were different from the means of the single unit measures. However, classification as a single unit or multi-unit did not significantly affect the way that units responded to the spatiotemporal stimuli. For measures of pairwise spike timing correlations, only single units were analyzed. While multi-unit cross-correlations can be more sensitive to detect relationships than single unit cross-correlations, changes in the correlations can be difficult to interpret since the number of cells recorded in the multi-units on each electrode could change, affecting the correlation value (Bedenbaugh and Gerstein, 1997). Since the focus of Chapter 4 was how the correlations change with stimulus conditions, we selected only single unit neuron pairs for the analysis.

Summary Analysis Methods

Data from each experiment were compiled in order to analyze the contributions to the variance in the observed measures of peak firing rate, response latency, or correlation magnitude. We followed a similar analysis strategy for all experiments because the data were collected simultaneously from the 100 electrodes in the array and were collected over time. Occasionally, neuron signals would be lost over the course of an experiment, or new neuron signals would be gained, leaving gaps in the time series of a given neuron. These gaps were considered missing observations. When a given neuron was recorded throughout a time series (such as all control stimulation and dual-site stimulation), the responses of that neuron during one stimulus block are likely to be related (or correlated) to the responses of that neuron during the next stimulus block. Thus, the errors in statistical predictions of these data are likely to be correlated. This knowledge led to

investigating analysis methods that have not been commonly described in neurophysiological literature.

In many other analysis methods typically used by neurophysiologists, individual neuronal recordings are typically considered independent observations, which meet the assumptions of parametric or nonparametric analysis of variance (ANOVA). However, simultaneously recorded neurons are likely to be correlated in their response properties, as outlined by Kenny and Judd (1986) and reviewed in Appendix A. Longitudinal clustered or correlated data are better analyzed using methods that do not require improper assumptions to be met regarding the independence of observations and the statistical distribution; therefore, we used Generalized Estimating Equations analysis introduced by Liang and Zeger (1986) for our simultaneously recorded data. While this method has not been commonly applied to neurophysiological data, its use is an improvement over traditional ANOVA of linear model theory when the data may not be normally distributed and when the observations are expected to be correlated rather than independent (e.g., Liang and Zeger, 1986; Zeger and Liang, 1986; Hardin and Hilbe, 2003). For a detailed description of Generalized Estimating Equations analysis and its applications for analyzing large-scale neuronal recording data, refer to Appendix A.

Research Limitations

At the time this research was conducted, the 100-electrode "Utah" array was increasingly used for studies in animals and humans, particularly related to applications for brain-computer-interfaces (e.g., Maynard et al., 1997; Buzsáki, 2004; Normann et al.,

2009). As this particular array was patented in 1994, perfecting its use and developing techniques to analyze the data obtained through the array recordings were still in relatively early stages of development (e.g., Nordhausen et al., 1994, 1996). The large numbers of neurons that could be simultaneously recorded using the 100-electrode array was an advance over previous array technologies; however, several complications arise from such recordings, many of which have been reviewed elsewhere (e.g., Gerstein and Kirkland, 2001; Buzsáki, 2004). One such complication is the large amount of time and computational resources required for procedures including spike sorting, calculating appropriate variable measures, and summarizing the data statistically. This dissertation relied on mostly well-established measures and analysis methods; however, methods appropriate to large-scale neuronal data recordings were applied with an eye to the current advances. Thus, this section explains some limitations of the methods applied in this dissertation, and briefly discusses alternate methods of analysis and future questions that could be addressed from these data.

Experiments were performed on anesthetized and paralyzed monkeys, which provided the benefits of stable recording conditions, prevention of the hand from moving during stimulus trials, and elimination of fluctuations in attention levels and other factors. However, experiments performed in anesthetized animals may not provide the same results as experiments performed in unanesthetized animals. Given the complications with training monkeys for somatosensory experiments in the awake state, we chose to perform experiments in anesthetized animals in order to describe the basic responses without the confounds of attention and other behavioral effects. Some of our effects were similar to those seen in unanesthetized macaque monkeys (e.g., Gardner and Costanzo,

1980a,b; Burton et al., 1998) and correspond well to results in awake humans (e.g., Tanosaki et al., 2002; Werhahn et al., 2002; Braun et al., 2005).

Individual neuron response properties including firing rate and response latency have been long-studied, especially from individual single-electrode recordings. The typical method of performing such single-electrode studies has involved the repeated presentation of a stimulus (or behavior-inducing event) in order to accumulate an average response of the neuron studied. This method assumes the likely scenario in which a postsynaptic neuron receives input from multiple single neurons that behave in similar ways, thus the averages accumulated in the peristimulus time histograms (PSTHs) theoretically reflect a population effect (e.g., Gerstner and Kistler, 2002). Although we recorded from a population of neurons simultaneously, we continued to follow the traditional method of accumulating average responses to repeated stimulus presentations, rather than attempting to "decode" stimulus information from the activity of multiple neuron responses within a single stimulus trial. While single-trial analysis of multiple neuron response is a worthy achievement to understand neuronal coding (Quiroga and Panzeri, 2009, review), complications in the interpretation of the results and in the implementation of the available analysis methods kept us from choosing such methods as our research focus. Rather than decoding the stimulus parameters from the population of neuronal responses, we asked how the stimulus parameters affect the response properties of neurons within the population.

Studying response magnitude and latency using the traditional PSTH-based methods appears to neglect some of the interesting aspects of neuronal population recording. Some may ask, "How is this analysis of simultaneously recorded data different

from accumulating many individual neuron recordings?" In some ways, the analyses used in this dissertation resemble those that would be used for individually recorded neuron responses. However, there are important differences in the way that these data were analyzed that are unique to simultaneous recordings. Specifically, individual neuronal recordings are traditionally considered independent observations and the contributions to the variance in the dependent variables of interest are then estimated using parametric or nonparametric ANOVA. Our experimental design was a repeated-measures design in which the same neurons were tested across several different stimulus conditions that were compared. Additionally, our data did not always appear to be drawn from a normal distribution. Therefore, our simultaneous recording data were better analyzed using Generalized Estimating Equations (e.g., Liang and Zeger, 1986; Zeger and Liang, 1986) to address the potential correlations among the clustered data. Thus, simultaneously recorded data required different analysis methods than individually recorded data allows, even when the dependent variables of interest (such as response magnitude and latency) were collected in traditional ways. There are alternative methods besides Generalized Estimating Equations analysis to apply to large-scale neuronal recordings, depending on the research question. A limitation of this research may be that we did not perform alternative analyses; however, some alternative methods could be applied to these data in the future to fully utilize these data. Several alternative analysis methods for simultaneous neuronal recordings are briefly reviewed in Appendix A.

Our use of traditional measures rather than exploring neuronal coding methods may be a limitation of this work. We described and quantified the occurrence of "spatiotemporal integration" without calculations based on information theory and other

neuronal coding strategies (e.g, Quiroga and Panzeri, 2009, review). An important point to clarify is how we can infer that widespread spatiotemporal integration occurs using our analysis of response properties without employing information theory. While the previous chapters of this dissertation were designed to address this question, it is worth the time to make the answer concrete. Individual neuron response properties may not come to mind when one thinks about neuron population analysis and widespread spatiotemporal integration. However, the key point in all of the chapters regarding neuronal response properties is that by using two stimuli, one in a non-preferred location and a second in a preferred location for a given neuron, interactions are revealed when the non-preferred stimulation affects the responses to the preferred stimulation. When a non-preferred stimulus that is presented far away in space or time from a preferred stimulus affects the neuron's response, spatiotemporal interaction related to the stimulus parameters has occurred. Thus, even by using traditional measures, we were able to investigate complex properties that occur in neuronal populations and determine how focal or widespread the interactions are, and this was aided by the ability to record from many neurons simultaneously.

In addition to measures described above, measures beyond individual neuron response properties should be studied using simultaneous recordings, and we studied one such measure out of the many possibilities. We examined the correlation coefficient derived from the joint peristimulus time histogram (JPSTH) analysis as a measure of the spike timing synchrony between two neurons. This method has been well-established, and we used a variation of the procedure by Aertsen et al. (1989), as described in Chapter 2. Simultaneous recordings are the only direct way to obtain spike timing correlations

between two neurons, and this method has been used to estimate the underlying functional connectivity between pairs of neurons within a population. We used JPSTH analysis to determine how spatiotemporal stimulation parameters may change the presence and magnitude of these functional connections. This traditional method is only designed to compute pair-wise interactions between neurons and is not able to quantify higher-order interactions between three or more neurons in the population, which may be a limitation.

Several other methods introduce the ability to identify clusters of three or more neurons with correlated firing and spike times, including those used by Bonds and colleagues (e.g., Samonds et al., 2003 [type analysis]; Bernard, 2008, p. 51-58 [dissertation introducing "PSP method"]) and NeuroXidence developed by Pipa et al. (2008) to detect excess or deficiency of joint spike timings in two or more neurons. Other methods can reveal clusters of correlated neurons but are more difficult to apply to quantitative analyses, or require subsequent analysis after clusters are identified, or still include pair-wise comparisons as their basis. Such methods include gravitational clustering (e.g., Gerstein and Aertsen, 1985; Baker and Gerstein, 2000) and various analyses involving hierarchical clustering (e.g., Eggermont, 2006; Hosoda et al., 2009). Additional methods to analyze large-scale neuronal recording data have been discussed by Kralik et al. (2001) and Pereda et al. (2005). We were interested in the effects of spatiotemporal stimulation on neuronal measures rather than identifying specific neuronal ensembles within each monkey that may have been active during the stimulations. JPSTH analysis allowed us to reveal some of the effects of spatiotemporal stimulation on neuron

pairs in our samples; however, we may be missing information by not having the capability of analyzing higher-order interactions through this method.

Since we were interested in how the functional connectivity (even between neuron pairs) may be affected by the spatiotemporal parameters of stimulation, we applied the Generalized Estimating Equations analysis to our dependent variable of the correlation coefficient in order to determine the spatiotemporal factors that account for the variance observed in this measure. As analysis methods are further developed, even the data we have already collected could be analyzed in new ways to extract information to better characterize spatiotemporal stimulation effects on small populations of neurons in area 3b. Thus, this work lays a foundation and points to promising directions for future studies.

Applications and Future Directions

This body of research has direct applications that the Kaas laboratory will pursue. Currently, we are comparing the response properties of neurons and spike timing correlations of neuron pairs in normal monkeys to those in monkeys who sustained injury to the dorsal column (sensory pathway) of the spinal cord (Qi et al., 2009 [abstract]). Additionally, we are comparing the properties of spike waveforms (i.e., duration, amplitude) between normal monkeys and monkeys after dorsal column injury. In these studies, lesions are made in the cervical spinal cord to disrupt the transmission of sensory information from part or all of the hand to the brain, with every effort made to keep the ventral spinal cord (motor pathway) intact. This procedure initially disrupts motor

behavior, as monkeys prefer not to use the hand from which they have no tactile sensation; however, behavioral training restores the hand use in behavioral tasks to normal or near-normal levels (e.g., Darian-Smith, 2009, review). In additional experiments that have not commenced, we plan to provide treatment beyond behavioral training for subsets of monkeys. These treatments are intended to promote the recovery of the spinal cord after injury and will be based on methods performed by Kaas and colleagues (2008) and others (Fawcett, 2009, review). We will be able to determine if the animals recover faster behaviorally and determine when and if neurons in the primary somatosensory cortex return to near-normal levels of responsiveness across the groups of monkeys. Some of the findings from this dissertation will be directly compared to findings in monkeys with spinal cord injuries, and all of our findings will be used to inform our predictions and analyses of the data recorded from primary somatosensory cortex neurons in monkeys after injury.

Beyond this work that we plan to pursue immediately, the knowledge gained from this research will be useful for understanding normal somatosensory cortical processing and for relating normal findings to human neurological conditions such as recovery from nerve injury and phantom limb syndrome. This dissertation work quantified aspects of surround modulation, including ipsilateral signals as contributing to surround modulation in primary somatosensory cortex of owl monkeys. Surround modulation has not been a well-studied aspect of somatosensory processing, and in the context of our passive stimulation experiments in anesthetized animals, such modulation was not related to attention (Burton and Sinclair, 2000; Hupe et al., 2001), but may have been related to how stimuli are perceived within a context rather than in isolation (e.g., Allman et al.,

1985; Albright and Stoner, 2002). The results from this dissertation apply to the underlying effects that occur in absence of conscious processing, and future studies can compare these effects in anesthetized animals to those that occur in awake, behaving animals to determine the differential contributions.

The work within this dissertation was intended to guide investigations of widespread integration that occurs during somatosensory processing. The effects of spatiotemporal stimulation are important for understanding normal somatosensory processing as well as understanding existing substrates for recovery from injury. In addition to the further analyses we have suggested could be performed on these existing data, we suggest that further studies could be performed in different brain regions, including the thalamus, to investigate the contributions of these regions to the stimulus integration effects. The contribution of feedback projections to the responses in the brain region of interest could be further elucidated with regional blocking studies, such as those performed by Chowdhury and Rassmusson (2003) in raccoon primary somatosensory cortex. Even the fine anatomical connectivity within the hand representation could be studied further with microiontophoretic injections of neuronal tracers, and the connection patterns could be compared to the observed cross-correlations and response properties recorded from the region of interest. An abstract presented at the Society for Neuroscience meeting in October combined optical imaging with neuronal tracer injections into area 3b in squirrel monkeys (Negyessy et al., 2009); therefore, studies comparing such anatomical connectivity results with functional connectivity results appear to be imminent. Several aspects of the anatomical and functional relationships between neurons in the somatosensory hand representation await full characterization. As

it is acquired, this knowledge will aid in the understanding of normal somatosensory processing of information from the hand and in how sensation and use of the hand may be recovered following injuries.

References

Aertsen AMHJ, Gerstein GL, Habib M, Palm G. 1989. Dynamics of neuronal firing correlation: modulation of "effective connectivity". *J Neurophysiol* 61:900-917.

Albright TD, Stoner GR. 2002. Contextual influences on visual processing. *Annu Rev Neurosci* 25: 339-379.

Allman J, Miezin F, McGuinness E. 1985. Stimulus specific responses from beyond the classical receptive field: Neurophysiological mechanisms for local-global comparisons in visual neurons. *Annu Rev Neurosci* 8: 407-430.

Alloway KD, Zhang M, Dick SH, Roy SA. 2002. Pervasive synchronization of local neural networks in the secondary somatosensory cortex of cats during focal cutaneous stimulation. *Exp Brain Res* 147: 227–242.

Alvarado JC, Vaughan JW, Stanford TR, Stein BE. 2007. Multisensory versus unisensory integration: contrasting modes in the superior colliculus. *J Neurophysiol* 97: 3193-3205.

Baker SN, Gerstein GL. 2000. Improvements to the sensitivity of gravitational clustering for multiple neuron recordings. *Neural Comput* 12: 2597-2620.

Bedenbaugh P, Gerstein GL. 1997. Multiunit normalized cross correlation differs from the average single-unit normalized correlation. *Neural Comput* 15: 1265-1275.

Bernard MR. 2008. Coding of natural features by neuronal synchronization in primary visual cortex. Ph.D. diss., Vanderbilt University.

Boloori AR, Stanley GB. 2006. The dynamics of spatiotemporal response integration in the somatosensory cortex of the vibrissa system. *J Neurosci* 26: 3767-3782.

Braun C, Hess H, Burkhardt M, Wühle A, Preissl H. 2005. The right hand knows what the left hand is feeling. *Exp Brain Res* 162: 366-373.

Burton H, Sinclair RJ. 2000. Tactile-spatial and cross-modal attention effects in the primary somatosensory cortical areas 3b and 1-2 of rhesus monkeys. *Somato Mot Res* 17: 213-228.

Burton H, Sinclair RJ, Whang K. 1998. Vibrotactile stimulus order effects in somatosensory cortical areas of rhesus monkeys. *Somatosens Mot Res* 15: 316-324.

Buzsáki G. 2004. Large-scale recording of neuronal ensembles. *Nat Neurosci* 7: 446-451.

Calford MB. 2002. Dynamic representational plasticity in sensory cortex. *Neuroscience* 111: 709-738.

Calford MB, Tweedale R. 1990. Interhemispheric transfer of plasticity in the cerebral cortex. *Science* 249: 805-807.

Calford MB, Tweedale R. 1991a. Acute changes in cutaneous receptive fields in primary somatosensory cortex after digit denervation in adult flying fox. *J Neurophysiol* 65: 178-187.

Calford MB, Tweedale R. 1991b. Immediate expansion of receptive fields of neurons in area 3b of macaque monkeys after digit denervation. *Somatosens Mot Res* 8: 249-260.

Chowdhury SA, Rasmusson DD. 2003. Corticocortical inhibition of peripheral inputs within primary somatosensory cortex: the role of GABAA and GABAB receptors. *J Neurophysiol* 90: 851-856.

Craig JC. 2009. Somatosensory perception. In *Encyclopedia of Neuroscience*, ed. LR Squire, 91-96. Amsterdam: Elsevier.

Darian-Smith C. 2009. Somatosensory plasticity. In *Encyclopedia of Neuroscience*, ed. LR Squire, 99-110. Amsterdam: Elsevier.

Davidson AG, O'Dell R, Chan V, Schieber MH. 2007. Comparing effects in spike-triggered averages of rectified EMG across different behaviors. *J Neurosci Methods* 163: 283-294.

De la Rocha J, Doiron B, Shea-Brown E, Josić K, Reyes A. 2007. Correlation between neural spike trains increases with firing rate. *Nature* 448: 802-807.

DiCarlo JJ, Johnson KO, Hsiao SS. 1998. Structure of receptive fields in area 3b of primary somatosensory cortex in the alert monkey. *J Neurosci* 18: 2626-2645.

Eggermont JJ. 2006. Properties of correlated neural activity clusters in cat auditory cortex resemble those of neural assemblies. *J Neurophysiol* 96: 746-764.

Fang P-C, Jain N, Kaas JH. 2002. Few intrinsic connections cross the hand-face border of area 3b of new world monkeys. *J Comp Neurol* 454: 310-319.

Fawcett JW. 2009. Spinal cord regeneration and functional recovery: strategies. In *Encyclopedia of Neuroscience* ed. LR Squire, 303-308. Amsterdam: Elsevier.

Fetz EE, Chen D, Murthy VN, Matsumura M. 2000. Synaptic interactions mediating synchrony and oscillations in primate sensorimotor cortex. *J Physiol (Paris)* 94: 323-331.

Friedman RM, Chen LM, Roe AW. 2008. Responses of areas 3b and 1 in anesthetized squirrel monkeys to single- and dual-site stimulation of the digits. *J Neurophysiol* 100: 3185-3196.

Gardner EP, Costanzo RM. 1980a. Spatial integration of multiple-point stimuli in primary somatosensory cortical receptive fields of alert monkeys. *J Neurophysiol* 43: 420-443.

Gardner EP, Costanzo RM. 1980b. Temporal integration of multiple-point stimuli in primary somatosensory cortical receptive fields of alert monkeys. *J Neurophysiol* 43: 444-468.

Gerstein GL. 2000. Cross-correlation measures of unresolved multi-neuron recordings. *J Neurosci Methods* 100: 41-51.

Gerstein GL, Aertsen AMHJ. 1985. Representation of cooperative firing activity among simultaneously recorded neurons. *J Neurophysiol* 54: 1513-1528.

Gerstein GL, Kirkland KL. 2001. Neural assemblies: technical issues, analysis, and modeling. *Neural Netw* 14: 589-598.

Gerstner W, Kistler WM. 2002. *Spiking neuron models: single neurons, populations, plasticity*. New York: Cambridge University Press. Available online. http://icwww.epfl.ch/~gerstner/SPNM/node1.html.

Greek KA, Chowdhury SA, Rasmusson DD. 2003. Interactions between inputs from adjacent digits in somatosensory thalamus and cortex of the raccoon. *Exp Brain Res* 151: 364-371.

Hanes DP, Thompson KG, Schall JD. 1995. Relationship of presaccadic activity in frontal eye field and supplementary eye field to saccade initiation in macaque: Poisson spike train analysis. *Exp Brain Res* 103: 85-96.

Hardin JW, Hilbe JM. 2003. *Generalized estimating equations*. Boca Raton: Chapman and Hall/CRC.

Hosoda K, Watanabe M, Wersing H, Körner E, Tsujino H, Tamura H, Fujita I. 2009. A model for learning topographically organized parts-based representations of objects in visual cortex: topographic nonnegative matrix factorization. *Neural Comput* 21: 2605-2633.

Hsiao SS, Fitzgerald PJ, Thakur PH, Denchev P, Yoshioka T. 2009. Somatosensory receptive fields. In *Encyclopedia of Neuroscience* ed. LR Squire, 111-119. Amsterdam: Elsevier.

Hupe JM, James AC, Girard P, Lomber SG, Payne BR, Bullier J. 2001. Feedback connections act on the early part of the responses in monkey visual cortex. *J Neurophysiol* 85: 134-145.

Jain N, Qi H-X, Kaas JH. 2001. Long-term chronic multichannel recordings from sensorimotor cortex and thalamus of primates. Chapter 5 In *Progress in Brain Research*, ed. MAL Nicolelis, 130: 1-10. Amsterdam: Elsevier Science B.V.

Kaas JH, Qi HX, Burish MJ, Gharbawie OA, Onifer SM, Massey JM. 2008. Cortical and subcortical plasticity in the brains of humans, primates, and rats after damage to sensory afferents in the dorsal columns of the spinal cord. *Exp Neurol* 209: 407-416.

Kenny DA, Judd CM. 1986. Consequences of violating the independence assumption in analysis of variance. *Psychol Bull* 99: 422-431.

Killackey HP, Gould HJ, III, Cusick CG, Pons TP, Kaas JH. 1983. The relation of corpus callosum connections to architectonic fields and body surface maps in sensorimotor cortex of new and old world monkeys. *J Comp Neurol* 219: 328-419.

Kralik JD, Dimitrov DF, Krupa DJ, Katz DB, Cohen D, Nicolelis MAL. 2001. Techniques for long-term multisite neuronal ensemble recordings in behaving animals. *Methods* 25: 121-150.

Liang K-Y, Zeger SL. 1986. Longitudinal data analysis using generalized linear models. *Biometrika* 73: 13-22.

Leiser SC, Moxon KA. 2006. Relationship between physiological response type (RA and SA) and vibrissal receptive field of neurons within the rat trigeminal ganglion. *J Neurophysiol* 95: 3129-3145.

Maynard EM, Nordhausen CT, Normann RA. 1997. The Utah Intracortical Electrode Array: a recording structure for potential brain-computer interfaces. *Electroencephalogr Clin Neurophysiol* 102: 228-239.

Merzenich MM, Kaas JH, Sur M, Lin CS. 1978. Double representations of the body surface within cytoarchitectonic areas 3b and 1 in "SI" in the owl monkey (Aotus trivirgatus). *J Comp Neurol* 181: 41-74.

Mountcastle VB, Talbot WH, Sakata H, Hyvarinen J. 1969. Cortical neuronal mechanisms in flutter-vibration studied in unanesthetized monkeys. Neuronal periodicity and frequency discrimination. *J Neurophysiol* 32: 452-484.

Negyessy L, Friedman R, Chen LM, Dillenburger BC, Palmer CT, Jákli B, Cserey G, Roe AW. Intrinsic and extrinsic connections of fingertip representation in the somatosensory cortex of the squirrel monkey. Program No. 656.12. 2009 Neuroscience Meeting Planner. Chicago, IL: Society for Neuroscience, 2009. Online.

Niebur E, Hsiao SS, and Johnson KO. 2002. Synchrony: a neuronal mechanism for attentional selection? *Curr Opin Neurobiol* 12: 190-194.

Nordhausen CT, Maynard EM, Normann RA. 1996. Single unit recording capabilities of a 100 microelectrode array. *Brain Res* 726: 129-140.

Nordhausen CT, Maynard EM, Normann RA. 1994. Optimizing recording capabilities of the Utah Intracortical Electrode Array. *Brain Res* 637: 27-36.

Normann RA, Greger BA, House P, Romero SF, Pelayo F, Fernandez E. 2009. Toward the development of a cortically based visual neuroprosthesis. *J Neural Eng* 6: 035001.

Pereda E, Quiroga RQ, Bhattacharya J. 2005. Nonlinear multivariate analysis of neurophysiological signals. *Prog Neurobio* 77: 1-37.

Pipa G, Wheeler DW, Singer W, Nikolić D. 2008. NeuroXidence: reliable and efficient analysis of an excess or deficiency of joint-spike events. *J Comput Neurosci* 25: 64-88.

Qi H, Reed JL, Gharbawie OA, Burish MJ, Zhou Z, Bernard MR, Bonds AB, Kaas JH. Spinal cord injury and multiple approaches of evaluation: behavioral consequences, neuronal response properties in deprived somatosensory cortex, and immunocytochemical changes in the brainstem and spinal cord. Program No. 563.9. 2009 Abstract Viewer/Itinerary Planner. Washington DC: Society for Neuroscience 2009. Online.

Quiroga RQ, Panzeri S. 2009. Extracting information from neuronal populations: information theory and decoding approaches. *Nat Rev Neurosci* 10: 173-185.

Roy SA, Alloway KD. 1999. Synchronization of local neural networks in the somatosensory cortex: a comparison of stationary and moving stimuli. *J Neurophysiol* 81: 999–1013.

Salinas E, Sejnowski TJ. 2001. Correlated neuronal activity and the flow of neural information. *Nat Rev Neurosci* 2: 539-550.

Samonds JM, Allison JD, Brown HA, Bonds AB. 2003. Cooperation between area 17 neuron pairs enhances fine discrimination of orientation. *J Neurosci* 23: 2416-2425.

Samonds JM, Bonds AB. 2005. Gamma oscillation maintains stimulus structure-dependent synchronization in cat visual cortex. *J Neurophysiol* 93: 223-236.

Samonds JM, Zhou Z, Bernard MR, and Bonds AB. 2006. Synchronous activity in cat visual cortex encodes collinear and cocircular contours. *J Neurophysiol* 95: 2602-2616.

Sripati AP, Yoshioka T, Denchev P, Hsiao SS, Johnson KO. 2006. Spatiotemporal receptive fields of peripheral afferents and cortical area 3b and 1 neurons in the primate somatosensory system. *J Neurosci* 26: 2101-2114.

Stanford TR, Quessy S, Stein BE. 2005. Evaluating the operations underlying multisensory integration in the cat superior colliculus. *J Neurosci* 25: 6499-6508.

Steinmetz PN, Roy A, Fitzgerald PJ, Hsiao SS, Johnson KO, Niebur E. 2000. Attention modulates synchronized neuronal firing in primate somatosensory cortex. *Nature* 404: 187–190.

Sur M, Wall, JT, Kaas JH. 1984. Modular distribution of neurons with slowly adapting and rapidly adapting responses in area 3b of somatosensory cortex in monkeys. *J Neurophysiol* 51: 724-744.

Tanosaki M, Suzuki A, Takino R, Kimura T, Iguchi Y, Kurobe Y, Haruta Y, Hoshi Y, Hashimoto I. 2002. Neural mechanisms for generation of tactile interference effects on somatosensory evoked magnetic fields in humans. *Clin Neurophysiol* 113: 672-680.

Tommerdahl M, Simons SB, Chiu JS, Favorov O, Whitsel BL. 2006. Ipsilateral input modifies the primary somatosensory cortex response to contralateral skin flutter. *J Neurosci* 26: 5970-5977.

Towe AL, Amassian VE. 1958. Patterns of activity in single cortical units following stimulation of the digits in monkeys. *J Neurophysiol* 21: 292-311.

Tutunculer B, Foffani G, Himes BT, Moxon KA. 2006. Structure of the excitatory receptive fields of infragranular forelimb neurons in the rate primary somatosensory cortex responding to touch. *Cereb Cortex* 16: 791-810.

Werhahn KJ, Mortensen J, Van Boven RW, Zeuner KE, Cohen LG. 2002. Enhanced tactile spatial acuity and cortical processing during acute hand deafferentation. *Nat Neurosci* 5: 936-938.

Zeger SL, Liang K-Y. 1986. Longitudinal data analysis for discrete and continuous outcomes. *Biometrics* 42: 121-130.

Zhang M, Alloway KD. 2004. Stimulus-induced intercolumnar synchronization of neuronal activity in rat barrel cortex: a laminar analysis. *J Neurophysiol* 92: 1464–1478.

Zhang M, Alloway KD. 2006. Intercolumnar synchronization of neuronal activity in rat barrel cortex during patterned airjet stimulation: A laminar analysis. *Exp Brain Res* 169: 311-325.

APPENDIX A

STATISTICAL ANALYSIS OF LARGE-SCALE NEURONAL RECORDING DATA

This appendix reproduces the work submitted by Reed JL and Kaas JH to *Neural Networks* on October 1, 2009 as an invited paper for a special issue on "Analysis and modeling of massively parallel neural signals".

Abstract

Relating stimulus properties to the response properties of individual neurons and neuronal networks is a major goal of sensory research. Many investigators implant electrode arrays in multiple brain areas and record from chronically implanted electrodes over time to answer a variety of questions. Technical challenges related to analyzing large-scale neuronal recording data are not trivial. Several analysis methods traditionally used by neurophysiologists do not account for dependencies in the data that are inherent in multi-electrode recordings. In addition, when neurophysiological data are not best modeled by the normal distribution and when the variables of interest may not be linearly related, extensions of the linear modeling techniques are recommended. A variety of methods exist to analyze correlated data, even when data are not normally distributed and the relationships are nonlinear. Here we review expansions of the Generalized Linear Model designed to address these data properties. Such methods are used in other research fields, and the application to large-scale neuronal recording data will enable investigators to determine the variable properties that convincingly contribute to the variances in the observed neuronal measures. Standard measures of neuron properties such as response magnitudes can be analyzed using these methods, and measures of neuronal network

activity such as spike timing correlations can be analyzed as well. We have done just that in recordings from 100-electrode arrays implanted in the primary somatosensory cortex of owl monkeys. Here we illustrate how one example method, Generalized Estimating Equations analysis, is a useful method to apply to large-scale neuronal recordings.

1. Introduction

1.1 Motivation

Recording large-scale neuronal data in vivo is an expanding field; however, methods that can best describe and quantify the results of these recordings are essential to utilizing these data. Our laboratory with our colleagues have implanted multi-electrode arrays into somatosensory and motor regions of the cortex in non-human primates (e.g., Nicolelis et al., 1998; Jain et al., 2001; Reed et al., 2008), and we recognize the challenges that performing such experiments and analyzing these data present. Data can be analyzed in traditional ways, treating simultaneous neuron recording as an efficient means of increasing the sample size of neurons recorded from each monkey at a time. However, these traditional analyses rely on the assumption that the data collected from each neuron is independent, which may not be a valid assumption. Thus, we intend to introduce alternative analysis methods that may not be widely considered or used in current neurophysiological research. From in vivo recordings, computational neuroscientists often make neural network models that can include complex properties of real neurons, such as the dependence of the observed firing rate on the spiking history (e.g., Lewi, Butera, and Paninski, 2009). Such models have been used to understand the

properties of individual neurons considered in isolation from the recorded population (e.g., Pei et al., 2009) as well as to understand network properties (e.g., Deadwyler and Hampson, 1997, review). Here, we review selected methods for analyzing the variance of in vivo recording measures of large-scale neuronal populations, while we intend for neural network modeling to be addressed by others (maybe some in this special issue).

We believe this review will be helpful as the special circumstances of large-scale neuronal recordings are not currently well-recognized in the literature. In particular, we focused on two extensions of the Generalized Linear Model (McCullagh and Nelder, 1989), the Generalized Estimating Equations (Liang and Zeger, 1986; Zeger and Liang, 1986) and the Generalized Linear Mixed Models (e.g., Laird and Ware, 1982; Searle, Casella, and McCulloch, 1992), as practical methods of estimating the contributions of selected factors to the variance in the dependent measures of interest due to the existence of correlations inherent in large-scale recording experiments. A Pubmed search for "generalized estimating equations" produced 1648 hits on September 1, 2009. However, a Pubmed search for "neuron generalized estimating equations" produced 6 hits. A Pubmed search for "neuron generalized linear model" resulted in 56 hits, but most of these articles focused on neuronal network models rather than ways to analyze data collected in vivo for the contributions to the variance in the dependent variables. Forms of the Generalized Linear Models are already commonly used to model individual neuron properties, with recent examples from Lewi, Butera, and Paninski (2009) and Song et al. (2009). Without a full review of the content of each hit from the search, it is still clear that few neuroscientists are applying the Generalized Linear Model to their data for analysis of variance. We hope that a straightforward review of analysis methods and

practical considerations for their use will aid researchers in making decisions about how to analyze the complex data sets obtained from large-scale neuronal recordings.

1.2 Use of Generalized Linear Model Analysis in Other Research Fields

Reviews have been written for other fields to explain and encourage the use of the Generalized Estimating Equations, Generalized Linear Mixed Models, and other extensions of the Generalized Linear Models. Edwards (2000) described both Generalized Estimating Equations and Generalized Linear Mixed Models analyses for biomedical longitudinal studies. Other examples include behavioral research (Lee et al., 2007); ecology (Bolker et al., 2008); epidemiology (Hanley et al., 2003); psychology and social sciences (Tuerlinckx et al., 2006); and even political science (Zorn, 2001) and organizational research (Ballinger, 2004). Within most of these reviews, the term "subjects" is applied to people (patients, participants in research, etc.) for the purpose of statistical analysis of "between-subjects" or "within-subjects" effects on the variance of the dependent variable of interest. The term "subjects" is a general one, and for longitudinal data or other studies with clustered observations, it refers to the variable for which observations may be correlated (with respect to standard errors). In many neurophysiological studies, subjects are individual neurons. These neurons are nested within individuals, monkeys, in our case. This situation is analogous to studies in which human participants are nested within communities, for example. Most neurophysiological studies, especially those on non-human primates, provide the number of animals used in the experiment, but pool all of the neurons across animals so that the number of subjects for analysis of variance is large (number of neurons) instead of small (number of

animals). By incorporating the nested effects of neurons within animals, neurophysiologists can continue to investigate neurons as subjects without violating important statistical assumptions (e.g., Kenny and Judd, 1986) as long as appropriate measures are used to try to account for the likely correlations within subjects. Section 2 of this review describes this issue and how extensions of the Generalized Linear Model can be used to address multielectrode recording data. Now that these methods are becoming more widely used in other fields and many options for these analyses are included in commercially available statistical software packages, re-introducing Generalized Estimating Equations and Generalized Linear Mixed Models analysis for applicability to parallel neural recordings appears to be overdue.

2. Complexities of Parallel Neuronal Recording Data and How to Address Them

2.1 Complexities of Parallel Neuronal Recordings and Experimental Designs

The use of multi-electrode array to simultaneously record from small populations of neurons allows neuroscientists to study how neural ensembles may work (e.g., Buzsáki, 2004, review) and has played a role in the study of brain-machine-interfaces for neuroprosthetics (e.g., Chapin, 2004, review). There are diverse questions that can be addressed using large-scale neuronal recordings. Here, we consider issues that typically apply to such studies. While individual experiments will have specific design considerations, many designs are aimed at recording the responses of large numbers of individual neurons in order to relate changes in activity to specific sensory or behavioral conditions. Some sensory experiments can be more easily performed in anesthetized animals than in awake animals, while behavioral experiments require animals to behave

in the awake state. All of our experiments have been performed in lightly anesthetized animals.

Experiments can also be divided into "chronic" and "acute" recording categories. We have implanted microwire multi-electrode arrays chronically for long-term studies in primary somatosensory and primary motor cortex of squirrel monkeys (Jain et al., 2001), and we have implanted the 100-electrode silicon "Utah" array in primary somatosensory cortex of owl monkeys (Reed et al., 2008) for acute studies (in which the electrodes are not fixed permanently as for animal recovery experiments). New World monkeys (such as squirrel monkeys and owl monkeys) are often used for multielectrode recording studies because many cortical areas of interest are available on the cortical surface rather than buried in a sulcus. We chose owl monkeys because the area of interest in our case, area 3b, is not buried in the central sulcus, and the somatosensory cortex has been well studied (e.g., Cusick et al. 1989; Garraghty et al. 1989; Merzenich et al. 1978; Nicolelis et al. 2003). The acute recording experiment is a relatively simple design that still requires special consideration. In such experiments, recordings are made from the multiple electrodes implanted in one subject during a single experiment, and data are collected from multiple subjects to obtain the sample population of neuronal recordings. A common, but more complicated experiment is the chronic or longitudinal recording experiment. In such experiments, electrodes are chronically implanted so that the position of the electrodes is the same over time, and the recordings are made periodically over an extended time, which sometimes encompasses a period in which changes are expected to occur (e.g., Jain et al., 2001). For example, long-term recordings could be made in behaving animals before learning a task and after learning a task or before and after

injury or treatment. Even in acute experiments, signals from the same neurons can be recorded under different conditions within the recording session, but unlike chronic recording studies, these neurons are not tracked over months of time. As the ability to track neuronal signals over days to months becomes more reliable (such as through the recent single neuron stability assessments introduced by Dickey et al., 2009), analysis methods concerned with the complexities of longitudinal recordings will increase in importance.

From a practical standpoint, these data require advanced techniques to process the signals to isolate single neuron signals from multi-neuron clusters (called "spike sorting"), careful organization and data management, and high-level analysis techniques. These data can be analyzed in traditional ways by looking at neurons individually for their response properties or looking at correlations across neurons. Often "snapshots" of neuronal activity distributed across the electrode arrays are generated from these data (e.g., Rousche et al., 1999 (rat whisker representation); Ghazanfar and Nicolelis, 1999 (rat whisker representation); Reed et al., 2008 (monkey hand representation); however, how such snapshots can be analyzed rather than described has not been clear. Snapshot of peak firing rates across the 100-electrode array in the primary somatosensory cortex hand representation of one owl monkey under two different conditions is shown in Figure A-1 as an example to illustrate changes that can be visualized.

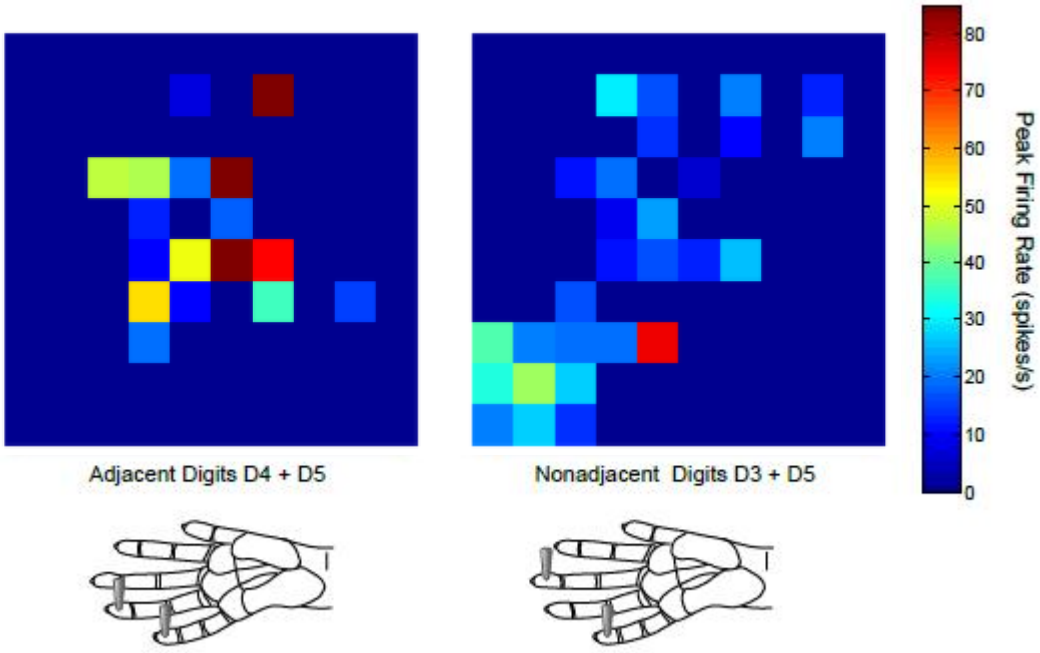

Figure A-1. Snapshots of activity recorded from a 100-electrode array under two different stimulation conditions. Activity snapshots were plotted in color maps of the peak firing rate measured across the 10 x 10 electrode array in monkey 3. Each square represents an electrode in the array and the color indicates the peak firing rate value during the 50 ms response window. Electrodes from which no significant responses (firing rate increases over baseline) were obtained during the stimulations shown are indicated in dark blue (no squares). The lower schematics indicate the locations of the stimulus probes on the owl monkey hand. Left panel shows the activity when adjacent digit locations on digit 4 (D4) and digit 5 (D5) were stimulated simultaneously (0 ms temporal onset asynchrony). Right panel shows the activity when nonadjacent digit locations on digit 3 (D3) and D5 were stimulated simultaneously. Differences between the patterns of activity during the two stimulation conditions are obvious and can easily be described visually, but quantitative measures are desired.

In somatosensory research, we are interested in contributions to the responses from stimulation across different parts of the skin to different parts of the brain. How neurons may integrate information from within and outside of their receptive fields is one question we ask to determine how the cortex processes tactile stimuli. Our research seeks to address how stimuli presented with varying spatial and temporal relationships affect neuron response properties in primary somatosensory cortex to reveal widespread stimulus integration. Here the term "widespread interaction" applies to when the effects of stimuli on the neurons occur when the stimuli are presented widely separated in space or time. We therefore categorize our stimulus parameters to use as predictor variables for analysis of variance (ANOVA) when we analyze these data to quantify spatiotemporal stimulus interactions. Data from both acute and chronic recording studies have properties that differ from those assumed by typical ANOVA procedures based on linear model theory. In the following sections, we illustrate properties of parallel neuronal recordings that could be better analyzed by extensions of the Generalized Linear Model. We have selected a particular route for analyzing the data, which we justify and illustrate in the following sections.

2.2 Correlated Instead of Independent Observations in Multi-Neuron Recordings

The data from large-scale neuronal recordings are likely to be correlated, but the types of correlations may vary depending on the experiment. Generally, the neuronal signals recorded during even acute experiments without repeated measures designs are best considered to be correlated rather than independent observations. Specifically, the errors in the predictions of the neuronal measures may be correlated. This violates the

assumption of linear model theory that the error is distributed independently with a zero mean and constant variance (Gill, 2001, p. 2). Biologically, correlations could take the form of the neurons in a particular brain area behaving similarly under the given experimental conditions since they are likely to be interconnected; thus, within each experimental human or animal subject, the neuron measures are correlated rather than independent. In a chronic recording experiment, measures of an individual neuron recorded at one time would also be expected to correlate with measures of the same neuron recorded at a later time. Many traditional analyses disregard the likely correlations and assume that each neuron measure is an independent observation. Most analyses also tend to assume that individual subjects do not vary enough to prevent pooling of the neuronal data between subjects without regard to subject identity. This may prove to be a reasonable assumption, but it seems worth testing as appropriate methods for accounting for non-independence have been developed.

An important article on the topic of assuming that neuron responses are independent observations in analysis of variance was published by Kenny and Judd in 1986. The review focused on identifying "nonindependent" observations and examining the consequences of violating the independence assumption of analysis of variance (ANOVA). When neurons are used as subjects and observations made from these neurons under different stimulus conditions are assumed to be independent in order to meet the assumptions of linear model theory, possible bias in the analysis can arise. Here we briefly recall the main points from Kenny and Judd (1986). Three main types of nonindependence were identified for typical neurophysiological recordings: "nonindependence due to groups", "nonindependence due to sequence", and

"nonindependence due to space". Nonindependence due to groups refers to correlations between members of a functional group; perhaps all of the neural responses collected from one subject will be grouped and slightly different from all of the responses collected from a second subject. Or perhaps neurons within an individual subject are linked in functional groups and these neurons will have similar responses and differ from other neurons outside the functional group. Nonindependence due to sequence will occur when observations are taken from the same neuron unit over time, as it is likely that observations taken close together in time will be more similar than observations that are separated by more time. Finally, nonindependence due to space occurs when neighbors in space are more similar than neurons farther away spatially; which is a reasonable assumption for most brain areas.

Kenny and Judd (1986) and others have demonstrated the general consequences of violating the assumption of independence; therefore, we do not repeat the derivations, but summarize the key points. When these effects of nonindependence are ignored, bias in the mean square for the independent variable and in the mean square for error can affect the F ratios in ANOVA and alter the type I errors in either direction (Kenny and Judd, 1986). Treating neurons collected from individual animals as independent greatly increases the sample size, and when between-subjects differences are the measures of interest, the type I errors (false positives) can be increased (e.g., Snijders and Bosker, 1999, p. 15). When within-subject differences are of interest, the type I errors can be too low (e.g., Snijders and Bosker, 1999, p. 16). To illustrate this situation, if the data are correlated but analyzed as though they are independent, the estimate of the variance may be larger than the estimate that would be obtained when the correlation is is included in

the analysis; and this affects the hypothesis testing (e.g., Fitzmaurice, Laird, and Ware, 2004, p. 44). When nonindependence due to groups (e.g., nesting of neurons within monkeys) is ignored, the bias introduced depends on the real correlation and the true effect of the independent variables on the dependent variables, as demonstrated in detail by Kenny and Judd (1986). Thus, parallel neuronal recording experiments with or without repeated measures within neurons should be analyzed using methods that take into account the potential for neuron measures to be correlated in the ways outlined by Kenny and Judd (1986).

2.3 Distribution Assumption May Be Violated By Neural Recording Data

The distribution assumption of linear model theory may be violated by parallel recordings of neuronal activity (i.e., it is not universally true that neuronal recording data are non-normally distributed). When the data do not fit the normal (Gaussian) distribution, the generalized linear model extends the linear model theory to accommodate measures which were drawn from non-normal distributions (Gill, 2001, p. 2) to select a variety of distributions from the exponential family of distributions (Hardin and Hilbe, 2003, p. 7-8). To be clear, the term "exponential family" does not imply restrictive relationship to the exponential probability density function. Instead, this refers to a method in which the terms in the probability functions are moved to the exponent to transform the functions to a common notation that is mathematically useful (Gill, 2001, p. 9-10). A "link function" is added to generalized linear models to define the relationship between the linear predictor and the expected value from the mean of the dependent variable (e.g., Zeger and Liang, 1986; Gill, 2001, p. 30; Hardin and Hilbe, 2003, p. 7-8).

Thus, the generalized linear model should be used when the distribution of the dependent variable is believed to be non-normal or even discontinuous, as in the binomial distribution; and when the relationship between the dependent variable and the predictor variables may not be linear (e.g., McCullagh and Nelder, 1989, review).

Models of the data will fit better when the appropriate probability distribution and link functions are selected, and the best fitting parameters can be tested within the model analysis. One can perform Kolmogorov-Smirnov tests and create Probability-Probability plots to assess whether the experimental distribution differs from the normal distribution (or other distributions). Inappropriate distribution and link function choices may result in under- or over-estimating the predicted values. One can use the Generalized Linear Models analyses since these methods generalize to data distributions beyond the normal distribution.

2.4 How to Analyze Neural Recording Data to Avoid Violating Assumptions

Given some examples in this section of the ways in which large-scale neuronal recording data can differ from the assumptions of standard linear model theory, the alternative methods should be able to account for these violations or be robust in the face of violations. We review two extensions of generalized linear models that are well-suited options for analyzing the sources variance associated with measures of interest from parallel neuronal recordings. Generalized Estimating Equations analysis was developed for longitudinal studies to account for the presence of clustered or correlated data (e.g., Liang and Zeger, 1986; Zeger and Liang, 1986; Hardin and Hilbe, 2003). Similarly, Generalized Linear Mixed Models can be used for clustered data and unbalanced

longitudinal studies, particularly when effects within subjects are of experimental interest (review, Breslow and Clayton, 1993; tutorial, Cnaan, Laird, and Slasor, 1997). Such methods should be considered for large-scale neuronal recordings, specifically due to the presence of correlated data as outlined by Kenny and Judd (1986) and for cases in which the data are not normally distributed (e.g., count data).

Recording studies can take advantage of repeated-measures or longitudinal experimental design and the inherent correlations can be accounted for using the Generalized Estimating Equations analysis and Generalized Linear Mixed Models. Around the same time that the Kenny and Judd (1986) article was published, the Generalized Estimating Equations analysis was introduced by Liang and Zeger (1986) for analysis of longitudinal data that were not necessarily normally distributed; however, neurophysiologists did not adopt the new method. The title of this article, "Longitudinal data analysis using generalized linear models" may not have revealed its potential significance to analyzing non-independent or correlated data to neurophysiologists. Generalized Linear Mixed Models analysis was introduced even earlier than Generalized Estimating Equations; and article titles such as, "Random-effects models for longitudinal data" by Laird and Ware in 1982 did not reveal relevance to neurophysiologists, particularly at a time when longitudinal or repeated measures studies were not widely performed in neurophysiology. The term "longitudinal data" in the titles may not have signaled to non-statisticians that the articles focused on alternative analyses for data that violate the independence assumption of linear model theory (while informed readers would be aware that "longitudinal" implied "non-independent" in statistical terms). In addition, perhaps the concerns of non-independence of observations seemed more

relevant to data from human behavioral research than from neuronal data. Thus, while these methods have not been conspicuously applied to neurophysiological data over the years since their development, these methods based on the Generalized Linear Model have been (and are currently) actively researched by statisticians and are currently used in other research fields, as highlighted in Section 1.2.

For the remainder of this article, we explain why the Generalized Estimating Equations and Generalized Linear Mixed Models analyses meet these criteria for alternative methods to analyze parallel recording data and the differences between the two approaches (Section 3). We then illustrate the use of Generalized Estimating Equations analysis with neurophysiological data from our experiments in Section 4. There are multiple alternative analysis methods depending on the research question, some of which are discussed in Section 5; however, we focus on Generalized Estimating Equations and Generalized Linear Mixed Models as two practical methods.

3. Generalized Estimating Equations and Generalized Linear Mixed Models Analysis for Neuronal Recordings

3.1 Comparisons of Generalized Estimating Equations and Generalized Linear Mixed Models

Both Generalized Estimating Equations and Generalized Linear Mixed Models use the correlation or covariance between observations when modeling longitudinal data. Longitudinal studies can be generally divided into two categories which affect their analysis. In the first category, the experimental focus is on how predictor variables influence the dependent variable, and the number of subjects must be larger than the number of observations per subject. In the second category, the experimental focus is on

the correlation or within-subjects effects, and the number of experimental subjects may be small. (Diggle et al., 2002, p. 20) Generalized Estimating Equations are well-suited to address the first category of experiments and Generalized Linear Mixed Models are well-suited to address the second category.

These methods have several differences and fall into separate categories of the basic extensions of generalized linear models. Generalized Estimating Equations is categorized as a marginal method which allows interpretation of population-average effects. Mixed models are random effects models which allow both the population effects and subject specific effects to be interpreted. (e.g., Edwards, 2000) Regarding the issue of correlated error in the data observations within subjects, dependence can be considered an interesting focus to be investigated or a nuisance that must be taken into account to properly investigate between subjects (Snijders and Bosker, 1999, p. 6-8). How non-independence is regarded by the investigator depends on the research questions. Generalized Estimating Equations regards dependence as a nuisance; thus, Generalized Estimating Equations may be the analysis method of choice when population-average effects between subjects are of interest. Mixed models include random effects for the within-subject variables and dependence within these effects is regarded as a characteristic of interest. Mixed models are preferred when within- subject effects are important to answer the research questions. In practical use, Generalized Linear Mixed Models can better handle multi-level correlations and complexity than Generalized Estimating Equations in conventional software packages, but Generalized Estimating Equations are robust to mis-specification of correlation structure (e.g., Tuerlinckx et al., 2006). When the data are normally distributed and related to the prediction with the

(linear) identity link, then the difference between the solutions from the two methods is slight. But when the data are non-normal and nonlinear, there can be differences in the results derived from the two methods.

Generalized Estimating Equations analysis requires large sample sizes, and Generalized Linear Mixed Models are preferred for small samples. Generalized Estimating Equations may underestimate the variance in the samples and have inflated type I errors (false positives) when the number of subjects with repeated observations is less than 40 (e.g., Kauermann and Carroll, 2001; Mancl and DeRouen, 2001; Lu et al., 2007). However, Lu et al. (2007) compared two correction methods (Kauermann and Carroll, 2001; Mancl and DeRouen, 2001) for small samples using Generalized Estimating Equations analysis and proposed corrections that may perform well when the number of samples (with repeated observations) is 10 or greater. The repeated measures taken within these samples should be balanced (taken at specific time points across subjects) and as complete as possible (few missing observations) when using the Generalized Estimating Equations approach. Neurophysiological experiments may comply with these guidelines better than some studies requiring observations from human subjects at strict time points.

It is not uncommon to have missing observations in any experiment, and Generalized Estimating Equations analysis and Generalized Linear Mixed Models have slight differences in their tolerances for missing data. Generalized Estimating Equations can account for missing values; however, the missing values are assumed to occur completely at random (MCAR) and without intervention by the investigator, the routine will proceed with an analysis of only complete observations (e.g., Hardin and Hilbe,

2003, p. 122). This method is still likely to be appropriate when the data are missing due to a dropout process (like losing the neuronal signal for the last observations in a series) if the process is not related to the parameters of interest (Hardin and Hilbe, 2003, p. 127). Generalized Linear Mixed Models is mathematically valid for data missing at random (MAR) and MCAR data. MAR is the term applied when the mechanism that causes the missing observations does not depend on the unobserved data. MCAR refers to the case when the probability of an observation being missing does not depend on the observed or the unobserved data (e.g, Hardin and Hilbe, 2003, p. 122-123). The problem when the missing data are "nonignorable" or are missing in a non-random pattern (MNAR) is briefly discussed in Section 5.2 on "Limitations". Here we focus on analyses that can be performed using the methods commonly available in statistical software for more widespread applicability, but readers are encouraged to investigate alternatives and extensions appropriate for the data.

3.2 Note on Practicality of Use

An incomplete list of software packages that contain commands for the Generalized Estimating Equations routine include SAS (SAS Institute Inc.), SPSS (SPSS Inc.), and Stata (Stata Corp). For a review of software for performing Generalized Estimating Equations analysis, see Horton and Lipsitz (1999). Note that their 1999 review excluded SPSS, which currently includes the Generalized Estimating Equations analysis. While these same software packages also have versions of linear mixed modeling analysis, SPSS does not currently allow users to choose probability distributions, thus, the linear model based on the normal distribution is the only option.

See Bolker et al. (2008) for a list of software packages for Generalized Linear Mixed Models analysis. Each software package has different directions and implementations, and the current review does not specify the steps to perform the analysis for each package. However, the ability for researchers and students to employ the Generalized Estimating Equations and Generalized Linear Mixed Models through the use of standard statistical software makes these methods relatively practical for widespread use to analyze large-scale neuronal recordings, particularly with the help of statisticians as needed.

4. Illustration of Use of Generalized Estimating Equations for Neuronal Recording Data

For our research question, we selected Generalized Estimating Equations instead of Generalized Linear Mixed Models for a few reasons. Our research question was specific to population average effects and we did not intend to determine neuron-specific predictions for our effects. Of a practical consideration, our data were highly complex and large numbers of neurons were sampled from a small number of monkeys, and this proved computationally challenging for our software and memory available on our computer to run linear mixed modeling. In addition, one feature of the Generalized Estimating Equations that we have highlighted is the ability to consistently estimate the parameters even when the correlation structure is mis-specified, as we illustrate in this section. For other research situations, including those related to subject-specific effects, Generalized Linear Mixed Models analysis is recommended.

Here we assume that data has been collected and measures of relevance have been determined. In many situations, the relevant neuronal data include the spike timings relative to some event. From this information, typical measures of response magnitude (firing rate) and response latency can be determined, along with measures of network activity such as the simple pairwise spike timing correlation. We obtained these measures from our recordings using a 100-electrode array (Reed et al., 2008). We measured neuron responses to several stimulation conditions over short periods of time and our simultaneously recorded neuronal data were likely to be correlated, we selected the Generalized Estimating Equations analysis to investigate the sources of the variance related to these neuron responses while accounting for the aspect of correlation that was most important in our experiment: the correlation within individual neurons measured over short periods of time. Generalized Estimating Equations are not able to "nest" measures within neurons within monkeys; however, we were able to allow the data dependencies within the repeated measures to differ in the three monkeys we studied rather than assuming that the repeated measures in all three monkeys had equivalent relationships. We related categorical factors (or predictor variables) to the variance observed in the measure of interest, peak firing rate. Our interest is directed toward the spatiotemporal stimulus effects on neuron response properties. Thus, our experiments involved presentations of paired stimuli that varied in spatial and temporal characteristics in relation to each other and to the Response Fields of the neurons. (These predictor variables are described in Section 4.2.) Based on the literature in somatosensory systems research, we formulated several hypotheses. We expected that when two stimuli were presented to locations on the hand with different temporal onset asynchronies, the

presence of the first, non-preferred stimulus would suppress the response (decrease the peak firing rate) to the second, preferred stimulus. Four measures of the temporal onset asynchronies were tested in each neuron: 0 ms, 30 ms, 50 ms, and 100 ms in a balanced design. The location of the paired stimulus probes may affect the peak firing rate of neurons, since stimuli close in proximity could have a suppressive or additive effect on the peak firing rate. Since neuron firing rates are related to the location of stimuli within their receptive fields, we predicted that when both stimulus probes were outside the Response Field, the peak firing rate would be low. When one stimulus probe was inside the Response Field and the other probe was outside the Response Field, we predicted that the peak firing rate would be higher, and the highest peak firing rates would occur when both stimulus probes were inside the Response Field. Finally, since all three of these effects act in concert, we expected possible interactions between these factors. For example, the spatial proximity could affect which level of the temporal onset asynchrony condition caused the greatest suppression, and the relationship of the stimulus probes to the Response Fields could affect these firing rate decreases.

For simplicity in this example, we focused on only one neuronal response property: response magnitude in the form of peak firing rate (spikes/s). Peak firing rate measures were calculated using Matlab and were collected from 100-electrode arrays implanted in three different monkeys in which varying spatiotemporal stimuli were presented to the monkeys' hands over the course of 2-3 days while the monkeys were anesthetized. Data were compiled in Excel (Microsoft) and imported into SPSS 17.0 for summary statistical analysis. Generalized Estimating Equations routines were performed

to determine the convincing contributions to the variance in the peak firing rate measures. The details are described in the remainder of this section.

4.1 Methods to Obtain Example Data

Procedures followed the guidelines established by the National Institutes of Health and the Vanderbilt University Animal Care and Use Committee. Three adult owl monkeys (*Aotus trivirgatus*) were prepared for electrophysiological recordings in primary somatosensory cortex as previously described (Reed et al., 2008, Reed et al., submitted). Animals were anesthetized with propofol and paralyzed with vecuronium bromide and artificially ventilated with a mixture of N_2O: O_2: CO_2 (75: 23.5: 1.5) during surgery to implant the electrode array and during experimental recordings. The 100-electrode array (Cyberkinetics, now Blackrock Microsystems, Salt Lake City, UT) was acutely implanted using a pneumatic inserter set to 600 μm depth, so that the electrode tips were expected to be within layer 3 of anterior parietal cortex. Recordings were made continuously for 2-3 days from each anesthetized monkey.

As previously described (Reed et al., 2008), recording data was acquired via the Bionics Data Acquisition System (now Blackrock Microsystems), and signals were amplified by 5000 and band-pass filtered between 250 Hz and 7.5 kHz. The waveforms were sampled at 30 kHz for 1.5 ms windows.

Computer-controlled mechanical stimulation was provided to the hand using two independent force- and position-feedback controlled motor systems (300B, Aurora Scientific Inc., Aurora, ON, CA), with contact made by round Teflon probes, 1 mm in diameter. Pulse stimuli that indented the skin 0.5 mm for 0.5 s, followed by 2.0 s off of

the skin were presented for at least 100 trials (~ 4 min). These stimuli were selected for experimental purposes beyond the scope of this review, but in general were selected to investigate how spatiotemporal stimulus relationships affected neuron response properties. For complete methods and details for obtaining the example data, see Reed et al. (2008).

4.2 Pre-Processing Methods for the Sample Data Set

The first step after obtaining extracellular recordings is to spike sort the data, and we performed spike sorting procedures offline as described previously (Reed et al., 2008). Spike sorting separates the data from each electrode into signals from single neuron units and multi-unit clusters. Data were then analyzed using programs written in Matlab (The Mathworks, Natick, MA) to determine the baseline firing rate, peak firing rate, and response latency for individual neurons, as well as the spike timing correlations between neuron pairs.

Data were classified based on the stimulus conditions and the relationship of individual neurons to the stimulus conditions. These stimulus conditions were the categorical predictors we expected would be associated with the variance in the neuronal measures. With the two tactile stimulus probes, we stimulated paired locations on the hand which could include adjacent digits or nonadjacent digits. The two tactile stimuli were presented at varying temporal onset asynchronies including 0 ms (simultaneous) and 30, 50, and 100 ms. The measurement intervals were consistent for the neurons recorded throughout the experiment. We selected data to include in the analysis such that

the preferred stimulus for a given neuron was presented second and the non-preferred stimulus was presented first, for the purposes of addressing our experimental hypothesis.

In addition to calculating response properties of the neurons, we determined the relationship of the tactile stimulus probes to the neuron's receptive field. To do this, we examined the firing rates of the neurons across all of the given set of stimulus locations on the hand. Since we used a classification measure based on the firing rate in response to indentation stimulation, we used the term "Response Field" to refer to the classification since the full receptive field properties of the neuron were not characterized. When the peak firing rate (after the average baseline firing rate was subtracted) was greater than or equal to 3 times the standard deviation of the average firing rate for the population of neurons recorded on the electrode array, then that stimulus site was classified as "Inside" the neuron's Response Field. Otherwise, the stimulus site was classified as "Outside" the neuron's Response Field. For a complete description, see Reed et al., submitted. Since the stimulus sites were paired, the combination of the Response Field categories for each single stimulus site was used to classify the Response Field relationship of the neuron to the two (paired) stimuli. Thus, the final categories for Response Field were: 1) both probes Outside of the Response Field (OUT_OUT); 2) one probe Inside the Response Field and one probe Outside (IN_OUT); and 3) both probes Inside the Response Field (IN_IN). This classification was important to our hypothesis that the location of the stimulation relative to the Response Field of the neurons would impact the changes in their firing rates. See Figure A-2 for a schematic representation of the predictor variables used in this example data set.

4.3 General Use of Generalized Estimating Equations

The Generalized Estimating Equations uses quasi-likelihood estimation for longitudinal data analysis of clustered or correlated data. Estimating equations are derived by specification of the quasi-likelihood for the marginal distributions of the observed (dependent) variable and the working correlation matrix, which refers to the time dependence for the repeated observations from each subject (e.g., Liang and Zeger, 1986; Zeger and Liang, 1986). There are a few aspects of the Generalized Estimating Equations procedure that require basic knowledge of the data in order to specify the model. However, even when the correlation matrix structure is mis-specified (since we use our best estimate to select how the observations may be time-dependent), the method is robust and produces consistent and asymptotically normal solutions for the estimates of the regression coefficients and their variances (Zeger and Liang, 1986).

4.3.1 Distribution and link function

The researcher must select the type of data distribution from which the dependent variable comes, and the Generalized Estimating Equations analysis allows one to select a variety of distributions from the exponential family of distributions along with a general link function that relates the linear predictor to the expected value (e.g., Zeger and Liang, 1986; Hardin and Hilbe, 2003, p. 7-8). (Distributions include the normal distribution, gamma, Poisson, binomial, Tweedie, etc. Link functions include, but are not limited to the identity link, log, logit, and reciprocal.)

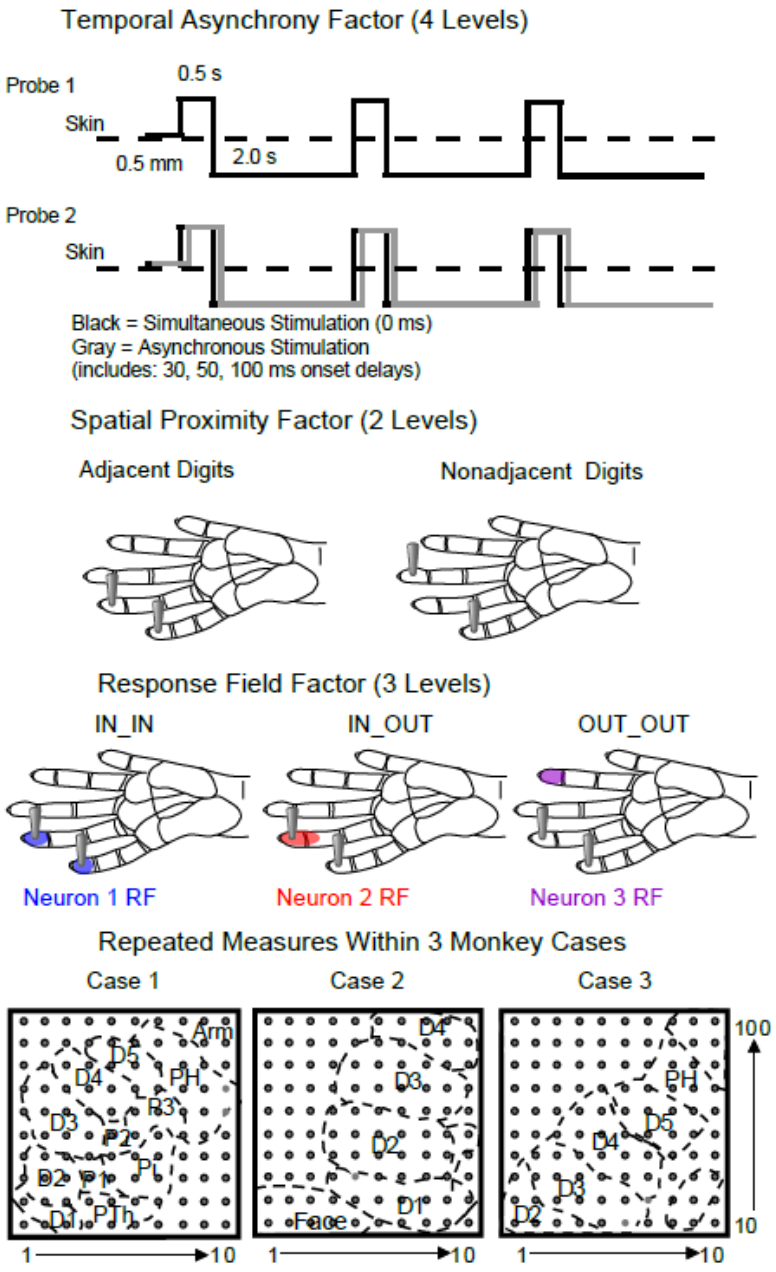

Figure A-2. Schematic of factors evaluated in the example data set. The categorical factors related to the stimulus parameters and the experimental subjects are shown with schematics to represent the levels over which the categories vary. The temporal stimulation asynchrony factor involves the relationship between the onset of stimulation by two tactile probes. The gray line represents how the onset of the second stimulation can be delayed in time relative to the onset of the stimulus provided by probe 1. The spatial proximity factor relates to the location of the two tactile probes on the hand. The signal isolation factor categorizes the neurophysiological recording signals as isolated from a single unit (neuron) or a cluster of neurons (multi-unit). The final factor categorizes the data from which monkey case the signals were recorded. Schematic representations of the location of the 100-electrode array relative to the hand representation in primary somatosensory cortex (area 3b) are shown to designate each monkey case. (D = digit; P = palm pad; Th = thenar; H = hypothenar; i = insular.)

4.3.2 Variable assignment, model effects to test

The dependent variable of interest must be selected. The subjects and the within-subjects measures specifying the repeated measurement condition must be specified in the model. First, the full factorial model can be selected, or main effects and interactions specific to a research hypothesis can be tested. In addition, the factors included in (or excluded from) the model can be varied to determine the best fit to achieve a final model of the data.

4.3.3 Working correlation matrix structure

The first model specification we describe is the working correlation matrix. The working correlation matrix structure can be selected based on the researcher's best estimate of the time dependence in the data, and this parameter can be varied to determine if alternative correlation structures better fit the data. Brief descriptions of a subset of the options are as follows (from Hardin and Hilbe, 2003, p. 59-73), and selected example working correlation matrices are shown from our experimental data. The "independent correlation" derived by Liang and Zeger (1986) assumes that repeated observations within a subject are independent (uncorrelated). All off-diagonal elements of the matrix are zero (compare with the exchangeable working correlation matrix example in Table A-1). In the case of repeated observations on the same subjects, the variance of the repeated measurements is usually not constant over time. The dependence among the repeated measurements is accounted for by allowing the off-diagonal elements of the correlation matrices to be non-zero (Fitzmaurice, Laird, and Ware, 2004, p. 30). The "exchangeable correlation" (or "compound symmetry") is appropriate when the

measurements have no time dependence and any permutation of the repeated measurements is valid. This type of structure may not be the most appropriate from repeated measures gathered across long periods of time, since the exchangeable structure does not account for the likelihood that measures obtained closely together in time are expected to have stronger correlations than measures obtained further apart in time. In our experiments, the first measure in the repeated measures series was taken less than 40 minutes before the last repeated measure in the series; therefore, we tested the exchangeable correlation structure (Table A-1), along with other structures. The "autoregressive correlation" is used when time dependence between the repeated measurements should be assumed, such as in a long-term recovery of function or other treatment study. An example of the first-order autoregressive correlation matrix tested from our data is found in Table A-2. The "unstructured correlation" is the most general correlation matrix, as it imposes no structure. While this unstructured option may seem the best for all situations, efficiency increases and better model fits will be obtained when the closest approximation to the actual correlation structure of the data is found (Zeger and Liang, 1986). This depends also on the number of time points relative to the number of subjects. An example of the unstructured correlation matrix tested using our data is found in Table A-3. Each of these example structures shows the matrices when only the repeated measures within neurons are considered. When we consider that the repeated measures on neurons may show dependencies within monkeys, the working correlation matrix structure increases in complexity. In fact, when we selected the unstructured working correlation matrix for repeated measures on neurons dependent within monkeys (Table A-4), the Generalized Estimating Equations routine failed to come to convergence

on a solution when the same model parameters resulted in convergence when structured (exchangeable, autoregressive) correlation matrices were selected. Similarly, the unstructured working correlation matrix was highly complex when we tested the effects of repeated measures dependent within neurons, and in turn dependent within monkeys, and given our large number of neurons, this working correlation matrix was too large to illustrate.

Table A-1. Exchangeable working correlation matrix from example data with simple repeated measures

Working Correlation Matrix

	Measurement			
Measurement	0 ms	30 ms	50 ms	100 ms
0 ms	1.000	.593	.593	.593
30 ms	.593	1.000	.593	.593
50 ms	.593	.593	1.000	.593
100 ms	.593	.593	.593	1.000

Table A-2. First-order autoregressive working correlation matrix from example data with simple repeated measures

Working Correlation Matrix

	Measurement			
Measurement	0 ms	30 ms	50 ms	100 ms
0 ms	1.000	.705	.498	.351
30 ms	.705	1.000	.705	.498
50 ms	.498	.705	1.000	.705
100 ms	.351	.498	.705	1.000

Table A-3. Unstructured working correlation matrix from example data with simple repeated measures

Working Correlation Matrix

	Measurement			
Measurement	0 ms	30 ms	50 ms	100 ms
0 ms	1.000	.488	.443	.505
30 ms	.488	1.000	.982	.836
50 ms	.443	.982	1.000	.764
100 ms	.505	.836	.764	1.000

Table A-4. Unstructured working correlation matrix from example data with repeated measures within monkeys

Working Correlation Matrix

	Measurement											
Measurement	0 ms* Monkey 1	0 ms* Monkey 2	0 ms* Monkey 3	30 ms* Monkey 1	30 ms* Monkey 2	30 ms* Monkey 3	50 ms* Monkey 1	50 ms* Monkey 2	50 ms* Monkey 3	100 ms* Monkey 1	100 ms* Monkey 2	100 ms* Monkey 3
0 ms* Monkey 1	1.000	.000	.000	.351	.000	.000	.461	.000	.000	.436	.000	.000
0 ms* Monkey 2	.000	1.000	.000	.000	.612	.000	.000	.270	.000	.000	.542	.000
0 ms* Monkey 3	.000	.000	1.000	.000	.000	.113	.000	.000	.376	.000	.000	.380
30 ms* Monkey 1	.351	.000	.000	1.000	.000	.000	.908	.000	.000	.908	.000	.000
30 ms* Monkey 2	.000	.612	.000	.000	1.000	.000	.000	.864	.000	.000	.745	.000
30 ms* Monkey 3	.000	.000	.113	.000	.000	1.000	.000	.000	.605	.000	.000	.251
50 ms* Monkey 1	.461	.000	.000	.908	.000	.000	1.000	.000	.000	.908	.000	.000
50 ms* Monkey 2	.000	.270	.000	.000	.864	.000	.000	1.000	.000	.000	.389	.000
50 ms* Monkey 3	.000	.000	.376	.000	.000	.605	.000	.000	1.000	.000	.000	.674
100 ms* Monkey 1	.436	.000	.000	.908	.000	.000	.908	.000	.000	1.000	.000	.000
100 ms* Monkey 2	.000	.542	.000	.000	.745	.000	.000	.389	.000	.000	1.000	.000
100 ms* Monkey 3	.000	.000	.380	.000	.000	.251	.000	.000	.674	.000	.000	1.000

4.3.4 Estimating equations and testing

In addition to the correlation matrix structure, the variance-covariance estimator must be selected. This variance estimator can be a "robust estimator" or a "model-based estimator". The mean and variance of the response must be correctly specified for the model based estimator. The robust estimator is consistent even when the working correlation matrix is mis-specified, so the robust estimator is usually recommended (e.g.,

Hardin and Hilbe, 2003, p 30). Using statistical software packages, the Generalized Estimating Equations routine runs for a selected number of iterations to reach the specified model convergence. The results of the analysis include estimated regression coefficients for the main effects and interactions in the model and estimated marginal means, along with estimates of significance. When the effects have multiple levels, the research selects the adjustment for multiple comparisons (e.g., the Bonferroni correction).

4.4 Performing Summary Data Analysis Using Generalized Estimating Equations

An important aspect of the analysis is choosing the best final model of the data. A guide for model selection is the goodness-of-fit statistic: either the quasi likelihood under independence model criterion (QIC) or the corrected quasi likelihood under independence model criterion (QICC) are often used, as they resemble Akaike's information criterion (AIC), which is a well-established goodness-of-fit statistic (Hardin and Hilbe, 2003, p. 139). The smallest value is best using the QIC and QICC. Note that the goodness-of-fit statistic should not be used as the sole criterion for selecting the best working correlation structure for the data—if there are experimental reasons to specify a particular correlation structure, follow this reasoning. Similarly, the QIC is particularly useful when choosing between models including various main effects and interactions between factors, but the effects of interest for the model may be determined by the research hypothesis rather than the goodness-of-fit statistics. (Hardin and Hilbe, 2003, p. 142).

The procedure for determining the best model for the data using Generalized Estimating Equations involves changing the model parameters to select the best fit based on goodness-of-fit statistics. We compared models which assumed the data were

normally distributed with models that assumed the data followed a gamma distribution. In addition to the distribution, several other characteristics of the data must be selected by the researcher, as described in Section 4.3, and some of these can be varied to test the best model fit. Here we describe the different selections specific to the models that we tested using the gamma and normal distribution functions.

In our models, we selected various correlation matrix structures in order to determine the best fit. For the normal distribution (linear relationship), the link function is typically the "identity" link function (Hardin and Hilbe, p. 8), and this is what we used for our models using testing the linear relationship of our variables. We used the typical link function for the gamma distribution, the "log link" function, in our models using the gamma distribution. The reciprocal link function is canonical for the gamma distribution; however, this link function does not preserve the positivity of the data distribution, so the log link function is commonly used (e.g., Lindsey, 2004, p. 30). For additional distributions and link functions, see Hardin and Hilbe (2003, p. 8). We always selected the robust estimator of the variance-covariance matrix since this selection is robust in the general case (e.g., Hardin and Hilbe, 2003, p 30).

The subject identification variables and the within-subjects measures indicating the repeated measurement condition must be specified in the model. In our case, the subjects were the individual neuron units from which the repeated measures were taken. We performed the analysis two ways. In the first, the within-subjects repeated measurements were the varying levels of the stimulation conditions (without regard to the individual monkeys). In the second, the varying levels of the stimulation conditions measured for the neurons were regarded as dependent within the individual monkeys.

These two methods affected the working correlation matrix structure used to determine the Generalized Estimating Equations solutions. (Compare the unstructured working correlation matrix in Table A-3 when only the repeated measures taken for each neuron were included with that in Table A-4 when the neuron measures were incorporated as dependent within monkeys.)

The Generalized Estimating Equations analysis only works on one dependent variable (unlike multivariate ANOVA), and this was the peak firing rate magnitude in our experiment. We selected several categorical predictor variables for the model: temporal stimulation asynchrony; spatial stimulation proximity; and Response Field relationship. For our example data, we used a final model with all three main effects and one three-way interaction effect. The tests of model effects for our best fit models using the gamma and normal distributions are shown in Tables A-5 and A-6, respectively.

4.5 Results of Data Analysis Using Generalized Estimating Equations

While neuronal signals were recorded from all 100 electrodes of the array, only the signals that were likely to come from single neurons (rather than multi-neuron clusters) were included in this analysis. During the selected stimulus conditions, only a subset of the electrodes implanted in each monkey recorded neural activity from which we were able to isolate single neurons. From monkey 1, results from 19 single neurons were collected and 4 repeated measures were collected from each neuron (except for 2 missing observations), for a total of 74 observations. From monkey 2, results from 46 single neurons were collected with 4 repeated measures each, for a total of 184 observations. From monkey 3, 61 single neurons were collected with 4 repeated measures

Table A-5. Tests of Generalized Estimating Equations model effects on peak firing rate using the gamma probability distribution with log link function

Tests of Model Effects

	Type III		
Source	Wald Chi-Square	df	Sig.
(Intercept)	552.354	1	<.0005
Temporal Asynchrony	28.564	3	<.0005
Spatial Proximity	9.037	1	.003
Response Field (RF)	11.380	2	.003
Temporal * Spatial * RF	35.417	17	.005

Dependent variable: peak firing rate (spikes/s). Model parameters: gamma distribution, log link, first-order autoregressive correlation matrix. Subject effects for 126 neurons, with four levels of within-subject repeated-measures stimulation (total N = 499, 5 missing)

Table A-6. Tests of Generalized Estimating Equations model effects on peak firing rate using the normal probability distribution with identity link function

Tests of Model Effects

	Type III		
Source	Wald Chi-Square	df	Sig.
(Intercept)	105.024	1	<.0005
Temporal Asynchrony	36.591	3	<.0005
Spatial Proximity	7.225	1	.007
Response Field (RF)	12.960	2	.002
Temporal * Spatial * RF	40.580	17	.001

Dependent variable: peak firing rate (spikes/s). Model parameters: normal distribution, identity link, first-order autoregressive correlation matrix. Subject effects for 126 neurons, with four levels of within-subject repeated-measures stimulation (total N = 499, 5 missing)

(except for 3 missing observations), for 241 observations. Thus, the total number of observations was N = 499, while 5 values were excluded due to missing observations from the repeated measures series. The mean response magnitude for the data set was 18.05 spikes/s, with a standard deviation of 23.81.

The results for model fitting using both the gamma and normal distributions are described here for illustration purposes. We investigated working correlation matrices of: first-order autoregressive, exchangeable, and unstructured for the normal distribution with the identity link function and for the gamma distribution with the log link function. For all working correlation matrices specified, the goodness-of-fit statistic QIC was substantially better using the gamma distribution compared to the normal distribution (e.g., 1480.789 and 239,348.869, respectively, under the same model parameters, described to follow). In addition, we tested correlation structures that incorporated only the repeated measures taken from individual neurons and those that included repeated measures within monkeys (which we term "complex model"). We again examined the QIC goodness-of-fit statistic to help determine the best correlation structure for the analysis. After reducing the effects included in the model from the full factorial model, we selected possible correlation matrices, and checked the QICC goodness-of-fit statistic to determine the best model parameters to fit the data. The QICC did not differ between models that included all main effects and the 3-way interaction and those that included the main effects, 3-way interaction, and 2-way interactions. Because the 2-way interactions were never significant sources of variance in the models, we selected the model that only included the significant effects (3 main effects and the 3-way interaction).

Under the model including 3 main effects and the 3-way interaction, the QIC values were very similar, sometimes identical when the repeated measures were considered to be dependent within monkeys. However, there was a dramatic difference in the QIC values for the simple and the complex models when the working correlation matrix was specified as unstructured. The Generalized Estimating Equations routine could not come to convergence on a solution when the within-subjects effects were complex and the gamma distribution was specified. The last iteration of the procedure produced the QIC value of 1535.166, while the solution was reached in the simple model with a QIC value of 1480.809. The QIC values and the parameter estimates when the exchangeable working matrix structure was selected was equivalent for the complex and simple within-subjects effects (1480.792). Including three levels of within-subjects variables so that repeated measures were dependent within neurons, which in turn were dependent within monkeys worsened the fit of the model and again, the routine could not come to convergence when the unstructured correlation matrix was specified (QIC for the last iteration was 1644.810). This illustrates a noteworthy aspect of Generalized Estimating Equations. The parameter estimates are typically the same in spite of differences in the covariance structure selected by the user (e.g., Liang and Zeger, 1986; Zeger and Liang, 1986). The standard errors of the effects used for confidence intervals and hypothesis testing can change based on these selections. In our case, the differences between the parameter estimates and the standard errors were negligible between models with different working correlation matrices.

The final model we selected used the gamma distribution with the log link function and the first-order autoregressive correlation matrix structure, and had a

goodness-of-fit QIC = 1480.789 (Model Effects shown in Table A-5). The equivalent model using the normal distribution and identity link function resulted in a QIC value of 239,348.869 (Model Effects shown in Table A-6). Although this model using the normal distribution reported significant effects similar to those reported using the gamma distribution, there are some differences in the effects that reach significance, different regression parameter estimates, and clearly a large difference in model fit. Thus, we rejected the Generalized Estimating Equations model using the normal distribution in favor of the Generalized Estimating Equations model using the gamma distribution, and for these data we reject other analysis methods that rely on the assumption of independent observations from the normal distribution.

From the Generalized Estimating Equations analysis, we obtained a model that included the factors that relate to the variance in the observed measurements (Table A-5); the estimated regression parameters that describe the relationships of the factors to the dependent variable the estimated marginal means of these factors (see one example Figure A-3); and pairwise comparisons for significance between the levels of each factor. We used the estimated marginal means and the significance calculations to determine how the spatiotemporal stimulus relationships affected the peak firing rates of the neurons we recorded within the three monkeys. Selected regression parameter estimates for the best model are shown in Table A-7. We can interpret the parameter estimates to describe the relationships between the factors in the data. In general, linear regression coefficients are interpreted such that the coefficient represents the amount of change to the response variable for a one-unit change in the variable associated with the coefficient, with the other predictors held constant (e.g., Hardin and Hilbe, 2007, p. 133). Examining

our data for example, as expected for the somatosensory system, the relationship of the location of the paired stimuli to the Response Field of the neuron influenced the peak firing rate. The parameter estimate for the case when the paired stimulus probes were both outside of the Response Field (OUT_OUT) was -1.309, which was less than the estimate for the case when one of the stimulus probes was inside the Response Field and the other probe was outside of the Response Field (IN_OUT) of the given neuron (-0.804), and these values refer to case when both stimulus probes were inside the Response Field (IN_IN).

Overall, the results are similar to those produced by repeated-measures ANOVA using linear model theory. These Generalized Estimating Equations results provide population average effects of the categorical predictor factors on the dependent variable of interest, while accounting for individual-level correlations. To focus on the individual data subjects, a subject-specific Generalized Estimating Equations model would need to be created (programmatically) that resemble within-subjects effects analysis, or alternative methods such as Generalized Linear Mixed Models could be performed. Our experimental questions referred to population averages rather than within-subjects effects; thus, we were able to find support for our hypotheses and determine quantitative estimates of the ways spatiotemporal stimulus properties affect neuron firing rates in primary somatosensory cortex of owl monkeys.

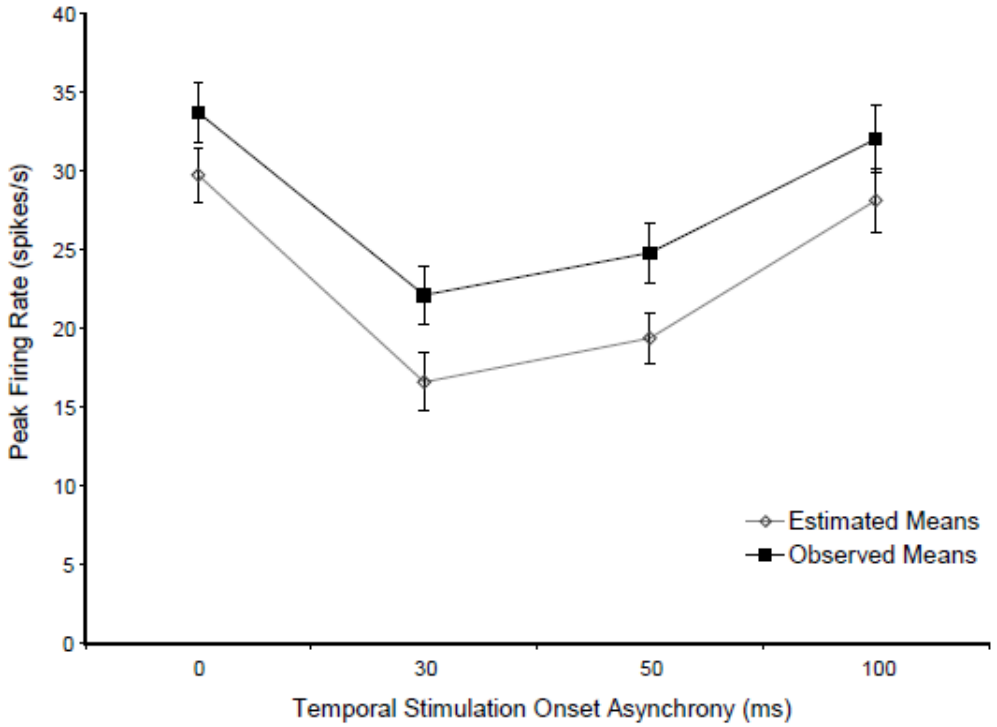

Figure A-3. Observed means and estimated means for the temporal asynchrony factor from the best model. The categories from one factor, temporal asynchrony, is plotted on the x-axis and the dependent variable, response magnitude (spikes/s) is plotted on the y-axis. Observed mean response magnitudes are shown by category with filled squares. Estimated marginal means from the best fitting Generalized Estimating Equations routine is shown by category with open diamonds. Although the values of the estimates are not equal to the observed values, the patterns of the effects of the predictor variable categories on the response magnitude are the same.

Table A-7. Regression parameter estimates from the Generalized Estimating Equations routine for peak firing rate using the gamma probability distribution with log link function (only main effects shown)

Parameter Estimates

			95% Wald Confidence Interval		Hypothesis Test		
Parameter	B	Std. Error	Lower	Upper	Wald Chi-Square	df	Sig.
(Intercept)	3.893	.2811	3.342	4.444	191.778	1	<.0005
Temporal 0 ms	-.053	.1967	-.438	.333	.072	1	.788
Temporal 30 ms	-1.603	.5124	-2.608	-.599	9.792	1	.002
Temporal 50 ms	-1.121	.4357	-1.975	-.267	6.623	1	.010
Temporal 100 ms	0[a]						
Spatial Adjacent	-.562	.4190	-1.383	.260	1.797	1	.180
Spatial Nonadjacent	0[a]						
RF OUT_OUT	-1.309	.5187	-2.326	-.293	6.372	1	.012
RF IN_OUT	-.804	.3150	-1.421	-.186	6.511	1	.011
RF IN_IN	0[a]						
(Scale)	1.653						

Redundant parameters set to 0 indicated by [a] . RF = Response Field. See text for other abbreviations.

5. Limitations and Alternatives

The example in Section 4 was intended to illustrate how specific types of data can be modeled using the Generalized Estimating Equations analysis. The Generalized Estimating Equations analysis is particularly useful for large samples of longitudinal or repeated measures data that are expected to be correlated or clustered and that may not have linear relationships or fit the normal distribution. Another advantage of the Generalized Estimating Equations approach is that it provides consistent estimates for the regression parameters of the model even if the working correlation selected by the researcher is not the most appropriate (Tuerlinckx et al., 2006). There are limitations to this analysis, which may not be ideal for all designs, and there are alternative analysis methods that may be generally applicable to large-scale neuronal recording data to consider.

5.1 Limitations of the Generalized Estimating Equations Analysis

A possible limitation of the Generalized Estimating Equations analysis for some designs is that interpretation of cluster-specific effects (within-subjects effects) is usually not included in the analysis within standard software packages, even though the analysis does take into account the correlated structure of the data for the between-subjects effects. The Generalized Estimating Equations method itself does include two main classifications that address between-subjects and within-subjects effects, respectively, the population-averaged model and the subject-specific model (Hardin and Hilbe, 2003, p. 49). Those who are concerned with the within-subjects variance and require methods

built into a commercial statistical package would be best served by an alternative analysis method, such as Generalized Linear Mixed Models, as described in Section 3.1.

Another limitation of Generalized Estimating Equations analysis is one that is shared by most other methods, and this involves the biases possible when accounting for nonignorable missing data values (also called informatively missing data or nonrandom missing data). By nonignorable, we refer to missing data that are caused by a nonrandom process related to the condition under study. Unlike ANOVA, Generalized Estimating Equations can account for missing values; however, the missing values are assumed to occur completely at random (MCAR) and without intervention by the investigator, the routine will proceed with an analysis of only complete observations. This method is still likely to be appropriate when the data are missing due to a dropout process (like losing the neuronal signal for the last observations in a series) if the process is not related to the parameters of interest (Hardin and Hilbe, 2003, p. 127). Hardin and Hilbe (2003, p 122-128) describe techniques to deal with missing data for Generalized Estimating Equations analysis. First, the data can be divided into complete and incomplete series, and then typically missing values are replaced with values imputed from the data. Investigators should carefully consider when to use data imputation methods. Alternative methods include modeling the complete data and the missing data separately, but models for the missing data sets are not built in to statistical software. There are a few occasions that come to mind in which missing data are unlikely to occur at random in neurophysiological experiments. For instance, in an experiment when one measures response latency, there will be missing values when the neuron fails to respond to specific stimulus conditions (no response = no response latency). This situation is not

simply random since the failure of the neuron to respond is related to the stimulus condition. Nonignorable missing data is a recognized problem in several types of clinical longitudinal studies, and methods accounting for such data have been described for use in Generalized Linear Mixed Models analysis (e.g., Ibrahim, Chen, and Lipsitz, 2001). Currently, there appear to be no standard ways to account for nonignorable missing data, such as occurs for latency observations. While the problem of nonignorable missing data does not plague all neurophysiological measurements, it is a concern that is not directly addressed without data imputation or other procedures, and certainly methods are not built into commercial statistics packages to specifically analyze data sets including nonignorable missing data.

Finally, as mentioned previously, the Generalized Estimating Equations analysis as implemented in software packages allows for one dependent variable (but multiple covariates) to be analyzed. Multivariate research questions may be better analyzed with an alternative method. In addition, complex clustering is not easily incorporated into the Generalized Estimating Equations. In our example using SPSS, we were able to include clustering of the repeated measures on neurons within our individual monkey subjects. However, as the complexity of the working correlation structure increased, the Generalized Estimating Equations routine was not able to come to convergence on a solution. Random effects models, such as Generalized Linear Mixed Models, can typically handle complicated nesting structures due to differences in the calculation of random effects compared to marginal models of residuals. In our case, recall that the model fits were equivalent when the complex dependence was used for the working correlation matrix and when the simple dependence (without accounting for dependencies

of neuron observations within monkeys) was used, except when the unstructured matrix was chosen rather than a structured (autoregressive or exchangeable) matrix. Thus, methods of choice depend on the measure of interest and computational considerations. Since the correlation matrix structure of the Generalized Estimating Equations analysis could not incorporate nested effects, we were not able to account for potential correlations in measures between neurons (which might be expected due to spatial proximity, for example). Dependency between neurons is not precisely known, and here we considered that neurons were independent; however, adaptations of Generalized Linear Mixed Models or other analysis methods may be able to model the possible dependencies better.

5.2 Some Alternatives to the Generalized Estimating Equations Analysis for Large-Scale Neuronal Recordings

Here we briefly describe selected alternatives to Generalized Estimating Equations analysis that may have useful applications to large-scale neuronal recording data. We assume that data from parallel microelectrode recordings are likely to have correlated or non-constant variability due to recording from clusters of neurons over time. We also suggest that good alternative analysis methods will allow for the dependent measure of interest to possibly come from non-normal distributions to account for the different types of data that may be obtained through such neuronal recordings.

As previously introduced, Generalized Linear Mixed Models are similar to Generalized Estimating Equations, in that both are extensions of Generalized Linear Models and may be used to analyze correlated or clustered data from non-normal distributions (e.g., Tuerlinckx et al., 2006, review). Generalized Linear Mixed Models

may be advantageous over Generalized Estimating Equations when the dependence or correlations within subjects is of interest (rather than a nuisance; e.g., Snijders and Bosker, 1999, p. 6-7) so that subject-specific predictions can be made and when the number of clustered observations is low (e.g., < 40), since Generalized Estimating Equations tend to underestimate the true variance in small samples (Lu et al., 2007).

An addition to some statistical packages (e.g., Amos, SAS) is structural equation modeling, which can link the dependent variables with independent observed variables and latent variables (e.g., Tuerlinckx, 2006). A benefit of structural equation modeling is that researchers may build models to express unobserved latent variables that are expected to contribute to the observed measures by expressing latent variables in terms of the observed variables, which could be of interest in some neuronal recording experiments. The use of structural equation modeling to examine latent variables is similar to the use of Principal Components Analysis and Independent Component Analysis to identify underlying sources of variance related to the observed measures.

Principal Component Analysis (PCA) has already been applied to neuronal recording data (e.g., Chapin and Nicolelis, 1999; Kralik et al., 2001; Devilbiss and Waterhouse, 2002), as a method to describe the linear relationship between variables (i.e., how stimulus information relates to neuron spike trains). Proportions of the variance are explained by each Principal Component, with the first PC accounting for the most variance in the data. The interpretation of PCA may not be intuitive in all experimental designs, and this analysis assumes linear relationships between variables and that the sources of the variance have a normal distribution. But given the right circumstances, PCA provides an interesting way to assess changes distributed among recorded neurons

(e.g., Devilbiss and Waterhouse, 2002) and to estimate relationships within neuronal ensembles (e.g., Chapin and Nicolelis, 1999).

Similar to PCA, Independent Components Analysis (ICA) has also been used to examine data from parallel neuronal recordings, and has been shown to identify groupings of neurons with correlated firing distributed over the recorded neuronal ensembles (Laubach, Shuler, and Nicolelis, 1999; Kralik et al., 2001). ICA was found to perform better than PCA at identifying groups of neurons with correlated firing when those neurons shared common input (Laubach, Shuler, and Nicolelis, 1999). Unlike PCA, ICA should be used when the sources of variance do not have a normal distribution (Makeig et al., 1999). However, ICA has limitations, one of which is that a given IC can represent a linear combination of sources of variance, rather than an "independent" source (Makeig et al, 1999), and similarly, ICA cannot identify the actual number of source signals. Thus the reliability, accuracy, and interpretation of results of ICA can be difficult to determine in general.

Pereda and colleagues (2005) reviewed nonlinear multivariate methods for analyzing parallel neurophysiological recordings to determine the synchronization across the signals. These methods are not limited to describing the linear features of neuronal signals, and neuronal signals may be intrinsically nonlinear. Such multivariate measures can assess the interdependence between simultaneously recorded neuronal signals or data types, and this assessment is a feature not possessed by standard Generalized Estimating Equations analysis methods. Nonlinear multivariate methods of "generalized synchronization" and "phase synchronization" have a wide range of applications to neurophysiology. These methods range from nonlinear correlation coefficients to

information-theory-based methods. Many of these methods examine pairwise interactions (e.g., cross-correlations) between neuronal signals (e.g., spike trains), but a subset can be used to analyze high-order interactions. (Pereda, Quiroga, and Bhattacharya, 2005) Most of these applications are not part of commercial statistical software, but sometimes the implementation of these analysis methods are made available by authors or can be found in neurophysiological analysis software. Kralik et al. (2001) suggested several strategies for analyzing neuronal data from multi-electrode recordings ranging from single neuron analysis techniques to employing artificial neuronal networks with information theory; and some of their methods are available in analysis software such as Matlab.

Many neurophysiological studies, including the example provided in this review, rely on multiple trials to average the responses (or other measurements) of individual neurons. This technique is rooted in the study of single neurons with single electrodes, in which the average over multiple trials resembles the information received by a postsynaptic neuron that receives input from several other neurons performing in a similar way to the recorded neuron. When the experimental system and research questions are appropriate, analyses of multiple-neuron recordings to extract information from neuronal populations within one or a few trials may provide a more realistic depiction of how the brain works. In their recent review, Quiroga and Panzeri (2009) described two main (and complementary) approaches to obtaining information from neuronal population recordings for the purpose of application to single-trial analysis: decoding and information theory. Decoding algorithms predict the likely stimulus (or behavior) related to the observed neuronal response. Using the information theory approach, one can quantify the average amount of information gained with each stimulus

presentation or behavioral event. (Quiroga and Panzeri, 2009) Typically, decoding neuronal responses and applying information theory requires carefully planned experiments, careful interpretation and knowledge of programming since such algorithms are not often found in commercial statistical packages. However, as knowledgeable users continue to employ these methods, their use will likely extend and become more widespread as experiments utilizing large-scale neuronal recordings increase.

6. Conclusions

Current statistics packages and incarnations of the Generalized Estimating Equations and Generalized Linear Mixed Models analyses can accomplish many of the data analysis goals required by the increasingly complex large-scale neuronal recordings. Specifically, these analyses address concerns that have been largely overlooked when analyzing parallel neuronal recording data collected over time: that these data are likely to be correlated or clustered and that the normal distribution may not be the appropriate distribution to test. We illustrated our use of Generalized Estimating Equations to address questions regarding stimulus-response relationships in simultaneously recorded neurons in monkey somatosensory cortex. The Generalized Estimating Equations analysis has limitations, and alternative methods may provide more appropriate answers to some research questions.

In addition to revealing stimulus-response relationships as described in our example data, the Generalized Estimating Equations and Generalized Linear Mixed Models analysis appear to be well-suited to studies involving plasticity, learning, and

attention processes, which can all be tested in longitudinal designs with various neuronal measures obtained from simultaneous recordings. In our data example, the goal was to determine how the responses of populations of neurons may be influenced by specific stimulus parameters recorded over relatively short periods of time; however, the technological advancements in chronic recording techniques and algorithms to determine when electrophysiological signals are stable over time and likely to originate from the same neuron will surely aid the progress of such longitudinal studies. Although we used the response magnitude example for simplicity, measures of correlated activity that can only be made by simultaneous neuronal recordings (such as those reviewed by Pereda, Quiroga, and Bhattacharya, 2005) can be used as the dependent measure when the goal is to determine how independent variables may affect the variance in these measures recorded longitudinally. The options are nearly unlimited. The analysis of long-term, large-scale neuronal recordings promises to increase our understanding of complex brain activity, and meeting the challenge to produce and employ efficient and appropriate analysis methods is important to reach this goal.

Acknowledgements

The example data used in this is work was collected with support by the James S. McDonnell Foundation (J.H. Kaas) and NIH grants NS16446 (J.H. Kaas), F31-NS053231 (J.L. Reed), EY014680-03 (Dr. A.B. Bonds). We thank Dr. Andrew Tomarken for invaluable comments on the manuscript.

References

Ballinger GA. 2004. Using generalized estimating equations for longitudinal data analysis. *Organizational Res Methods* 7: 127-150.

Bolker BM, Brooks ME, Clark CJ, Geange SW, Poulsen JR, Stevens HH, White JS. 2008. Generalized linear mixed models: a practical guide for ecology and evolution. *Trends Ecol Evol* 24: 127-135.

Breslow NE, Clayton DG. 1993. Approximate inference in generalized linear mixed models. *J Am Stat Assoc* 88: 9-25.

Buzsáki G. 2004. Large-scale recording of neuronal ensembles. *Nat Neurosci* 7: 446-451.

Chapin JK. 2004. Using multi-neuron population recordings for neural prosthetics. *Nat Neurosci* 7: 452-455.

Chapin JK, Nicolelis MA. 1999. Principal component analysis of neuronal ensemble activity reveals multidimensional somatosensory representations. *J Neurosci Methods* 94: 121-140.

Cnaan A, Laird NM, Slasor P. 1997. Tutorial in biostatistics: using the general linear mixed model to analyze unbalanced repeated measures and longitudinal data. *Stat Med* 16: 2349-2380.

Cusick CG, Wall JT, Felleman DJ, Kaas JH. 1989. Somatotopic organization of the lateral sulcus of owl monkeys: area 3b, S-II, and a ventral somatosensory area. *J Comp Neurol* 282: 169-190.

Czanner G, Eden UT, Wirth S, Yanike M, Suzuki WA, Brown EN. 2008. Analysis of between-trial and within-trial neural spiking dynamics. *J Neurophysiol* 99: 2672-2693.

Deadwyler SA, Hampson RE. 1997. The significance of neural ensemble codes during behavior and cognition. *Ann Rev Neurosci* 20: 217-244.

Devilbiss DM, Waterhouse BD. 2002. Determination and quantification of pharmacological, physiological, or behavioral manipulations on ensembles of simultaneously recorded neurons in functionally related circuits. *J Neurosci Methods* 121: 181-198.

Dickey AS, Suminski A, Amit Y, Hatsopoulos NG. 2009. Single-unit stability using chronically implanted multielectrode arrays. *J Neurophysiol* 102: 1331-1339.

Diggle PJ, Heagerty P, Liang K-Y, Zeger SL. 2002. *Analysis of longitudinal data*. 2nd ed. New York: Oxford University Press, Inc.

Edwards LJ. 2000. Modern statistical techniques for the analysis of longitudinal data in biomedical research. *Pediatr Pulmonol* 30: 330-344.

Fitzmaurice GM, Laird NM, Ware JH. 2004. *Applied longitudinal analysis*. Hoboken, NJ: John Wiley & Sons, Inc.

Garraghty PE, Pons TP, Sur M, Kaas JH. 1989. The arbors of axons terminating in middle cortical layers of somatosensory area 3b in owl monkeys. *Somatosens Motor Research* 6: 401-411.

Ghazanfar AA, Nicolelis MAL. 1999. Spatiotemporal properties of layer V neurons of the rat primary somatosensory cortex. *Cereb Cortex* 9: 348-361.

Gill J. 2001. *Generalized linear models: a unified approach*. Quantitative applications in the social sciences, ed. M.S. Lewis-Beck, vol. 134. London: SAGE Publications.

Hanley JA, Negassa A, Edwardes MD, Forrester JE. 2003. Statistical analysis of correlated data using generalized estimating equations: an orientation. *Am J Epidemiol* 157: 364-75.

Hardin JW, Hilbe JM. 2003. *Generalized estimating equations*. Boca Raton: Chapman and Hall/CRC.

Hardin JW, Hilbe JM. 2007. *Generalized linear models and extensions*. 2nd ed. College Station, TX: Stata Press.

Horton NJ, Lipsitz SR. 1999. Review of software to fit generalized estimating equations regression models. *Am Stat* 53: 160-69.

Ibrahim JG, Chen M-H, Lipsitz SR. 2001. Missing responses in generalized linear mixed models when the missing data mechanism is nonignorable. *Biometricka* 88: 551-564.

Kauermann G, Carroll RJ. 2001. A note on the efficiency of sandwich covariance matrix estimation. *J Am Stats Assoc* 96: 1387-1398.

Kenny DA, Judd CM. 1986. Consequences of violating the independence assumption in analysis of variance. *Psychol Bull* 99: 422-431.

Kralik JD, Dimitrov DF, Krupa DJ, Katz DB, Cohen D, Nicolelis MAL. 2001. Techniques for long-term multisite neuronal ensemble recordings in behaving animals. *Methods* 25: 121-150.

Laird NM, Ware JH. 1982. Random-effects models for longitudinal data. *Biometrics* 38: 963-974.

Laubach M, Shuler M, Nicolelis MAL. 1999. Independent component analyses for quantifying neuronal ensemble interactions. *J Neurosci Methods* 94: 141-154.

Lee J-H, Herzog TA, Meade CD, Webb MS, Brandon TH. 2007. The use of GEE for analyzing longitudinal binomial data: a primer using data from a tobacco intervention. *Addict Behav* 32: 187-193.

Lewi J, Butera R, Paninski L. 2009. Sequential optimal design of neurophysiology experiments. *Neural Comput* 21: 619-687.

Liang K-Y, Zeger SL. 1986. Longitudinal data analysis using generalized linear models. *Biometrika* 73: 13-22.

Lindsey JK. 2004. *Statistical analysis of stochastic processes in time*. New York: Cambridge University Press.

Lu B, Preisser JS, Qaqish BF, Suchindran C, Bangdiwala SI, Wolfson M. 2007. A comparison of two bias-corrected covariance estimators for generalized estimating equations. *Biometrics* 63: 935-941.

Makeig S, Westerfield M, Jung TP, Covington J, Townsend J, Sejnowski TJ, Courchesne E. 1999. Functionally independent components of the late positive event-related potential during visual spatial attention. *J Neurosci* 19: 2665-2680.

Mancl LA, DeRouen TA. 2001. A covariance estimator for GEE with improved small-sample properties. *Biometrics* 57: 126-134.

McCullagh P, Nelder JA. 1989. *Generalized Linear Models*. 2nd ed. London: Chapman & Hall.

Merzenich MM, Kaas JH, Sur M, Lin CS. 1978. Double representations of the body surface within cytoarchitectonic areas 3b and 1 in "SI" in the owl monkey (*Aotus trivirgatus*). *J Comp Neurol* 181: 41-74.

Nicolelis MAL, Ghazanfar AA, Stambaugh CR, Oliveira LMO, Laubach M, Chapin JK, Nelson RJ, Kaas JH. 1998. Simultaneous encoding of tactile information by three primate cortical areas. *Nat Neurosci* 1: 621-630.

Nicolelis MAL., Dimitrov D, Carmena JM, Crist R, Lehew G, Kralik JD, Wise SP. 2003. Chronic, multisite, multielectrode recordings in macaque monkeys. *Proc Natl Acad Sci USA* 100: 11041-11046.

Pei Y-C, Denchev PV, Hsiao SS, Craig JC, Bensmaia SJ. 2009. Convergence of submodality-specific input onto neurons in primary somatosensory cortex. *J Neurophyisol* 102: 1843-1853.

Pereda E, Quiroga RQ, Bhattacharya J. 2005. Nonlinear multivariate analysis of neurophysiological signals. *Prog Neurobio* 77: 1-37.

Quiroga RQ, Panzeri S. 2009. Extracting information from neuronal populations: information theory and decoding approaches. *Nat Rev Neurosci* 10: 173-185.

Reed JL, Pouget P, Qi H-X, Zhou Z, Bernard MR, Burish MJ, Haitas J, Bonds AB, Kaas JH. 2008. Widespread spatial integration in primary somatosensory cortex. *Proc Natl Acad Sci USA* 105: 10233-10237.

Rousche PJ, Petersen RS, Battiston S, Giannotta S, Diamond ME. 1999. Examination of the spatial and temporal distribution of sensory cortical activity using a 100-electrode array. *J Neurosci Methods* 90: 57-66.

Searle SR, Casella G, McCulloch CE. 1992. *Variance Components*. New York: Wiley.

Snijders TAB, Bosker RJ. 1999. *Multilevel analysis: an introduction to basic and advanced multilevel modeling*. London: SAGE Publications.

Song D, Chan RSM, Marmarelis VZ, Hampson RE, Deadwyler SA, Berger TW. 2009. Nonlinear modeling of neural population dynamics for hippocampal prostheses. *Neural Networks* 73: 13-22.

Tuerlinckx F, Rijmen F, Verbeke G, De Boeck P. 2006. Statistical inference in generalized linear mixed models: A review. *Br J Math Stat Psychol* 59: 225-255.

Zeger SL, Liang K-Y. 1986. Longitudinal data analysis for discrete and continuous outcomes. *Biometrics* 42: 121-130.

Zorn CJW. 2001. Generalized estimating equation models for correlated data: a review with applications. *Am J Political Sci* 45: 470-490.